LA-UR-16-29078
Approved for public release; distribution is unlimited.

Title: 2016 T Division Lightning Talks

Author(s): Ramsey, Marilyn Leann; Adams, Luke Clyde; Ferre, Gregoire Robing; Grantcharov, Vesselin; Iaroshenko, Oleksandr; Krishnapriyan, Aditi; Kurtakoti, Prajvala Kishore; Le Thien, Minh Quan; Lim, Jonathan Ng; Low, Thaddeus Song En; Lystrom, Levi Aaron; Ma, Xiaoyu; Nguyen, Hong T; Pogue, Sabine Silvia; Orandle, Zoe Ann; Reisner, Andrew Ray; Revard, Benjamin Charles; Roy, Julien; Sandor, Csanad; Slavkova, Kalina Polet; Weichman, Kathleen Joy; et al.

Intended for: Report

Issued: 2016-11-29

2016 T Division Lightning Talks

Marilyn L. Ramsey

2016 Lightning Talk Authors

Adams. Luke
Ferre, Gregorie
Grantcharov, Vesselin
Iaroshenko, Oleksandr
Krishnapriyan, Aditi
Kurtakoti, Prajvala
Le Thien, Minh Quan
Lim, Jonathan
Low, Thaddeus
Lystorm, Levi
Ma, Xiaoyu
Nguyen, Hong
Pogue-Zentgraf, Sabine
Orandle, Zoe
Reisner, Andrew
Revard, Benjamin
Roy, Julien
Sandor, Csandor
Slavkova, Kalina
Weichman, Kathleen
Wu, Fei
Yang, Yang

Accelerating RPMD with Hyperdynamics

Luke Adams (UGS)
Whitman College

Mentor: Arthur Voter, T-1

Outline

- Infrequent event systems
- Hyperdynamics
- Ring polymer molecular dynamics (RPMD)
- Example system
- Results and challenges

Infrequent Event Systems

The system spends most of its time vibrating in a 3-N dimensional basin before finding an escape path.

We would like spend less of our computational budget on simulating this boring vibrational activity, so that we can observe more interesting events.

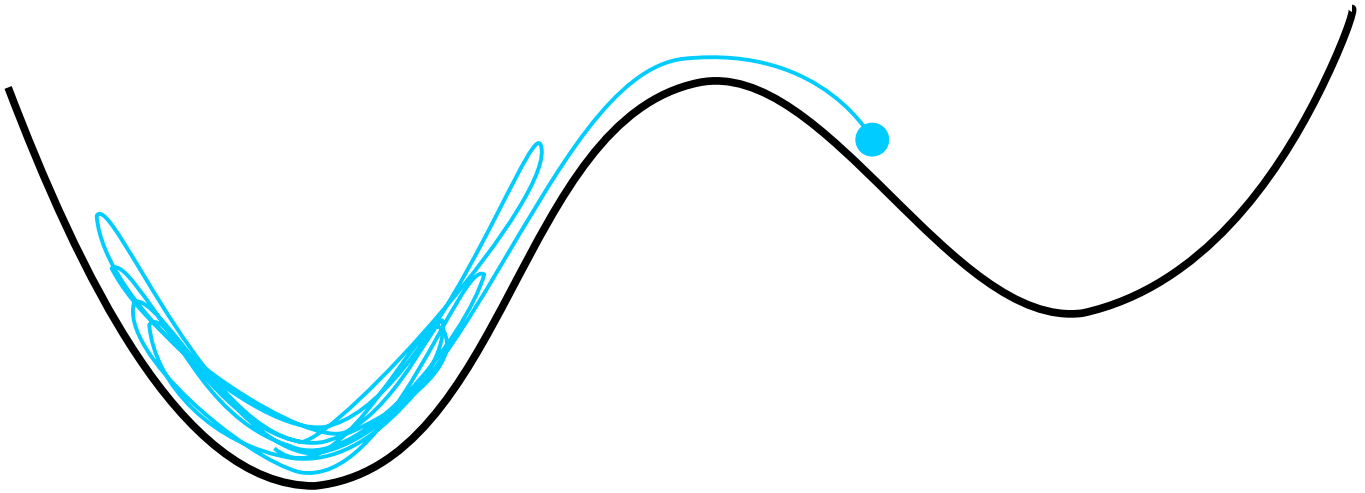

Hyperdynamics

Procedure:

- design bias potential
- run simulation on biased surface (V + ΔV)
- accumulate *hypertime* as

$$t_{\mathrm{hyper}} = \sum \Delta t_{\mathrm{MD}} \cdot \exp\left(\frac{\Delta V(x)}{k_B T}\right)$$

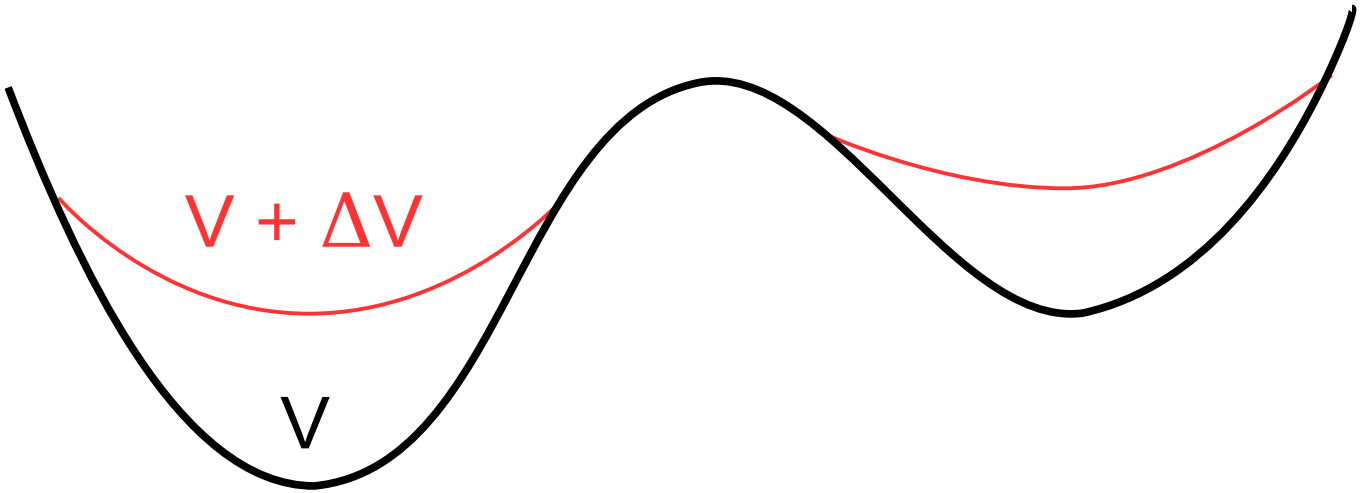

Hyperdynamics

Procedure:

- design bias potential
- run simulation on biased surface (V + ΔV)
- accumulate *hypertime* as

$$t_{\mathrm{hyper}} = \sum \Delta t_{\mathrm{MD}} \cdot \exp\left(\frac{\Delta V(x)}{k_B T}\right)$$

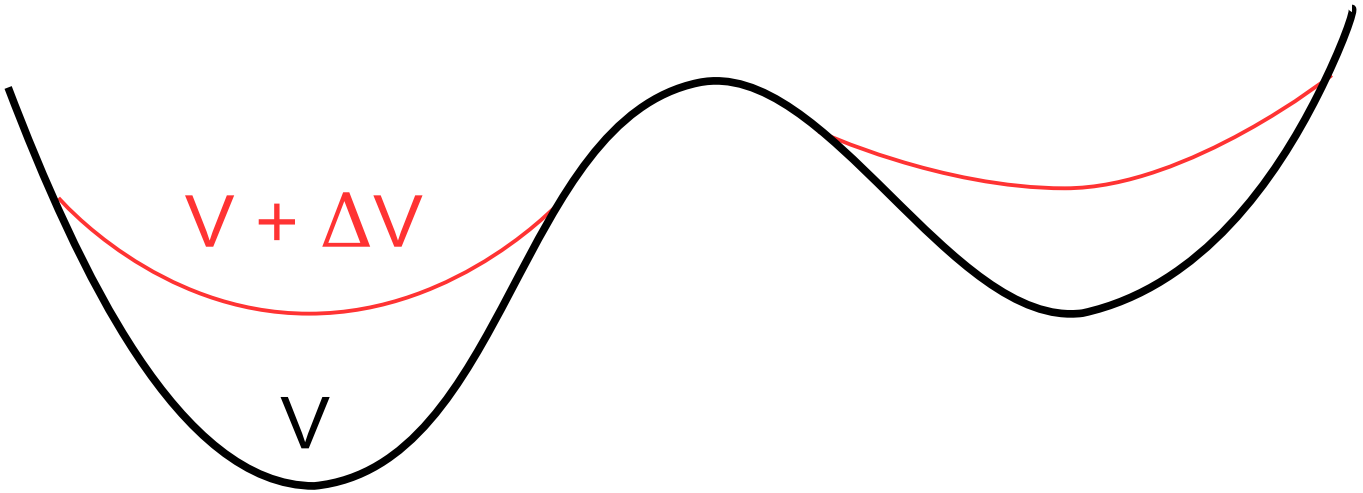

Hyperdynamics

Assumptions:

- infrequent events
- no recrossings
- bias potential ΔV is zero at dividing surface

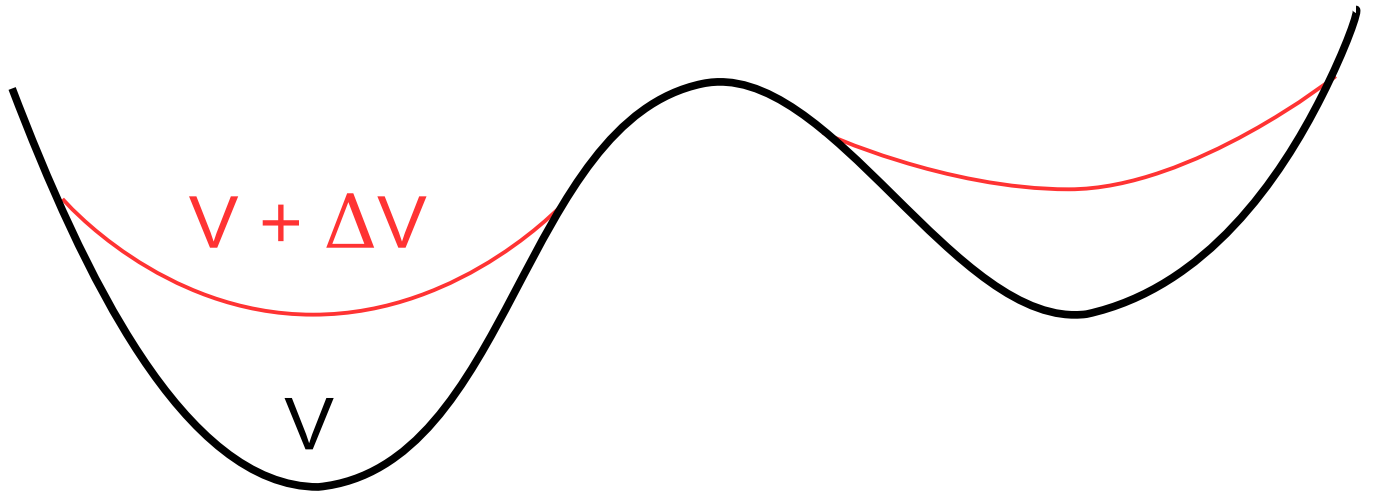

Ring Polymer MD (RPMD)

Replaces each atom with a ring of n beads; exact equilibrium quantum results in the infinite bead limit.

Each set of beads evolves in its own 'universe' while also interacting with its two neighboring universes.

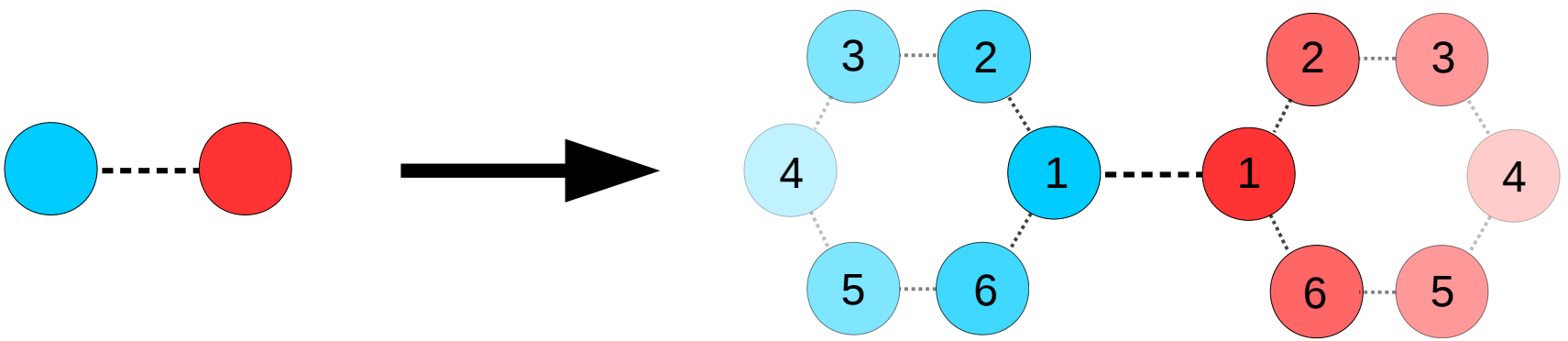

Ring Polymer MD (RPMD)

Each bead is connected to its two neighbors by a spring with a spring constant given by

$$\text{spring constant} = m \cdot \left(\frac{n k_B T}{\hbar} \right)^2$$

The spring frequency often limits the length of timesteps in the simulation.

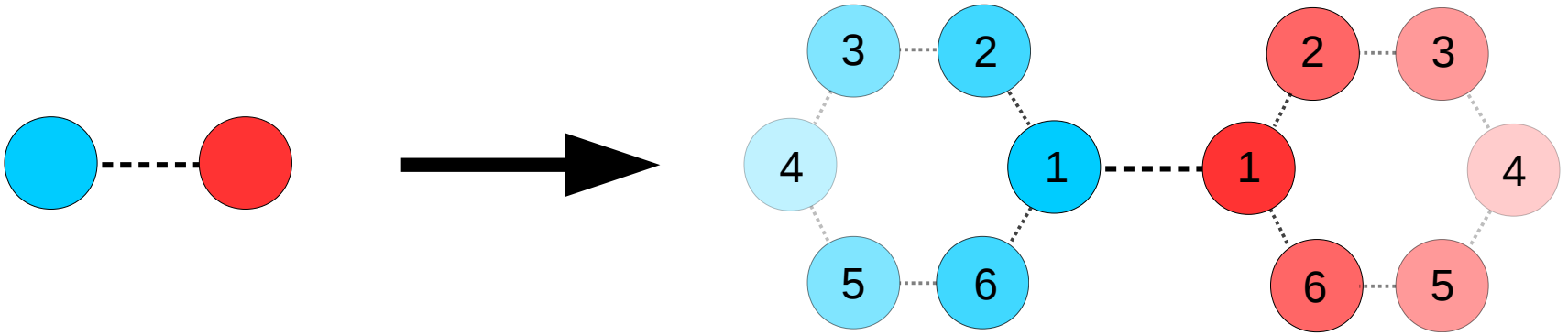

RPMD and Hyperdynamics

The most difficult part of adapting hyperdynamics to RPMD is choosing an appropriate bias potential.

We must choose a bias that gives a significant boost, but is zero along all dividing surfaces.

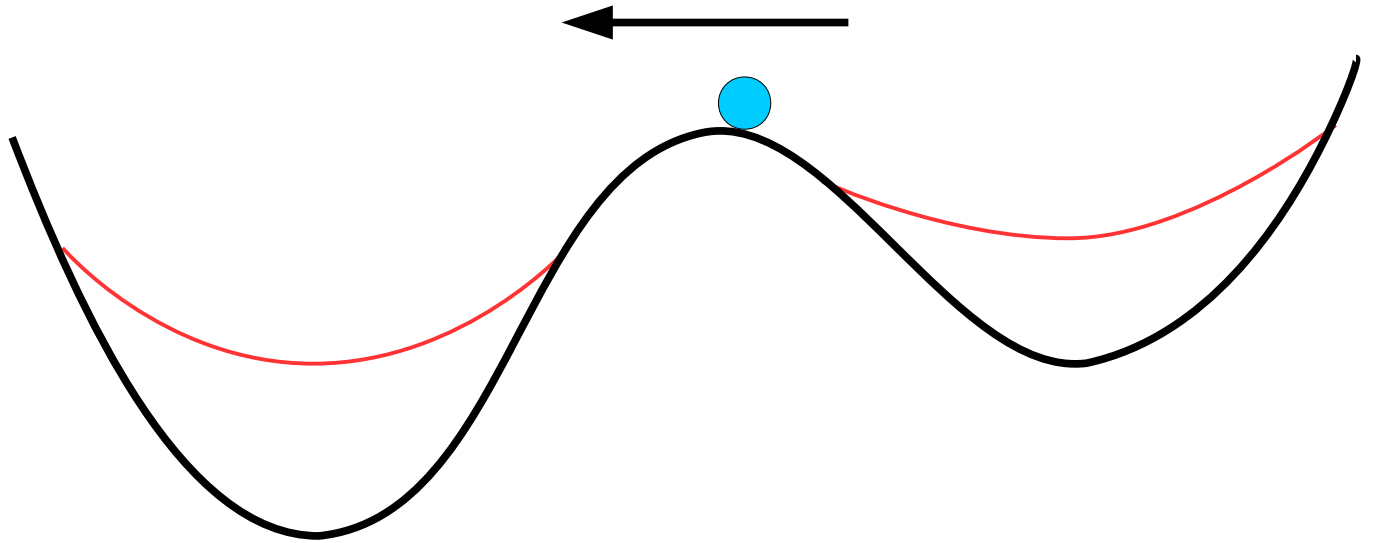

RPMD and Hyperdynamics

The most difficult part of adapting hyperdynamics to RPMD is choosing an appropriate bias potential.

We must choose a bias that gives a significant boost, but is zero along all dividing surfaces.

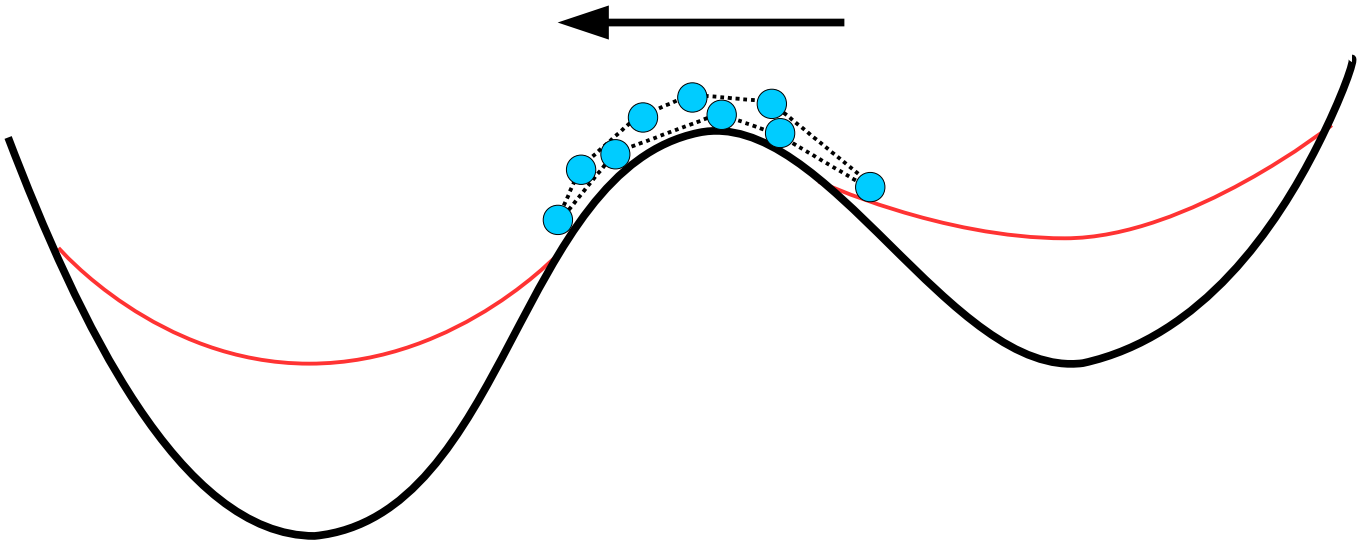

RPMD and Hyperdynamics

We define the bias force as the gradient of the bias potential at the centroid of the ring, and assign each bead $1/n$ of the bias force.

We assume that the centroid will be near the dividing surface when the system is making a transition.

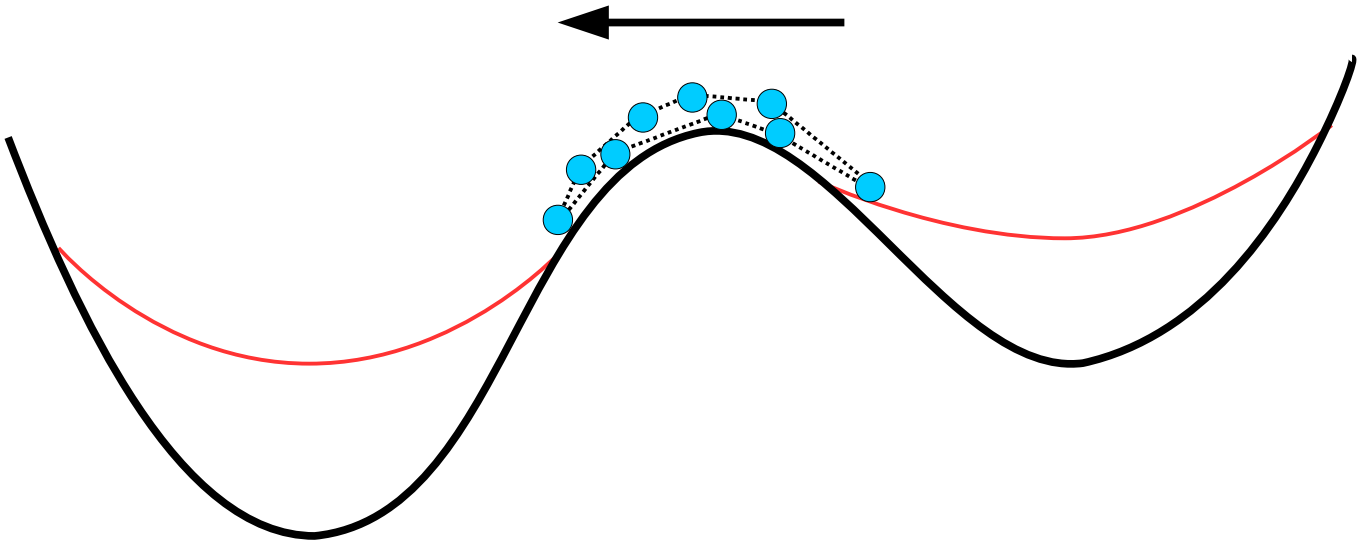

Example System

Symmetric Eckart barrier:

$$V(x) = \frac{V_0}{\cosh^2(x/a)}$$

$$\begin{aligned} V_0 &= 0.425 \text{ eV} \\ a &= 0.3884 \text{ Å} \\ m &= 9.7 \times 10^{-28} \text{ kg} \end{aligned}$$

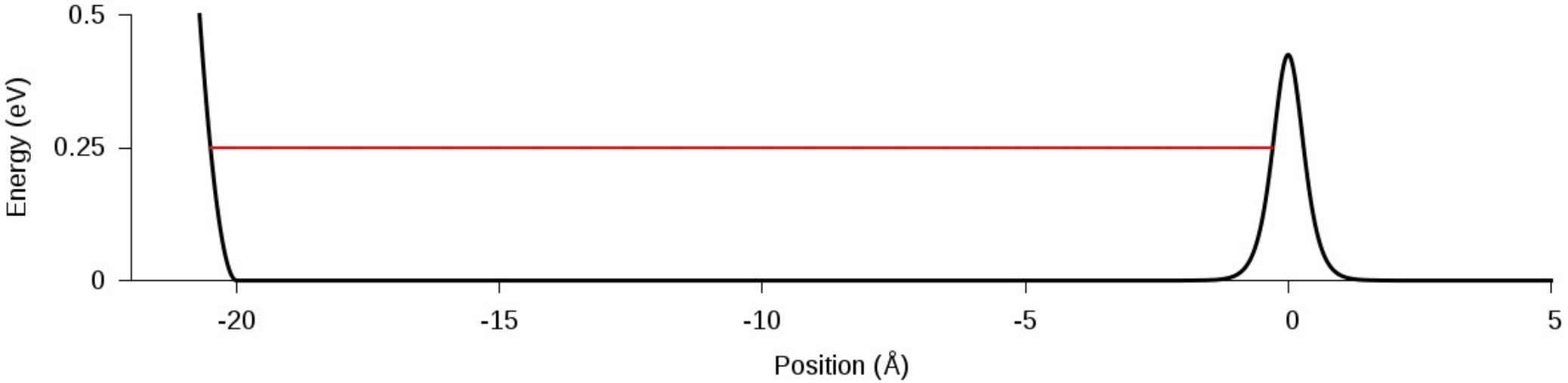

Results

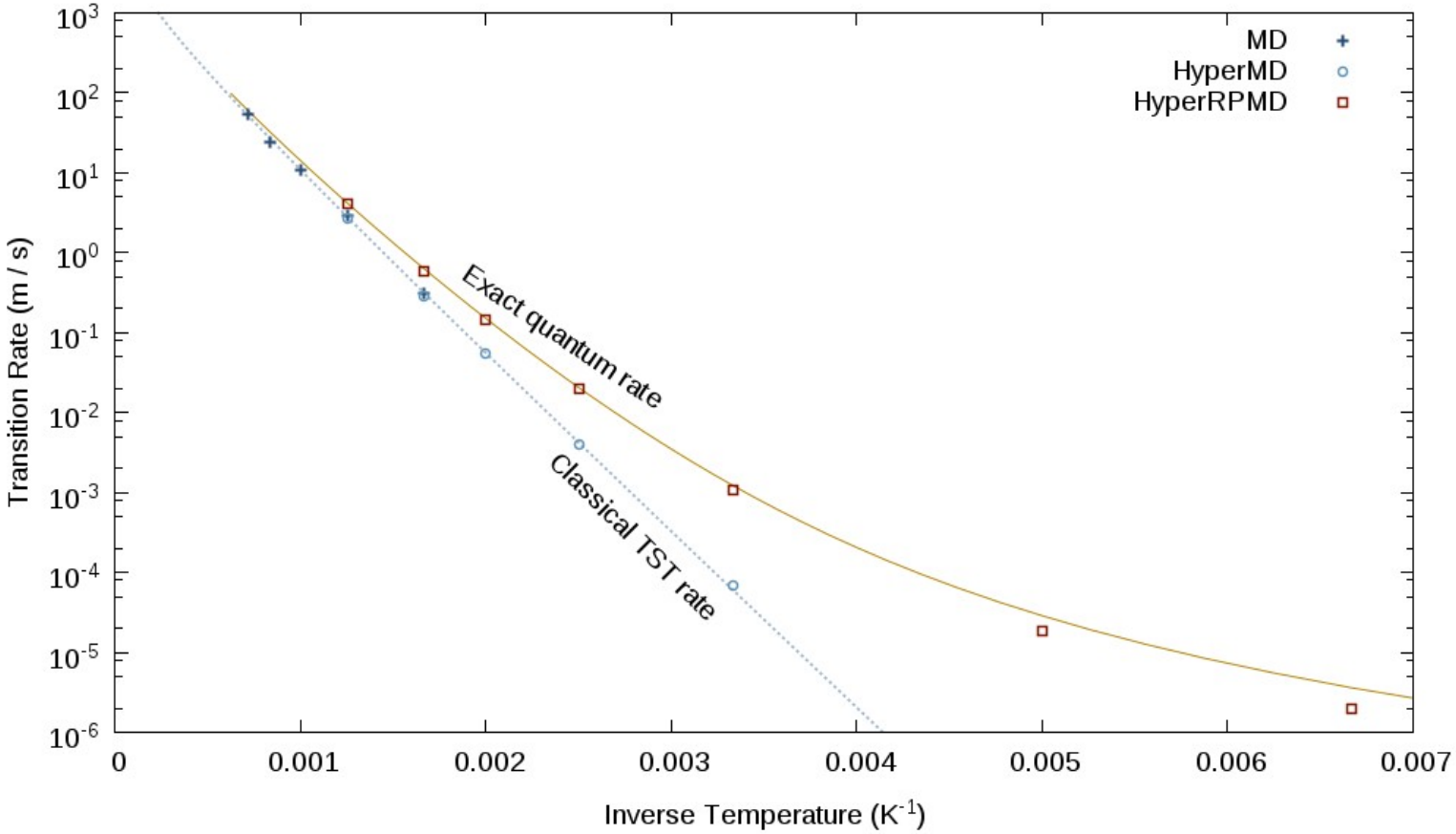
MD
HyperMD
HyperRPMD
Exact quantum rate
Classical TST rate
Transition Rate (m / s)
Inverse Temperature (K-1)
10^3
10^2
10^1
10^0
10^-1
10^-2
10^-3
10^-4
10^-5
10^-6
0
0.001
0.002
0.003
0.004
0.005
0.006
0.007

Results

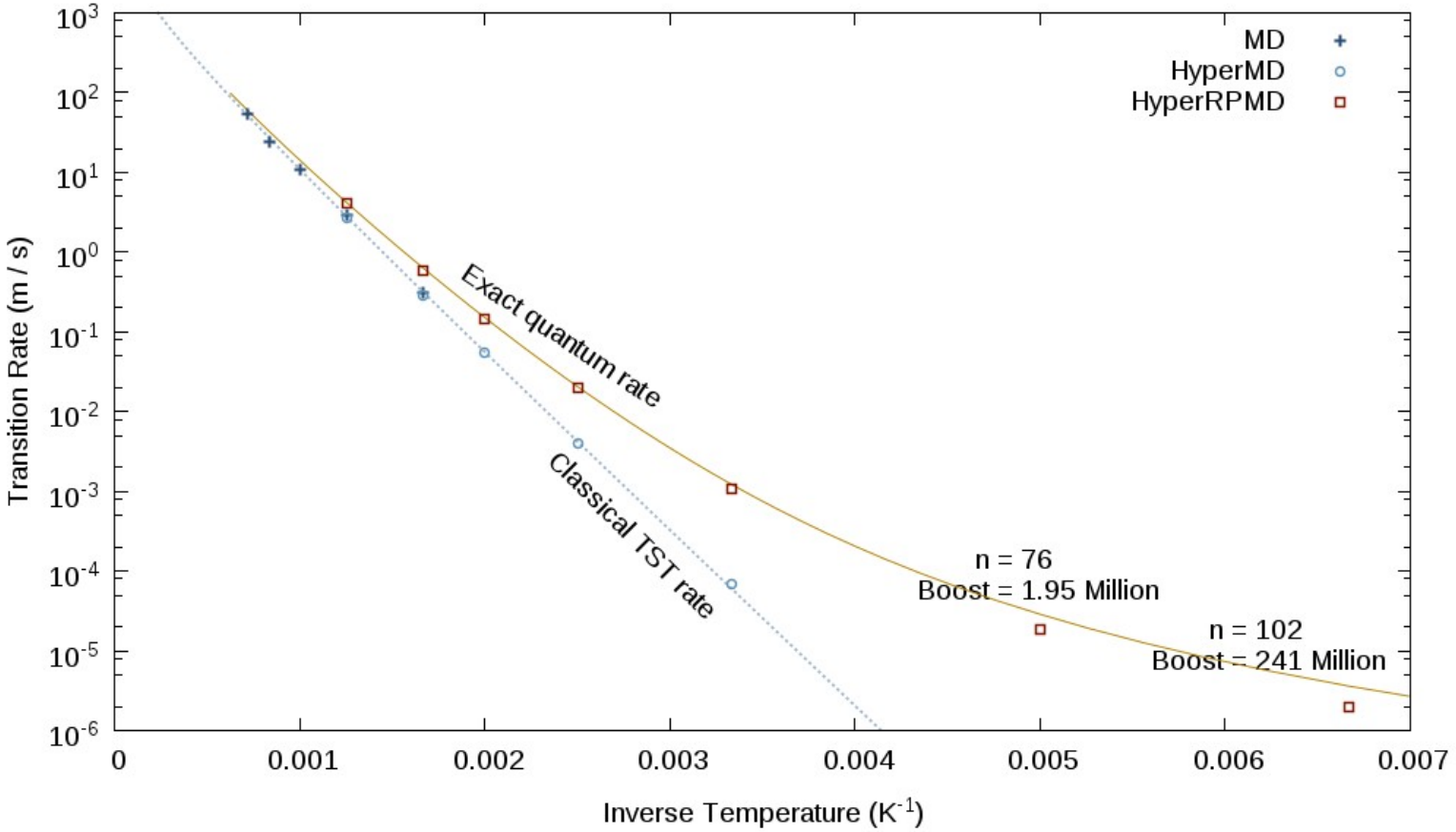
MD
HyperMD
HyperRPMD
Exact quantum rate
Classical TST rate
n = 76
Boost = 1.95 Million
n = 102
Boost = 241 Million
Transition Rate (m / s)
Inverse Temperature (K-1)
10^3
10^2
10^1
10^0
10^-1
10^-2
10^-3
10^-4
10^-5
10^-6
0
0.001
0.002
0.003
0.004
0.005
0.006
0.007

Active Matter on Dynamical Optical Traps

Cs. Sándor[1,2] A. Libál[1,2] C. Reichhardt[2] C. J. Olson Reichhardt[2]

[1]Faculty of Mathematics and Computer Science
Babeș-Bolyai University

[2]Los Alamos National Laboratory
Theoretical Division and Center of Nonlinear Studies

Lightning Talk, 2016

Active Matter

- Nonequilibrium particle-based systems with internal, propulsion.
- Possible collective behaviors

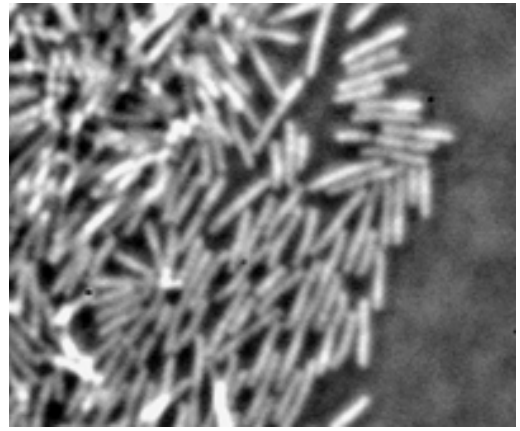

Simulation

System parameters:

- number of particles: $N_s = 8000 - 20000$
- particle radius: $R_i = 1.0$
- system size: $L = 300 \times 300$

Equation of motion:

$$\eta \frac{dr_i}{dt} = F^i_{inter} + F^i_m \qquad (1)$$

- repulsive disk-disk interaction force: $\mathbf{F}^i_{inter} = \Theta(d-2R)k(d-2R)$
- particle motor force : $\mathbf{F}^i_m = 1.0$
- run length: $l_r = 300 - 600$

Run-and-thumble dynamics:

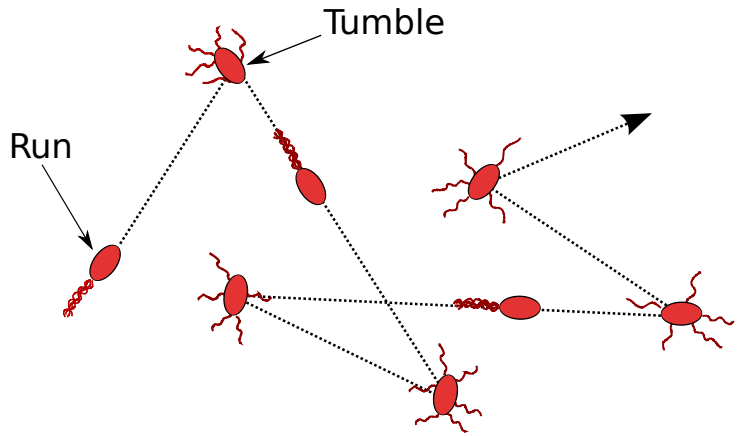

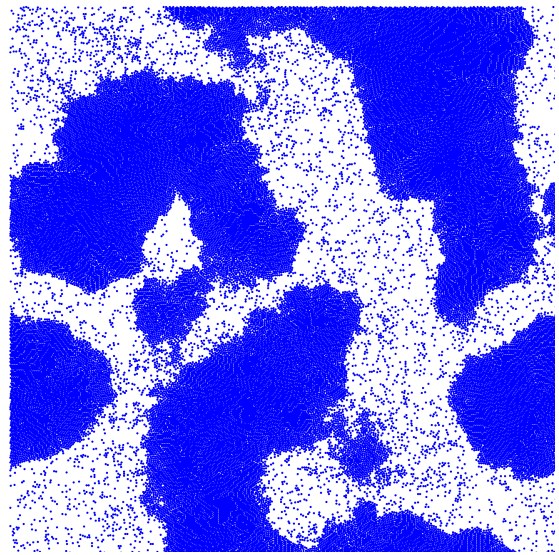

Random Pinning Substrate

Equation of motion:

$$\eta \frac{dr_i}{dt} = F^i_{inter} + F^i_m + \mathbf{F}^i_p \quad (2)$$

- pinning force:
  $\mathbf{F}^i_p = \Theta(r - R_p) r / R_p F_p$

System parameters:

- number of particles:
  $N_s = 8000 - 20000$
- number of pinning sites:
  $N_p = 8000$
- pinning site force:
  $F_p = 0 - 8$

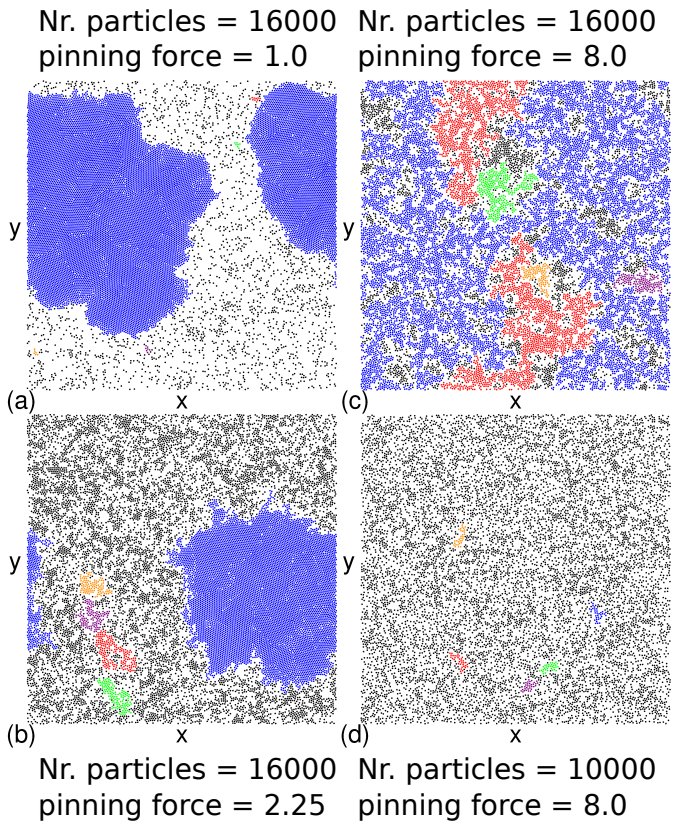

- *a.*: C_l/N_s : fraction of particles in the largest cluster
- *b.*: P_6/N_s: fraction P_6 of sixfold coordinated disks

Phases:

- I. dewetted phase
- II. partially wetted phase
- III. wetted labyrinth phase
- IV. pinned liquid phase

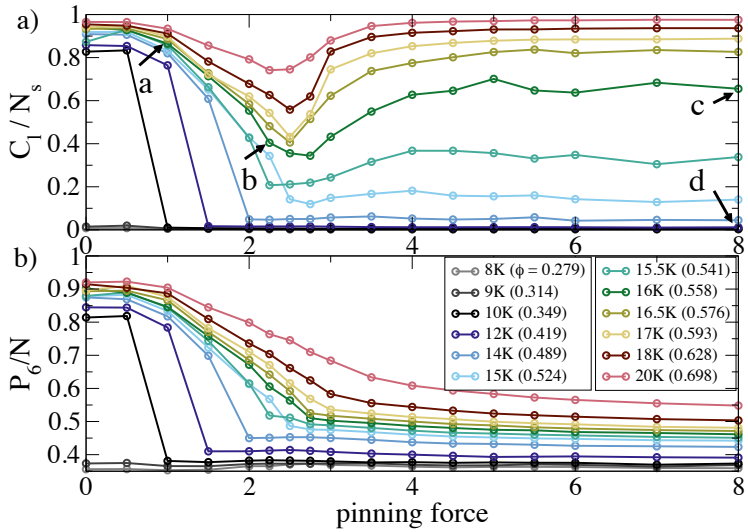

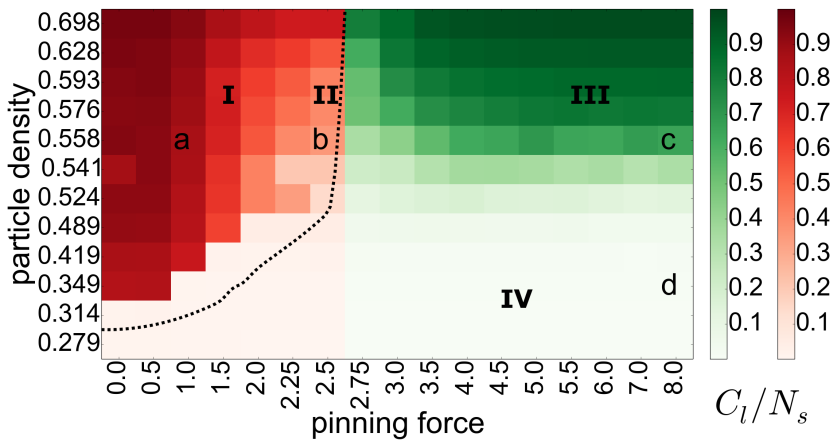

Drift Force

Equation of motion:

$$\eta \frac{dr_i}{dt} = F^i_{inter} + F^i_m + \mathbf{F}^i_d \quad (3)$$

- drift force: $\mathbf{F}^i_d = 0 - 7$
- number of particles: $N_s = 6000 - 24000$
- number of pinningsites: $N_p = 8000$
- pinning force: $F_p = 5.0$

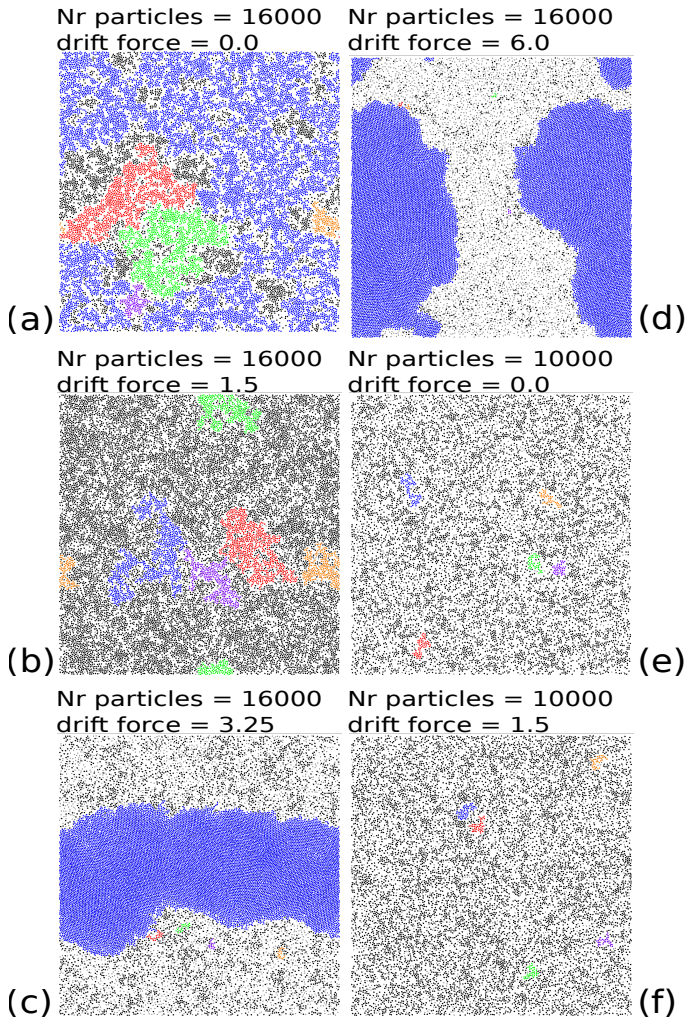

Phases:

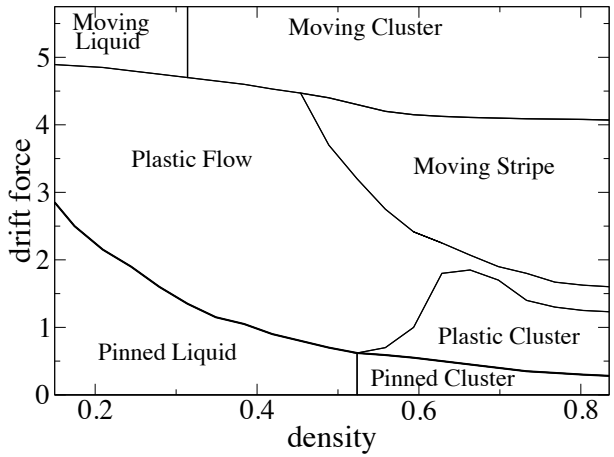

Velocity:

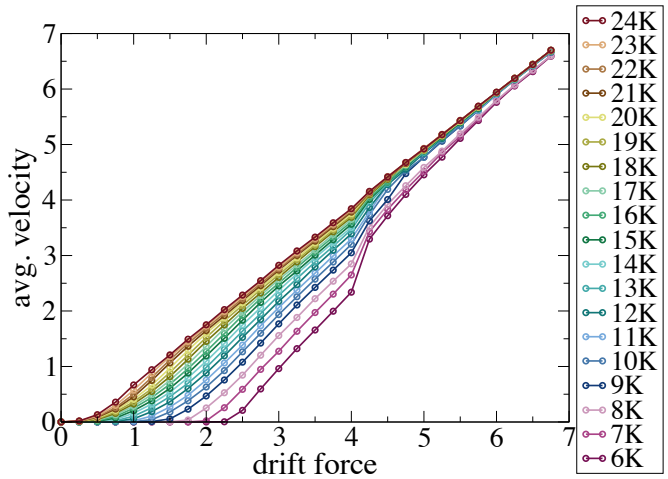

Cluster length:

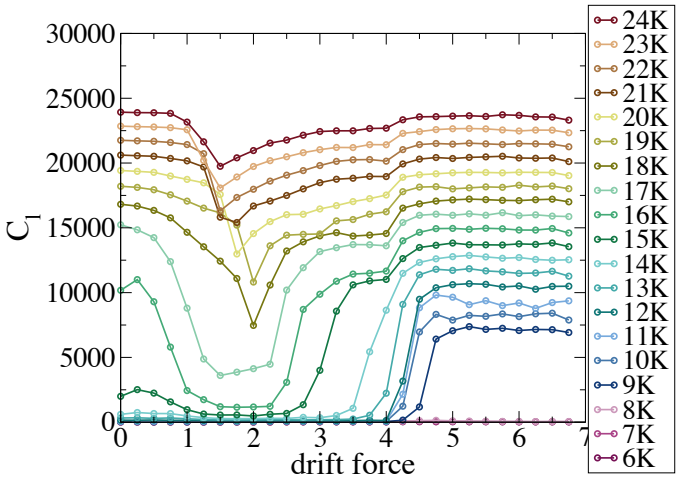

Derivative velocity:

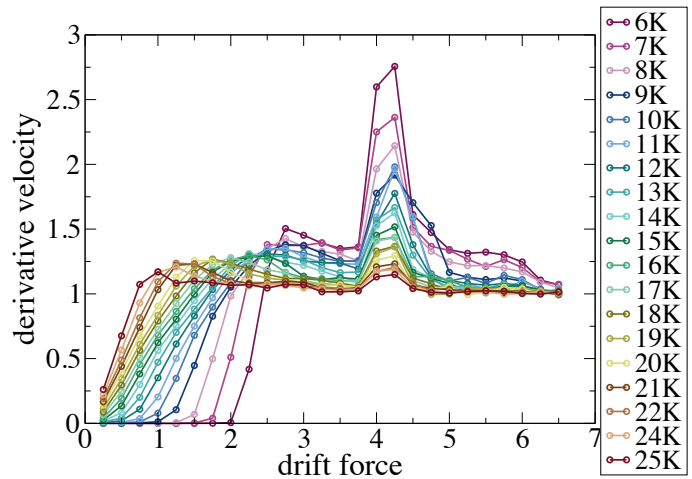

Acknowledgments

I would like to thank to

- T4
- T1

for hosting, and for my mentors:

- Charles Reichhardt
- Cynthia Reichhardt
- András Libál

for mentoring me

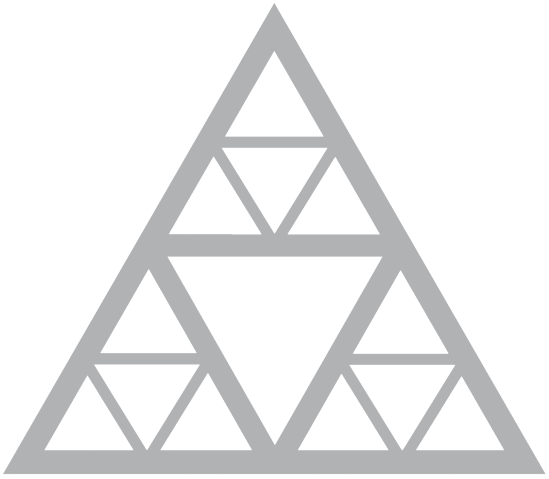

École des Ponts

ParisTech

www.enpc.fr

Kernels over graphs for fitting potential energy landscape

Lightning Talk

Grégoire Ferré – Kipton Barros – Gabriel Stoltz

Center for Non-Linear Studies – École des Ponts ParisTech

Thusday, July 28th, 2016

Outline

1. Motivation and Tools

Classical Molecular Dynamics

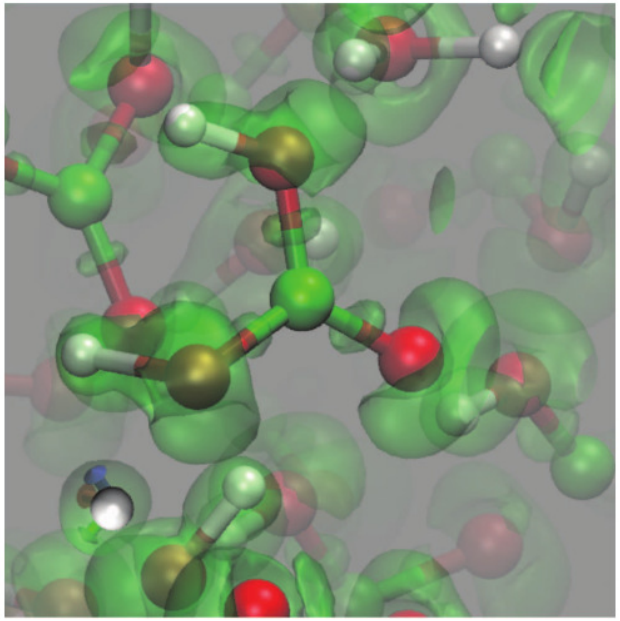

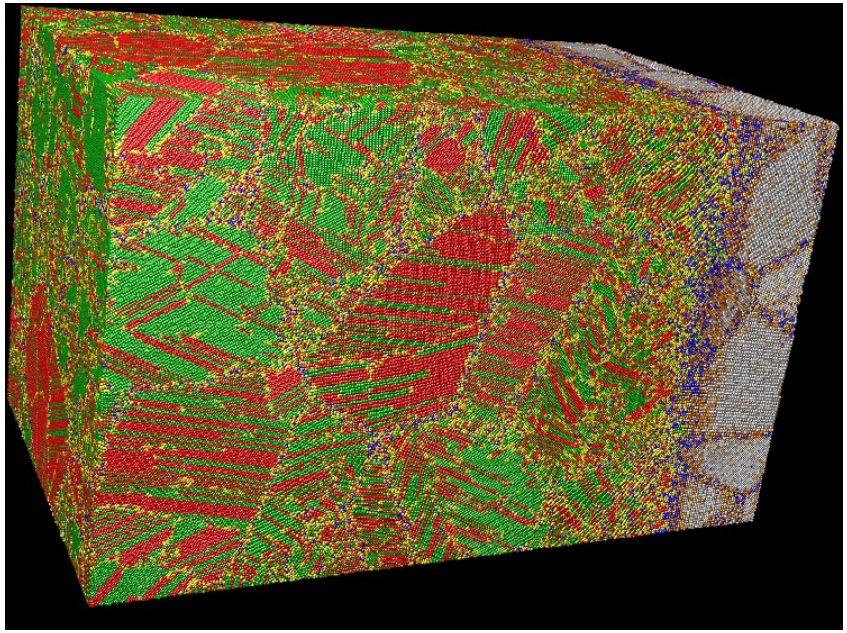

From Ab Initio Calculation to MD: a scaling issue

$$H\psi = E\psi$$

Classical Molecular Dynamics

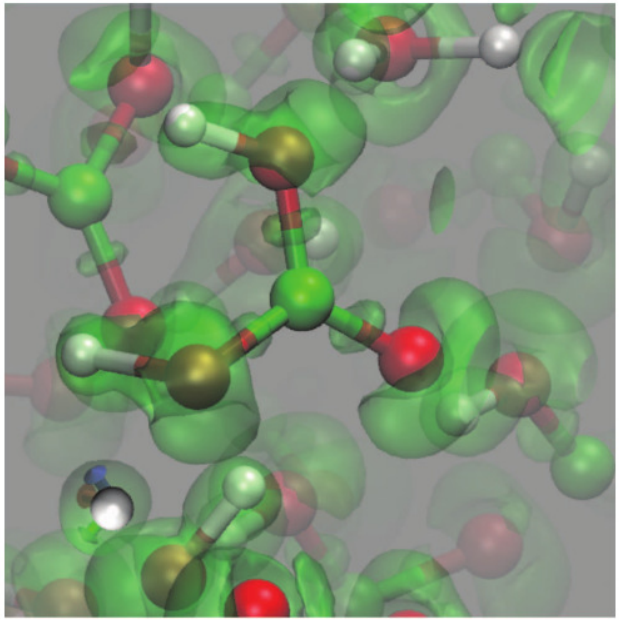

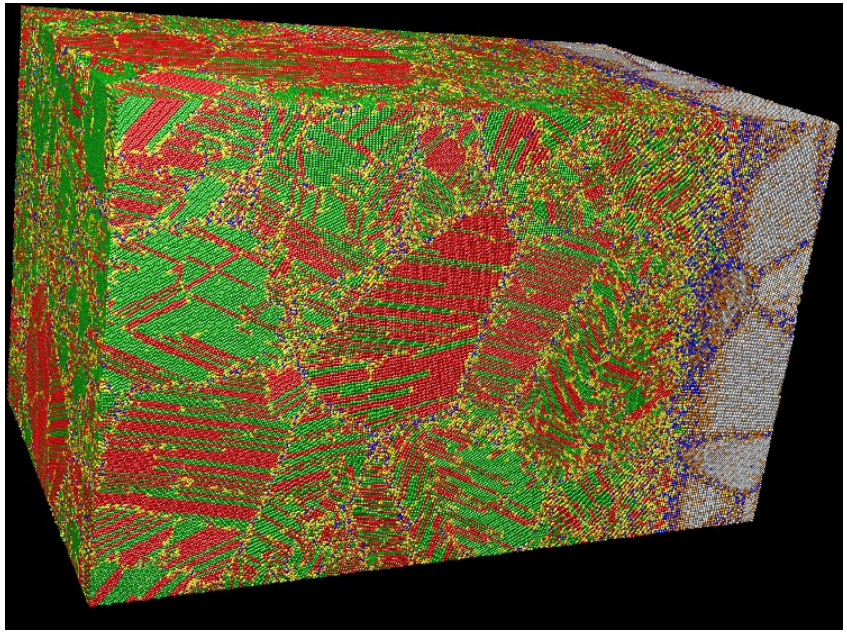

From Ab Initio Calculation to MD: a scaling issue

$$H\psi = E\psi$$

Motivation of Numerical Potentials

MD requires the computation of forces for many configurations

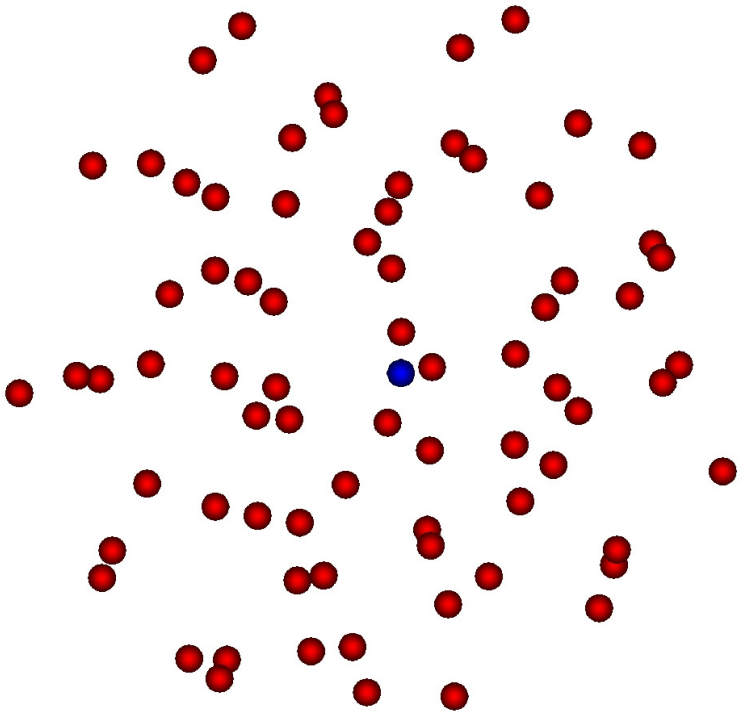

Atomic environment

Objective

Estimate for the central particle:

- the energy $V(C)$
- the forces $-\nabla V(C)$

Motivation of Numerical Potentials

MD requires the computation of forces for many configurations

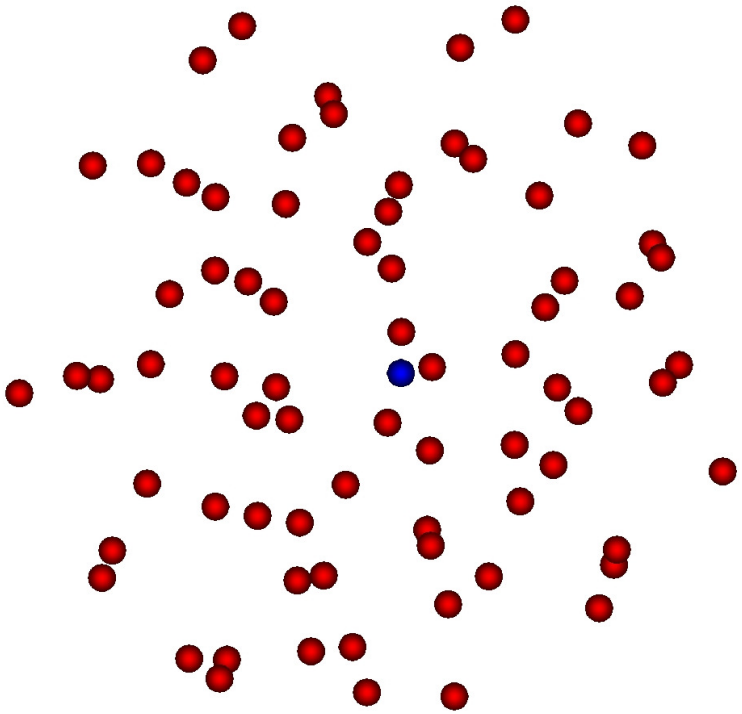

Atomic environment

Objective

Estimate for the central particle:

- the energy $V(C)$
- the forces $-\nabla V(C)$

Motivation of Numerical Potentials

Potential at an intermediate level

Ab Initio Calculation

Accurate, long to compute, depends on the number of electrons

Numerical Potentials and Forces

Ab Initio accuracy with lower computational cost

Classical Potentials and Forces

Unable to reproduce all the properties of a complex material

Motivation of Numerical Potentials

Potential at an intermediate level

Ab Initio Calculation

Accurate, long to compute, depends on the number of electrons

Numerical Potentials and Forces

Ab Initio accuracy with lower computational cost

Classical Potentials and Forces

Unable to reproduce all the properties of a complex material

Motivation of Numerical Potentials

Potential at an intermediate level

Ab Initio Calculation

Accurate, long to compute, depends on the number of electrons

Numerical Potentials and Forces

Ab Initio accuracy with lower computational cost

Classical Potentials and Forces

Unable to reproduce all the properties of a complex material

Motivation of Numerical Potentials

Potential at an intermediate level

Ab Initio Calculation

Accurate, long to compute, depends on the number of electrons

Numerical Potentials and Forces

Ab Initio accuracy with lower computational cost

Classical Potentials and Forces

Unable to reproduce all the properties of a complex material

Machine Learning Tools

Database:

- atoms′ positions, configurations (C_i) for $i = 1, \ldots, N$
- associated forces $(\nabla V(C_i))$ for $i = 1, \ldots, N$

Machine Learning Tools

Database:

- atoms' positions, configurations (C_i) for $i = 1, \ldots, N$
- associated forces $(\nabla V(C_i))$ for $i = 1, \ldots, N$

Regression methods

- Support Vector Machine
- Neural Networks
- **Kernel methods**
- invariant polynomials ...

Machine Learning Tools

Database:

- atoms' positions, configurations (C_i) for $i = 1, \ldots, N$
- associated forces $(\nabla V(C_i))$ for $i = 1, \ldots, N$

Regression methods

- Support Vector Machine
- Neural Networks
- **Kernel methods**
- invariant polynomials ...

Kernel methods

For two configurations C_1 and C_2, a kernel $K(C_1, C_2)$ is a **measure of similarity** between C_1 and C_2.
Result: if we can compare, we can interpolate.

Difficulties

Physical properties:

- the number of atoms may vary,
- invariance with respect to ordering of atoms,
- rotation invariance.

Difficulties

Physical properties:

- the number of atoms may vary,
- invariance with respect to ordering of atoms,
- rotation invariance.

Extensive literature on this problem:

- symmetry functions (Behler et al., 2007),
- Smooth Overlap of Atomic Position (SOAP, Csanyi et al., 2010),
- Internal Vector coordinates (Li, Kermode, De Vita, 2015)
- scattering transform (Mallat et al., 2015),
- Moment Tensor Polynomials (MTP, Shapeev, 2016)

2. Graph Representation

Graph Representation

Define an adjacency matrix :

$A_{i,j} =$«weight between particles i and j»$= \varphi_\sigma(|q_i - q_j|)$

Graph Representation

Define an adjacency matrix :

$A_{i,j} =$«weight between particles i and j»$= \varphi_\sigma(|q_i - q_j|)$

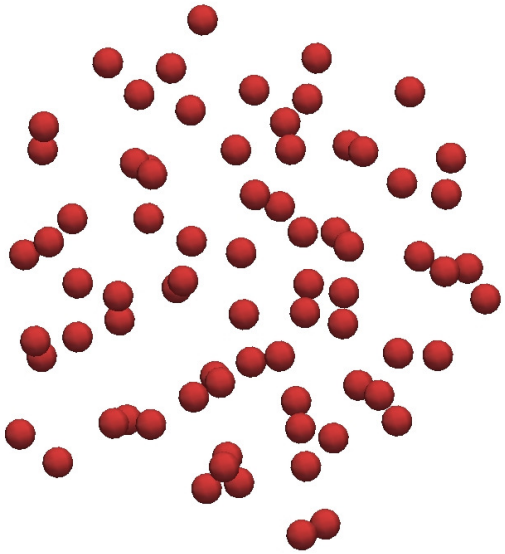

Graph Representation

Define an adjacency matrix :

$A_{i,j}$ =«weight between particles i and j»= $\varphi_\sigma(|q_i - q_j|)$

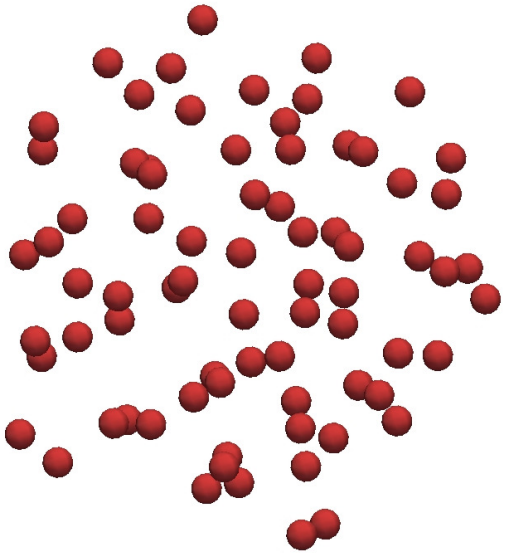

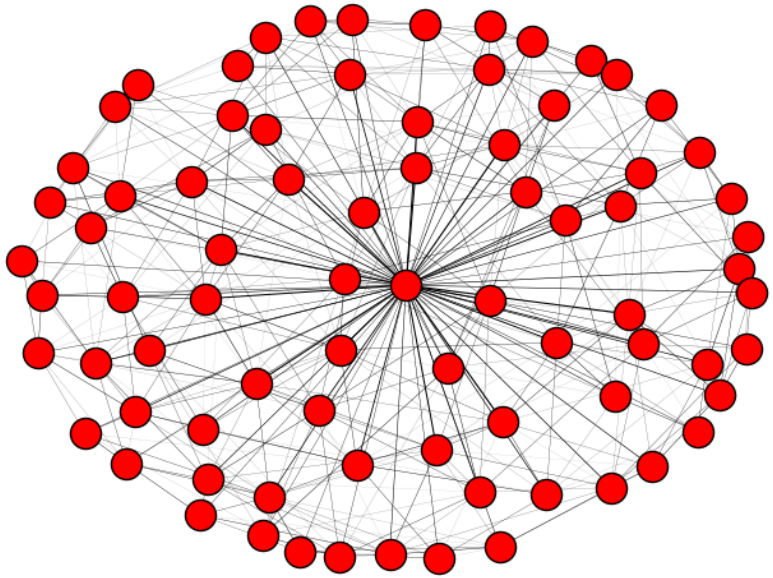

Graph Representation

Define an adjacency matrix :

$A_{i,j} =$«weight between particles i and j»$= \varphi_\sigma(|q_i - q_j|)$

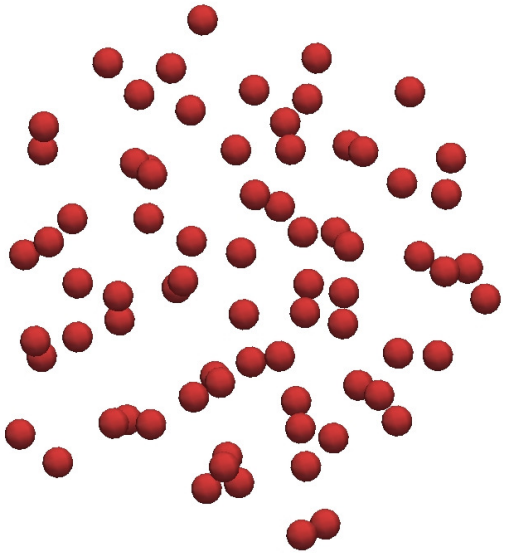

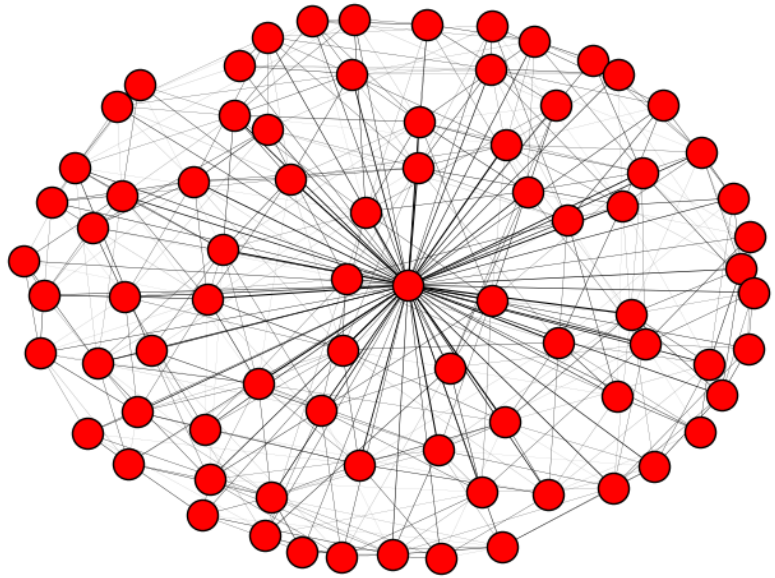

Idea

Rotation invariant description of the system

Graphs in the Literature

Important interest in the last 15 years:

- web/internet,
- social networks,
- disease propagation,
- chemoinformatics.

Graphs in the Literature

Important interest in the last 15 years:

- web/internet,
- social networks,
- disease propagation,
- chemoinformatics.

Many graph kernels have been developed (Gärtner, 2002):

- spectral properties (Kondor et. al, 2002),
- shortest paths (Borgwadt et al., 2005),
- graphlets (Shervashidze & Vishwanathan, 2009),
- random walks (Vishwanathan, Schraudolph, Kondor & Borgwardt, 2010),
- functional embedding (Shrivastava & Li, 2014).

Graph kernels and random walks

Adjacency matrix $(A_{i,j})_{i,j=1}^{n}$ as generator of a Markov process.

Graph kernels and random walks

Adjacency matrix $(A_{i,j})_{i,j=1}^{n}$ as generator of a Markov process.

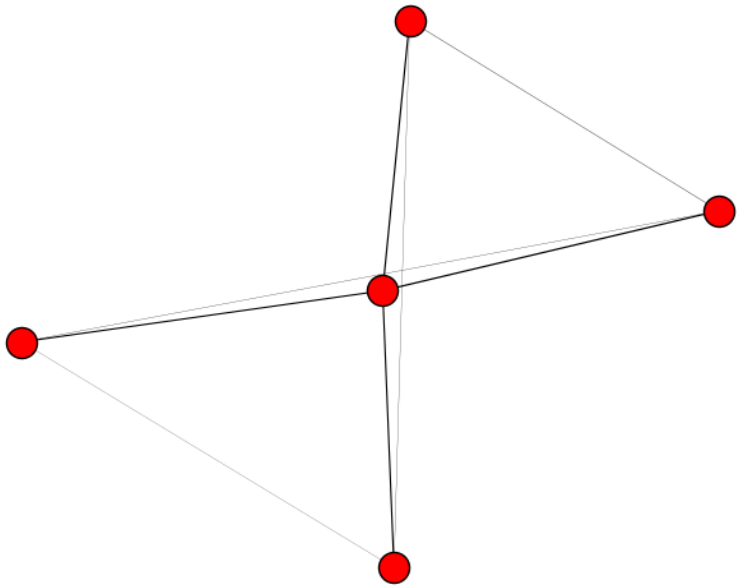

Graph kernels and random walks

Adjacency matrix $(A_{i,j})_{i,j=1}^{n}$ as generator of a Markov process.

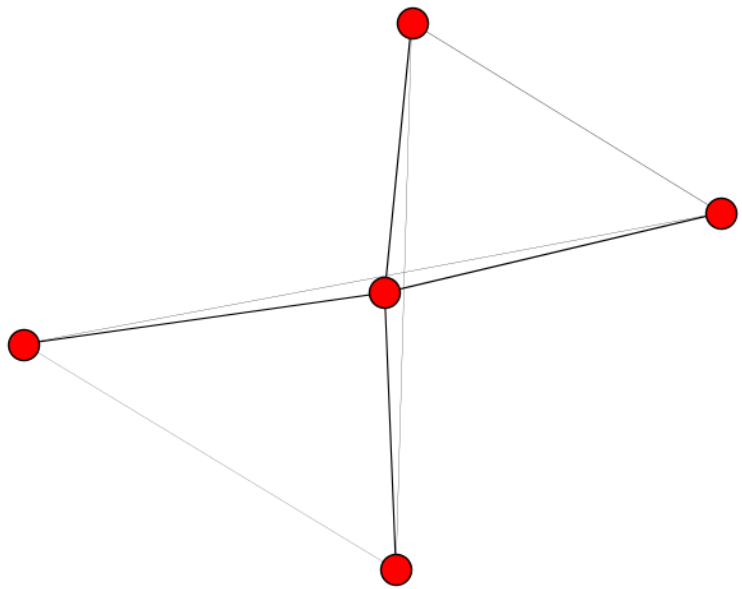

Random walk from an initial distribution $x_0 \in \mathbb{R}^n$

$$x_1 = Ax_0$$

$$x_2 = A^2 x_0$$

$$\dots$$

$$x_k = A^k x_0.$$

Graph kernels and random walks

Adjacency matrix $(A_{i,j})_{i,j=1}^{n}$ as generator of a Markov process.

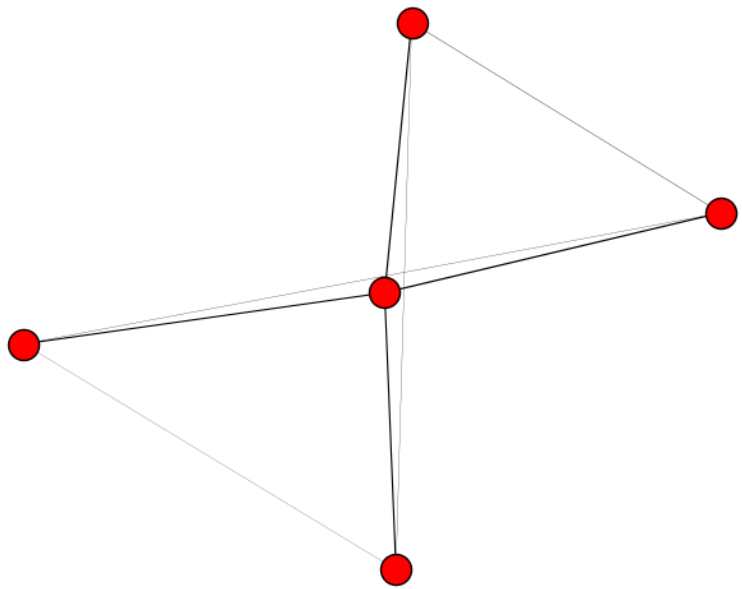

Random walk from an initial distribution $x_0 \in \mathbb{R}^n$

$$x_1 = Ax_0$$

$$x_2 = A^2 x_0$$

$$\dots$$

$$x_k = A^k x_0.$$

Bonus: if x_0 is chosen **uniform**, graph properties are made **permutation invariant**, so we use $x_0 = e = (1, \dots, 1)$.

Toy application

Fitting the pair interaction between a central atom and 4 neighbors with random perturbations.

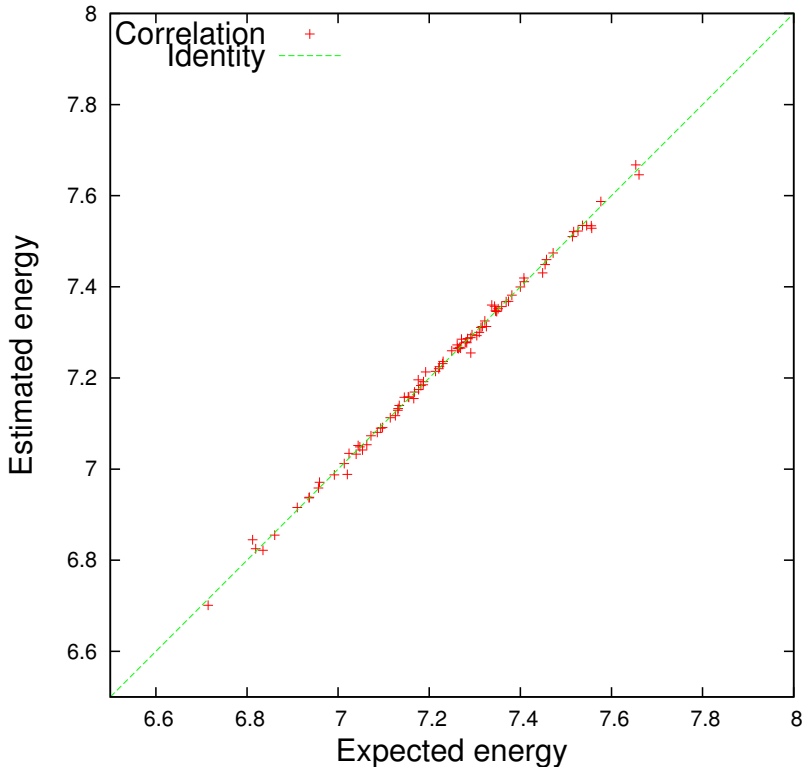

Good interpolation capacity with a small database ($\approx$ 400 elements)

Conclusion & Tracks

Conlusion

New methodology for fitting potential energy landscapes:

- represent a configuration by a graph,
- random graph theory for kernel design,
- proof of principle.

Ongoing work

- test on DFT database,
- insert more physics into the graph,
- discrepancy between tight-binding and DFT,
- approximation of the graph's probability density.

Conclusion & Tracks

Conlusion

New methodology for fitting potential energy landscapes:

- represent a configuration by a graph,
- random graph theory for kernel design,
- proof of principle.

Ongoing work

- test on DFT database,
- insert more physics into the graph,
- discrepancy between tight-binding and DFT,
- approximation of the graph's probability density.

RKHS: Kernel

Definition - Kernel

We consider a compact metric space $\mathcal{X}$.
A positive definite kernel is a function $K : \mathcal{X} \times \mathcal{X} \mapsto \mathbb{R}$, that verifies:

- K is symmetric: $\forall (x, x') \in \mathcal{X}^2, K(x, x') = K(x', x)$,
- for all $N \in \mathbb{N}^*$, $(x_1, \ldots, x_N) \in \mathcal{X}^N$, the matrix $K(x_i, x_j)_{i,j \leq N}$ is positive semidefinite, or for all $(a_1, \ldots, a_N) \in \mathbb{R}^N$,

$$\sum_{i=1}^{N} \sum_{j=1}^{N} a_i a_j K(x_i, x_j) \geq 0.$$

In this context

For data $(x_i)_{i=1}^n$, $K(x_i, x_j)$ is a matrix of correlation.
Typically,

$$\forall\, x, y \in \mathbb{R}^m, \quad K(x, y) = e^{-\frac{(x-y)^2}{2\sigma^2}}.$$

RKHS: Kernel

Definition - Kernel

We consider a compact metric space $\mathcal{X}$.
A positive definite kernel is a function $K : \mathcal{X} \times \mathcal{X} \mapsto \mathbb{R}$, that verifies:

- K is symmetric: $\forall (x, x') \in \mathcal{X}^2, K(x, x') = K(x', x)$,
- for all $N \in \mathbb{N}^*$, $(x_1, \ldots, x_N) \in \mathcal{X}^N$, the matrix $K(x_i, x_j)_{i,j \leq N}$ is positive semidefinite, or for all $(a_1, \ldots, a_N) \in \mathbb{R}^N$,

$$\sum_{i=1}^{N} \sum_{j=1}^{N} a_i a_j K(x_i, x_j) \geq 0.$$

In this context

For data $(x_i)_{i=1}^n$, $K(x_i, x_j)$ is a matrix of correlation.
Typically,

$$\forall x, y \in \mathbb{R}^m, \quad K(x, y) = e^{-\frac{(x-y)^2}{2\sigma^2}}.$$

Rkhs : basics

Reproducing Kernel Hilbert Spaces

Consider a space of real functions $\mathcal{H} \subset \mathbb{R}^{\mathcal{X}}$ forming a Hilbert space with inner product $\langle \cdot, \cdot \rangle_{\mathcal{H}}$. A kernel K is a reproducing kernel of $\mathcal{H}$ if:

- $\mathcal{H}$ contains all function of the form

$$\forall\, x \in \mathcal{X},\, K_x : t \mapsto K(x,t)$$

- for all $x \in \mathcal{X}$ and $f \in \mathcal{H}$,

$$f(x) = \langle K_x, f \rangle_{\mathcal{H}}.$$

Example

$$f(x) = \int_{\mathbb{R}^m} K(x,y) f(y) \mathrm{d}y.$$

RKHS : basics

Reproducing Kernel Hilbert Spaces

Consider a space of real functions $\mathcal{H} \subset \mathbb{R}^{\mathcal{X}}$ forming a Hilbert space with inner product $\langle \cdot, \cdot \rangle_{\mathcal{H}}$. A kernel K is a reproducing kernel of $\mathcal{H}$ if:

- $\mathcal{H}$ contains all function of the form

$$\forall\, x \in \mathcal{X},\, K_x : t \mapsto K(x,t)$$

- for all $x \in \mathcal{X}$ and $f \in \mathcal{H}$,

$$f(x) = \langle K_x, f \rangle_{\mathcal{H}}.$$

Example

$$f(x) = \int_{\mathbb{R}^m} K(x,y) f(y) \mathrm{d}y.$$

Understanding RKHS

Consider the operator:

$$\begin{array}{rccc} L_K: & L^2 & \to & L^2 \\ & f & \mapsto & \displaystyle\int_{\mathbb{R}^m} K(\cdot, y) f(y) \mathrm{d}y, \end{array}$$

and associated eigenvalues (λ_k, ψ_k), $\lambda_k \to 0$. Any L^2 function reads

$$f(x) = \sum_{k \geq 1} c_k \psi_k(x) \text{ with } c_k = \int_{\mathbb{R}^m} f(x) \psi_k(x) \mathrm{d}x.$$

Alternative definition

$$\mathcal{H} = \left\{ f = \sum_{k \geq 1} c_k \psi_k \;\middle|\; \sum_{k \geq 1} \frac{c_k^2}{\lambda_k} < +\infty \right\}$$

Functions of finite energy

$$L^2 = \left\{ f = \sum_{k \geq 1} c_k \psi_k \;\middle|\; \sum_{k \geq 1} c_k^2 < +\infty \right\}$$

Understanding RKHS

Consider the operator:

$$\begin{array}{rccc} L_K : & L^2 & \to & L^2 \\ & f & \mapsto & \displaystyle\int_{\mathbb{R}^m} K(\cdot, y) f(y) \mathrm{d}y, \end{array}$$

and associated eigenvalues (λ_k, ψ_k), $\lambda_k \to 0$. Any L^2 function reads

$$f(x) = \sum_{k \geq 1} c_k \psi_k(x) \text{ with } c_k = \int_{\mathbb{R}^m} f(x) \psi_k(x) \mathrm{d}x.$$

Alternative definition

$$\mathcal{H} = \left\{ f = \sum_{k \geq 1} c_k \psi_k \;\middle|\; \sum_{k \geq 1} \frac{c_k^2}{\lambda_k} < +\infty \right\}$$

Functions of finite energy

$$L^2 = \left\{ f = \sum_{k \geq 1} c_k \psi_k \;\middle|\; \sum_{k \geq 1} c_k^2 < +\infty \right\}$$

Understanding RKHS

Consider the operator:

$$\begin{array}{rccc} L_K: & L^2 & \to & L^2 \\ & f & \mapsto & \displaystyle\int_{\mathbb{R}^m} K(\cdot,y)f(y)\mathrm{d}y, \end{array}$$

and associated eigenvalues (λ_k, ψ_k), $\lambda_k \to 0$. Any L^2 function reads

$$f(x) = \sum_{k\geq 1} c_k \psi_k(x) \text{ with } c_k = \int_{\mathbb{R}^m} f(x)\psi_k(x)\mathrm{d}x.$$

Alternative definition

$$\mathcal{H} = \left\{ f = \sum_{k\geq 1} c_k \psi_k \;\middle|\; \sum_{k\geq 1} \frac{c_k^2}{\lambda_k} < +\infty \right\}$$

Functions of finite energy

$$L^2 = \left\{ f = \sum_{k\geq 1} c_k \psi_k \;\middle|\; \sum_{k\geq 1} c_k^2 < +\infty \right\}$$

Gabriel's Graph

Taking into account the angular information

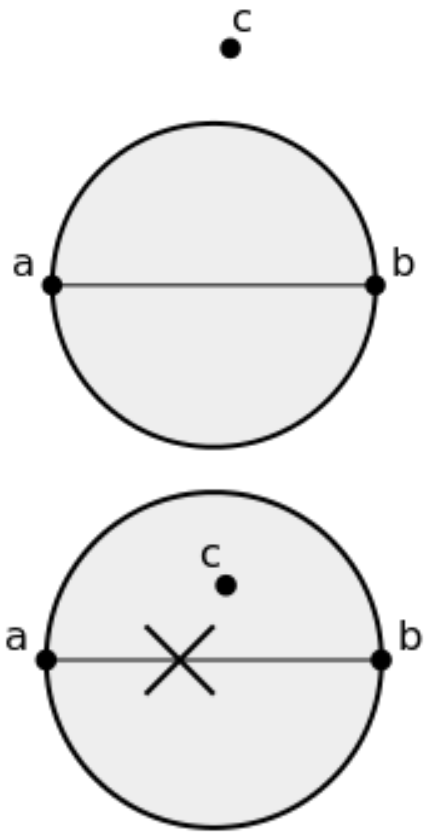

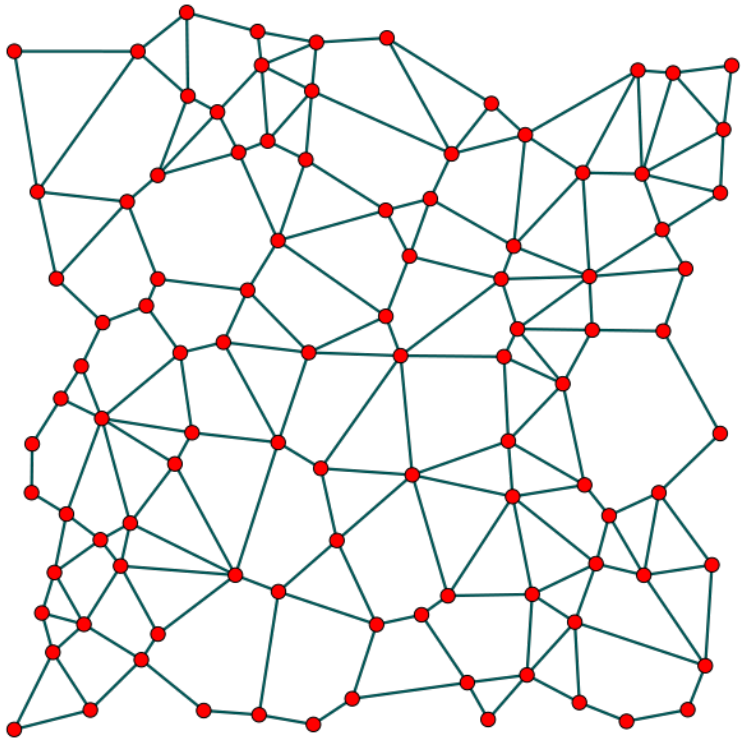

(Source: Wikipedia)

Embedding parallel LIBSVM in Julia for SVR analysis

Vesselin Grantcharov
and LANL T-1 Group

Outline

- Support Vector Machines (SVM) and Support Vector Regression (SVR) models
- LIBSVM
- JULIA language
- LIBSVM JULIA embedding in MADS.Julia

Support Vector Machine (SVM) models

SVM: Linear Separators

Binary classification is a task to separate classes in the feature space:

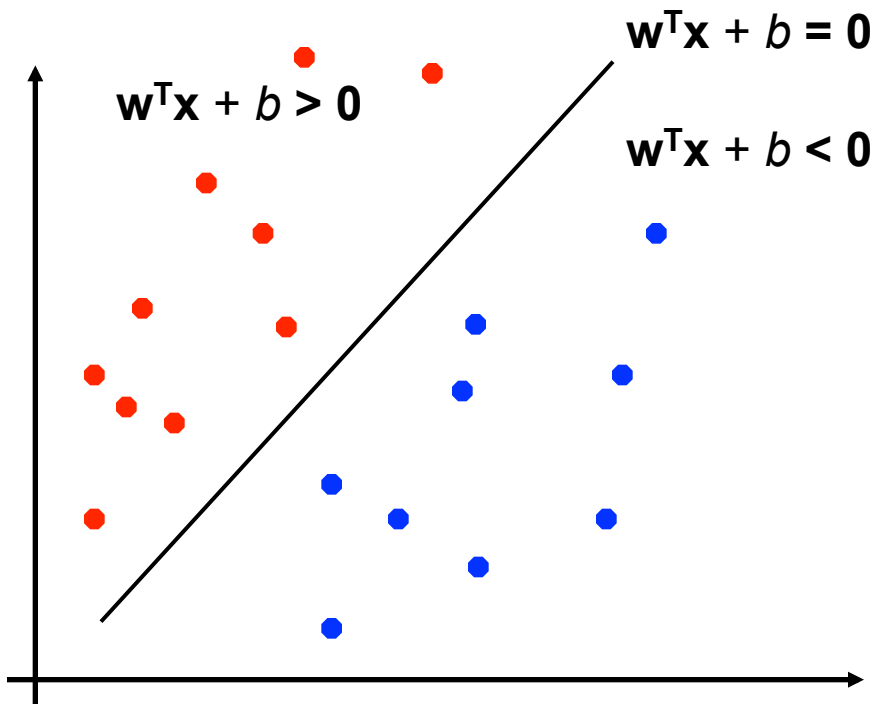

$$f(\mathbf{x}) = \text{sign}(\mathbf{w}^T\mathbf{x} + b)$$

Classification Margin

- Distance from $\mathbf{x}_i$ to the separator is $r = \dfrac{\mathbf{w}^T \mathbf{x}_i + b}{\|\mathbf{w}\|}$
- Examples closest to the optimal hyperplane are ***support vectors***.
- ***Margin*** ρ of the separator is the distance between support vectors.

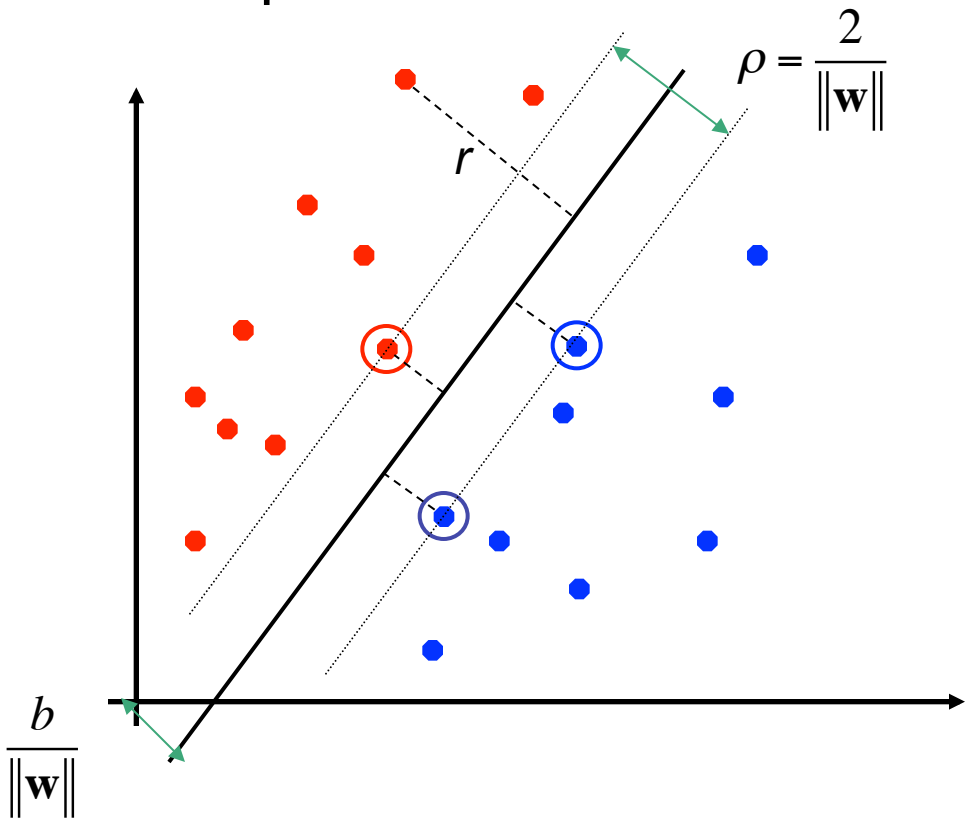

Linear SVM: Mathematically

A *quadratic optimization problem:*

Find **w** and *b* such that

$$\rho = \frac{2}{\|\mathbf{w}\|}$$ is maximized

and for all $(\mathbf{x}_i, y_i)$, i=1..n : $y_i(\mathbf{w}^T\mathbf{x}_i + b) \geq 1$

Which can be reformulated as:

Find **w** and *b* such that

$\Phi(\mathbf{w}) = \|\mathbf{w}\|^2 = \mathbf{w}^T\mathbf{w}$ is minimized

and for all $(\mathbf{x}_i, y_i)$, i=1..n : $y_i (\mathbf{w}^T\mathbf{x}_i + b) \geq 1$

Non-linear SVMs: Feature spaces

- General idea: the original feature space can always be mapped to some higher-dimensional feature space where the training set is separable:

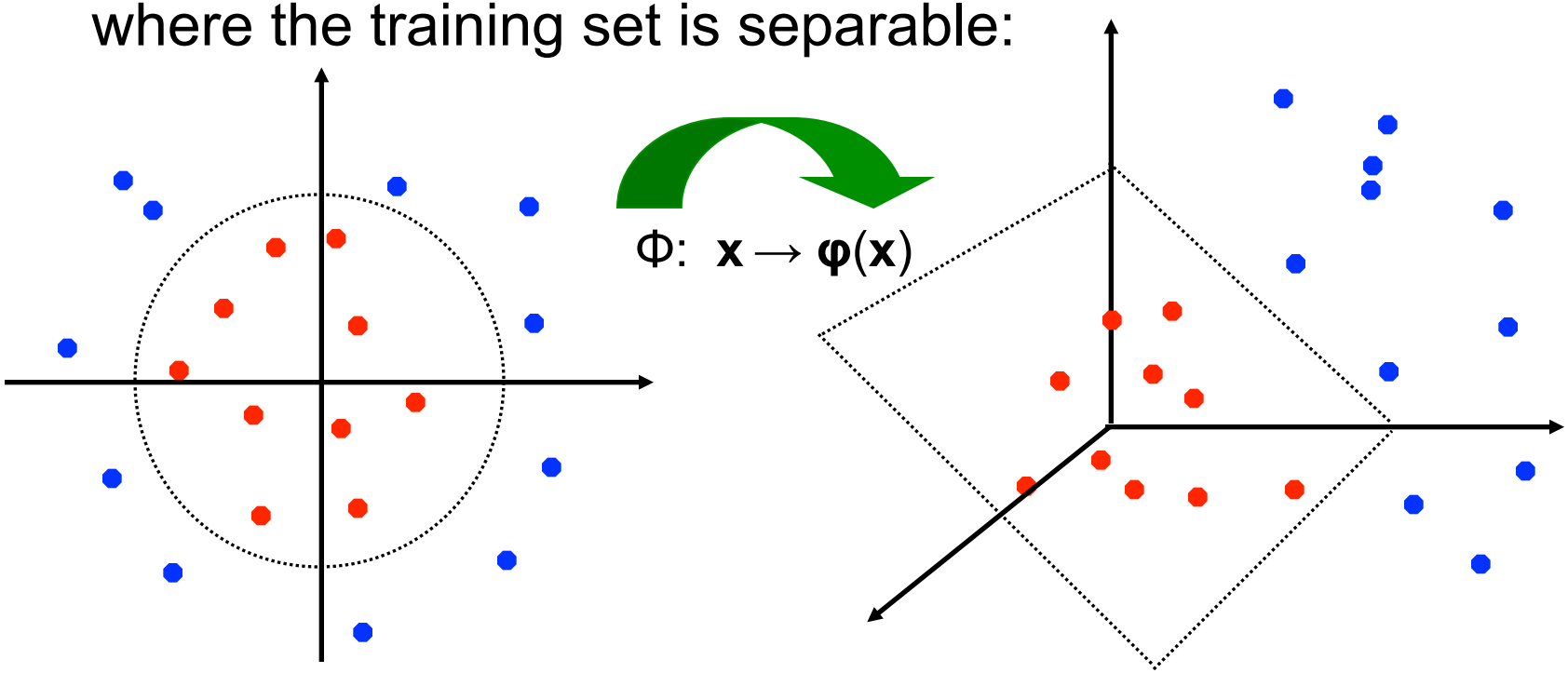

The Kernel Trick

- Mapping between two spaces $\varphi: X \rightarrow Z$
- Every dot product is a kernel
- It allows the algorithm to find the max-margin hyperplane in a transformed feature space

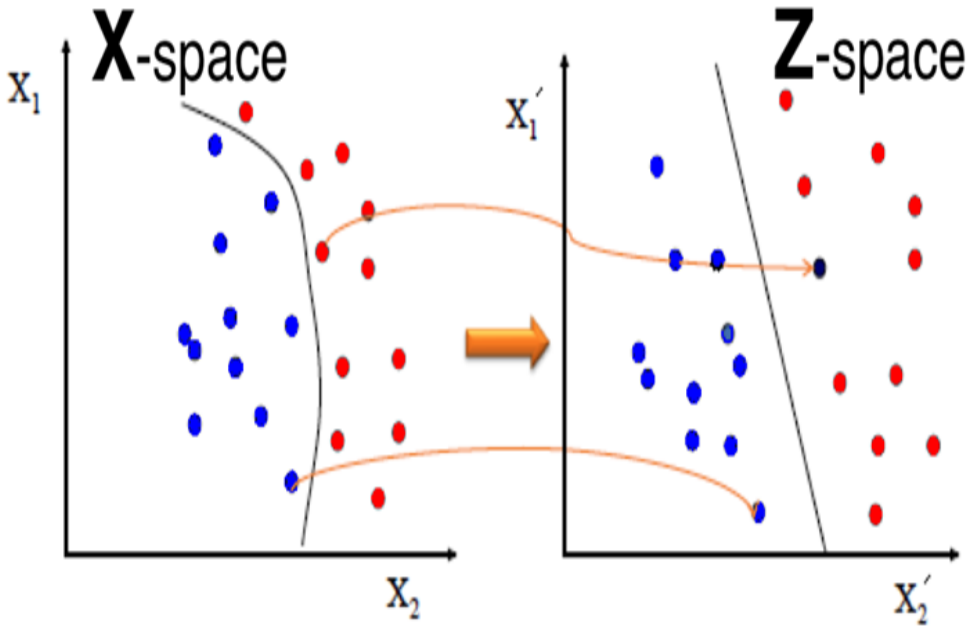

Linear SVM $x_i \cdot x_j$

Non-linear SVM $\phi(x_i) \cdot \phi(x_j)$

Kernel function $k(x_i \cdot x_j)$

Kernel functions	Type of classifier
$K(\mathbf{x}, \mathbf{x}_i) = (\mathbf{x}^T \mathbf{x}_i)$	Linear, dot product, kernel, CPD
$K(\mathbf{x}, \mathbf{x}_i) = [(\mathbf{x}^T \mathbf{x}_i) + 1]^d$	Complete polynomial of degree d, PD
$K(\mathbf{x}, \mathbf{x}_i) = e^{-\frac{1}{2}[(\mathbf{x}-\mathbf{x}_i)^T \Sigma^{-1} (\mathbf{x}-\mathbf{x}_i)]}$	Gaussian RBF, PD
$K(\mathbf{x}, \mathbf{x}_i) = \tanh[(\mathbf{x}^T \mathbf{x}_i) + b]^*$	Multilayer perceptron, CPD
$K(\mathbf{x}, \mathbf{x}_i) = \frac{1}{\sqrt{\|\mathbf{x}-\mathbf{x}_i\|^2 + \beta}}$	Inverse multiquadric function, PD

*only for certain values of b, (C)PD = (conditionally) positive definite

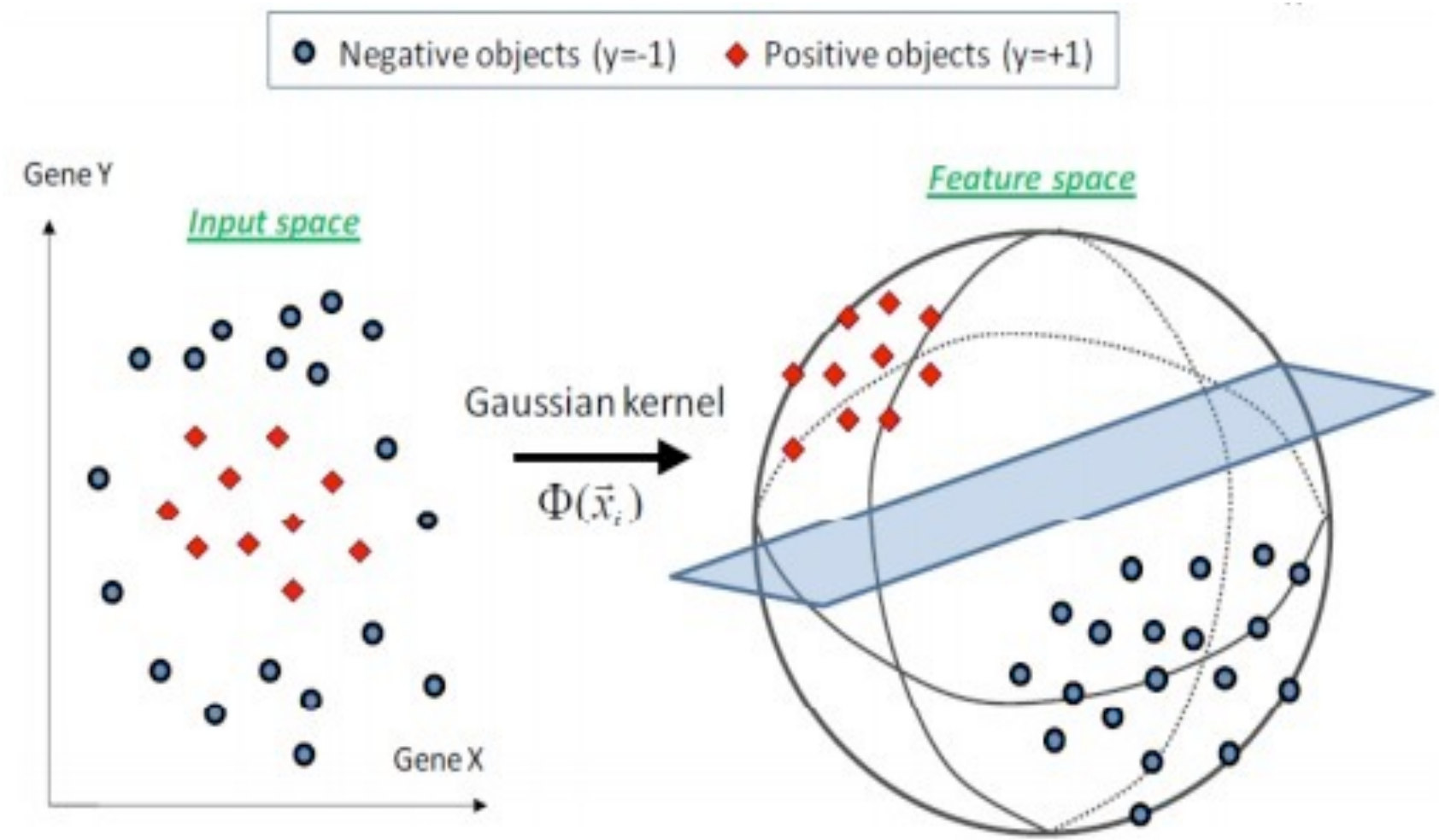
Negative objects (y=-1)
Positive objects (y=+1)
Gene Y
Input space
Gene X
Gaussian kernel
$\Phi(\vec{x}_i)$
Feature space

Support Vector Regression (SVR) models

Linear Support Vector Regression (SVR)

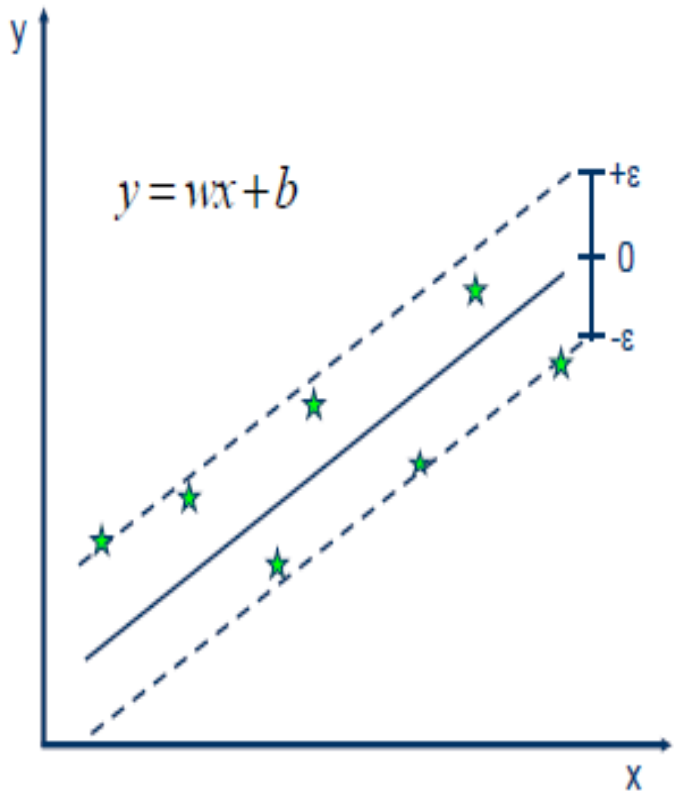

- Solution:

$$\min \frac{1}{2}\|w\|^2$$

- Constraints:

$$y_i - wx_i - b \leq$$

$$wx_i + b - y_i \leq$$

- Data M=$\{(x_1, y_1), (x_2, y_2), \ldots, (x_l, y_l), \}$,
- x_i – vectors X $\in R^n$, $y_i \in R, 1 \leq i \leq l$
- Find a function $f(x)$, that has at most ε deviations from the obtained targets y_i for all data points and it is as flat as possible (meaning that$\|w\|$ is minimun)
- We will not accept errors more than ε
- No errors inside of the ε-tube
- Equation of hyperplane: $f(x) =< \mathrm{w}, \mathrm{x} > +\mathrm{b}, \mathrm{w} \in R^n$, $\mathrm{b} \in R$
- Solving a convex quadratic optimization problem

ε–SVR: Hyperparameters

The solution to SVR we just saw is referred to as ε–SVR

Two Hyperparameters

$$\text{minimize } \frac{1}{2}\|w\|^2 + \frac{C}{M}\sum_{i=1}^{M}\left(\xi_i + \xi_i^*\right)$$

$$\text{subject to } \begin{cases} \langle w, x^i \rangle + b - y^i \le \varepsilon + \xi_i \\ y^i - \langle w, x^i \rangle - b \le \varepsilon + \xi_i^* \\ \xi_i \ge 0, \quad \xi_i^* \ge 0 \end{cases}$$

C controls the penalty term on poor fit
ε determines the minimal required precision

SVR: Mathematically

Given a training set $\mathcal{D} = \{(\mathbf{x}_1, y_1), \cdots, (\mathbf{x}_D, y_D)\}$ the linear SVR finds an optimal linear function by solving the following constrained convex optimization problem

$$\text{P0(SVR)}: \min_{\eta,\xi,\xi^\star} \frac{1}{2}\|\eta\|_2^2 + C\sum_{d=1}^{D}(\xi_d + \xi_d^\star)$$

$$\text{s.t. } \forall d: \begin{cases} y_d - \eta^\top \mathbf{f}(\mathbf{x}_d) \leq \epsilon + \xi_d \\ -y_d + \eta^\top \mathbf{f}(\mathbf{x}_d) \leq \epsilon + \xi_d^\star \\ \xi_d, \xi_d^\star \geq 0 \end{cases},$$

where $\mathbf{f} = \{f_1, \cdots, f_I\}$ is a vector of feature functions

η is the corresponding weight vector

$\|\eta\|_2^2 = \eta^\top \eta$ is the ℓ_2-norm; ξ_d and $\xi_d^\star$ are slack variables and ϵ is the precision parameter

The Kernel Trick

- Mapping between two spaces $\varphi: X \rightarrow Z$
- Every dot product is a kernel
- It allows the algorithm to find the max-margin hyperplane in a transformed feature space

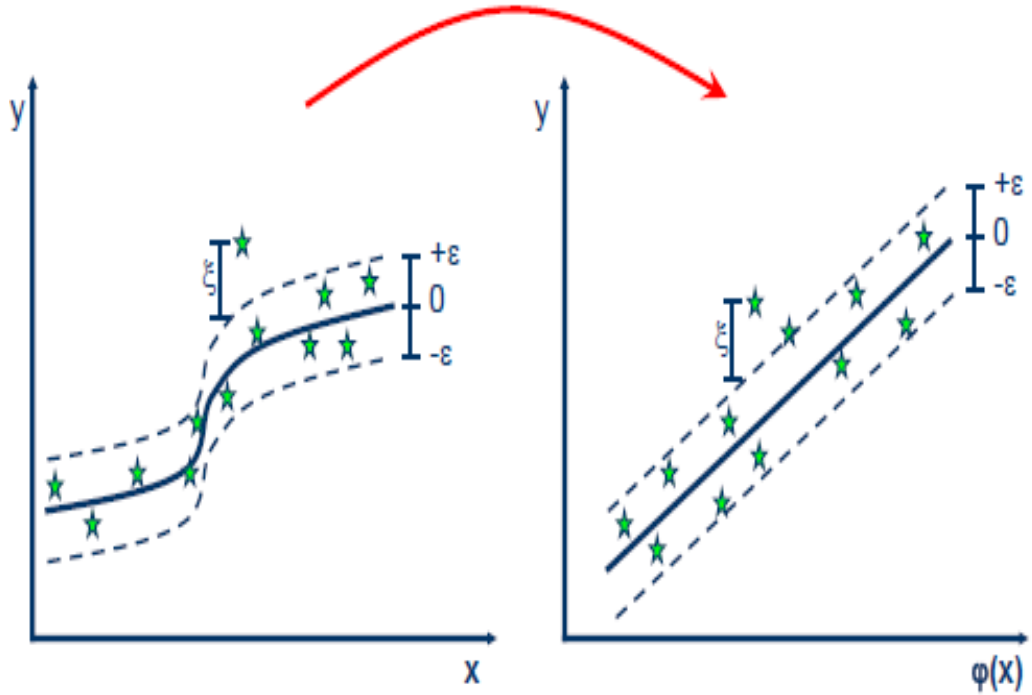

Linear SVM $x_i \cdot x_j$

Non-linear SVM $\phi(x_i) \cdot \phi(x_j)$

Kernel function $k(x_i \cdot x_j)$

Kernel functions	Type of classifier
$K(\mathbf{x}, \mathbf{x}_i) = (\mathbf{x}^T \mathbf{x}_i)$	Linear, dot product, kernel, CPD
$K(\mathbf{x}, \mathbf{x}_i) = [(\mathbf{x}^T \mathbf{x}_i) + 1]^d$	Complete polynomial of degree d, PD
$K(\mathbf{x}, \mathbf{x}_i) = e^{-\frac{1}{2}[(\mathbf{x}-\mathbf{x}_i)^T \Sigma^{-1} (\mathbf{x}-\mathbf{x}_i)]}$	Gaussian RBF, PD
$K(\mathbf{x}, \mathbf{x}_i) = \tanh[(\mathbf{x}^T \mathbf{x}_i) + b]^*$	Multilayer perceptron, CPD
$K(\mathbf{x}, \mathbf{x}_i) = \frac{1}{\sqrt{\|\mathbf{x}-\mathbf{x}_i\|^2 + \beta}}$	Inverse multiquadric function, PD

*only for certain values of b, (C)PD = (conditionally) positive definite

LIBSVM, JULIA and MADS

LIBSVM – The best Library for Support Vector Machines

Chih-Chung Chang and Chih-Jen Lin

LIBSVM is an integrated parallel software for support vector classification, (C-SVC, nu-SVC), regression (epsilon-SVR, nu-SVR) and distribution estimation (one-class SVM). It supports also multi-class classification.

Main features of LIBSVM include

- Different SVM\SVR formulations
- Efficient multi-class classification
- Cross validation for model selection
- Probability estimates
- Various kernels (including precomputed kernel matrix)
- Weighted SVM for unbalanced data
- Both C++ and Java sources
- Python, R, MATLAB, Perl, Ruby, Weka, Common LISP, CLISP, Haskell, implementations

“Because We Are Greedy.”

“We want a language that’s **open source**, with a liberal license.
We want the **speed** of C
with the **dynamism** of Ruby.
We want a language that’s **homoiconic**,
with true **macros** like Lisp,
but with obvious, familiar **mathematical notation** like Matlab.
We want something as usable for **general programming** as Python,
as easy for **statistics** as R,
as natural for **string processing** as Perl,
as powerful for **linear algebra** as Matlab,
as good at **gluing programs together** as the shell.
Something that is **dirt simple** to learn,
yet keeps the most **serious hackers** happy.”

Computational Framework MADS

http://madsjulia.lanl.gov

- **MADS** (Model Analysis & Decision Support) is an **open-source high-performance parallel** computational framework for **model analyses**, developed in Computational Earth Science Group at LANL, and supported by DOE Office of Science (LA-CC-11-035).
- **MADS** includes advanced adaptive computational techniques:
  - **Sensitivity analysis** (local / global);
  - Uncertainty quantification (local / global);
  - Optimization / calibration / parameter estimation (local / global);
  - Model ranking & selection
  - Decision support (Bayesian, GLUE, Info-gap, BIG-DT)
- **MADS** allows **external coupling** with any existing physics simulator

LIBSVM embedded in Mads.Julia

- Runs and controls parallel code
- Calls python that calls Julia (grid regression)
- Wrappers that allow for easy interactive mode rather than writing C code, compiling, running, debugging
- Integrate software from LIBSVM which is downloaded or modified separately from the standard library – grid search for regression, dense data version, etc.
- More flexible code to predict data in different formats than standard LIBSVM data format and read more than one file to make predictions, thus reducing constraints due to memory size

Thank you for your time

Arbitrary Order Mixed Mimetic Finite Difference Method with Nodal Degrees of Freedom

Oleksandr Iaroshenko

Penn State University

Mentor: Vitaliy Gyrya (LANL)

Co-mentor: Gianmarco Manzini (LANL)

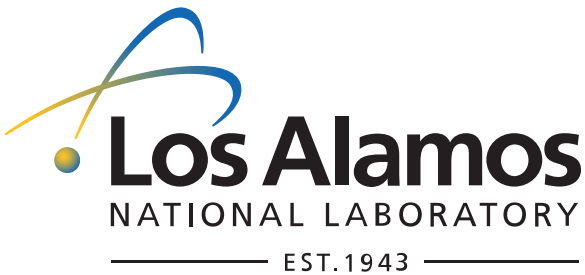

August 16, 2016

Outline

Diffusion equation

Stationary diffusion equation

$$-\operatorname{div}(K\nabla p) = f$$

Examples: conductivity (electrical, thermal), chemical diffusion, etc.

Mixed formulation with boundary conditions

$$\begin{aligned} \mathbf{u} &= -K\nabla p && \text{in } \Omega, \\ \operatorname{div}\mathbf{u} &= f && \text{in } \Omega, \\ p &= g && \text{on } \partial\Omega. \end{aligned}$$

p – potential (unknown scalar)

$\mathbf{u}$ – flux (unknown vector)

$\Omega \subset \mathbb{R}^2$

K – diffusion tensor (symmetric positive definite matrix)

Weak Formulation and Discretization

Weak formulation

Find $(\mathbf{u}, p) \in H(\mathrm{div}\,, \Omega) \times L^2(\Omega)$ such that

$$\begin{aligned} \langle K^{-1}\mathbf{u}, \mathbf{v}\rangle_\Omega - \langle p, \mathrm{div}\,\mathbf{u}\rangle_\Omega &= -\langle g, \mathbf{v}\cdot\nu\rangle_{\partial\Omega} && \forall \mathbf{v} \in H(\mathrm{div}\,, \Omega), \\ \langle \mathrm{div}\,\mathbf{u}, q\rangle_\Omega &= \langle f, q\rangle_\Omega && \forall q \in L^2(\Omega). \end{aligned}$$

Mimetic Finite Difference method: discretization scheme that mimics important calculus properties (Divergence Theorem, Green's formula, etc.).

Discrete mixed formulation

$$\begin{aligned} [\mathbf{u}_h, \mathbf{v}_h]_{X_h} - [p_h, \mathcal{DIV}\mathbf{v}_h]_{Q_h} &= -\langle g_h, \mathbf{v}_h\cdot\nu\rangle_h && \forall \mathbf{v}_h \in X_h, \\ [\mathcal{DIV}\mathbf{u}_h, q_h]_{Q_h} &= [f_h, q_h]_{Q_h} && \forall q_h \in Q_h. \end{aligned}$$

h – size of the mesh Ω_h

X_h – discrete space for fluxes $\mathbf{u}_h$

Q_h – discrete space for potentials p_h

Meshes

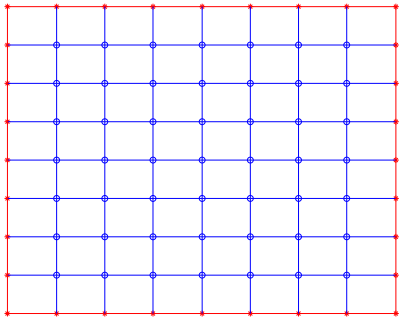
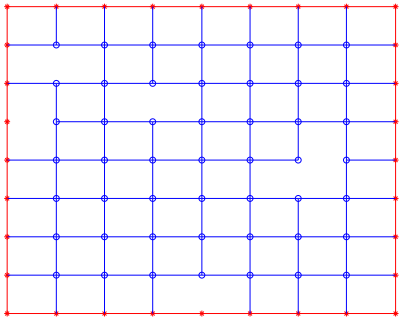
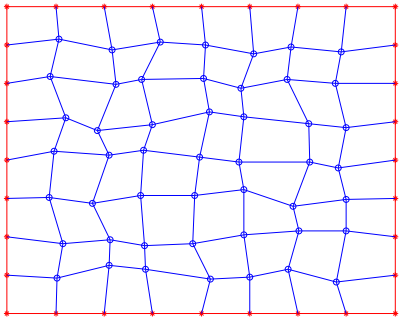
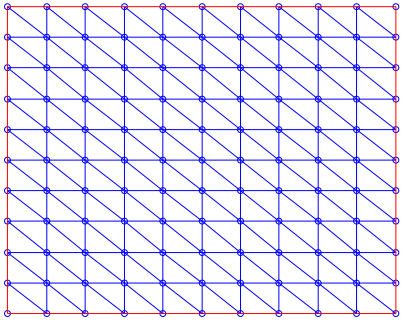
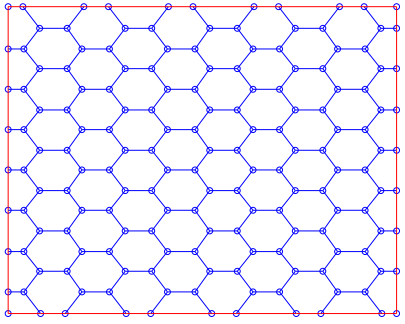
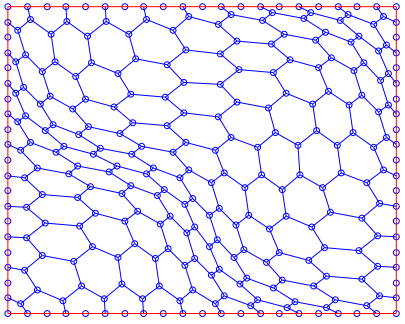
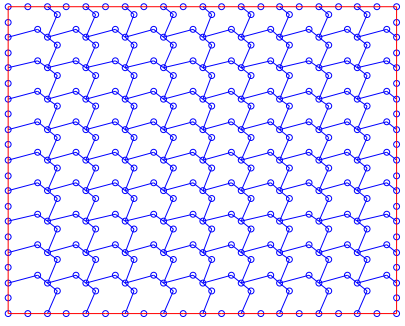

Implementation of MFD Scheme

Discrete mixed formulation

$$[\mathbf{u}_h, \mathbf{v}_h]_{X_h} - [p_h, \mathcal{DIV}\mathbf{v}_h]_{Q_h} = -\langle g_h, \mathbf{v}_h \cdot \nu \rangle_h \qquad \forall \mathbf{v}_h \in X_h,$$

$$[\mathcal{DIV}\mathbf{u}_h, q_h]_{Q_h} = [f_h, q_h]_{Q_h} \qquad \forall q_h \in Q_h.$$

Implementation

All matrices are constructed additively from their local analogs for each element $E \in \Omega_h$.

- Construct the matrix $\mathcal{M}_{X_E}$ that corresponds to the bilinear form that defines the mimetic inner product on X_E:

$$\langle \mathcal{M}_{X_E}\mathbf{u}_h, \mathbf{v}_h \rangle = [\mathbf{u}_h, \mathbf{v}_h]_{X_E} \approx \int_E \langle K^{-1}\mathbf{u}, \mathbf{v} \rangle dx$$

- Construct the matrix $\mathcal{M}_{Q_E}$ that corresponds to the bilinear form that defines the mimetic inner product on Q_E:

$$\langle \mathcal{M}_{Q_E} p_h, q_h \rangle = [p_h, q_h]_{Q_E} \approx \int_E pq \, dx$$

- Construct the discrete divergence operator $\mathcal{DIV}_E$ using commutation property:

$$\mathcal{DIV}_E \mathbf{v}^I = (\operatorname{div} \mathbf{v})^I \text{ on } E \in \Omega_h$$

Degrees of Freedom (original)

Local interpolation – discretization $\mathbf{u}^I$ and p^I for one element $E \in \Omega_h$.

$\mathcal{P}_k(E)$ – the space of all polynomials on E with degree less or equal to k.

DoF of potential p

- the polynomial coefficients of the approximation of p in the space $\mathcal{P}_{k-1}(E)$

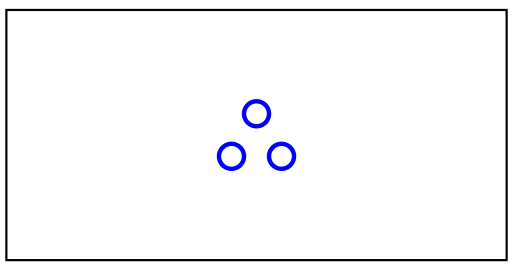

Figure: Degrees of freedom for potential on a quadrilateral element ($k = 2$)

Degrees of Freedom (original)

DoF of flux **u**

- the moments of $\mathbf{u}$ with respect to $\nabla\phi_{E,i}$, basis of $\mathcal{P}_{k-1}(E)$:

$$u^I_{E,i} := \frac{1}{|E|}\int_E \langle \mathbf{u}, \nabla\phi_{E,i}\rangle dx \quad \text{for } i = 1,\ldots,n_{k-1}$$

- the moments of $\langle \mathbf{u}, \nu_{E,e}\rangle$ with respect to $\phi_{e,i}$, basis of $\mathcal{P}_k(e)$:

$$u^I_{e,i} := \frac{1}{|e|}\int_e \langle \mathbf{u}, \nu_{E,e}\rangle\phi_{e,i}(s)ds \quad \text{for } i = 0,\ldots,k \quad \forall e \in \mathcal{E}_E$$

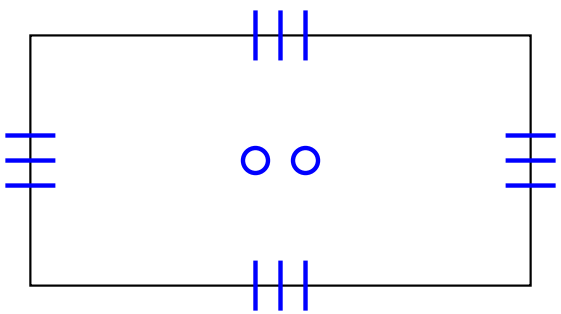

Figure: Degrees of freedom for flux on a quadrilateral element ($k = 2$)

Moving Edge DoF to Vertices

Locally: one-to-one correspondence for elements with no hanging nodes

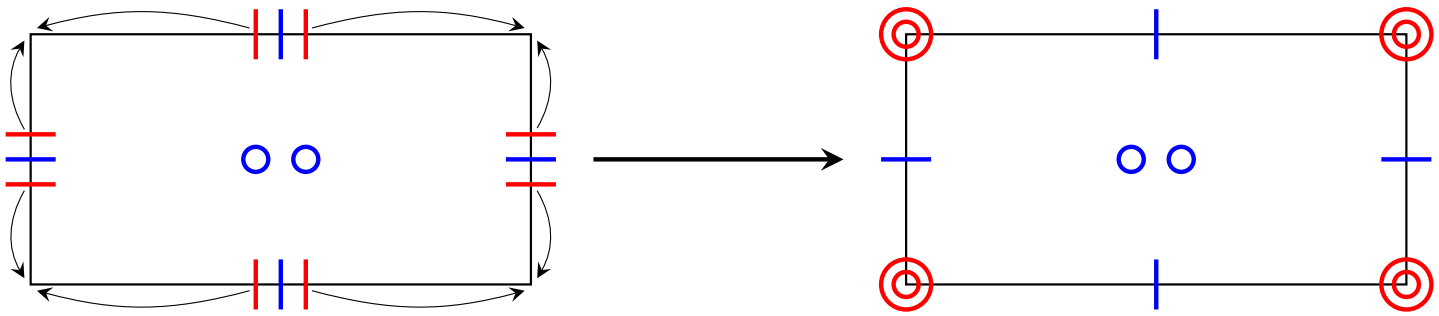

Figure: Old and new degrees of freedom (locally)

Globally: the number of degrees of freedom is reduced

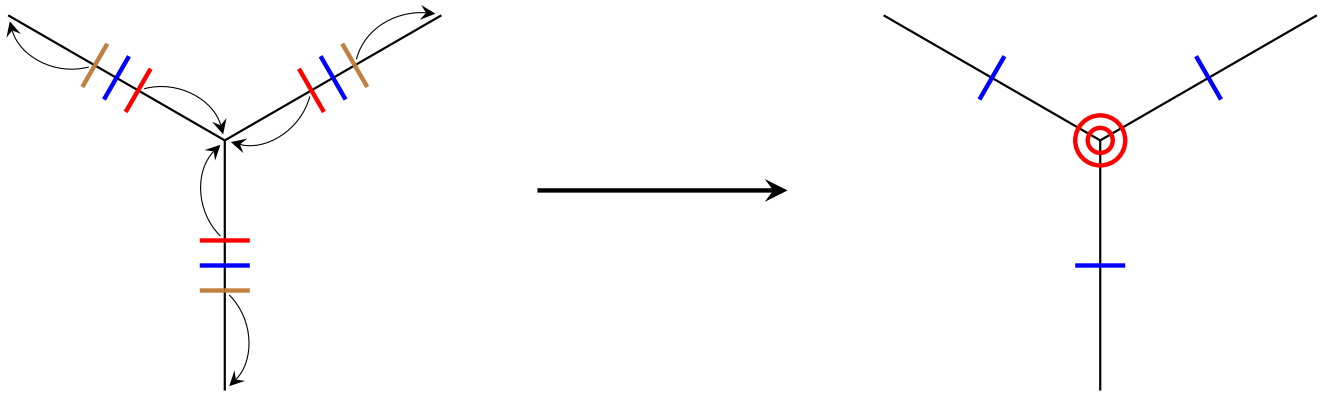

Figure: Old and new degrees of freedom (globally)

DoF on Perturbed Square Mesh

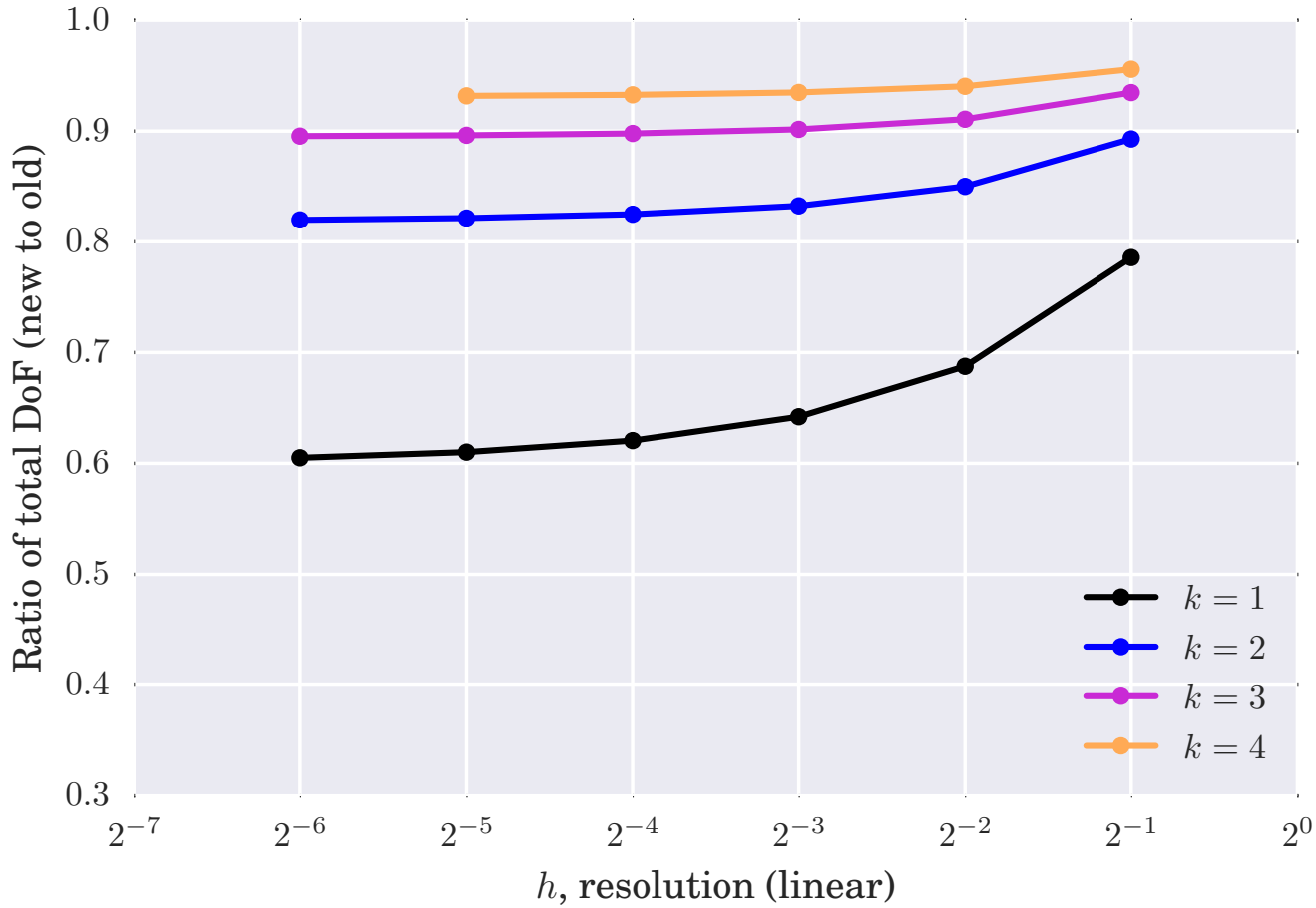

FIGURE: Ratio of number of new DoF to number of old DoF

Properties

Locally: same number of DoF, nothing changes for the elements with no hanging nodes (vertices with parallel adjacent edges).

Pros (globally):

- Fewer degrees of freedom:

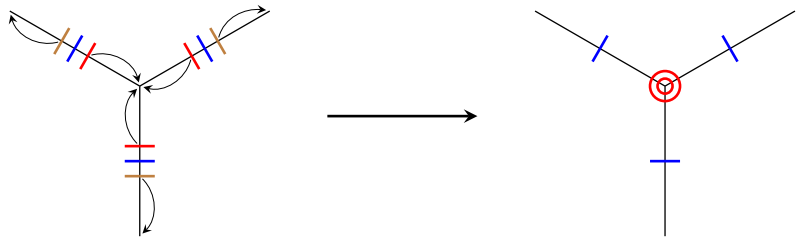

- Additional continuity of the flux:

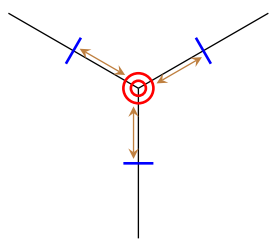

Cons: Discontinuous diffusion coefficient requires special consideration.

Test Problem

The results below were calculated for the following problem:

- $\Omega = [0, 1]^2$
- $K = \begin{bmatrix} 2 + x^2 & 0 \\ 0 & 2 + y^2 \end{bmatrix}$
- $p(x, y) = \sin \pi x \cos \pi y$
- The perturbed square mesh is used.

Error Comparison

Old method	New method

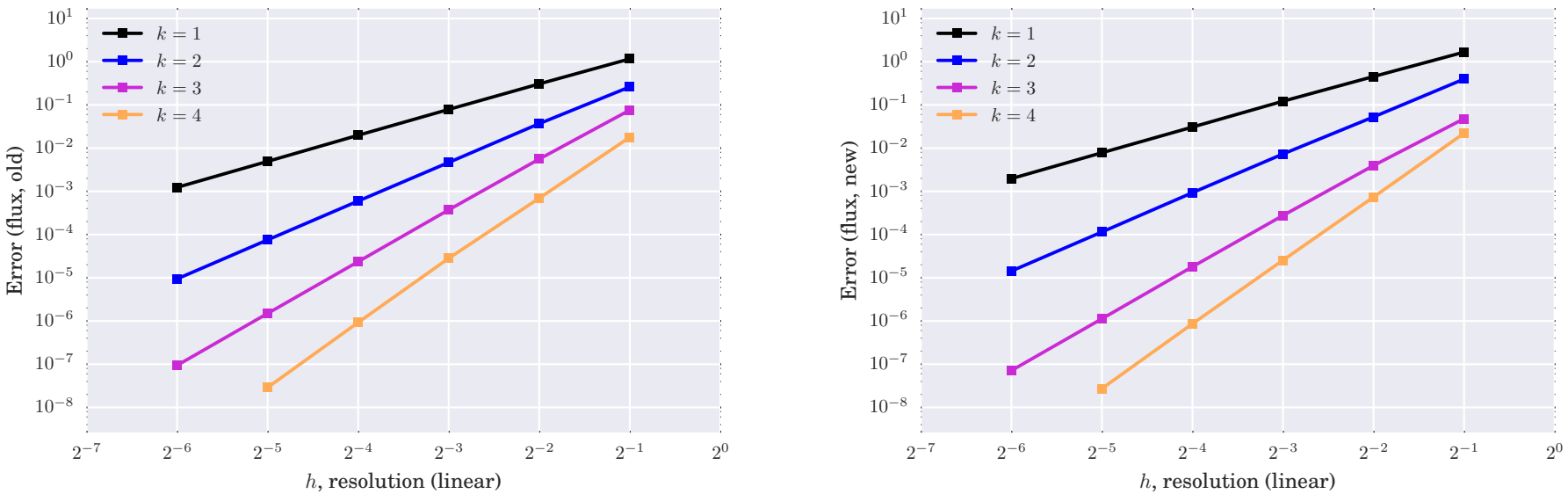

Figure: Error for flux

Error Comparison

Old method	New method

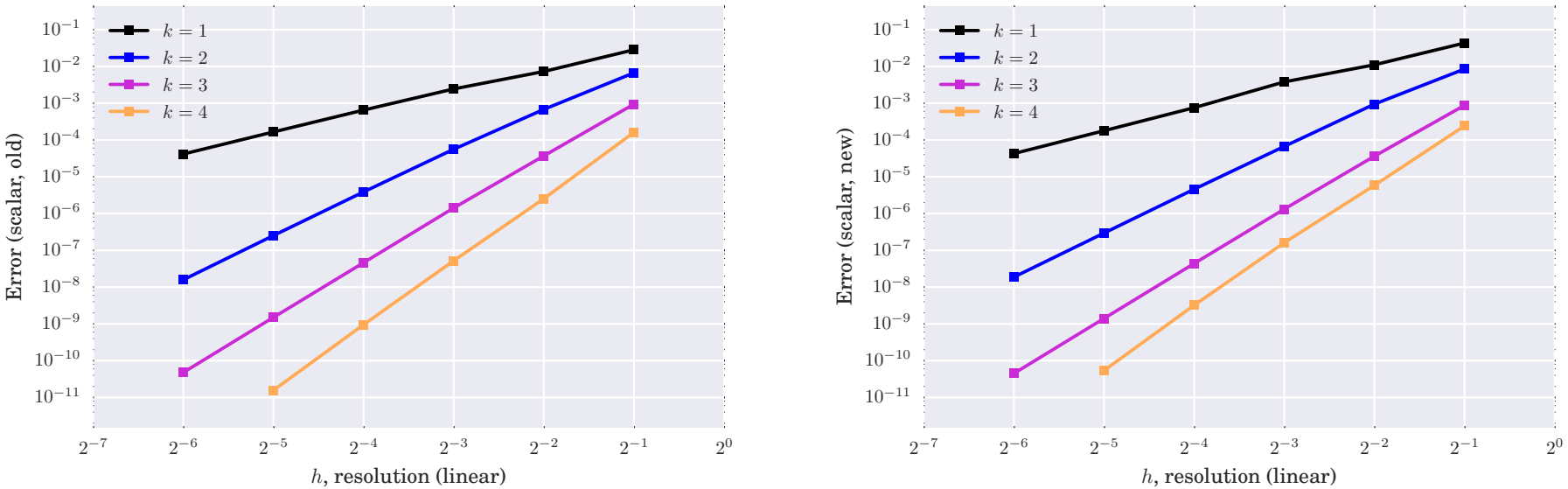

Figure: Error for potential

Rate of Convergence (New Method)

Flux	Potential

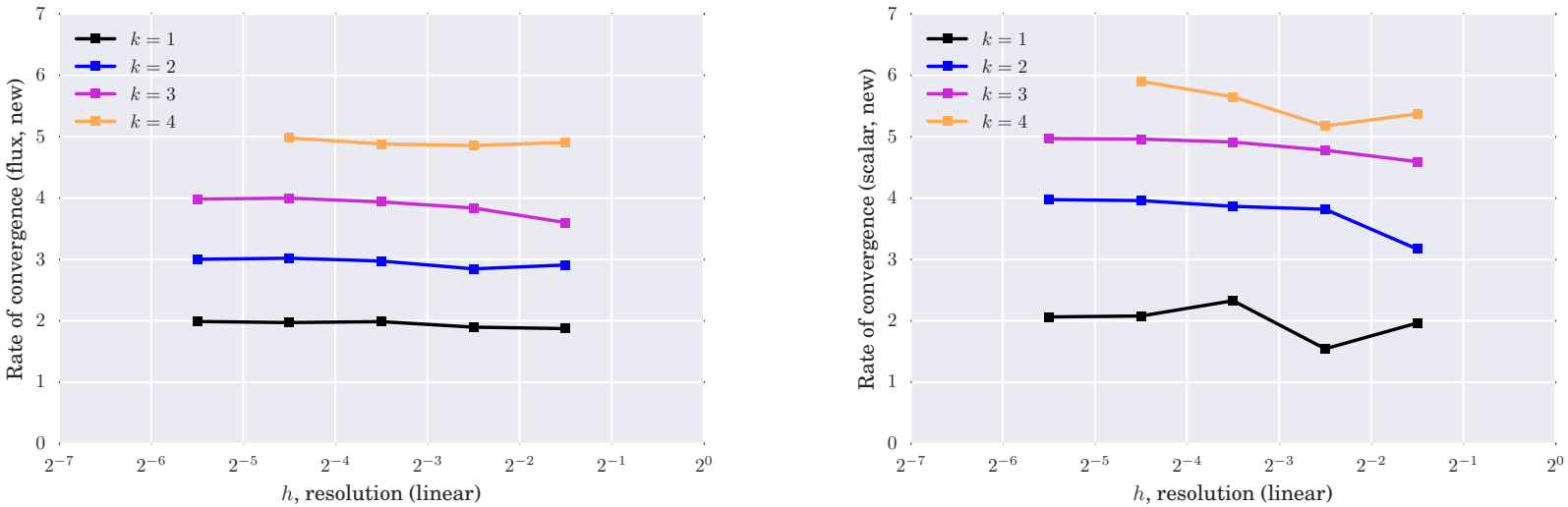

Figure: Rate of convergence

Numerical experiment shows the following rate of convergence:

- $k + 1$ for flux
- $k + 2$ for potential when $k \geq 2$
- $k + 1$ for potential when $k = 1$

Condition Number (New Method)

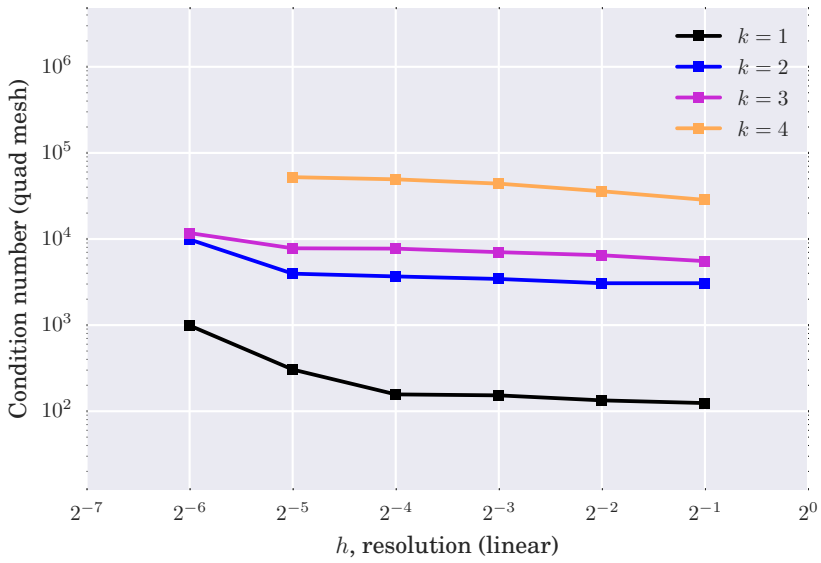

(A) Perturbed square mesh

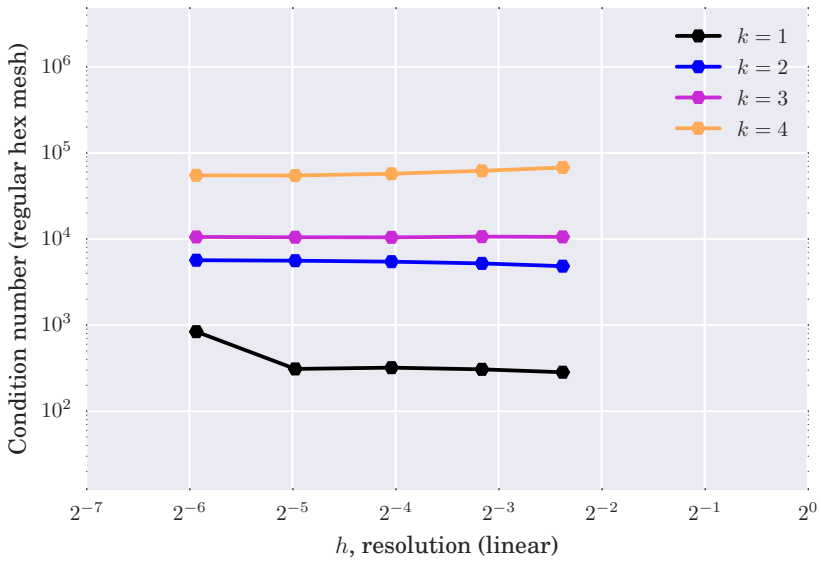

(B) Regular hexagonal mesh

Figure: Condition number of a global coefficient matrix for $[\mathbf{u}, p]^T$ for (a) perturbed square and (b) regular hexagonal meshes

The condition number of a coefficient matrix for a fixed order k does not grow much in the new method.

Conclusion

Conclusion

- The new method gives the same convergence results as the original method.
- The performance is increased due to decrease of number of variables:
  - up to 40% in the low-order case;
  - up to $10 - 18\%$ in the high-order cases.
- The new method adds the additional continuity of the discrete approximation.

Future work

- Special consideration of discontinuous diffusion tensor (e.g., add additional degrees of freedom to the vertices where K is discontinuous).
- Find problems where additional continuity plays an essential role.

Thank you!

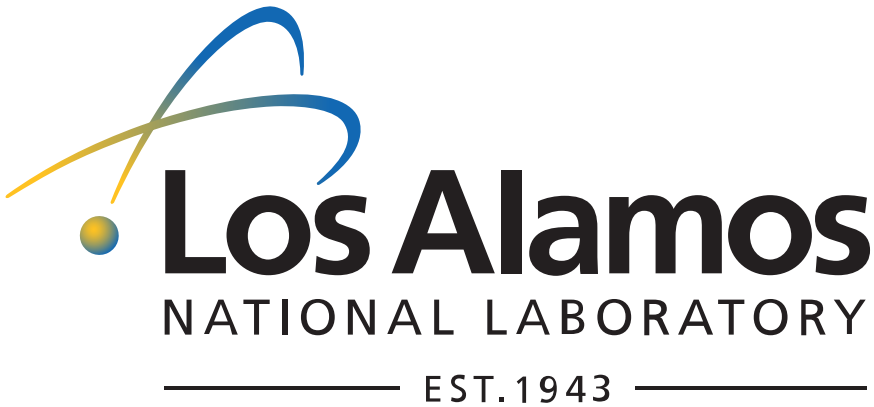

Acknoledgement: ASC Hydro

Discontinuous Case

Diffusion coefficient K can be discontinuous.

Analytical solution: flux is continuous through the edges where K jumps (normal component) but its tangential component may have jumps.

The edge DoFs possess this property automatically. The vertex DoFs force the approximation $\mathbf{u}_h$ to be continuous at each vertex (cannot have tangential jumps).

Optimization of interatomic potentials using machine learning

Aditi Krishnapriyan

Mentors: Marc Cawkwell, Ping Yang

August 23, 2016

Reactive quantum MD with LATTE

- Fast, parameterized electronic structure models (DFTB)
- Covalent bonding and charge transfer
- LANL-developed open-source code:
  - Extended Lagrangian Born-Oppenheimer MD
  - Fast, parallel O(*N*) and O(N^3) algorithms for the density matrix, **P**

Orbital overlap

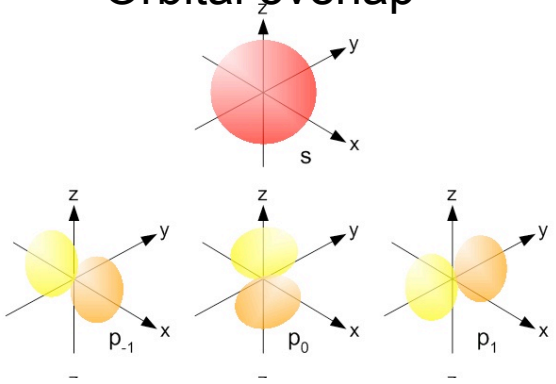

H: 1 × s
C, N, O: 1 × s + 3 × p

Potential energy: $U(\mathbf{R};\mathbf{P}) = 2\mathrm{Tr}\left[\mathbf{PH}\right] + \frac{1}{2}\sum\frac{q_i q_j}{R} + E_{\mathrm{pair}}$

Electronic energy | Electrostatics | Repulsion

Automatically tuning parameterizations

Bond integrals: $h_{ll'\tau}(R) = h_{ll'\tau}(R_0)\exp(A_1(R-R_0)+A_2(R-R_0)^2)$

Pair potentials: $\phi(R) = \phi_0 \prod_{i=1}^{4} \exp(B_i R^i)$

`bondints.nonortho`

Overlap matrix from wavefunction overlap

```
Noints= 7
Element1 Element2  Kind      H0    B1       B2        B3          B4          B5  R1     Rcut H0    B1       B2        B3          B4          B5  R1     Rcut
H C sss  -8.569940 -1.463764 -0.280323 0.000000 0.000000 1.100000 3.000000 3.500000 0.393139 -1.559300 -0.659087 0.074430 -0.017004 1.100000 3.000000 3.500000
H C sps  7.892364 -1.079786 -0.288107 0.000000 0.000000 1.100000 3.000000 3.500000 -0.469300 -1.018870 -0.997495 0.301138 -0.081795 1.100000 3.000000 3.500000
C C sss  -7.893027 -1.531314 -0.482302 0.000000 0.000000 1.500000 3.000000 3.500000 0.275515 -1.688130 -0.523751 0.041905 -0.010372 1.500000 3.000000 3.500000
C C sps  8.004860 -1.184291 -0.525113 0.000000 0.000000 1.500000 3.000000 3.500000 -0.332137 -1.243440 -0.739495 0.176080 -0.049828 1.500000 3.000000 3.500000
C C pps  5.659036 -0.800774 -0.503255 0.000000 0.000000 1.500000 3.000000 3.500000 -0.331087 -0.460593 -1.562450 0.924350 -0.298106 1.500000 3.000000 3.500000
C C ppp  -2.611850 -2.008940 -0.163584 0.000000 0.000000 1.500000 3.000000 3.500000 0.155671 -2.073180 -0.432304 0.024030 -0.011508 1.500000 3.000000 3.500000
H H sss  -8.827050 -1.119400 -0.440439 0.000000 0.000000 0.740000 3.000000 3.500000 0.563921 -1.450000 -0.756144 0.000000 0.000000 0.740000 3.000000 3.500000
```

H S

`ppots.nonortho`

```
Nopps= 3
Ele1  Ele2  A0         A1        A2        A3        A4        A5        A6        C     R1  Rcut
C H 622.109477 -7.494398 4.304384 -3.176901 0.000000 0.000000 0.000000 0.000000 1.500000 1.700000
C C 4.719818 20.460516 -40.187100 28.078400 -7.506860 0.000000 0.000000 0.000000 1.800000 2.000000
H H 25.489000 7.692560 -52.078700 79.678800 -48.738600 0.000000 0.000000 0.000000 1.000000 1.200000
```

Reference data from DFT for optimization

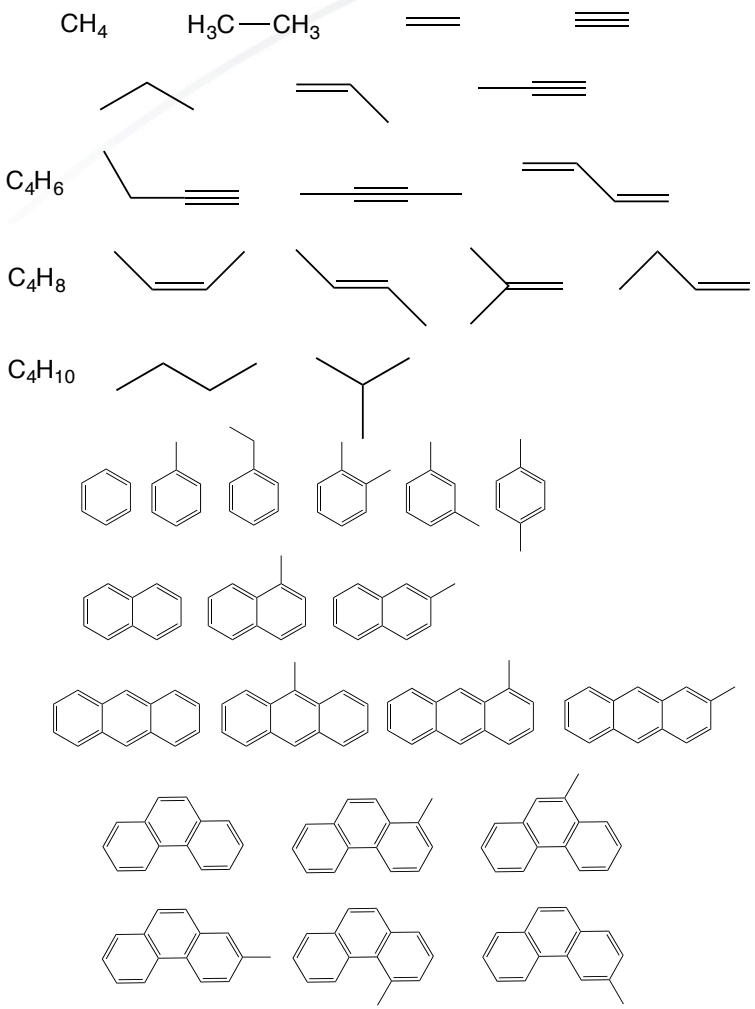

- 32 molecules
- 200 distortions per molecule
- Species + coordinates
- Atomization energy
- Forces
- Dipole moment

+…. e.g. stresses

Objective function measures error in parameterization

$$\chi_E^2 = \frac{1}{N_{mol}} \sum_{i=1}^{N_{mol}} \left(\frac{E_i^{Ref} - E_i^{TB}}{\sigma_E} \right)^2$$

$$\chi_F^2 = \frac{1}{N_{mol}} \sum_{i=1}^{N_{mol}} \left[\left(\frac{f_x^{Ref} - f_x^{TB}}{\sigma_x} \right)_i^2 + \left(\frac{f_y^{Ref} - f_y^{TB}}{\sigma_y} \right)_i^2 + \left(\frac{f_z^{Ref} - f_z^{TB}}{\sigma_z} \right)_i^2 \right]$$

$$\chi_D^2 = \frac{1}{N_{mol}} \sum_{i=1}^{N_{mol}} \left(\frac{D_i^{Ref} - D_i^{TB}}{\sigma_D} \right)^2$$

$$\chi^2 = \chi_E^2 + \chi_F^2 + \chi_D^2 + \ldots$$

- Stress, ionization potentials, HOMO-LUMO gap, polarizibility…
- Normalized per molecule by standard deviation: dimensionless

EPO ("Empirical Potential Optimizer"): Python + MPI (mpi4py)

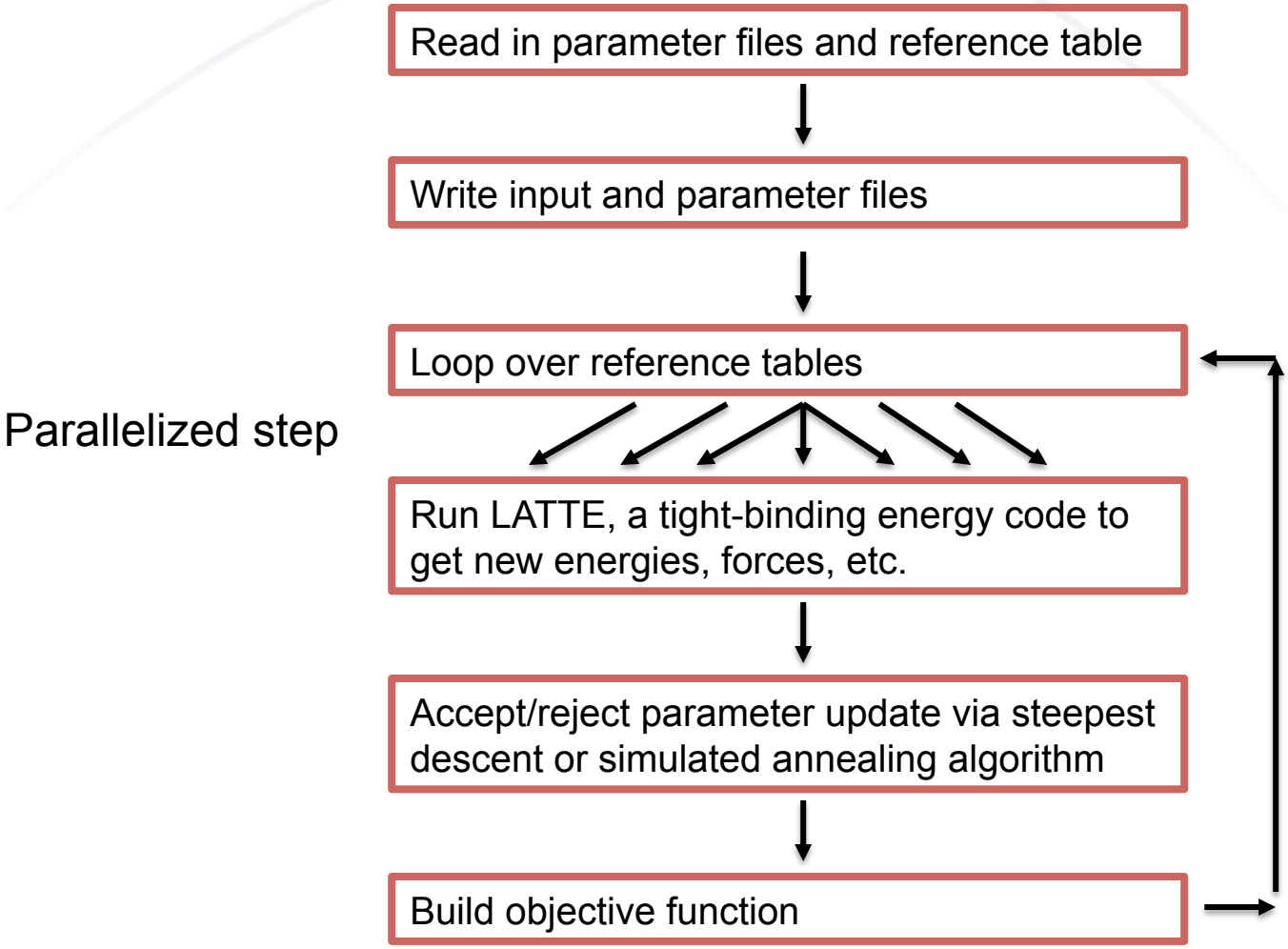

Parallel Scaling

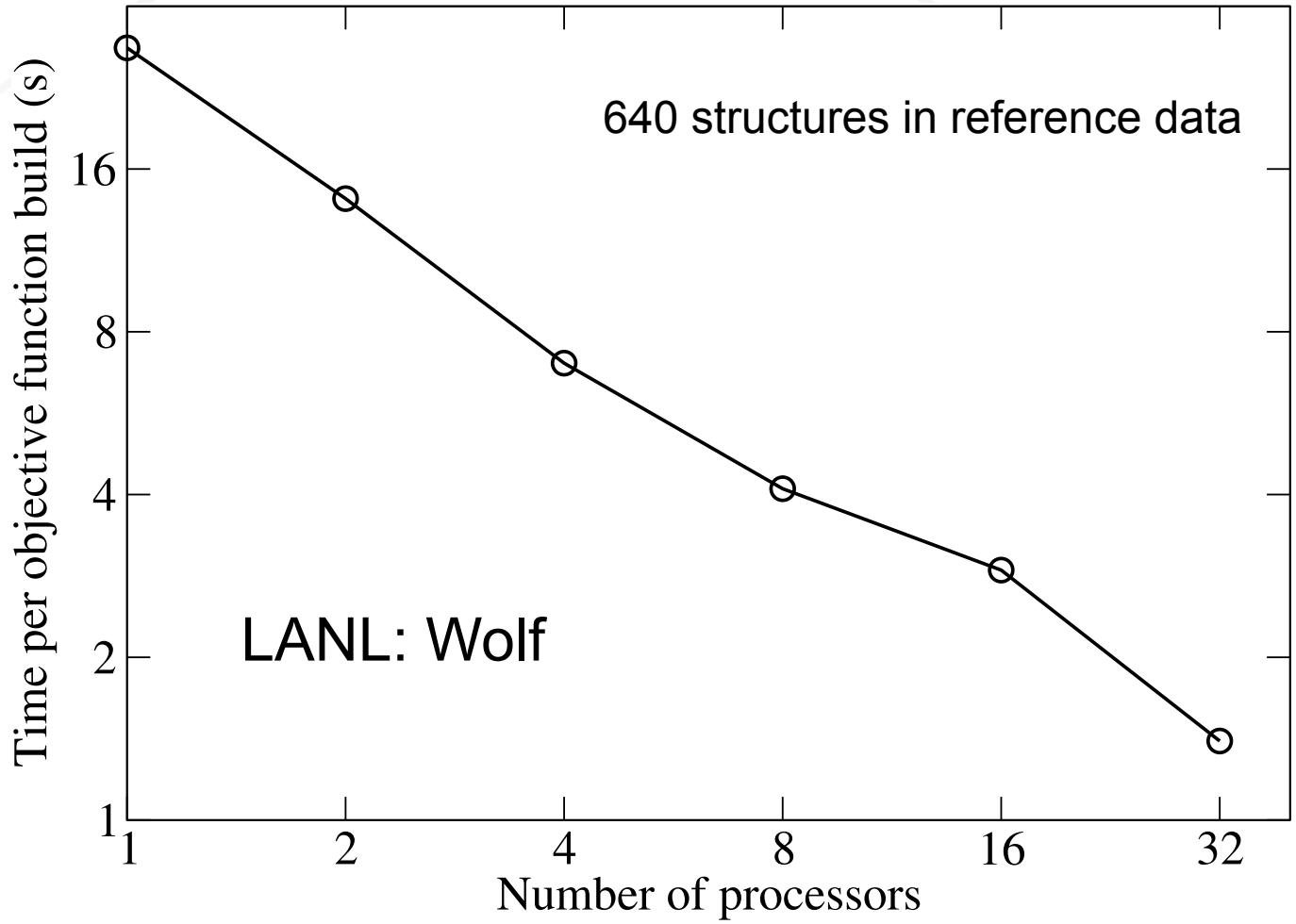

Steepest Descent: Number of iterations vs. Objective Function for perturbed parameters

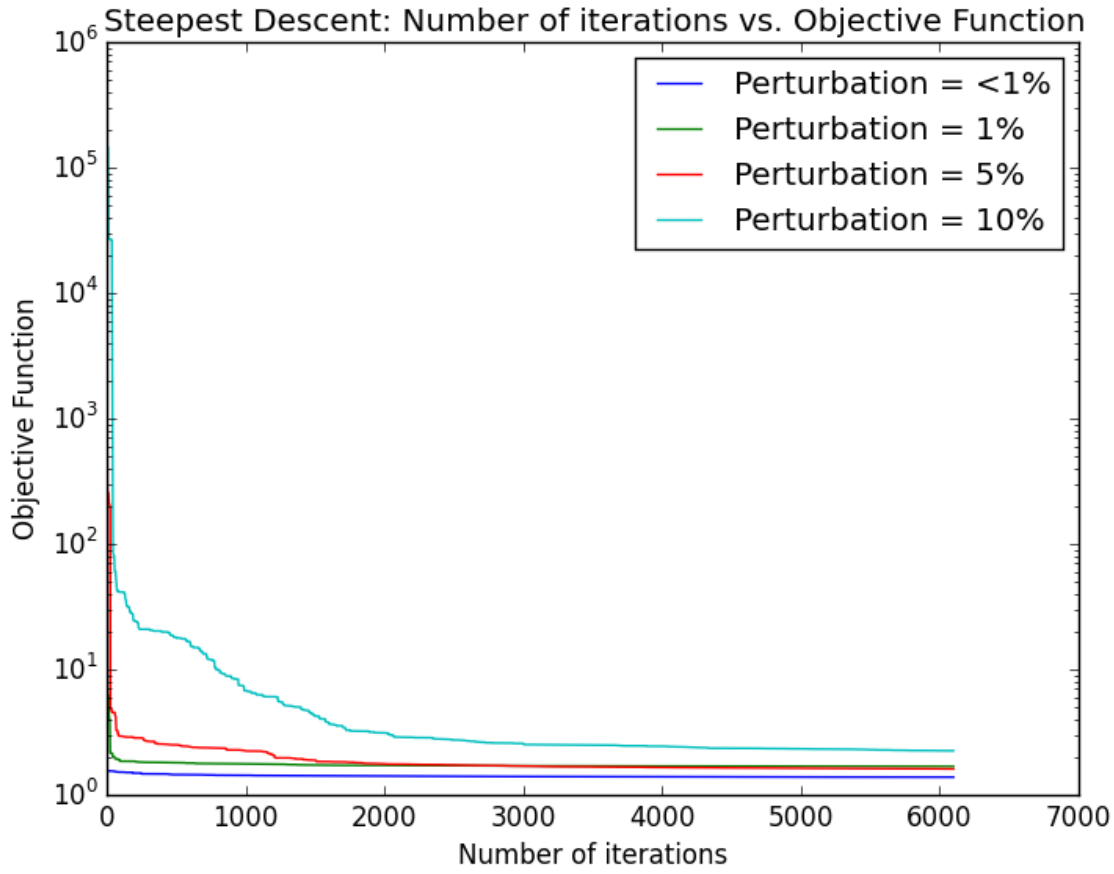

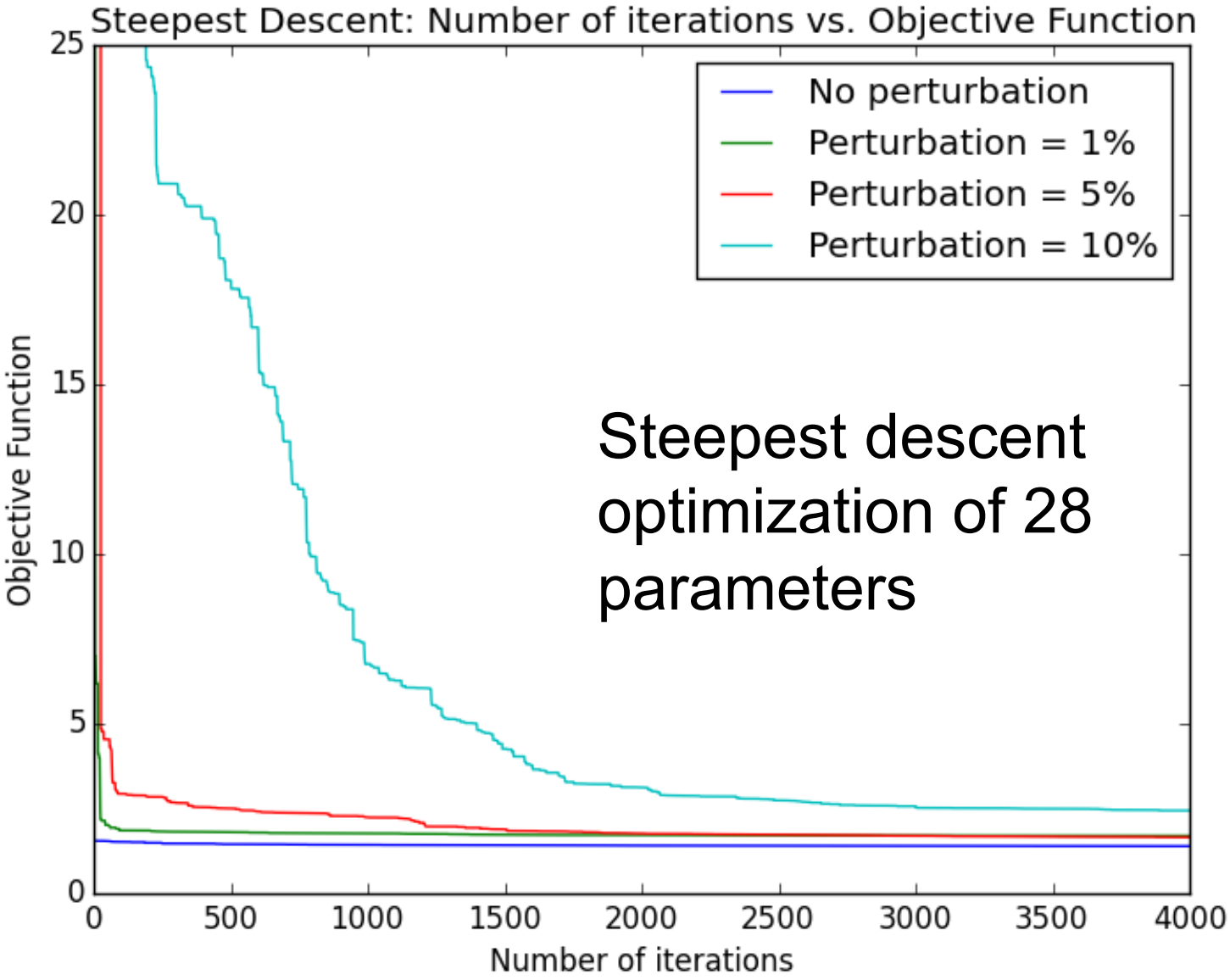

Steepest descent optimization of 28 parameters

Perturbed Parameters Error

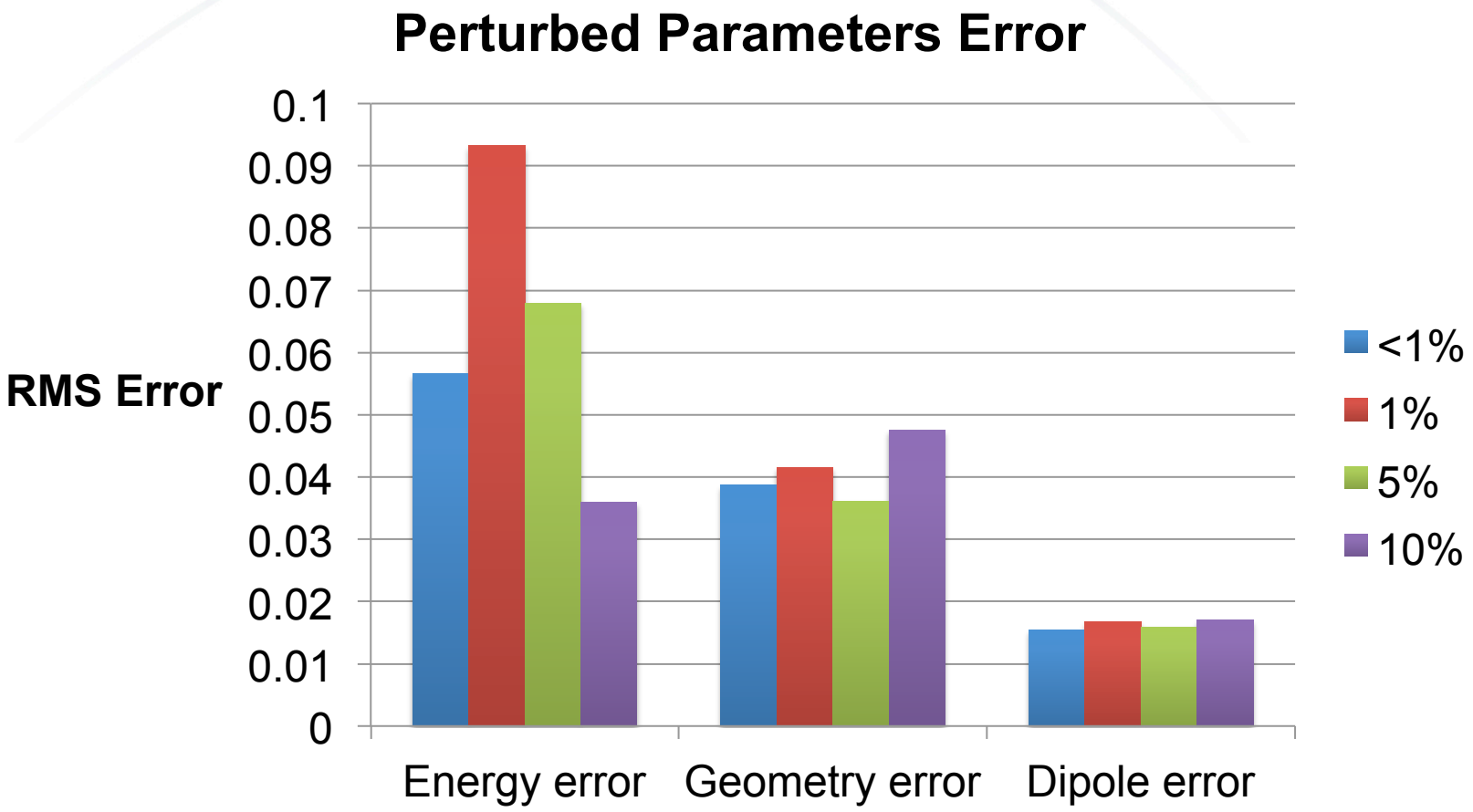

Error in atomization energy

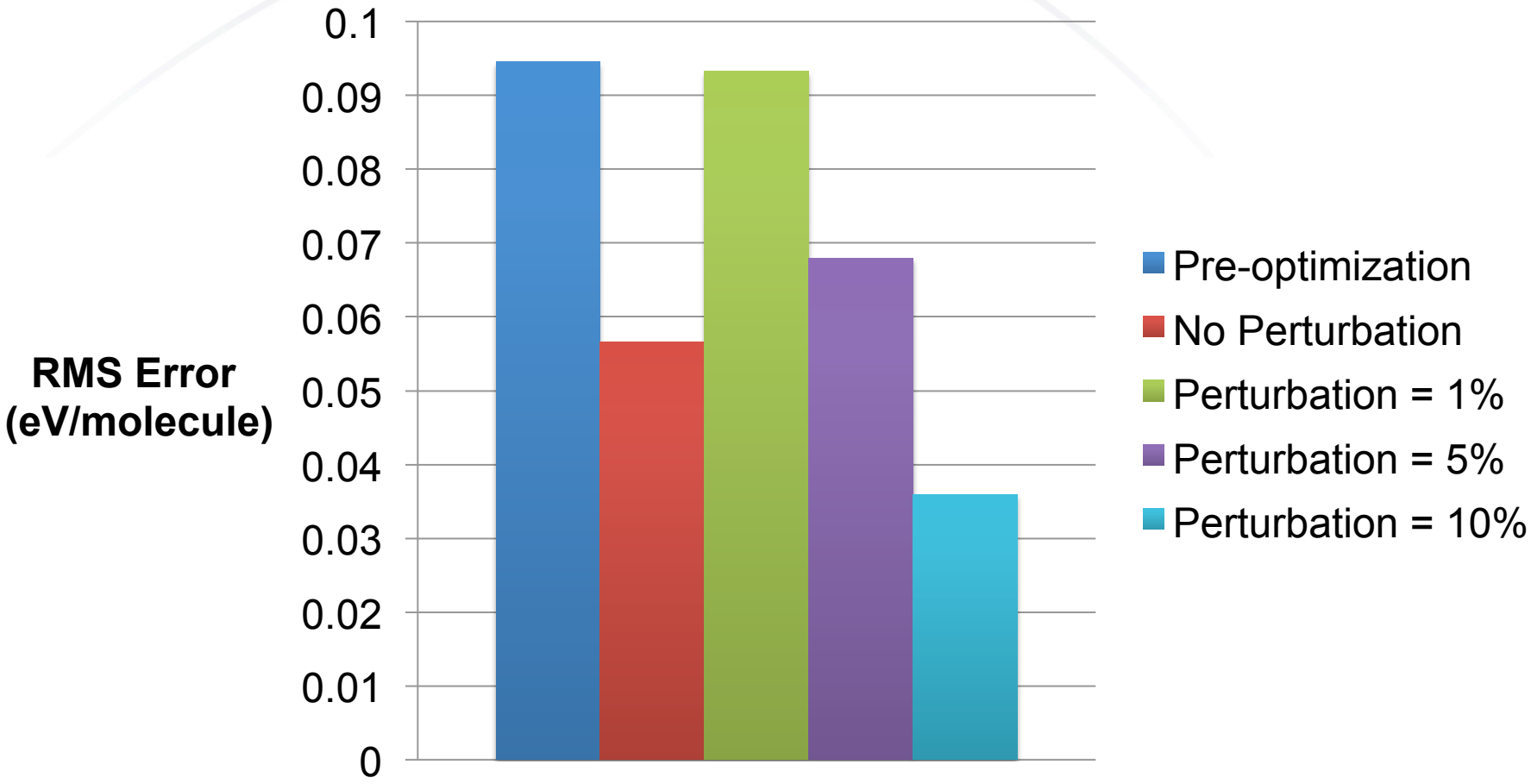

Error in molecular geometry

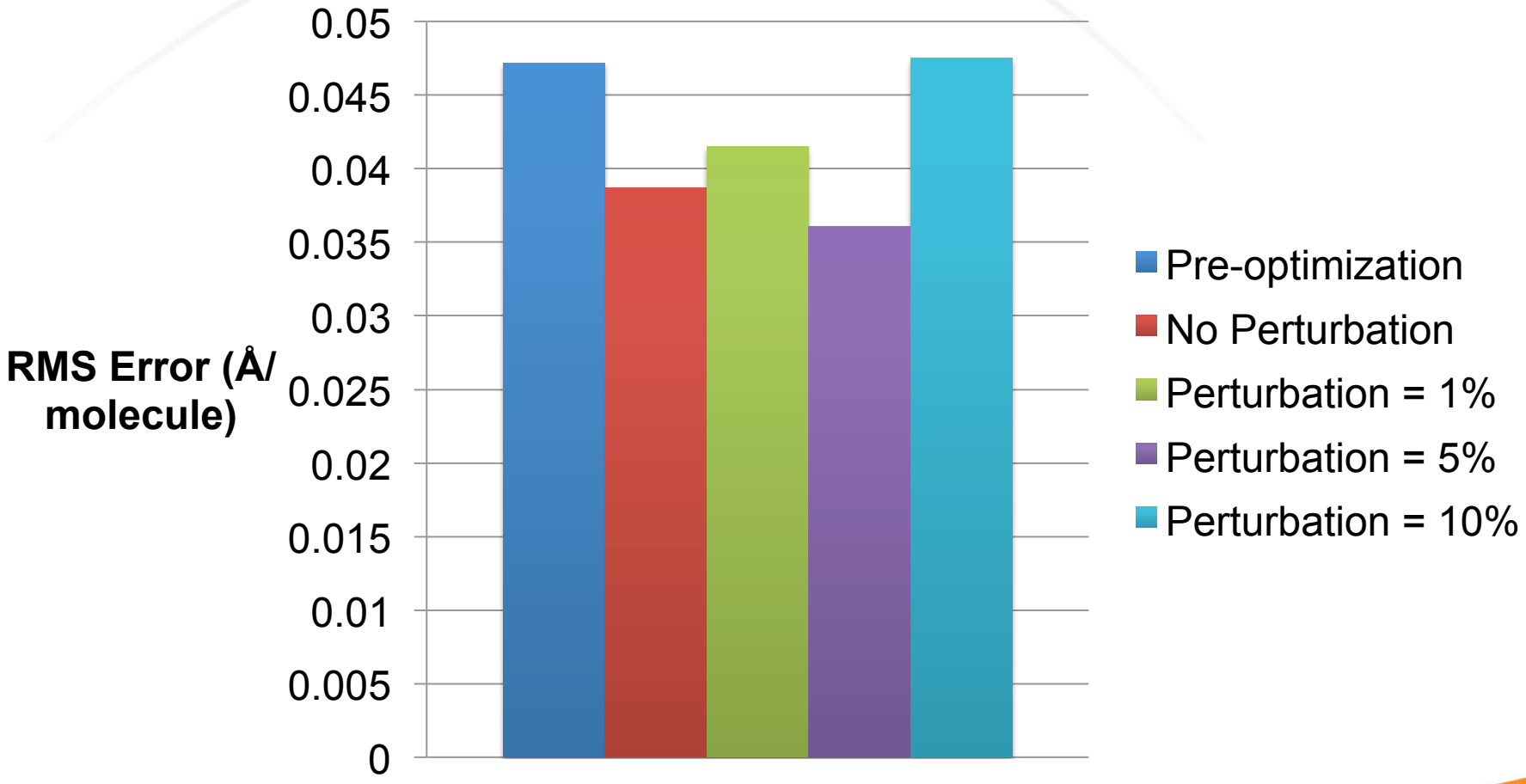

Error in molecular dipole moment

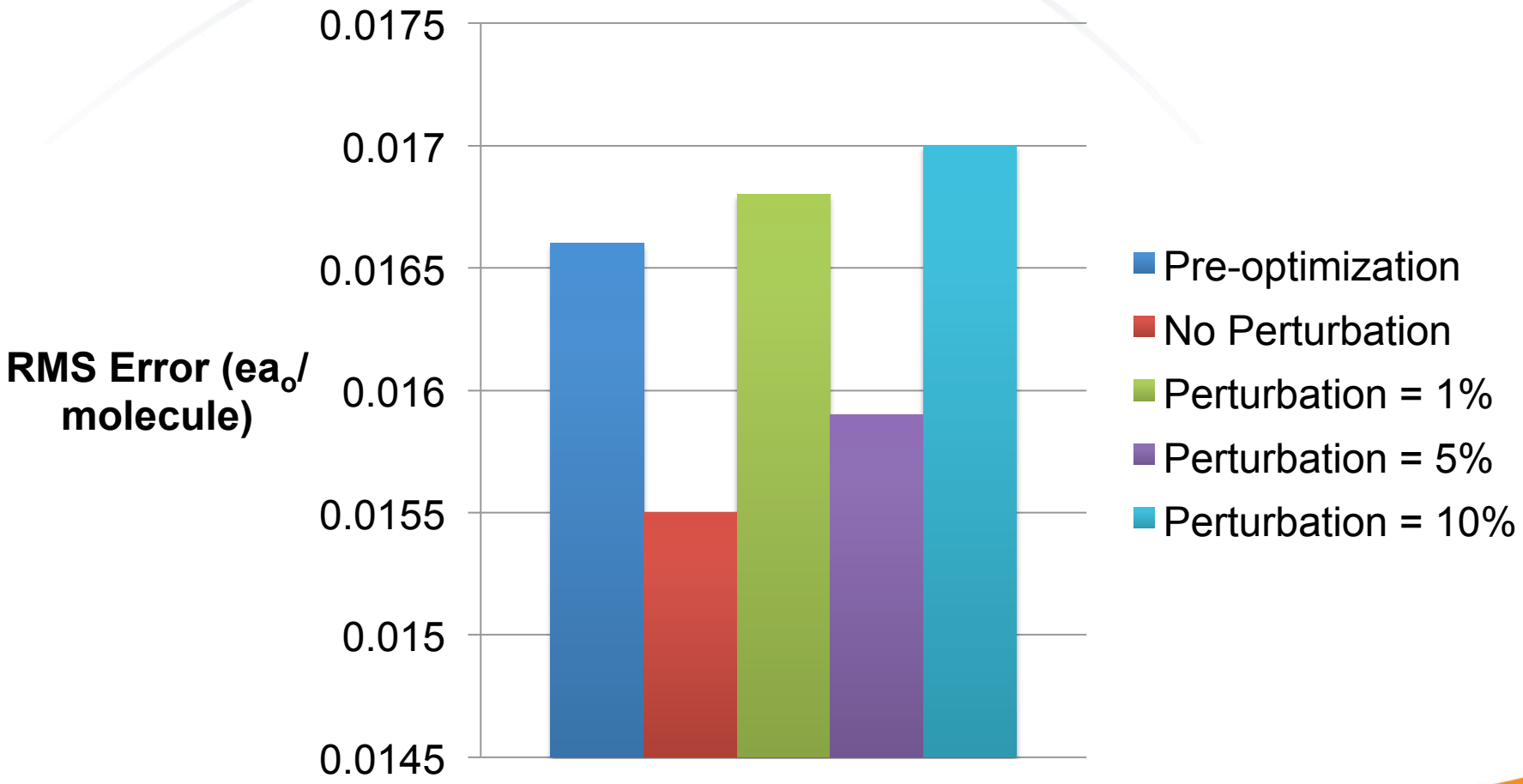

Future work: EPO

- Release code
- New optimizers
  - differential evolution
  - neural networks
- Improve portability and compatibility with other codes via modules/ functions
- Additional objective functions
  - stress tensors
  - polarizability
  - ionization potential
  - HOMO/LUMO eigenstates

Maud Rise Polynyas

Prajvala Kurtakoti
Texas A&M University
Advisor
Achim Stössel
Texas A&M University
Mentors
Milena Veneziani, Wilbert Weijer
Los Alamos National Laboratory

Schematic representation of physical processes taking place in deep water (open ocean) and shelf water (coastal) polynyas.

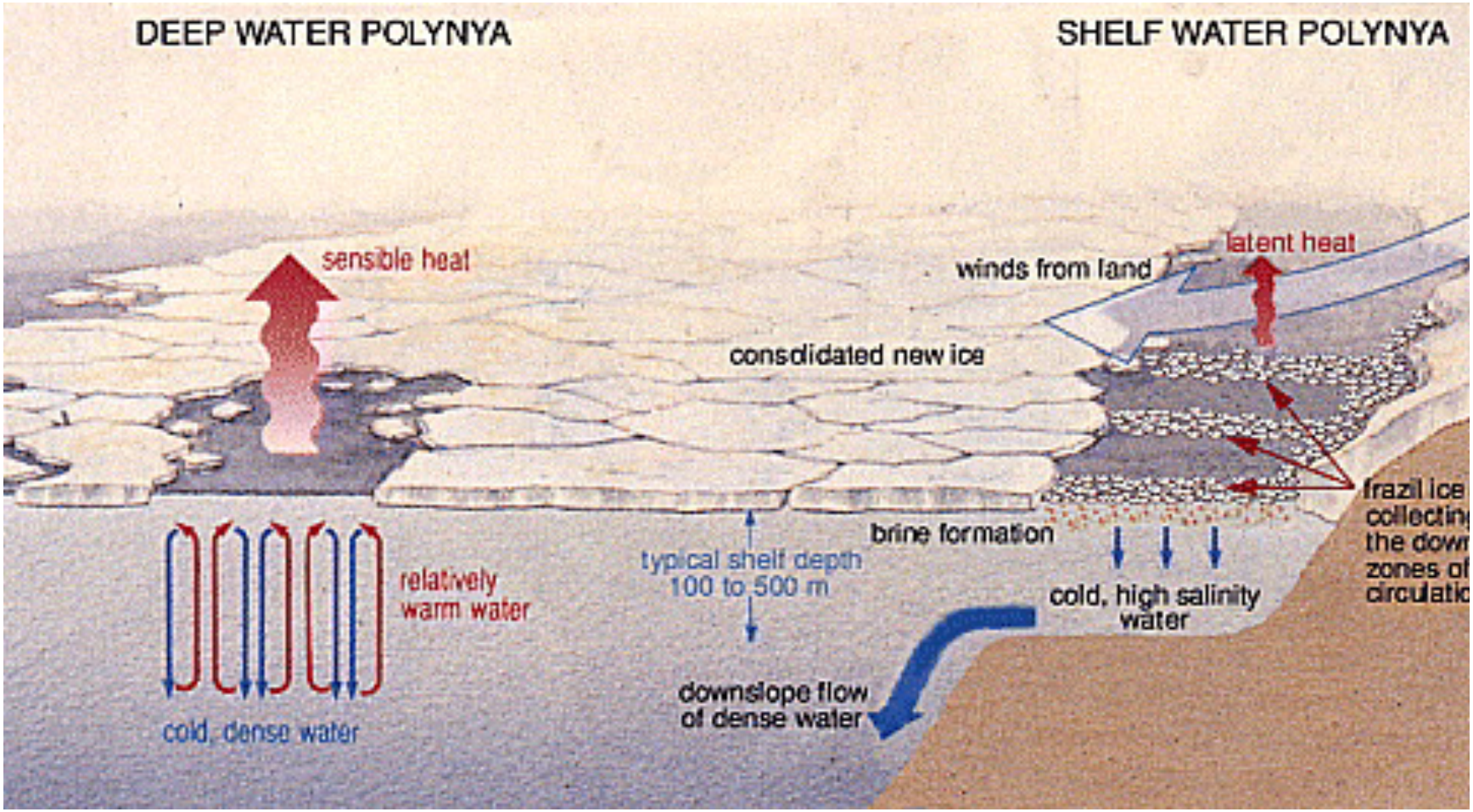

Reviews of Geophysics
Volume 42, Issue 1, RG1004, 18 MAR 2004 DOI: 10.1029/2002RG000116
http://onlinelibrary.wiley.com/doi/10.1029/2002RG000116/full#rog1583-fig-0001

Model details

- High resolution run:
  - Accelerated Climate Modeling for Energy (**ACME**) v0.1 baseline simulation.
  - Horizontal resolution of 0.1° for the ocean (POP) and sea-ice components (CICE).
  - 0.25° for the atmosphere (CAM) and land model components.
  - 95 years run (pre-industrial scenario).
- Low resolution run:
  - Horizontal resolution of 1° for the ocean (POP) and sea-ice components (CICE).
  - 1° for the atmosphere (CAM) and land model components.
  - 197 years run (pre-industrial scenario).

2 locations for Open Ocean Polynyas in the Weddell Region (**OOP**)

- Maud Rise Polynyas (**MRP**) :
  - ➢ Over Maud Rise Seamount
- Weddell Sea Polynyas (**WSP**)
  - ➢ Over Central and Eastern Weddell Sea.

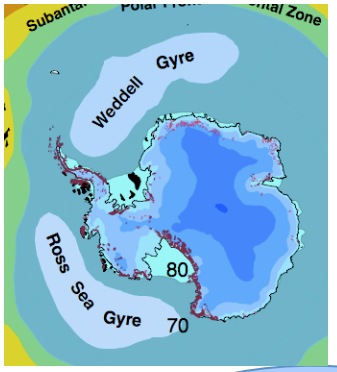

(Image: www.wikipedia.org/wiki/Weddell_Gyre)

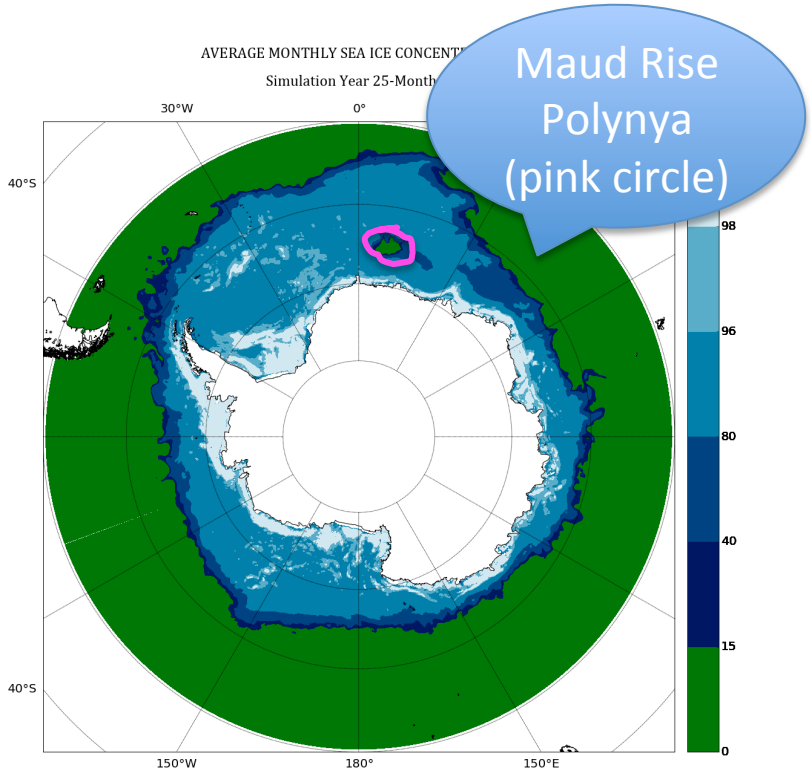

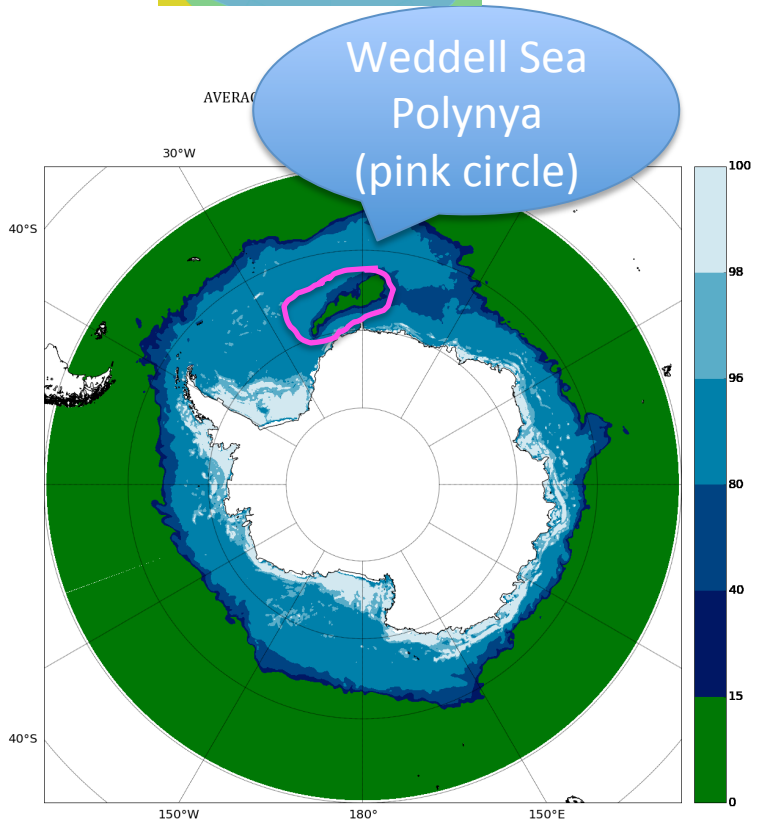

AVERAGE MONTHLY SEA ICE CONCENTRATION (%)

Simulation Year 15-Month 1

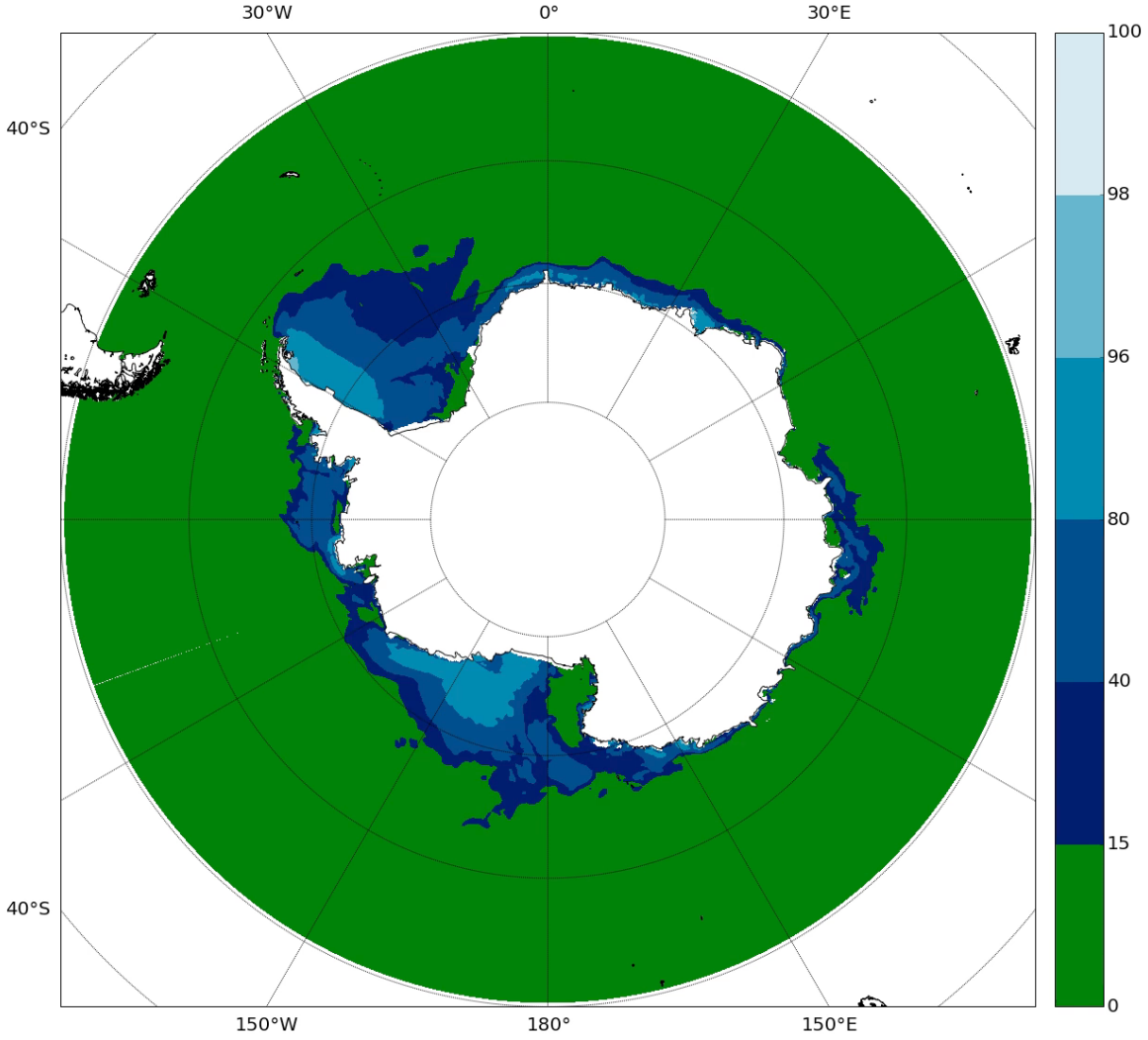

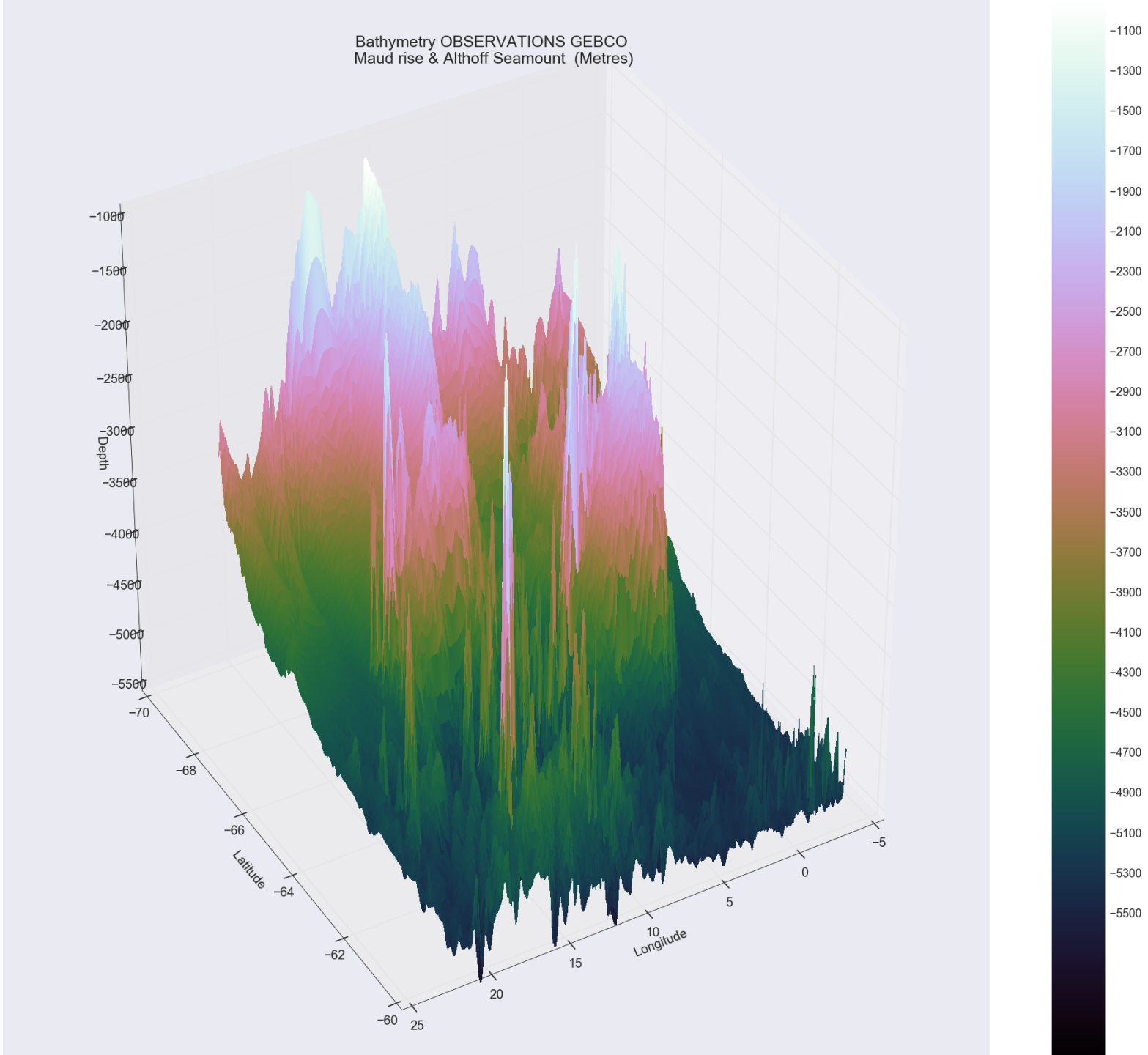
Bathymetry OBSERVATIONS GEBCO
Maud rise & Althoff Seamount (Metres)
Depth
−1000
−1500
−2000
−2500
−3000
−3500
−4000
−4500
−5000
−5500
Latitude
−70
−68
−66
−64
−62
−60
Longitude
25
20
15
10
5
0
−5
−1100
−1300
−1500
−1700
−1900
−2100
−2300
−2500
−2700
−2900
−3100
−3300
−3500
−3700
−3900
−4100
−4300
−4500
−4700
−4900
−5100
−5300
−5500

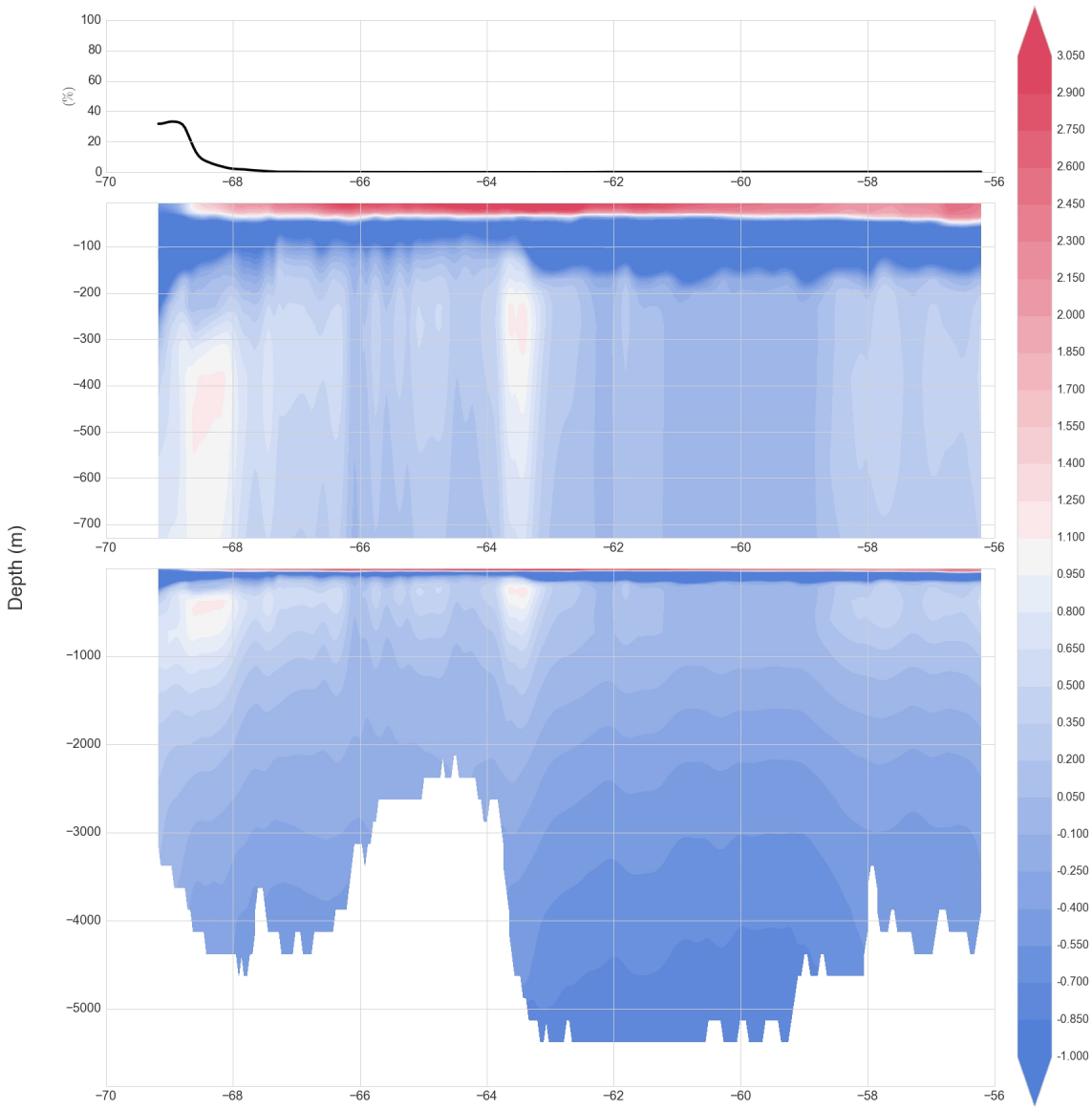
North-South cross section of Maud Rise Seamount
Ice Concentration (top)
Temperature (°C) upper 700m (centre) and full depth (bottom)
Year 28 Month 1
(%)
Depth (m)
Latitude
3.050
2.900
2.750
2.600
2.450
2.300
2.150
2.000
1.850
1.700
1.550
1.400
1.250
1.100
0.950
0.800
0.650
0.500
0.350
0.200
0.050
-0.100
-0.250
-0.400
-0.550
-0.700
-0.850
-1.000

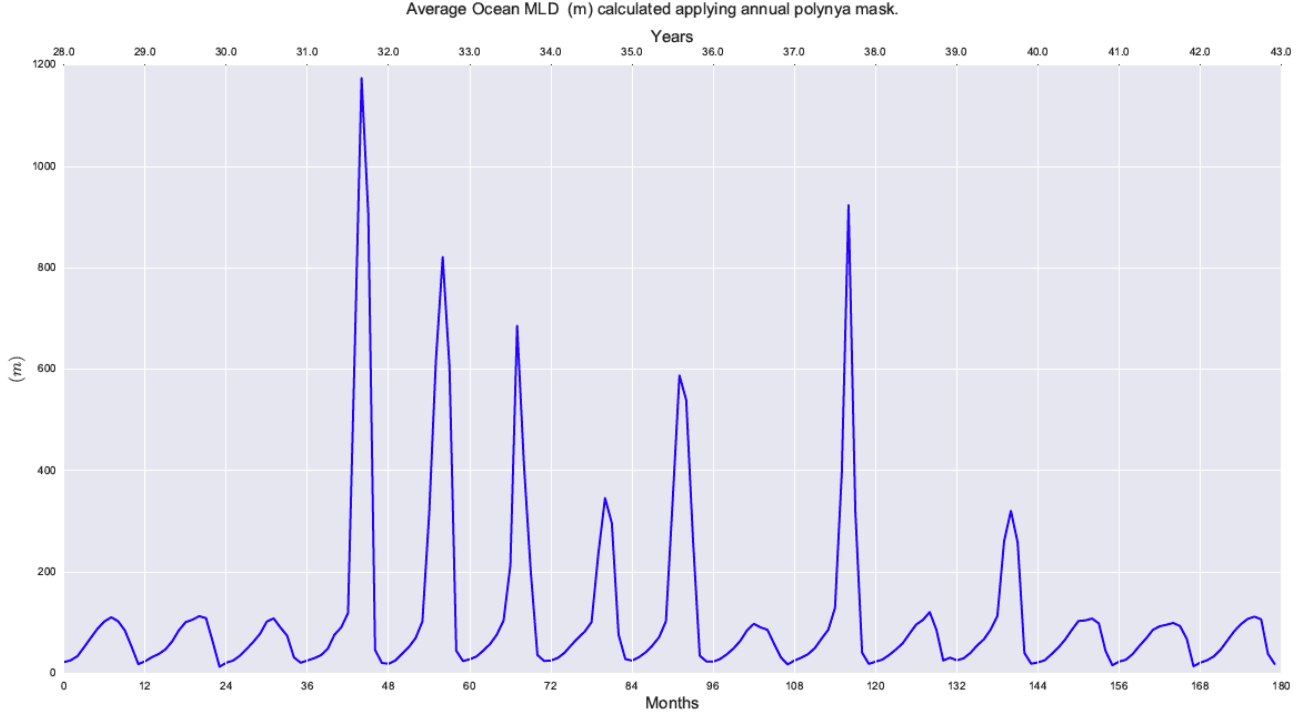
Average Ocean MLD (m) calculated applying annual polynya mask.
Years
28.0 29.0 30.0 31.0 32.0 33.0 34.0 35.0 36.0 37.0 38.0 39.0 40.0 41.0 42.0 43.0
1200
1000
800
600
400
200
0
(m)
0 12 24 36 48 60 72 84 96 108 120 132 144 156 168 180
Months

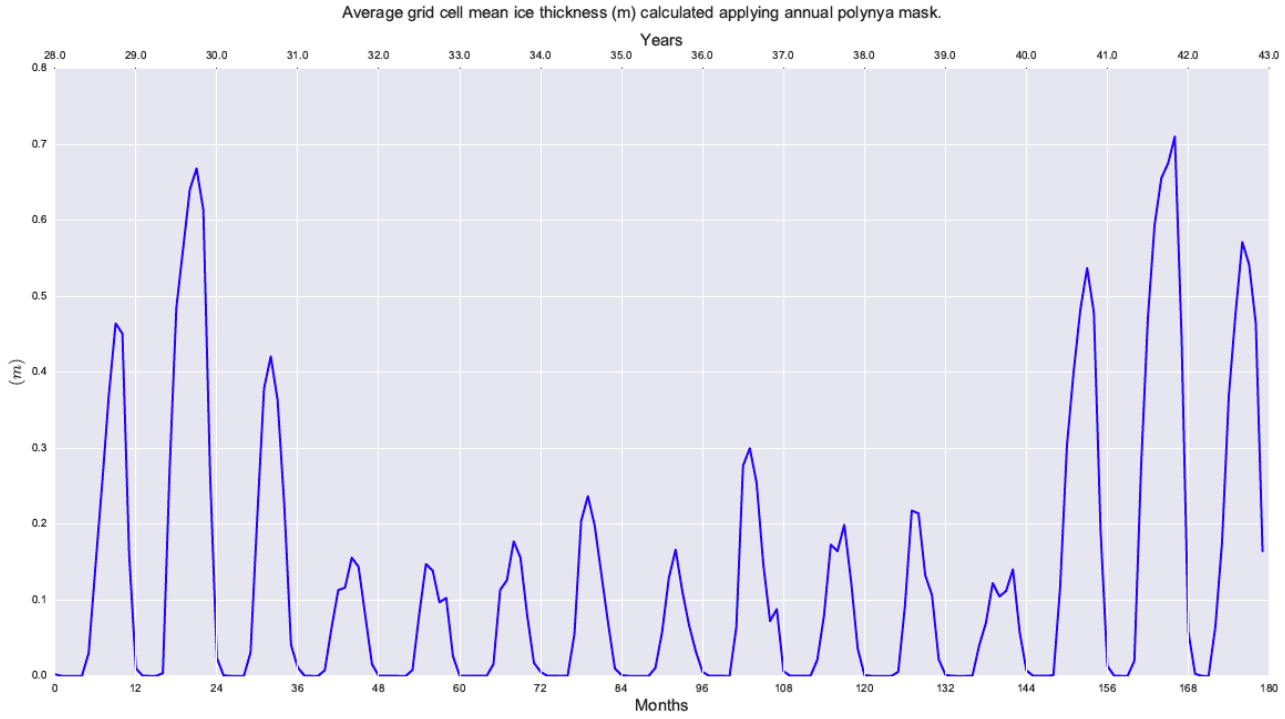
Average grid cell mean ice thickness (m) calculated applying annual polynya mask.
Years
28.0 29.0 30.0 31.0 32.0 33.0 34.0 35.0 36.0 37.0 38.0 39.0 40.0 41.0 42.0 43.0
0.8
0.7
0.6
0.5
0.4
0.3
0.2
0.1
0.0
(m)
0 12 24 36 48 60 72 84 96 108 120 132 144 156 168 180
Months

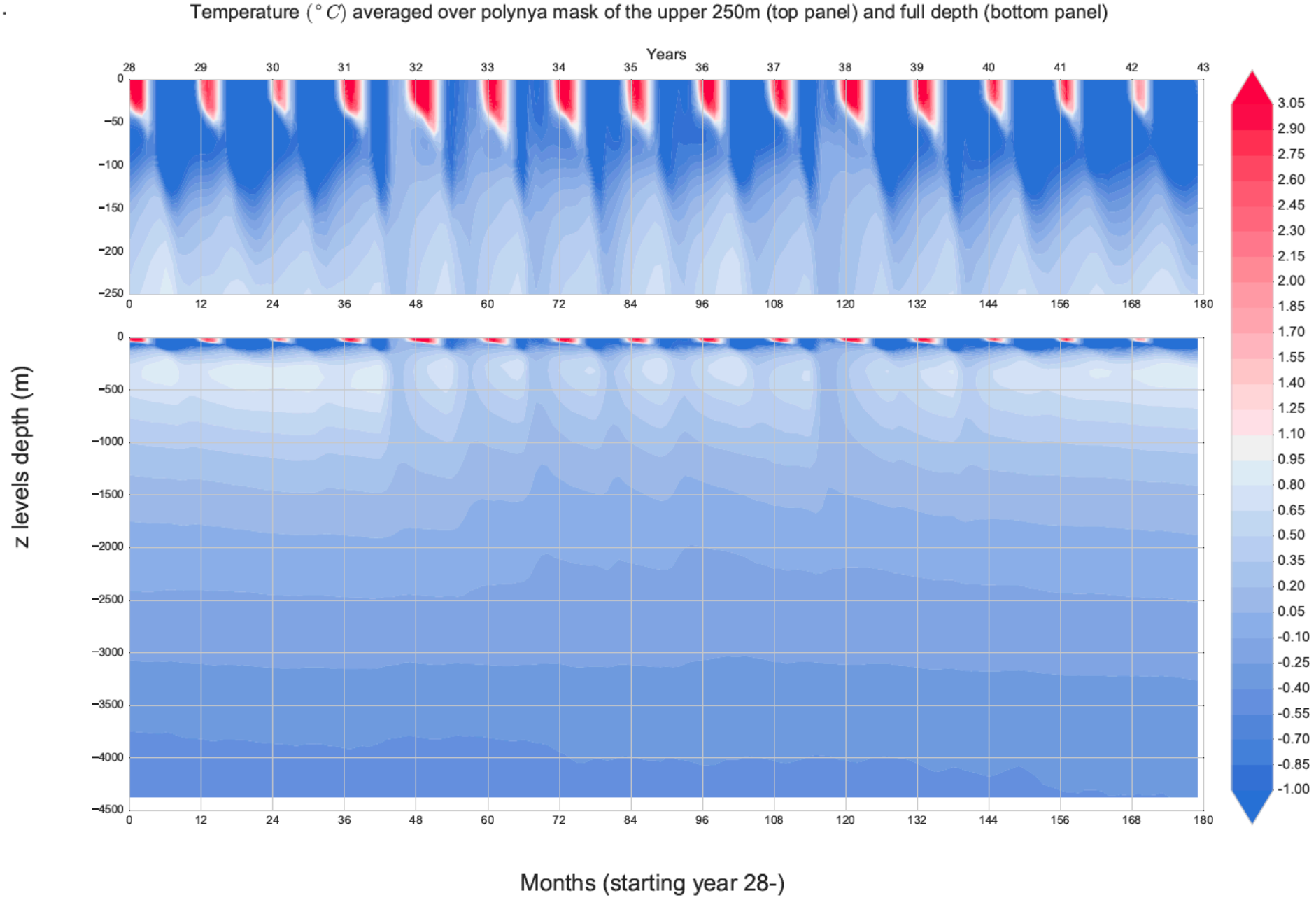
Temperature (°C) averaged over polynya mask of the upper 250m (top panel) and full depth (bottom panel)
Years
28 29 30 31 32 33 34 35 36 37 38 39 40 41 42 43
0 −50 −100 −150 −200 −250
0 12 24 36 48 60 72 84 96 108 120 132 144 156 168 180
0 −500 −1000 −1500 −2000 −2500 −3000 −3500 −4000 −4500
z levels depth (m)
3.05 2.90 2.75 2.60 2.45 2.30 2.15 2.00 1.85 1.70 1.55 1.40 1.25 1.10 0.95 0.80 0.65 0.50 0.35 0.20 0.05 -0.10 -0.25 -0.40 -0.55 -0.70 -0.85 -1.00
Months (starting year 28-)

Comparison of Bathymetry in Observation *vs.* model (high-resolution & low-resolution simulation)

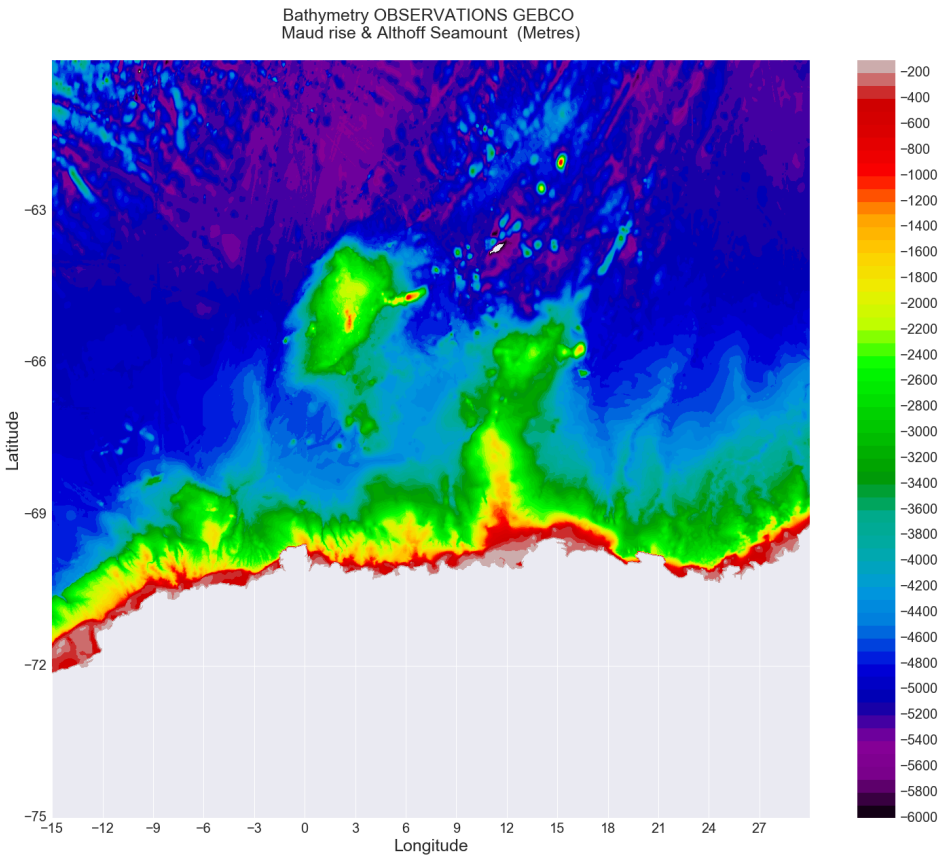

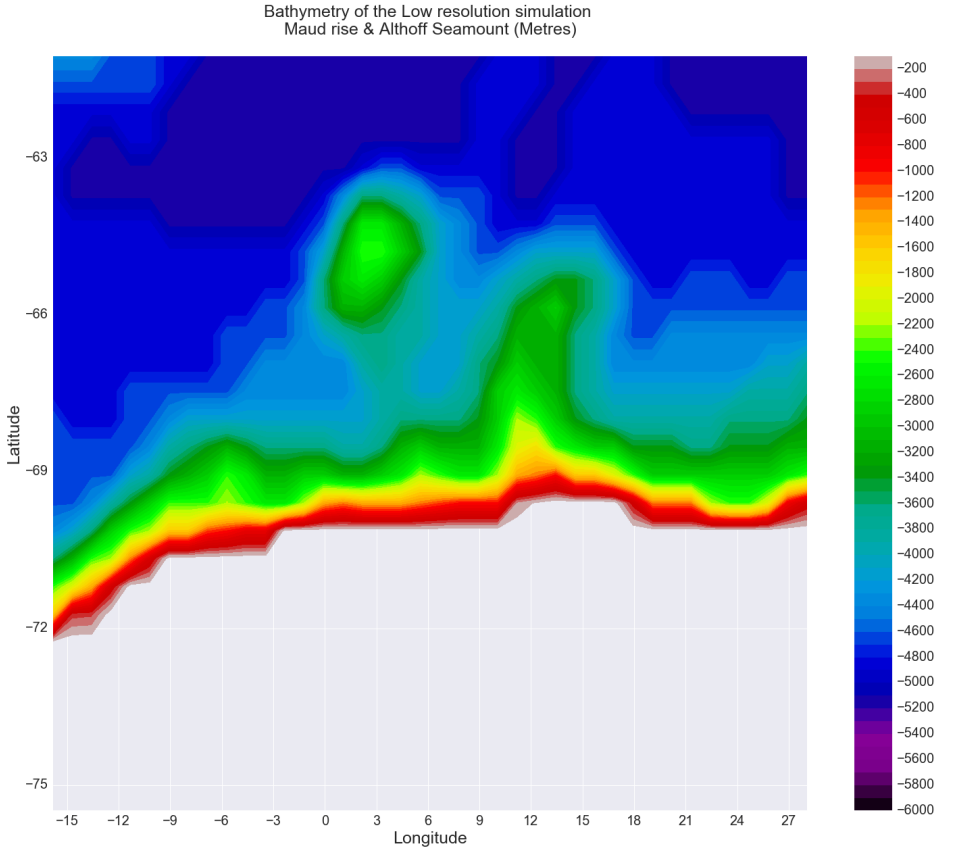

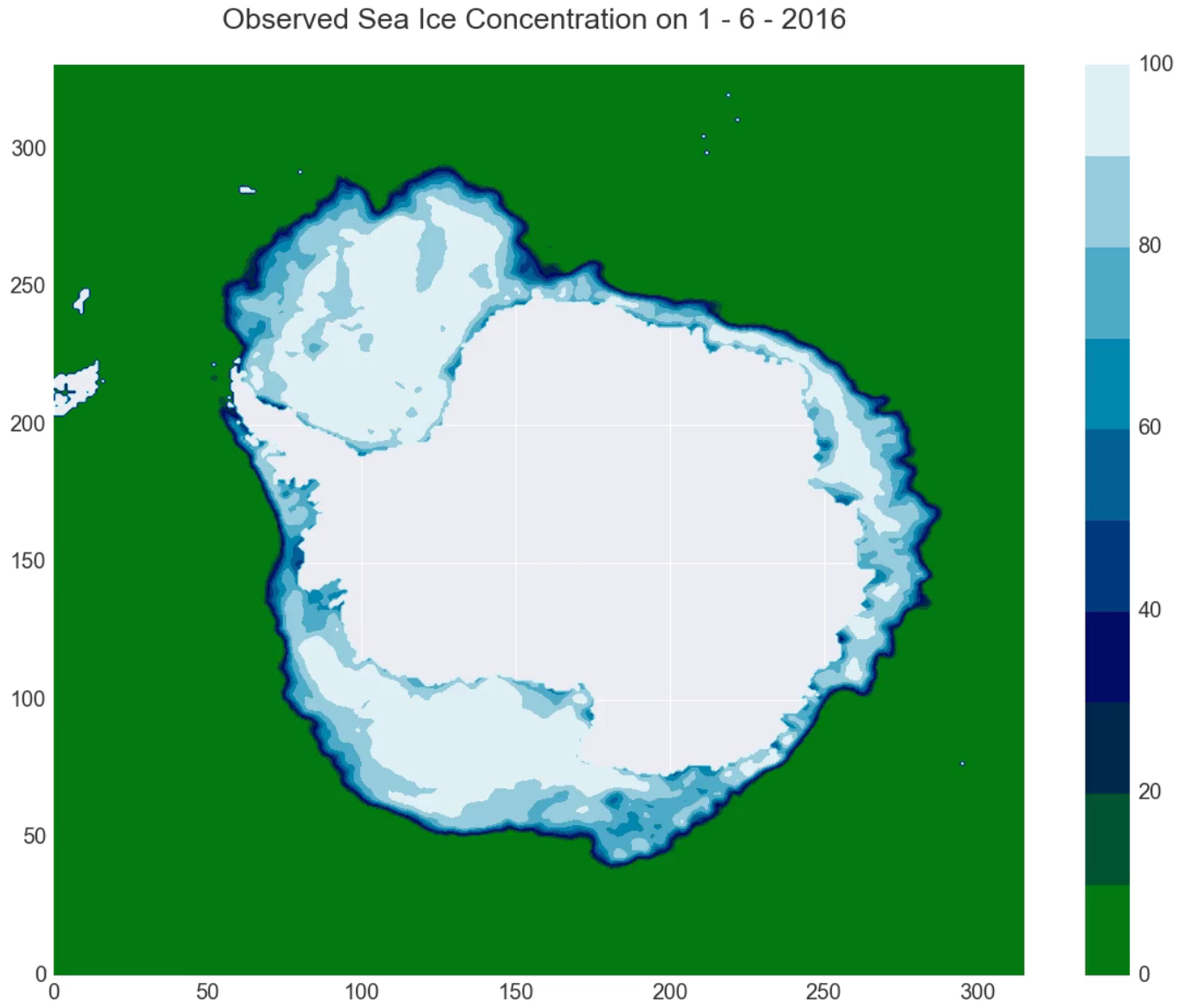
Observed Sea Ice Concentration on 1 - 6 - 2016
300
250
200
150
100
50
0
0
50
100
150
200
250
300
100
80
60
40
20
0

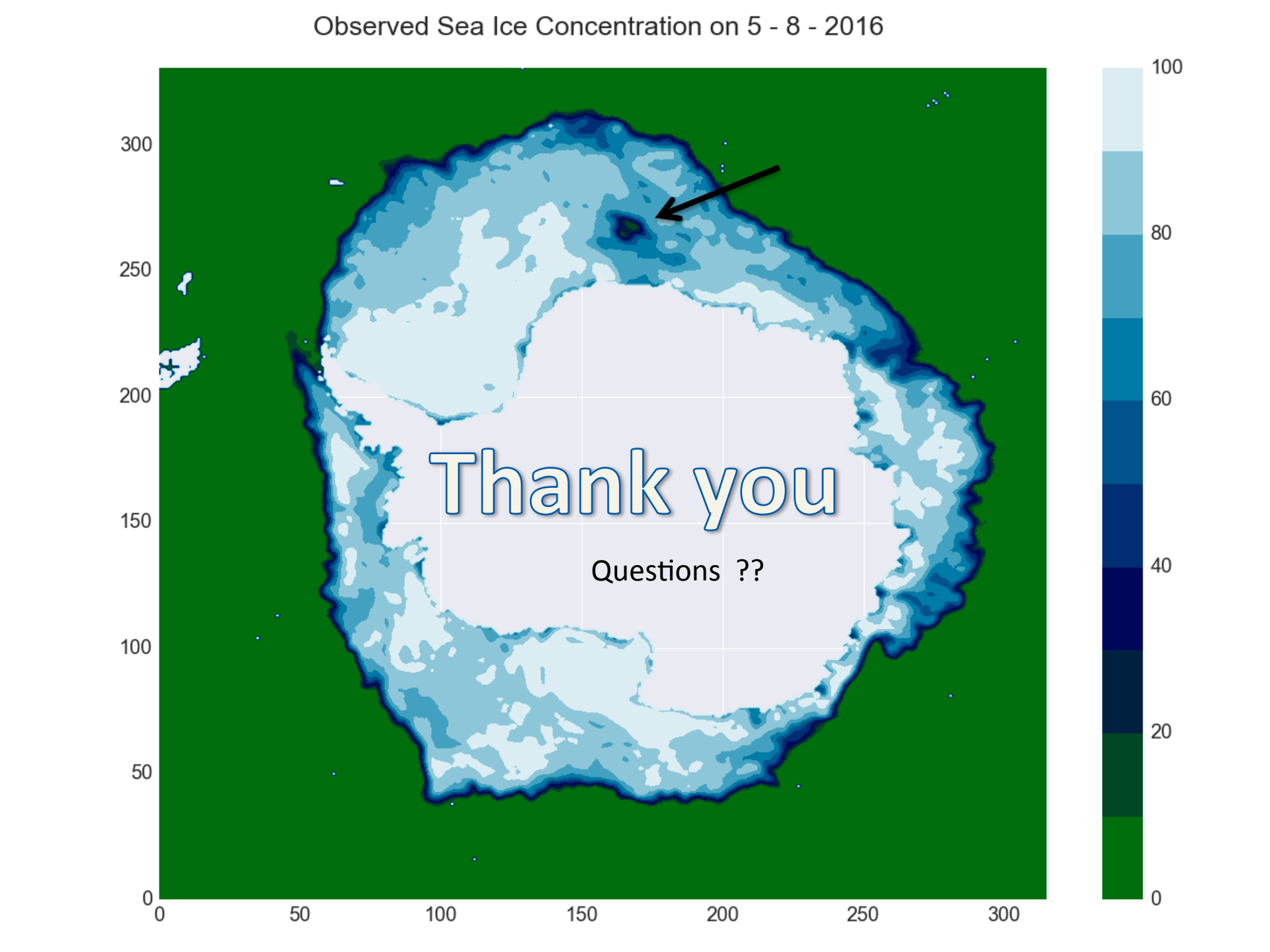
Observed Sea Ice Concentration on 5 - 8 - 2016
Thank you
Questions ??
0
50
100
150
200
250
300
0
20
40
60
80
100

Jonathan Lim
Mentor: Thomas K Leitner
Davidson College, UGS
T-6 Theoretical Biology and Biophysics

Reconstructing HIV Populations from Population Sequences

Direct population sequencing is a molecular biology technique that collapses the genomes of a whole population into a single file, yielding scope at the cost of resolution. In epidemiology, sequencing a patient's viral population is preferable to sequencing individual clones because physicians need to scan the entire population for drug resistance. Recently however, we found that phylogenetic analysis is greatly enhanced by the inclusion of many individual viral sequences from each patient. Since population sequences are widely available in regional databases, we are now interested in developing computational methods for reconstructing the viral populations of patients from their population sequences. First, we formulated into rules the logic used by humans to interpret sequencing chromatograms, both at the level of determining bases from peaks and at the level of determining consensuses from multiple reads. Second, we began efforts to optimize this logic for our application of obtaining phylogenetic signal while rejecting noise. We are validating these algorithms on a dataset in which patient viral samples were sequenced as clones and as populations, and we plan to include next-generation sequencing data from the same patients as well.

Title: Alpha to Omega: Modelling phase transformations in Ti under shock loading

Thaddeus Song En Low (GRA)
The Ohio State University
Group: T-3
Mentor: Curt Bronkhorst

Thanks,
Thad

Abstract: Under shock loading conditions resulting in pressures > 7 GPa, Ti experiences a phase transformation from the ambient stable alpha phase to the brittle and metastable omega phase. Although experimental work on this topic spans several decades, there remains much to uncover concerning the interaction between the phase transformation and plastic mechanisms. As a step towards further insight, the focus of this work is to incorporate a previously developed model into an FEM implementation via a VUMAT. Current features of the model include an EOS to account for elastic property changes, twinning/slip, and phase transformation adapted from martensitic theory. A brief overview of the model will be presented in addition to preliminary results of a pseudo-1D FEM simulation.

Photon induced Excited-State Dynamics

Lightning Talk 7/28/2016

By: Levi Lystrom, Tammie Nelson, Shawn McGrane, David Chavez, Jason Scharff, Sergei Tretiak

Ground State and Linear Absorption

- Optimization of Ground State
  - AM1 semiempirical
  - Ground State Dynamics
    - AM1 semiempirical
    - Thermalized for 6ps with δt=0.5fs classical time steps /w 3 electron steps.
- Absorption
  - CIS level of theory for static and thermalized geometries.

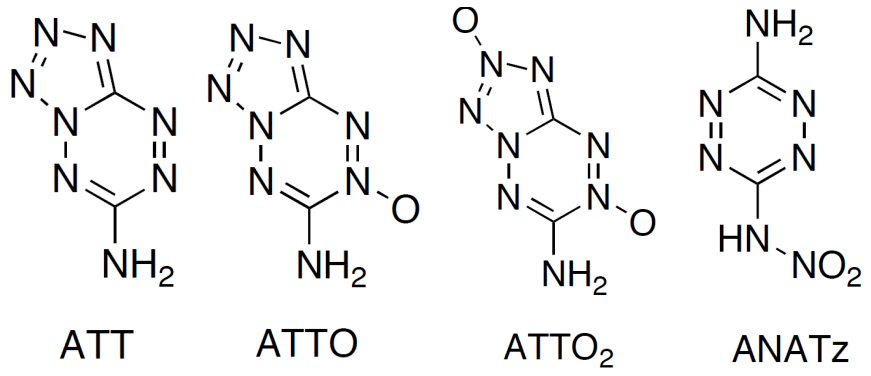

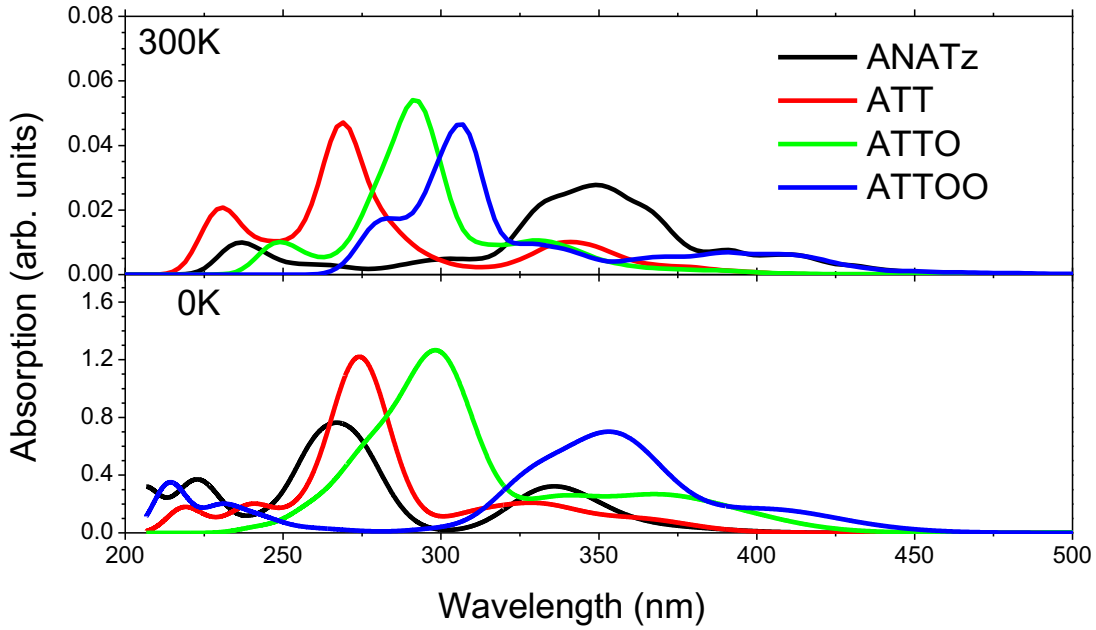

Pathways

Time = 0000fs

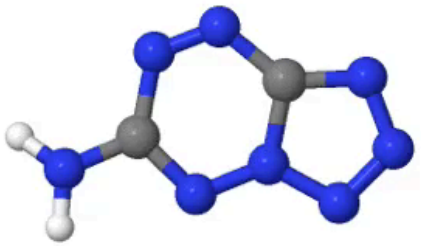

Time = 0000fs

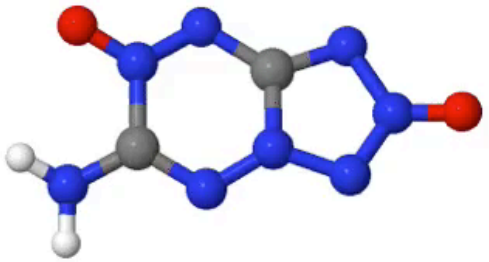

Branching Pathway Algorithm

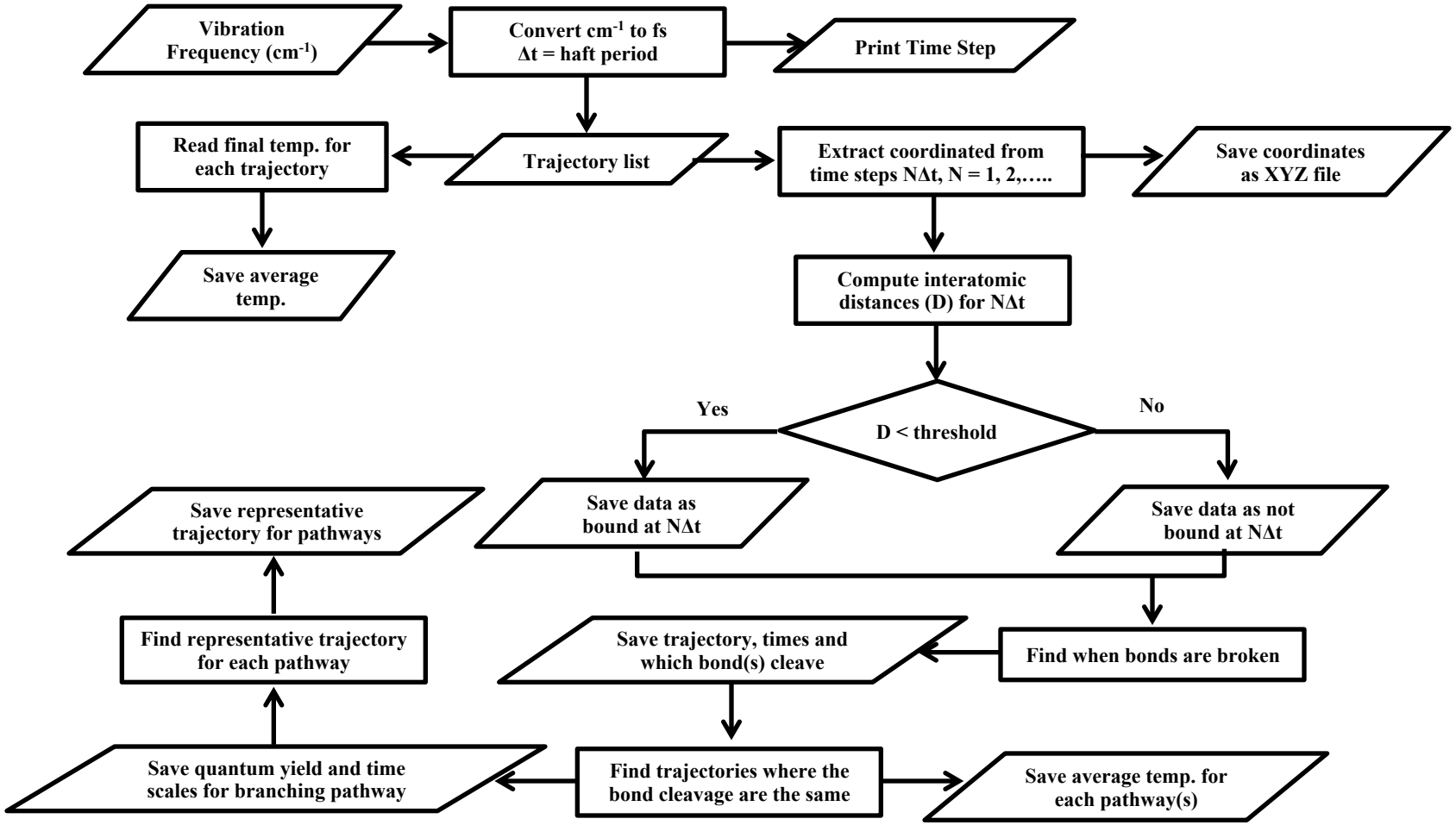

Algorithm Output

Compound		QY	Molecular Dynamics	
			Time (fs)	Snapshot
ATT	ATT	24%	144	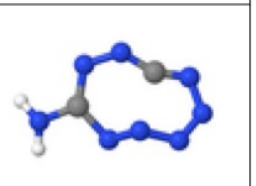
ATTO	ATTO	16%	144	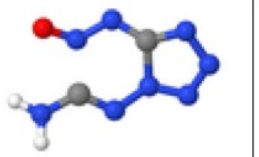
			192	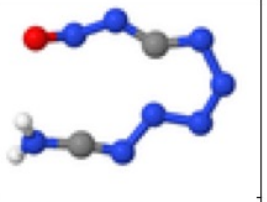
ATTO	ATTO	57%	144	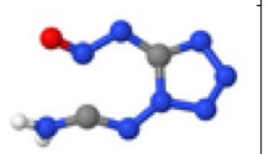

Compound		QY	Molecular Dynamics	
			Time (fs)	Snapshot
ATTOO	ATTOO	15%	112	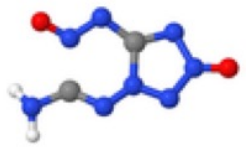
ATTOO	ATTOO	11%	128	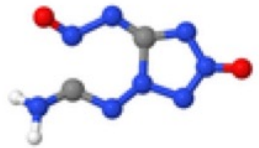
			192	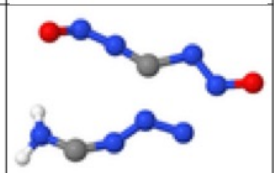
ATTOO	ATTOO		256	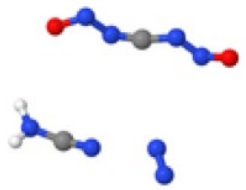

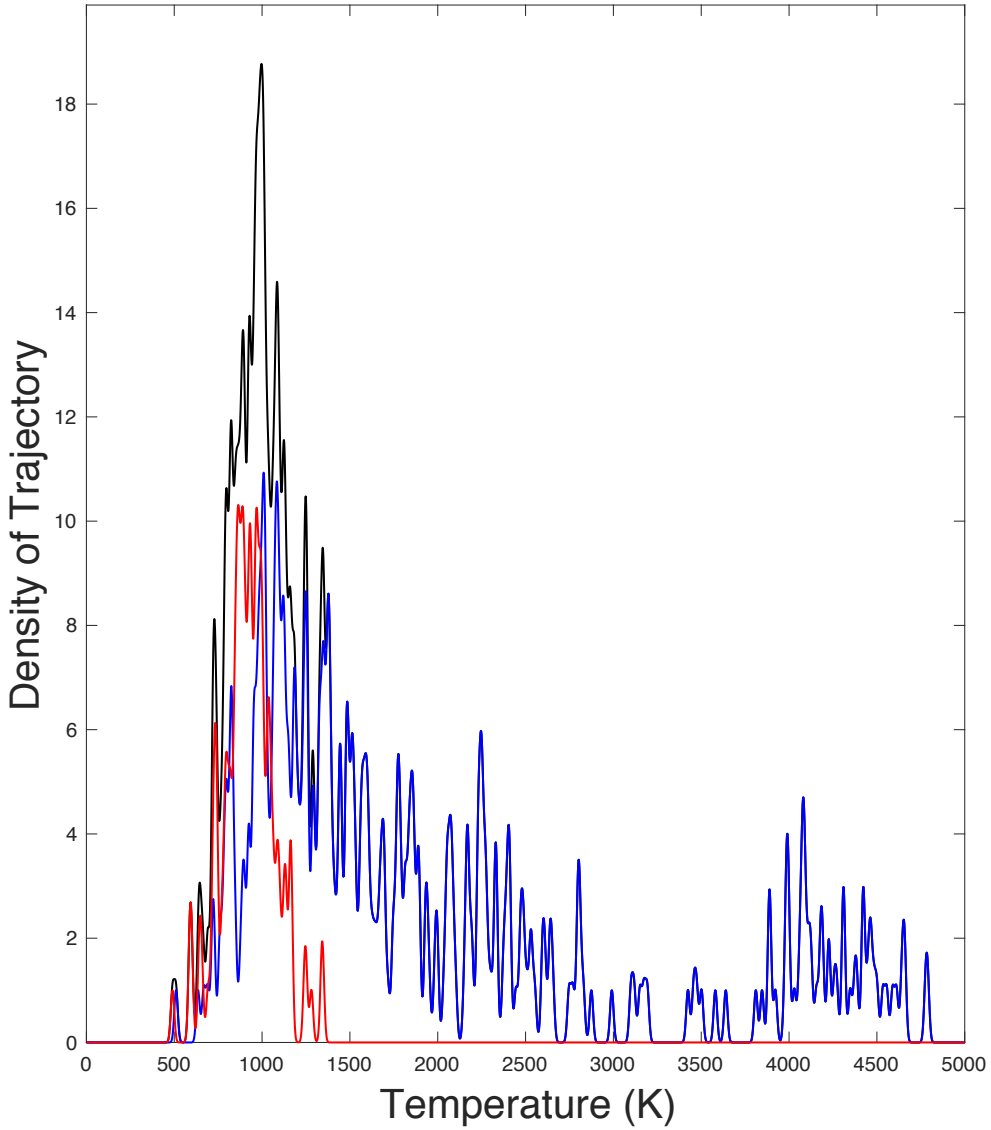

Conclusions

- The Branching Pathway Algorithm Performs
  - Extraction of time resolved XYZ coordinates
    - Saves in XYZ formatted files
    - Find interatomic distances
  - Classifies All trajectories into Branching Pathways
    - Finding Bond(s) cleaving events
  - Finds represented trajectory for each Pathway
  - Finds temperature dependency
    - Average Temperature for various pool
    - Dress the distribution of temperature
      with Gaussian distribution

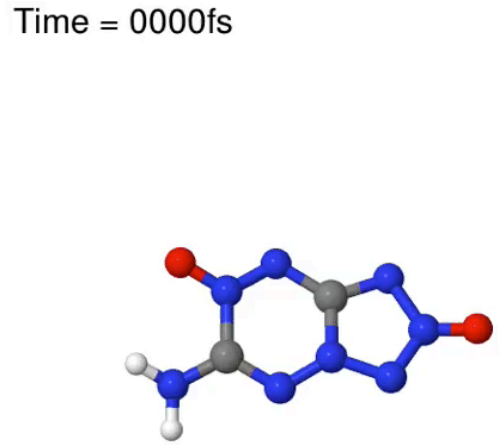

Acknowledgements

- Center for Nonlinear Study
- LDRD
- Los Alamos National Laboratory
- Sergei Tretiak Group

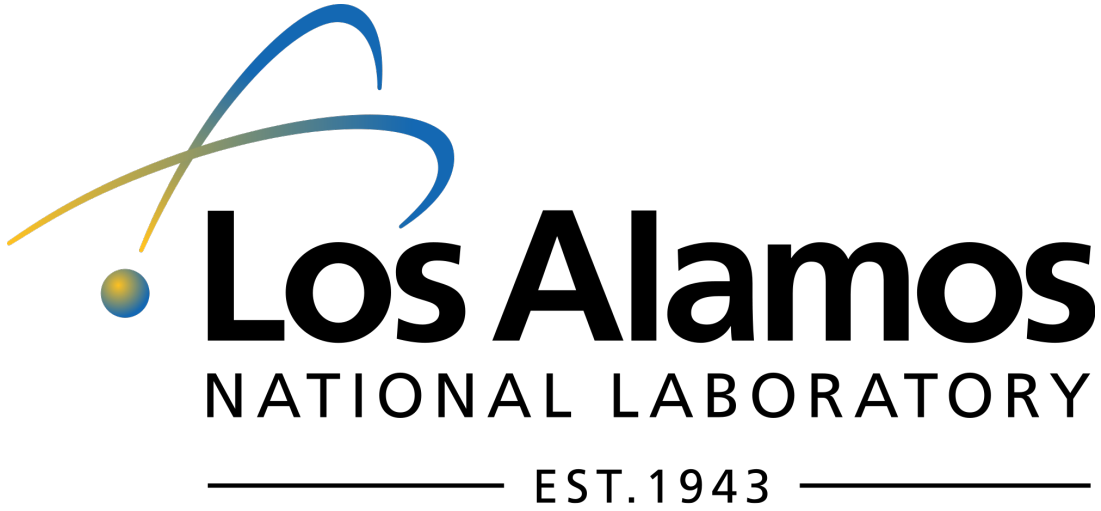

Questions?

Conclusions

- The Branching Pathway Algorithm Performs
  - Extraction of time resolved XYZ coordinates
    - Saves in XYZ formatted files
    - Find interatomic distances
  - Classifies All trajectories into Branching Pathways
    - Finding Bond(s) cleaving events
  - Finds represented trajectory for each Pathway
  - Finds temperature dependency
    - Average Temperature for various pool
    - Dress the distribution of temperature
      with Gaussian distribution

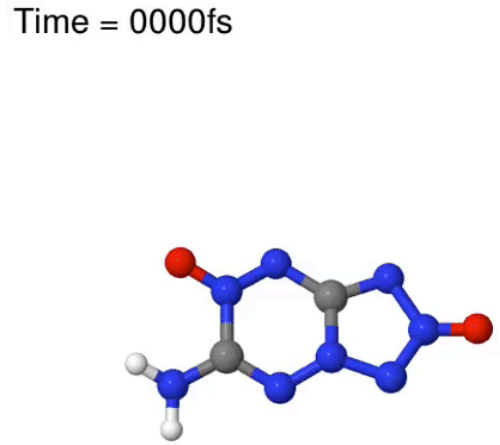

Collective Transport Properties of Driven Skyrmions with a Conformal Pinning Array

Xiaoyu Ma
University of Notre Dame

Mentors: Cynthia Reichhardt
(T-1)

Charles Reichhardt
(T-4)

07/14/2016

Outline

- Introduction to skyrmions, system description, and experiment results
- Particlelike skyrmion model and interaction of skyrmions with parabolic pin
- Collective transport properties of skyrmions with a conformal pinning array

Magnetic System

$$E=\int V\uparrow\blacksquare dr\uparrow 3\ \{A\sum i\uparrow\blacksquare(\nabla n\downarrow i)\uparrow 2\ +U(n)-\mu\downarrow 0\ M\downarrow 0\ H\cdot n\}+E\downarrow m$$

[1]

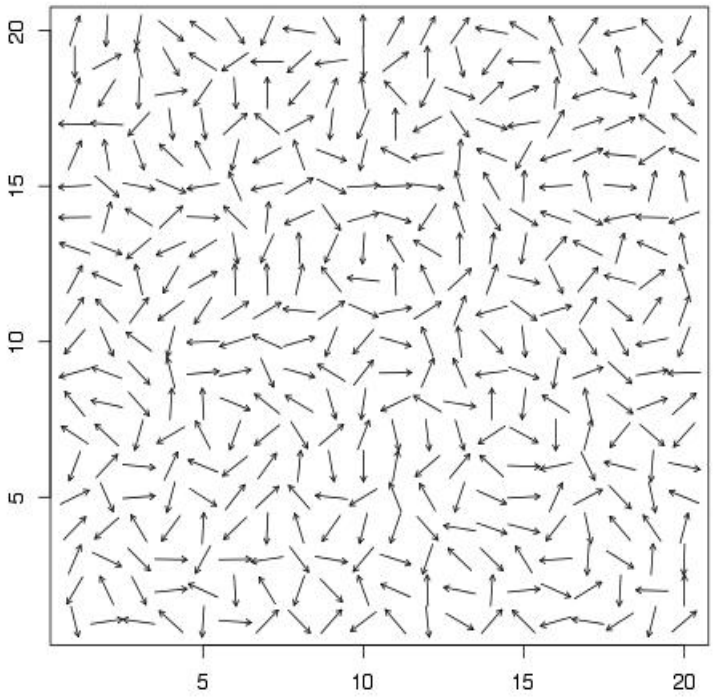

Exchange energy

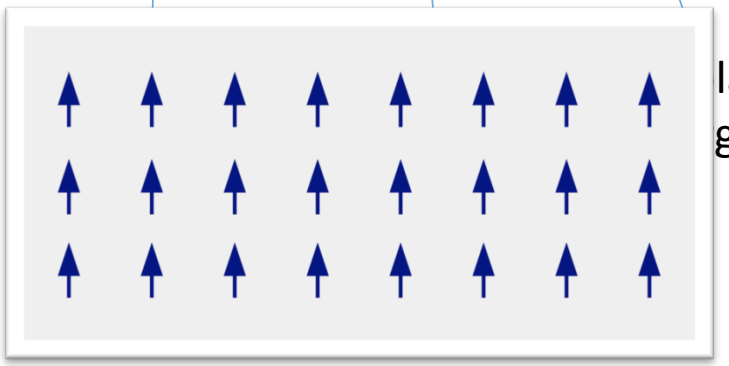

lar gy

$\{\blacksquare A>0$
$FerromagneticA<0$
$Antiferromagnetic$

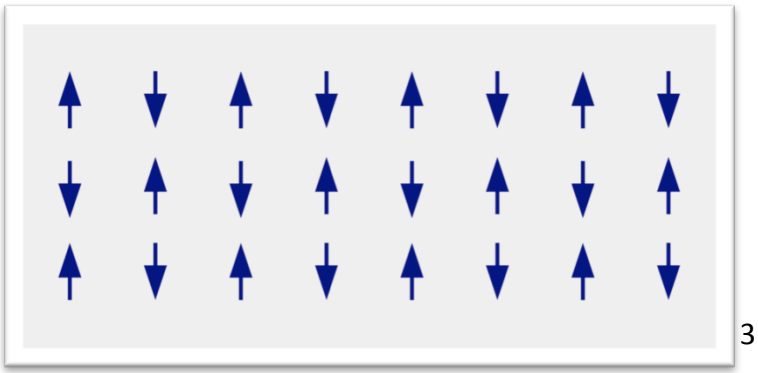

---

[1] H. Braun, Advances in Physics, Vol. 61, 1–116, 2012

Skyrmion

Dzyaloshinskii-Moriya Interaction (DMI): $\boldsymbol{D}\boldsymbol{n}\cdot(\boldsymbol{\nabla}\times\boldsymbol{n})$

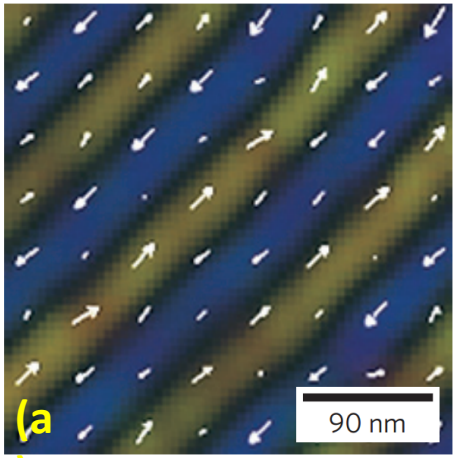

(a)

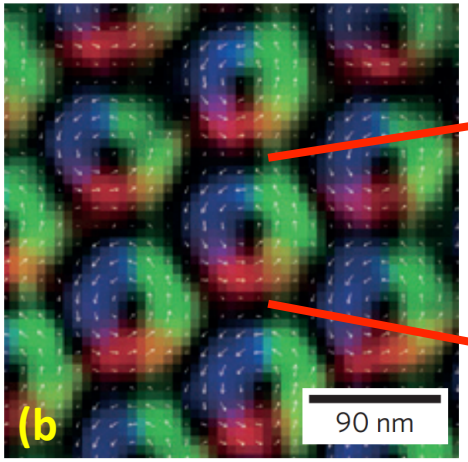

(b)

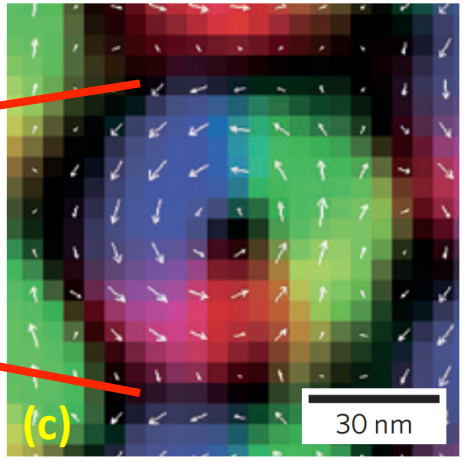

(c)

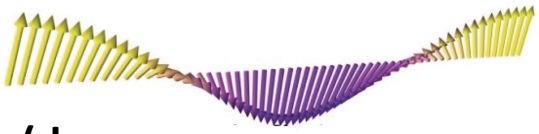

(d)

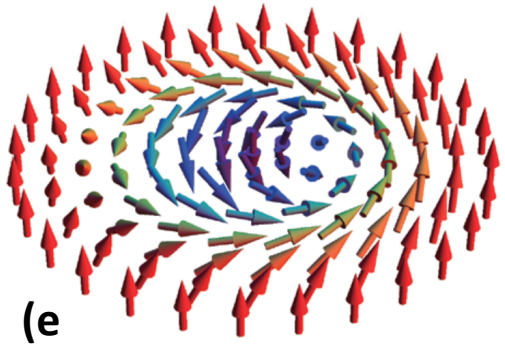

(e)

(a) Real-space observation of helical state and (b) skyrmion crystal state. (c) a magnified skyrmion from (b) [2]. (d) schematic spin configuration of helical state [3]. (e) schematic configuration of a skyrmion [4].

---

[2] X. Z. Yu, et al, Nat. Mater. 465, 901-904, 2010
[3] C. M. Jin, et al, Chinese Physics B, 24(12), 2015
[4] I. Kézsmárki, et al, Nat. Mater. 14, 1116-1123, 2015

Equation of Motion

The dynamics of a single skyrmion i [5] [6]

$$\alpha_d v_i + \alpha_m z \times v_i = F_i^{ss} + F_i^{sp} + F^D = F^{tot}$$

Dissipative component

Nondissipative component from Magnus term

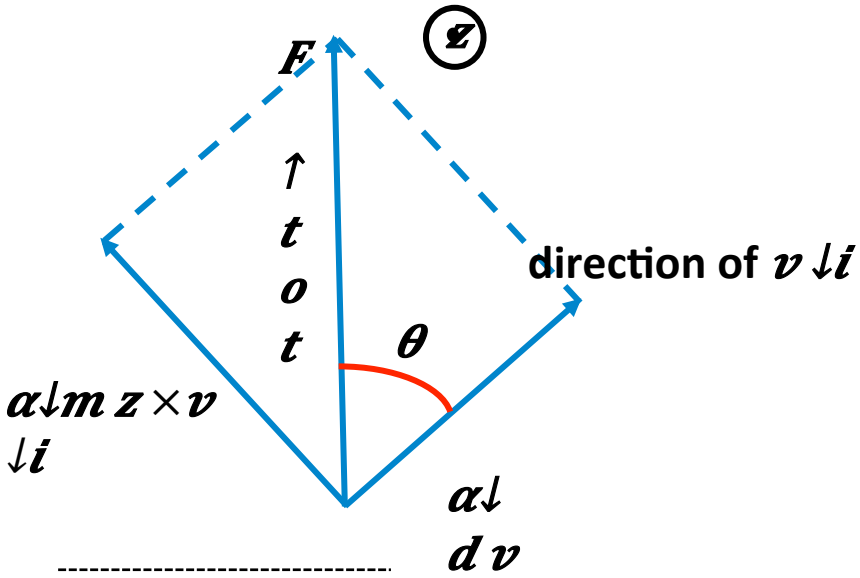

$F_i^{ss} = \sum_{j=1}^{N_s} r_{ij} K_1(R_{ij})$,

$R_{ij} = |r_i - r_j|$

F_i^{sp} non-overlapping harmonic traps

F^D Lorentz force from applied current

Hall angle: $\theta = \tan^{-1}(\alpha_m / \alpha_d)$

[5] S.-Z. Lin, et al, Phys. Rev. B 87, 214419, 2013

[6] C. Reichhardt, D. Ray, C. J. Olson Reichhardt, Phys. Rev. Lett. 114, 217202, 2015

Isolated Skyrmion within a Harmonic Trap with AC Drive (x direction)

(a) Fac=0.03, α_m/α_d =10

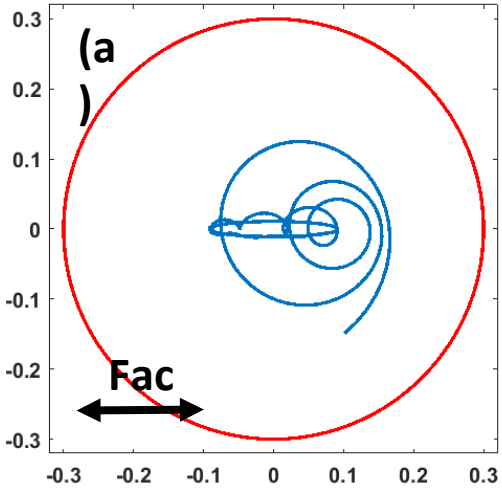

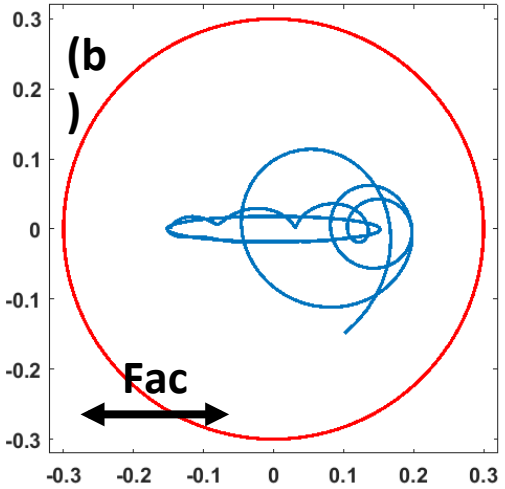

(b) Fac=0.05, α_m/α_d =10

(c) Fac=0.03 α_m/α_d =1

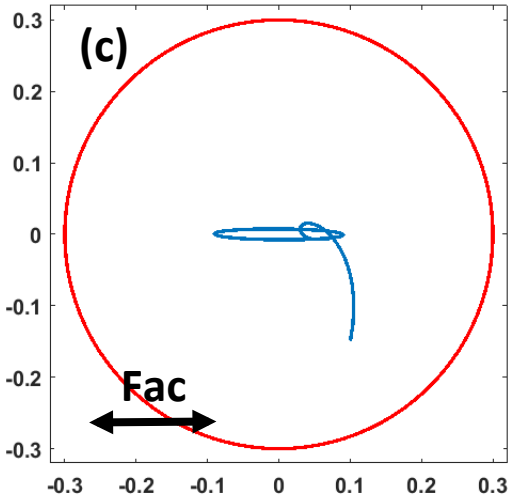

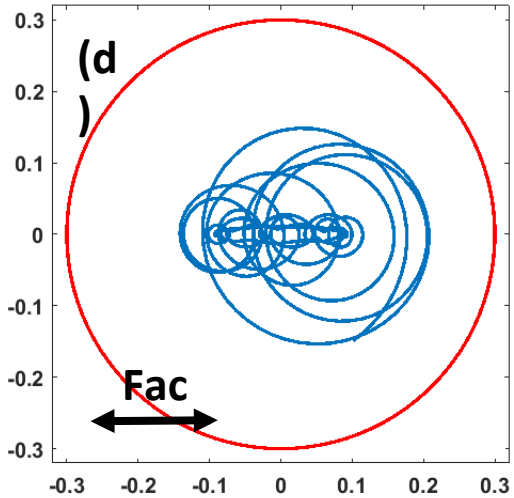

(d) Fac=0.03, α_m/α_d =30

Isolated Skyrmion within a Harmonic Trap with AC Drive (x direction, α_m/α_d=10)

(a) Fac=0.05, Fdc=0.04

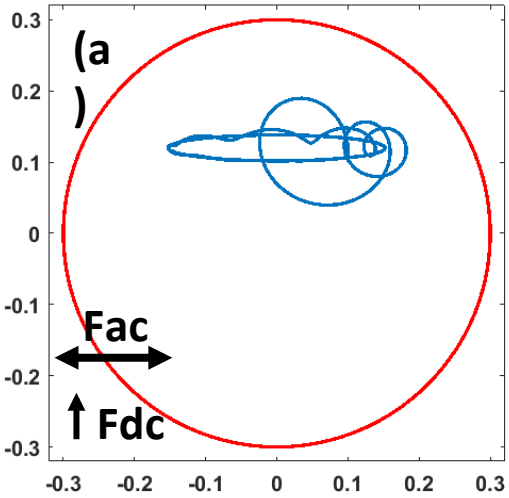

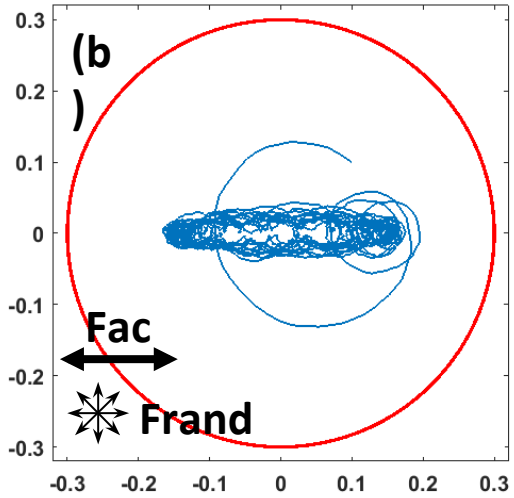

(b) Fac=0.05, Frand=0.02

(c) Fac=0.05, Frand=0.05

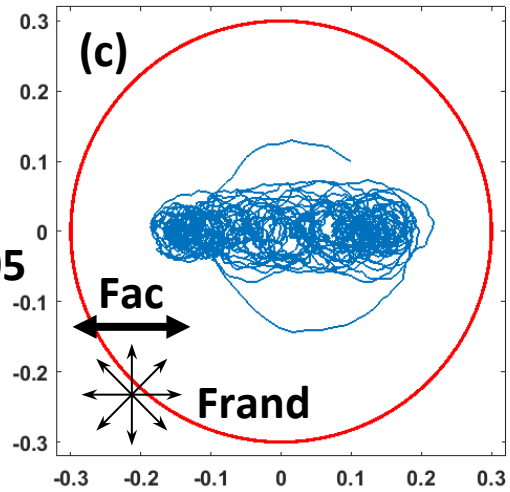

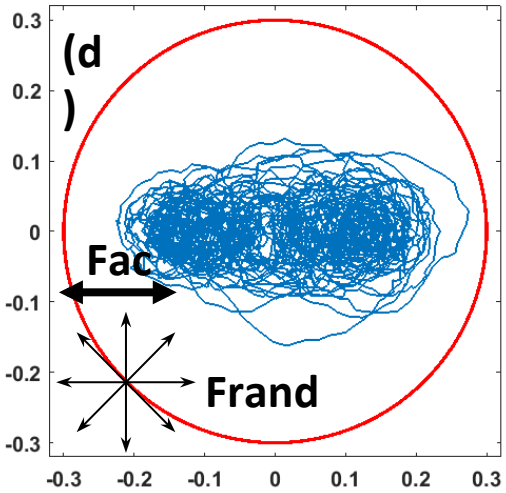

(d) Fac=0.05, Frand=0.09

Conformal Pinning Array [7]

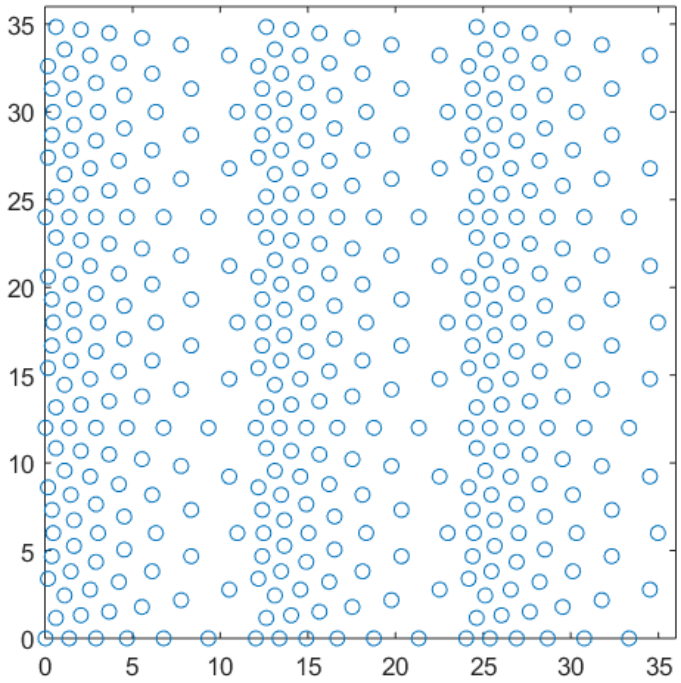

System size: 36×36

Same density: $n_p = n_s = 0.3$

$F_{pmax} = 0.1$ $r_p = 0.3$

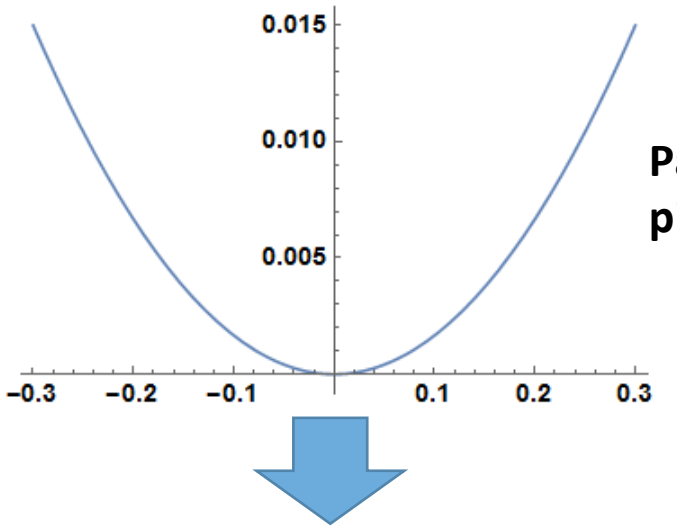

Parabolic pinning site

Hook's law: $F = -k \cdot r$, $k = 0.1/0.3$, $|r| \leq 0.3$

---

[7] C. Reichhardt, D. Ray, C. J. Olson Reichhardt, Phys. Rev. B 91, 184502, 2015

DC property (α_m / α_d=9.962)

Hall angle: $tan^{-1}|\langle V_\perp \rangle| / |\langle V_{drive} \rangle|$

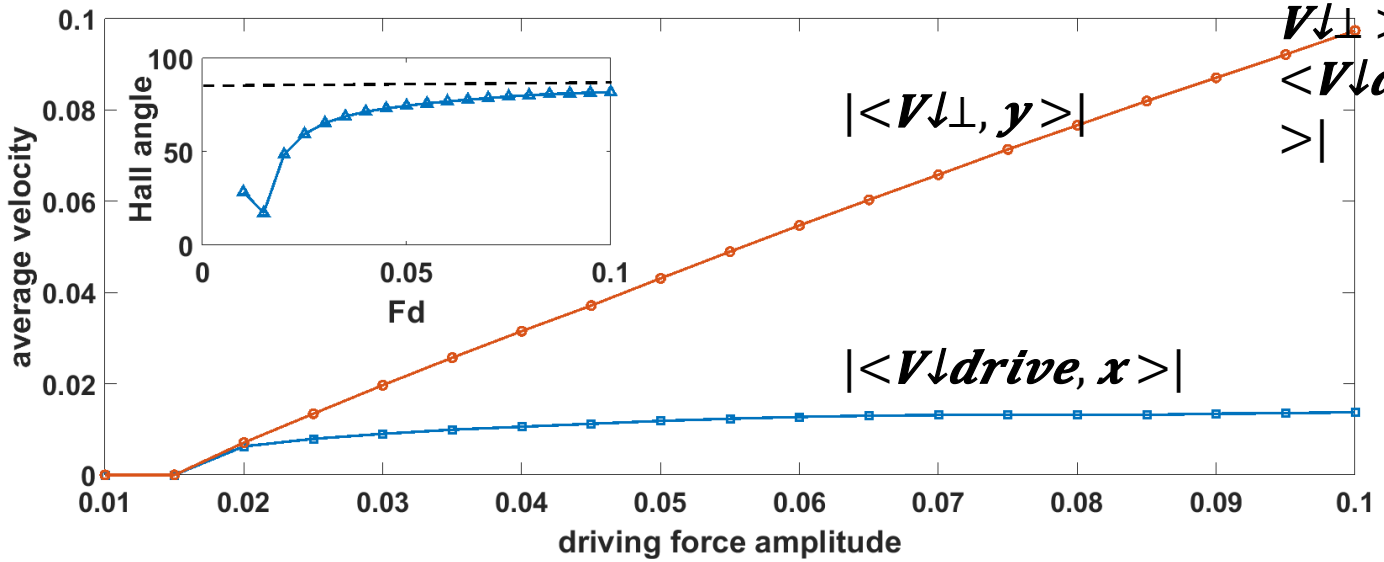

drive in x direction

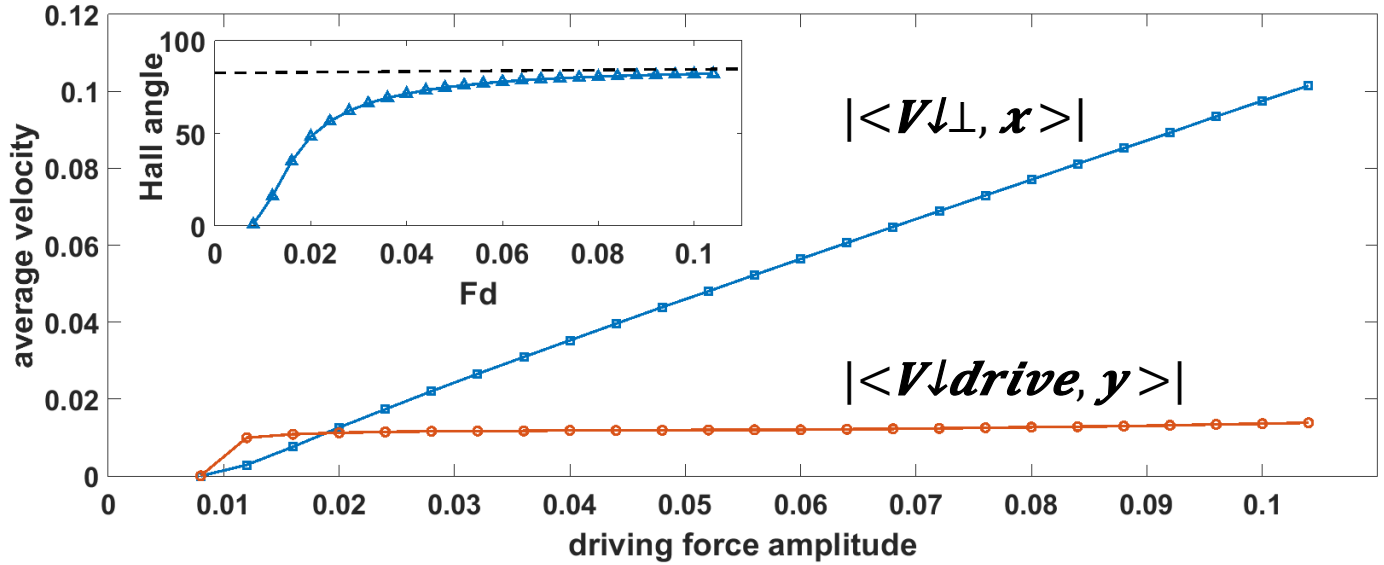

drive in y direction

AC Property & Ratchet Effect

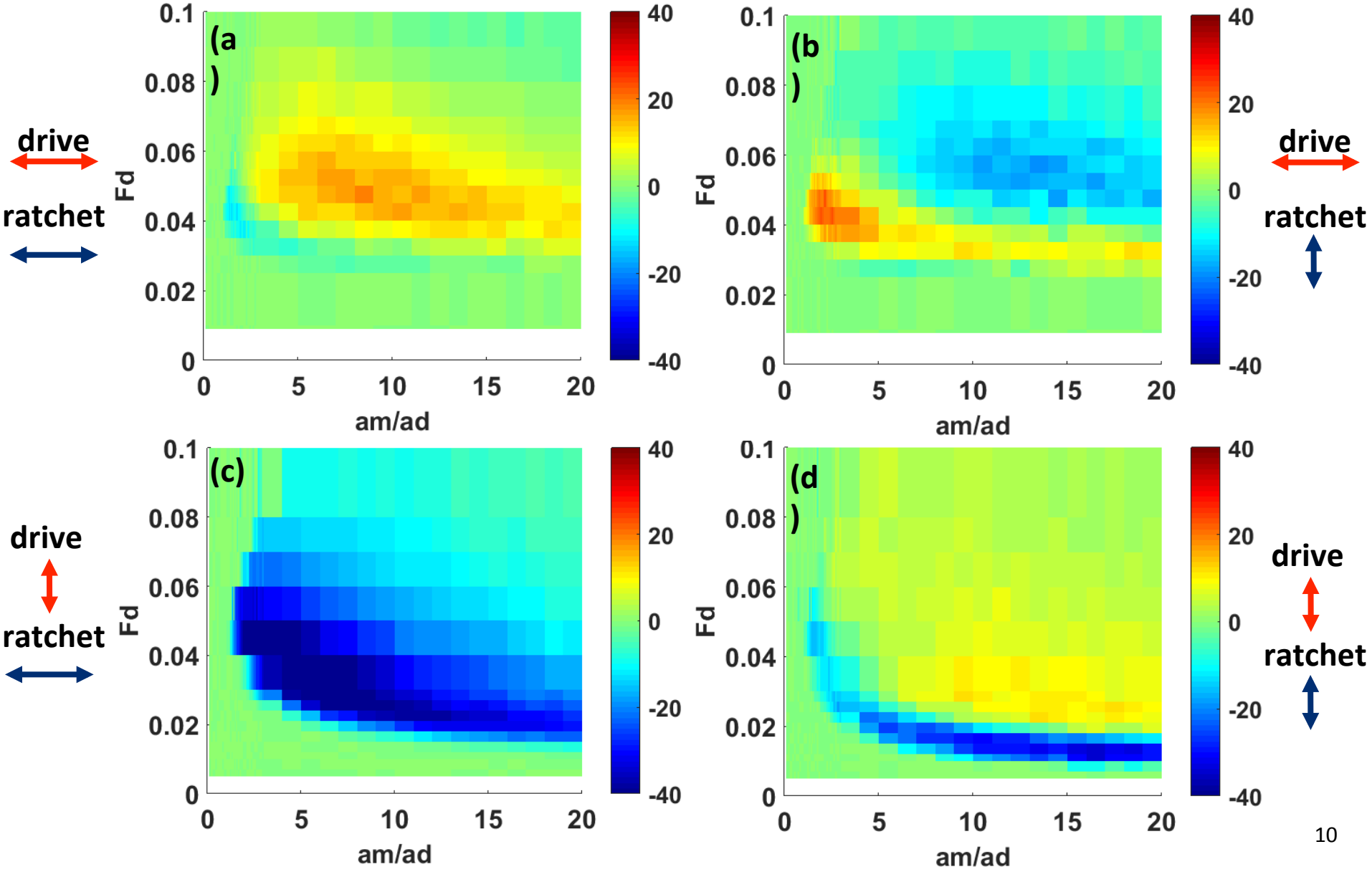

Strongly Pinned Region (α_m / α_d=9.962)

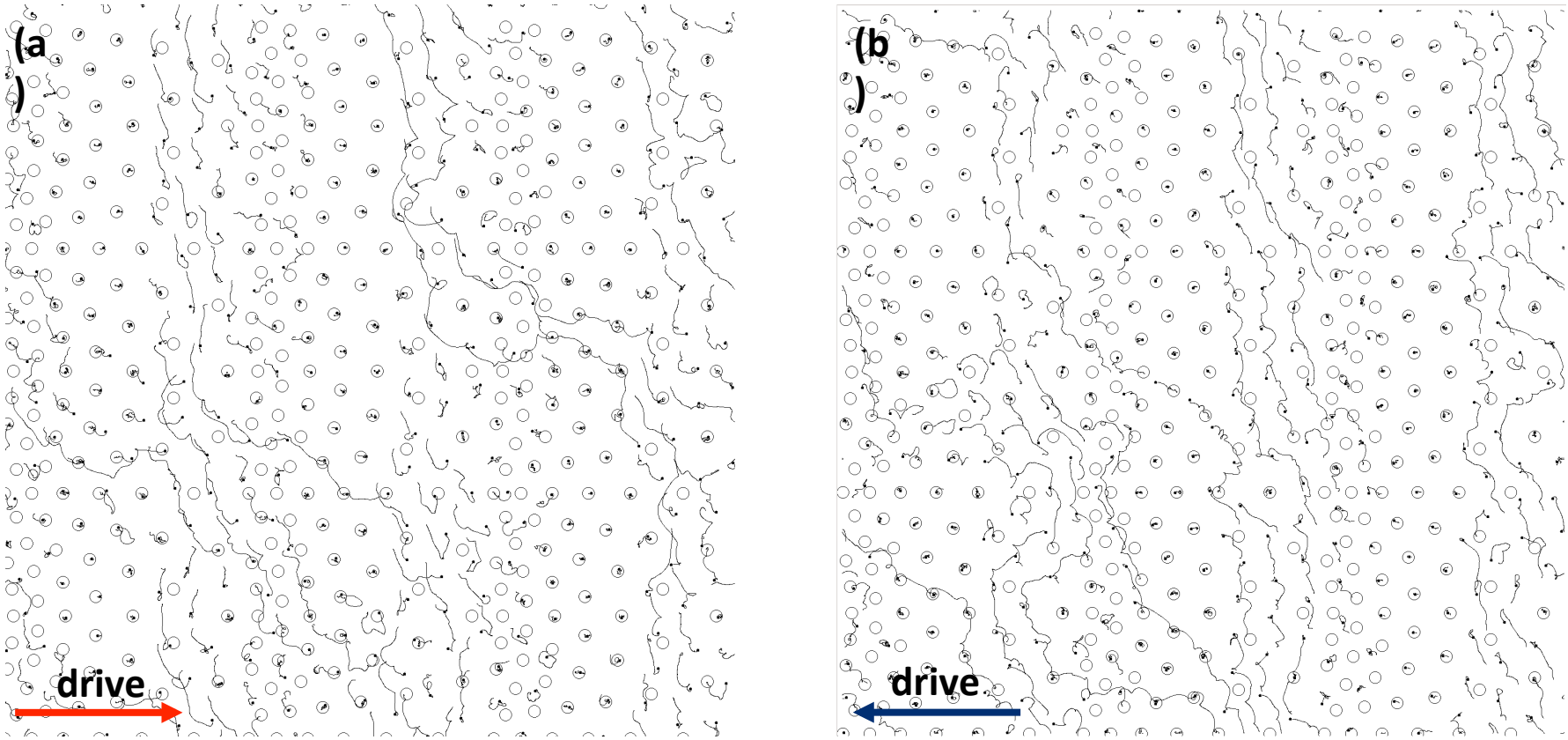

AC drive in x direction with amplitude 0.03. (a) trajectory in positive half cycle, (b) trajectory in negative half cycle.

Strongly Pinned Region ($\alpha_{\downarrow m}/\alpha_{\downarrow d}$=9.962)

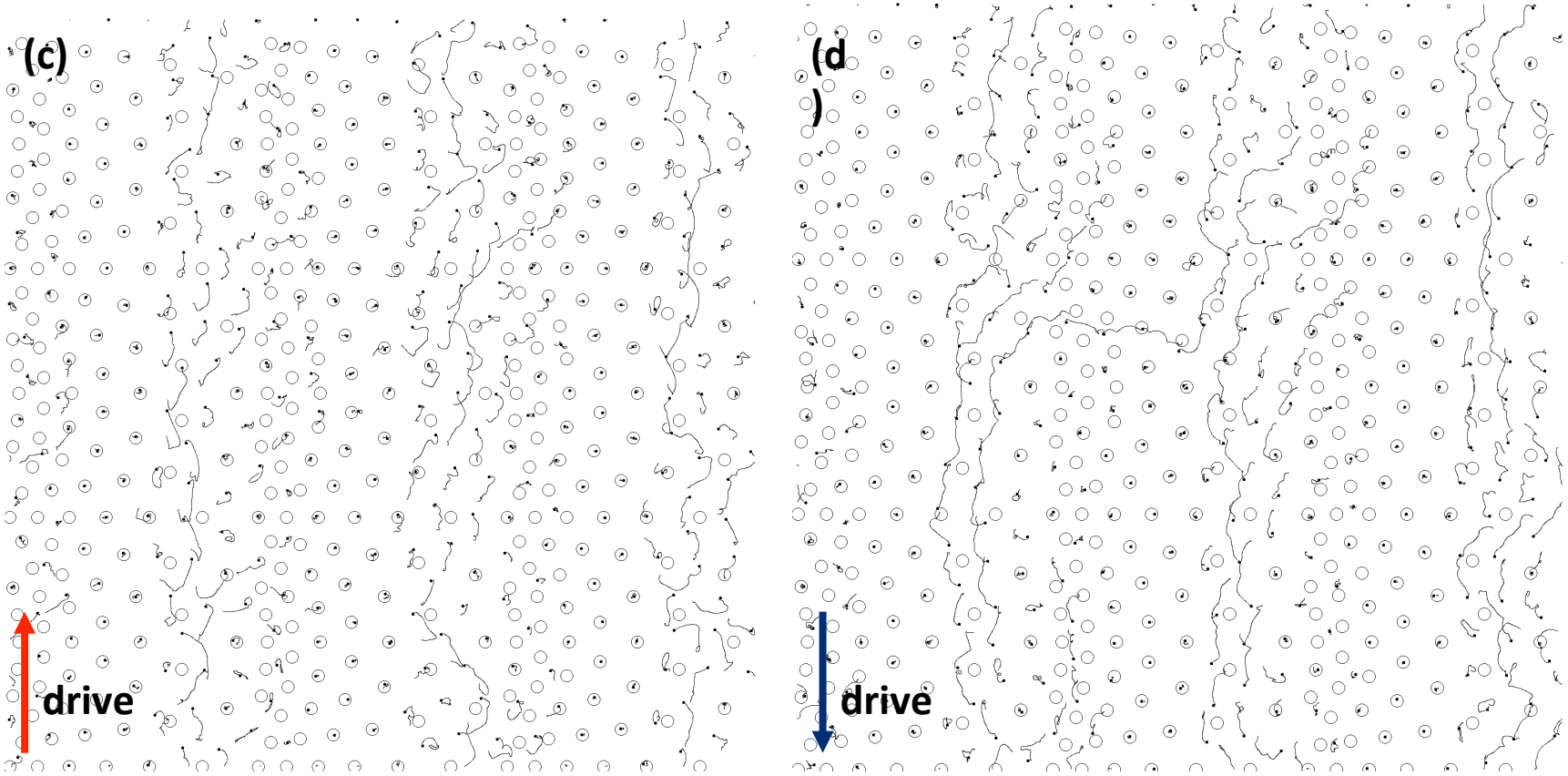

AC drive in y direction with amplitude 0.013. (c) trajectory in positive half cycle, (d) trajectory in negative half cycle.

Strongly Pinned Region (α_m / α_d=9.962)

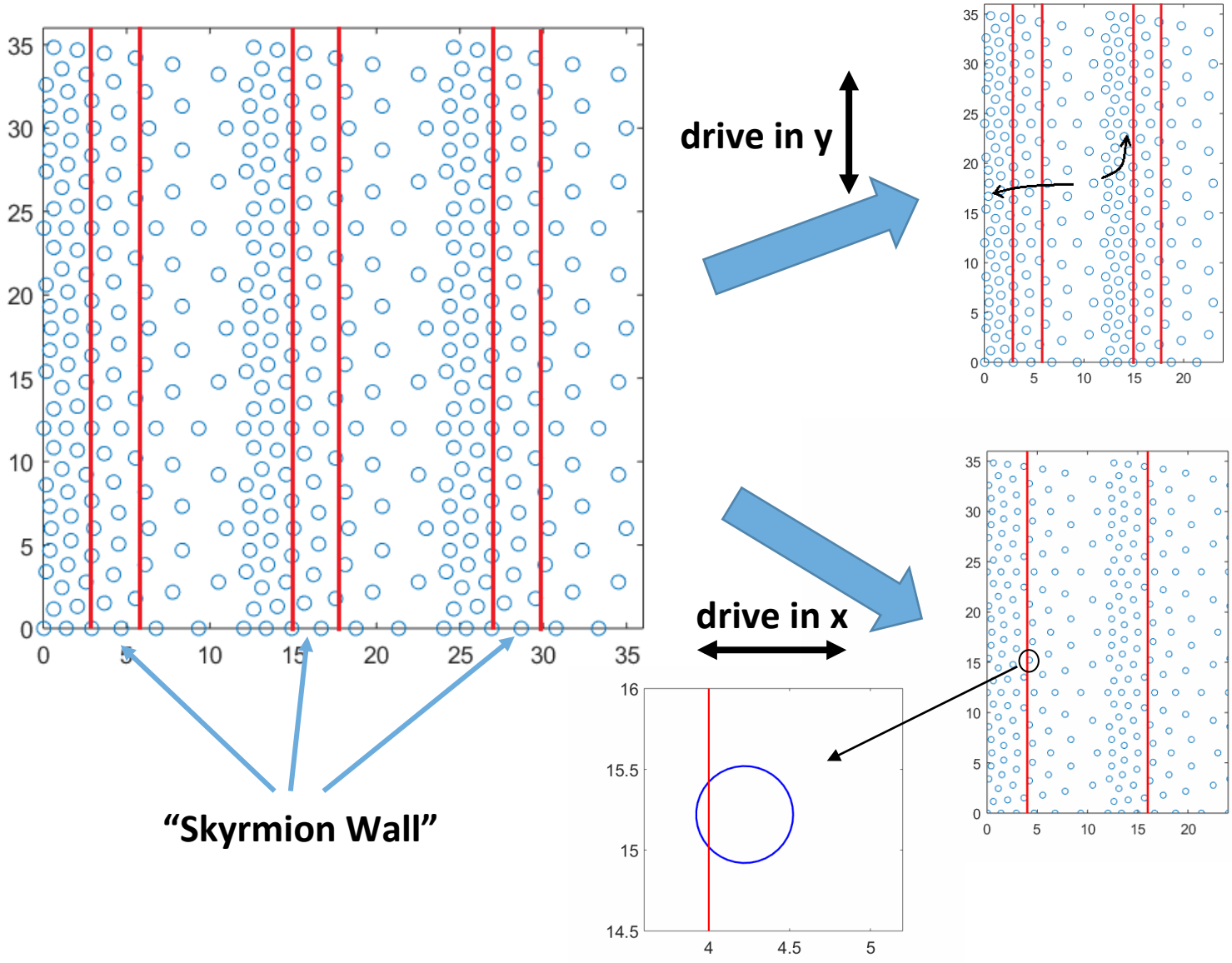

Conclusion

- **Interaction of an isolated skyrmion within a parabolic pinning site**
- **Collective transport properties with a conformal pinning array, ratchet effect**
- **Ratchet effect due to different depinning process**

Acknowledgement

- **Cynthia Reichhardt (LANL T-1)**

  Charles Reichhardt (LANL T-4)

  Boldizsar Janko (University of Notre Dame)

- **Yang Yang (Wabash College)**

  Minh Quan Le Thein (Wabash College)

  Hong Nguyen (University of South Florida)

Superconducting Vortices on a Disordered Hyperuniform Pinning Array

Le Thien Minh Quan

Wabash College
LANL T-1

Mentor: Dr. Cynthia Reichhardt
Professor Danielle McDermott
Dr. Charles Reichhardt

Superconductors

- No Apparent Electrical Resistance
- Zero-point energy levitation
- **Critical current is important!**

https://en.wikipedia.org/wiki/Superconductivity#/media/File:Stickstoff_gek%C3%BChlter_Supraleiter_schwebt_%C3%BCber_Dauermagneten_2009-06-21.jpg

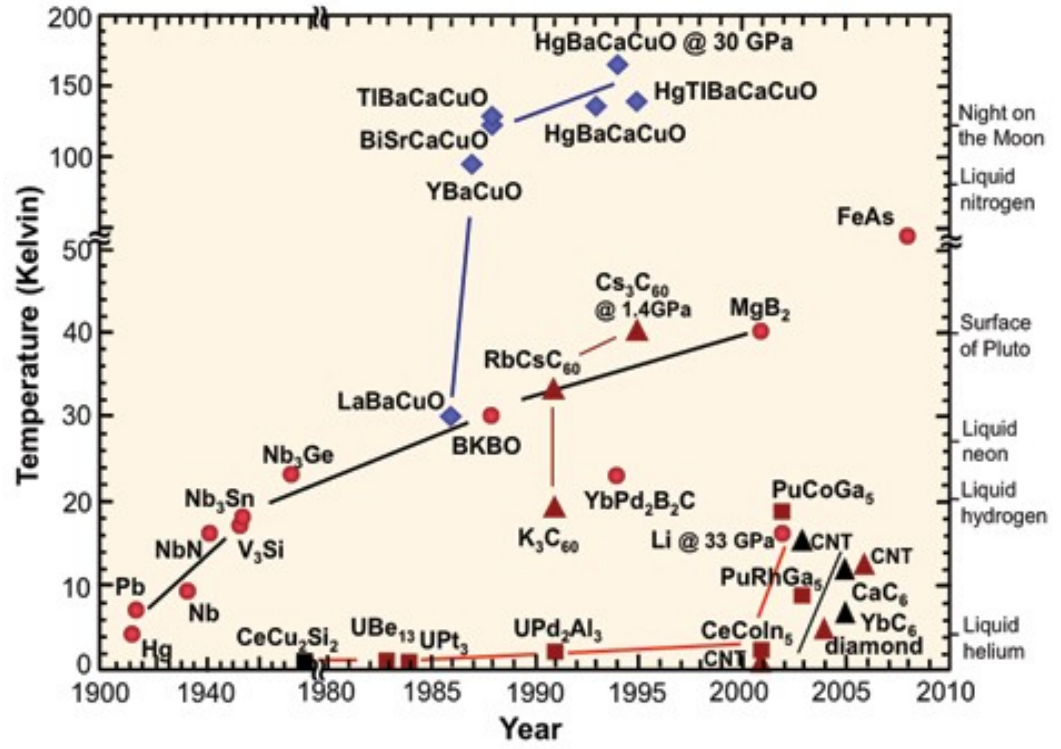

http://www.ccas-web.org/superconductivity/#image1

Quantum Vortices in Type-II Superconductor

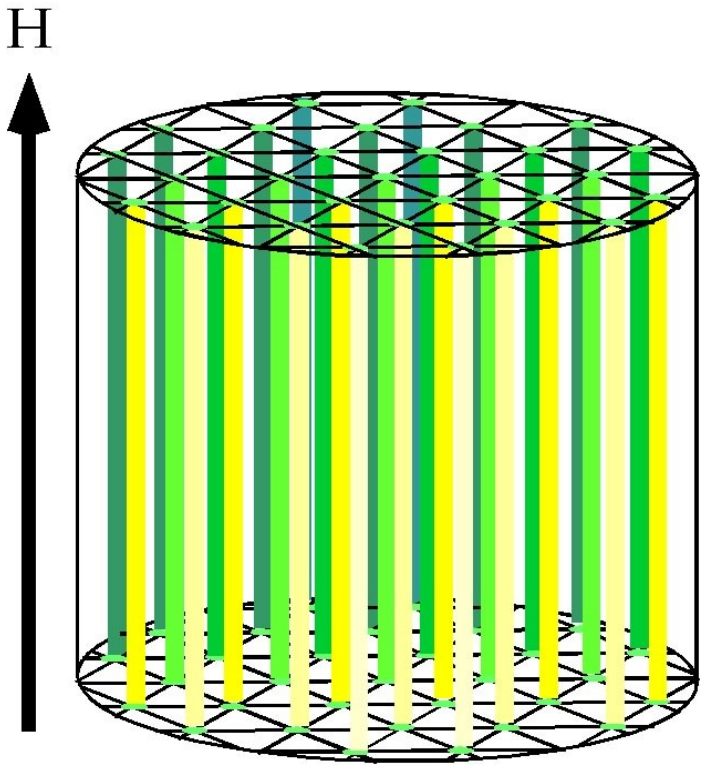

http://www.mmp.ph.qmul.ac.uk/~drew/?p=110

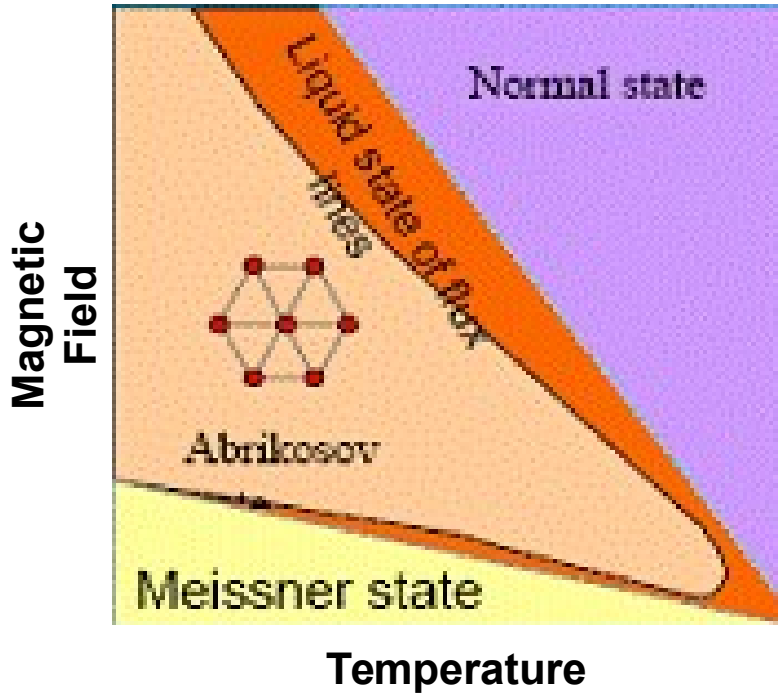

http://www.ims.demokritos.gr/people/mpissas/superconductivity.htm

Vortex Pinning

- The movement of the vortices creates resistive mixed state in type-II superconductors.
- Enhancement of pinning mechanisms via artificial pinscapes.

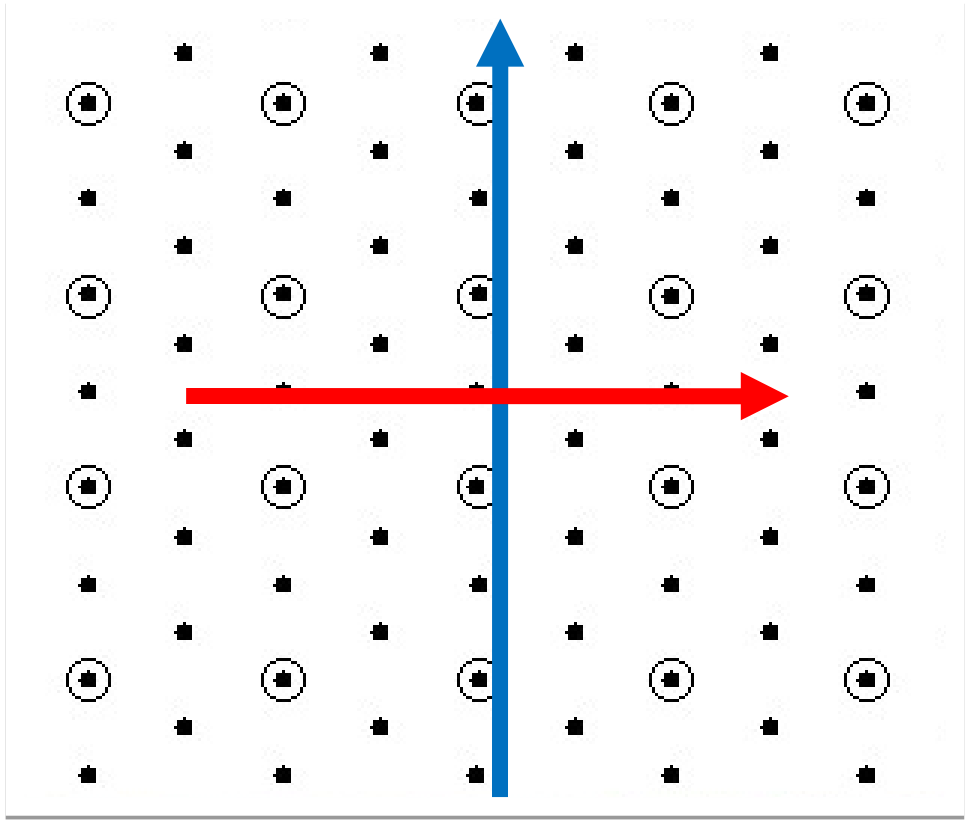

Electrical Current

$F_{Lorentz}$

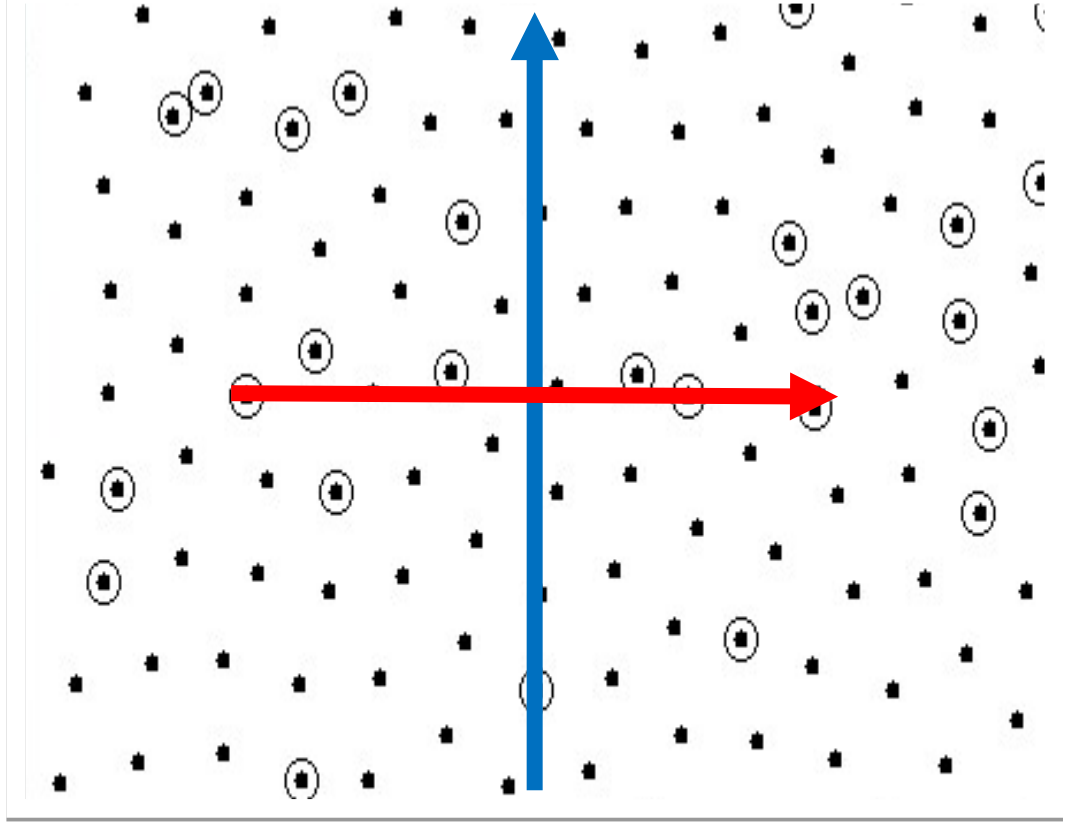

Vortex Pinning

- Effective channels created by periodicity.
- Distributing the pinning force evenly through out the system

  → Limits on long-scale variation of density fluctuation of a Disordered Structure.

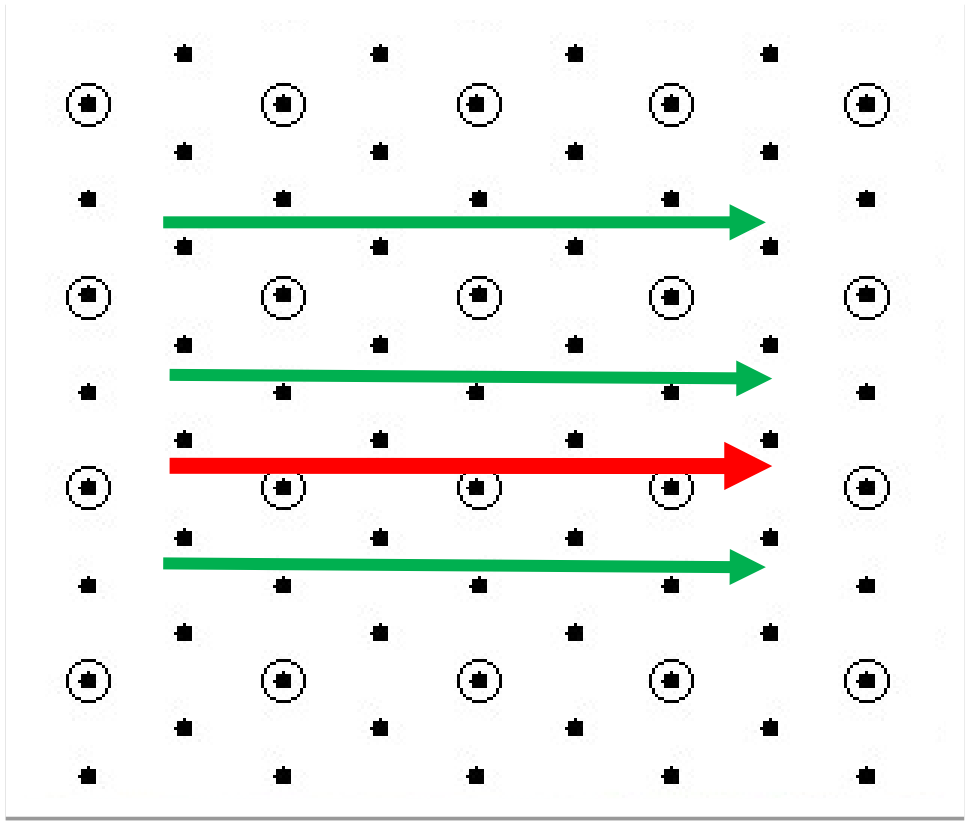

Effective Channels

$\vec{F}_{Lorentz}$

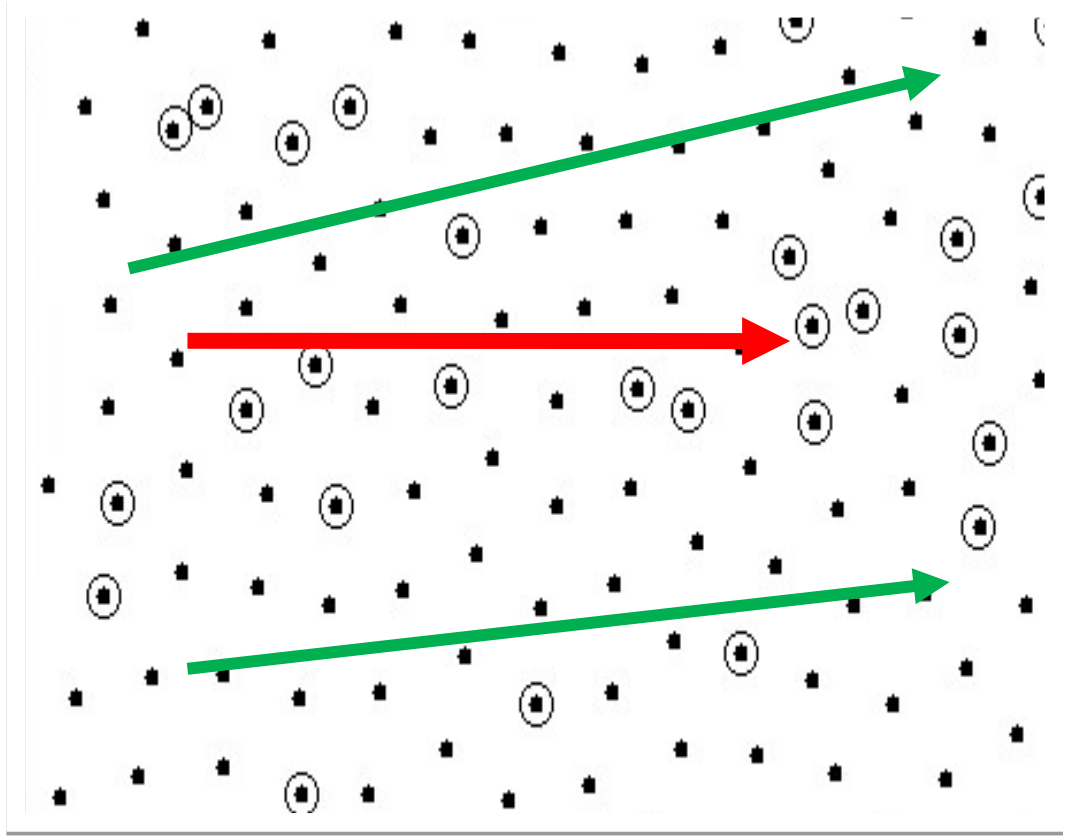

Hyperuniformity

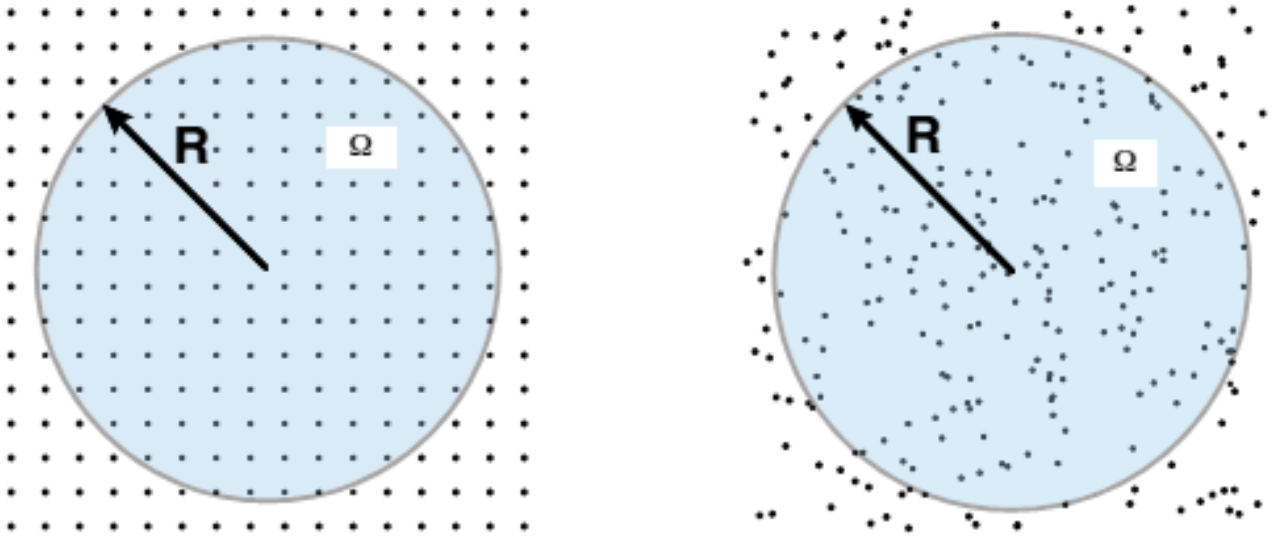

- $N(R)$: Number of points in Region Ω
- $Var(N(R)) = \langle N^2(R) \rangle - \langle N(R) \rangle^2$
- For a Poisson Random Process, $Var(N(R)) \sim R^2$.
- If $Var(N(R)) \sim R^{\alpha}$ and $\alpha < 2$, the system is said to have a hyperuniform structure.

S. Torquato and F. H. Stillinger, Phys. Rev. E 68, 041113 (2003)

Disordered Hyperuniform Pinning Array

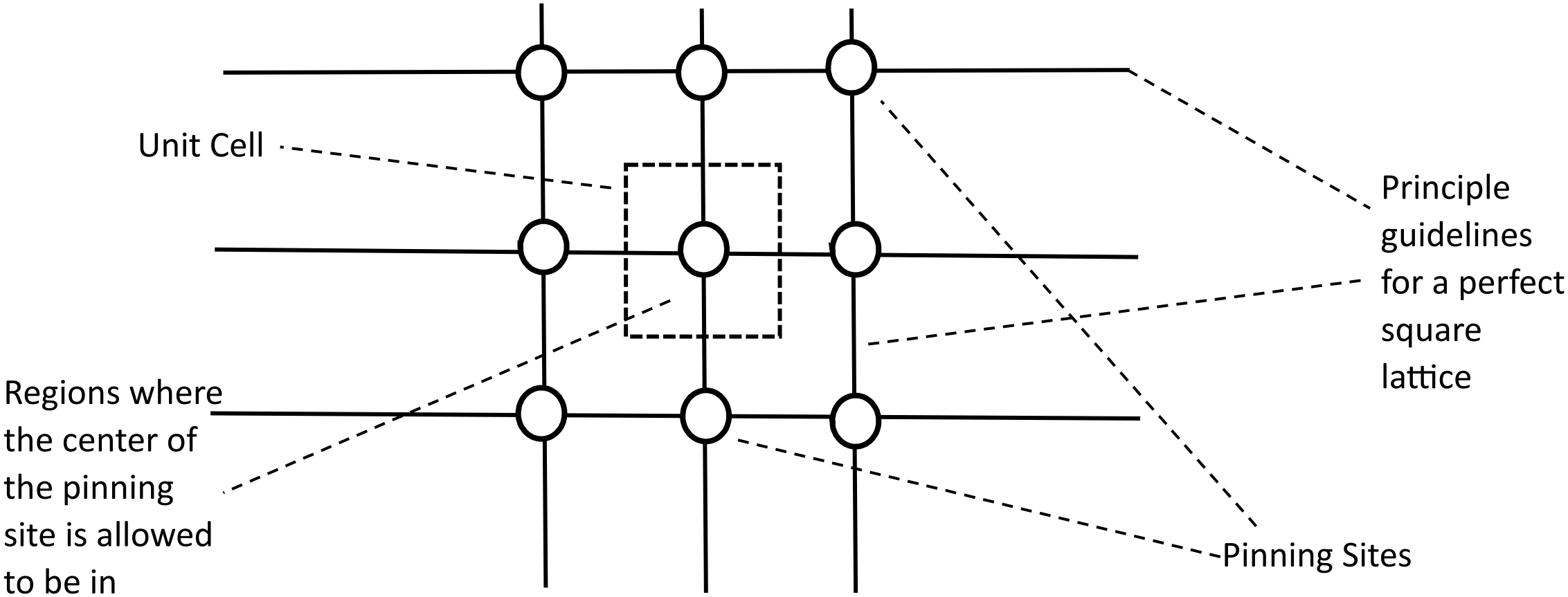

Disordered Hyperuniform Pinning Array

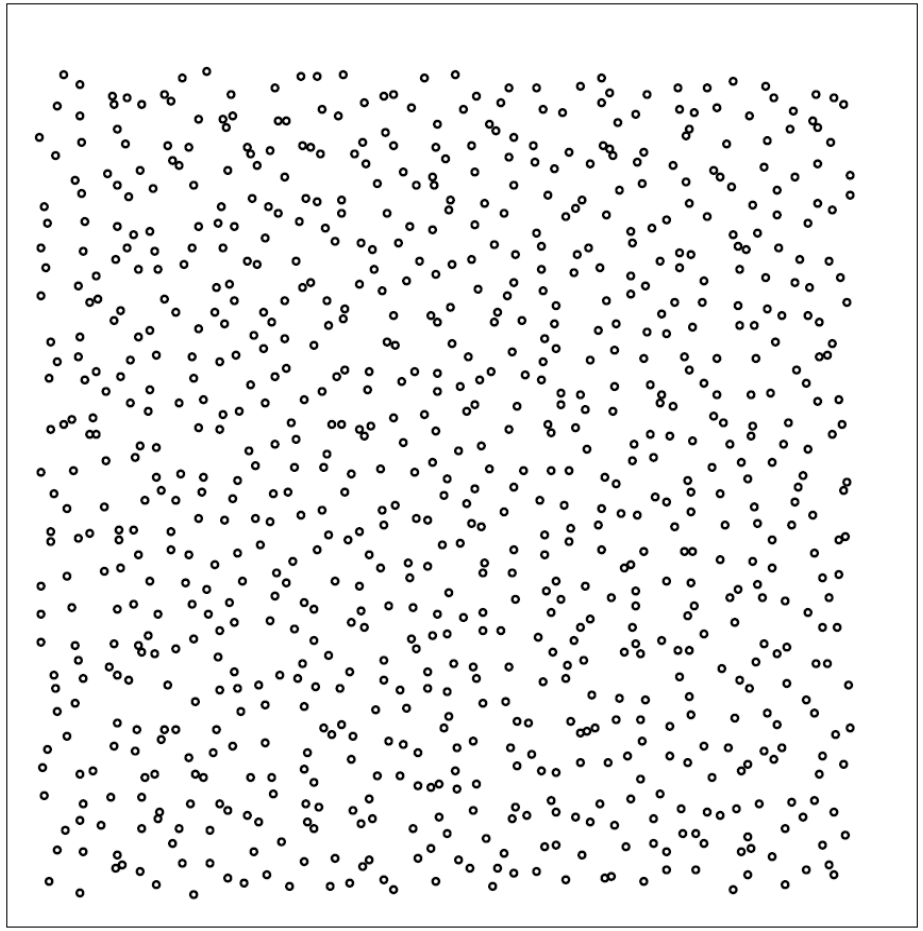

Disordered Hyperuniform

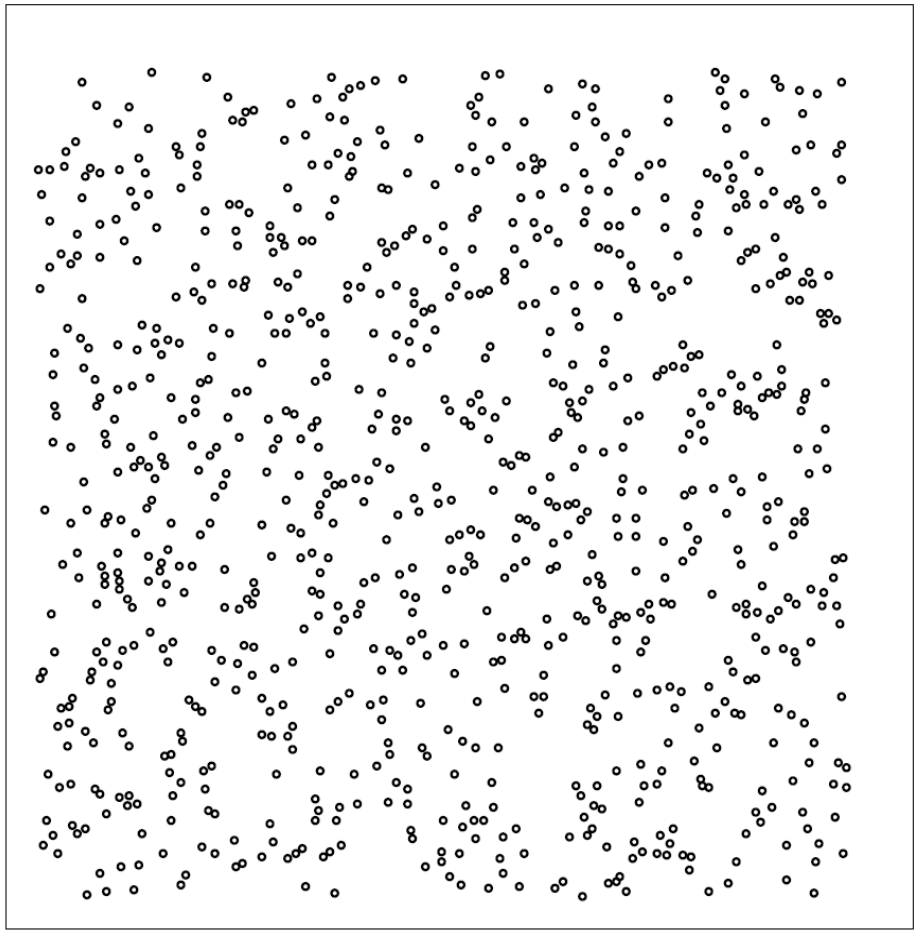

Poisson Random

Model of Superconducting Vortices

- London approximation where quantum vortices can be treated as classical particles.

- Molecular Dynamics (Langevin Dynamics):

$$\vec{F}_i = \vec{F}_i^{vv} + \vec{F}_i^{vp} + \vec{F}_i^{th} + \vec{F}_i^{d} = \eta\, \vec{v}_i$$

Viscosity of the surrounding media

Overdamped motion, thus the velocity is proportional to the net force

Net Force on Vortices

Repulsive Vortex-Vortex interaction

Spring-like pinning force with cut-off range

Thermal Force to simulate Brownian motion

Induced Lorentz Driving Force

Enhancement of Critical Current

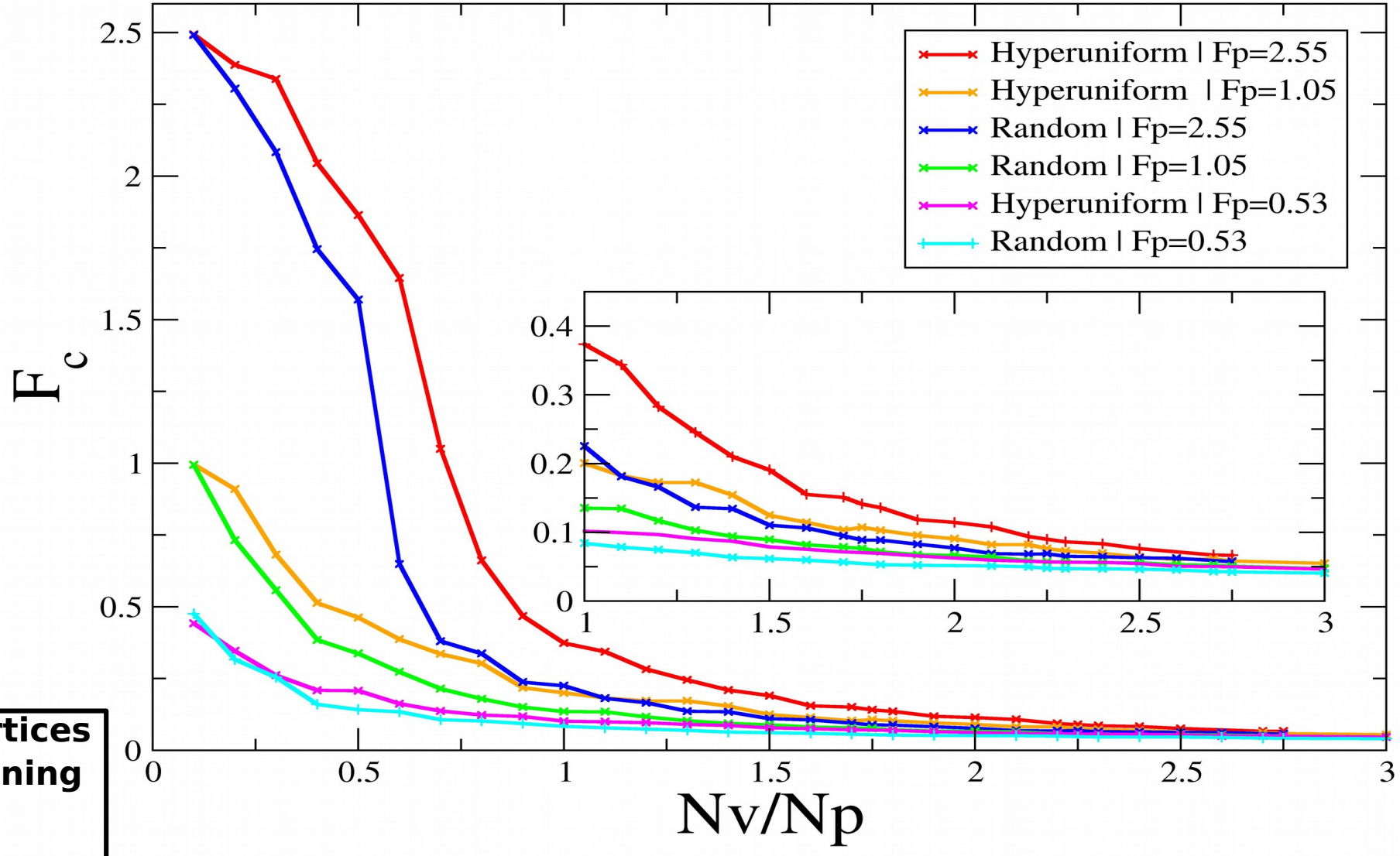

Nv: Number of Vortices
Np: Number of pinning sites

Structural Analysis

- Voronoi Algorithm
- Polygon-6

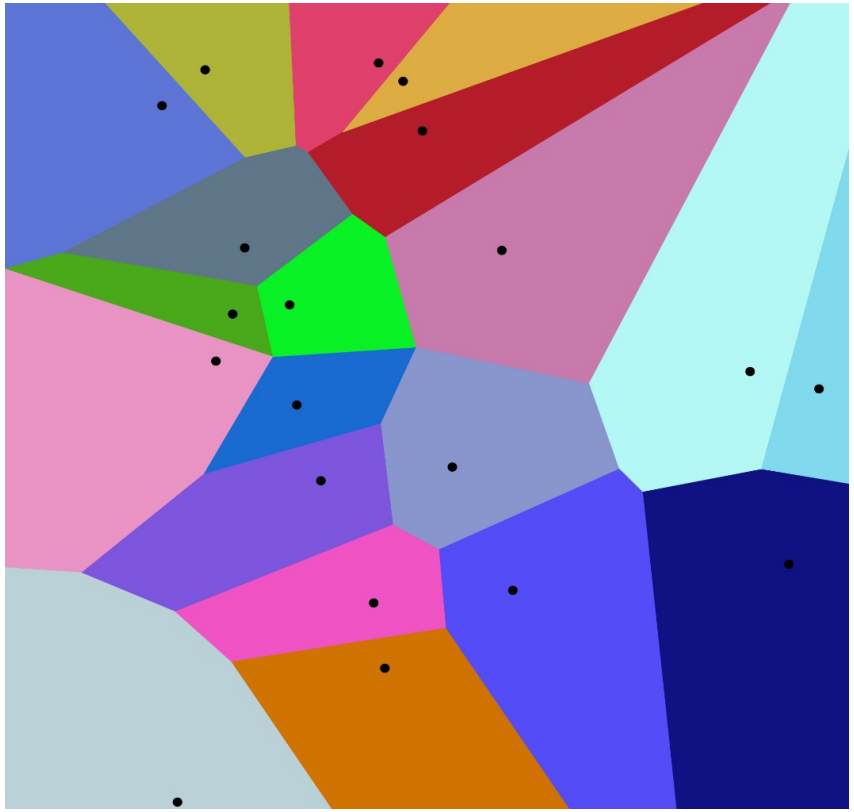

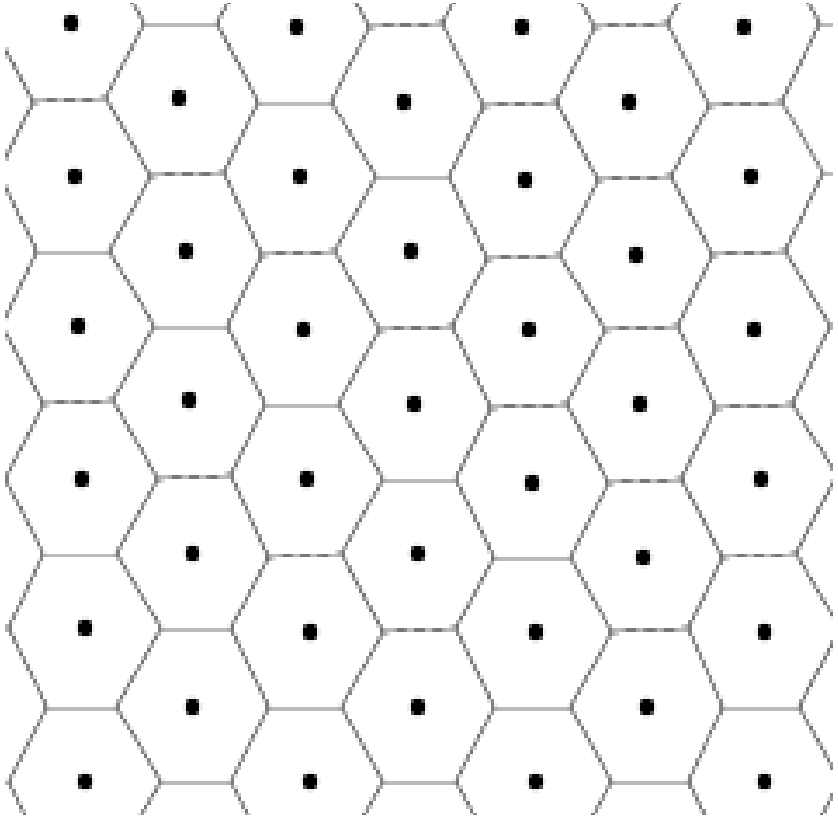

https://en.wikipedia.org/wiki/Voronoi_diagram

Local Induced Disorder

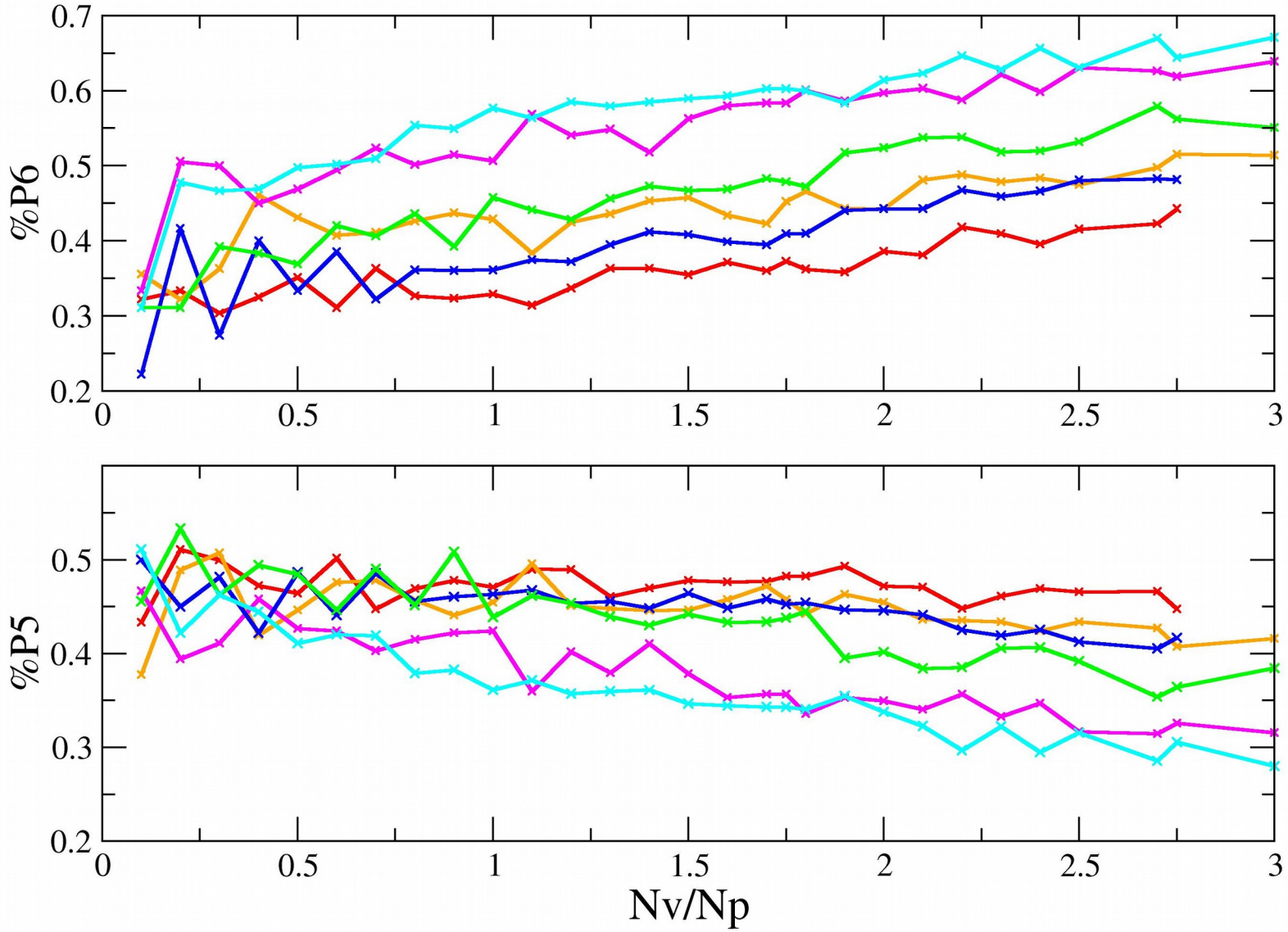

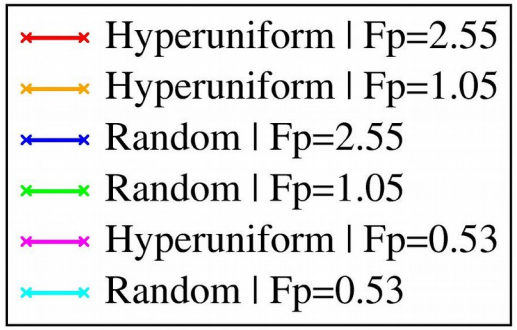

Nv: Number of Vortices
Np: Number of pinning sites

Suppression of Plasticity

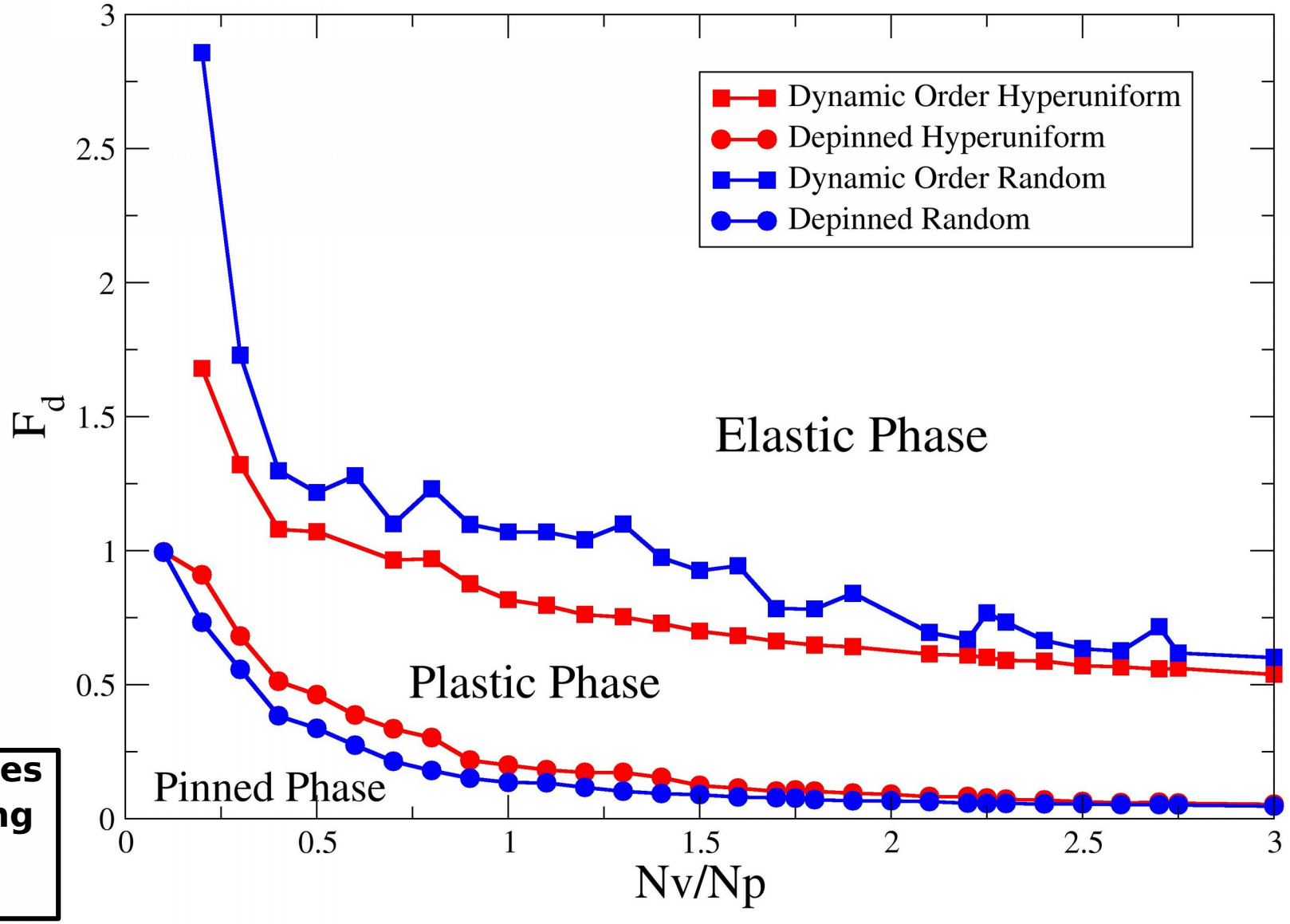

Nv: Number of Vortices
Np: Number of pinning sites

Conclusion

- Disordered Hyperuniform Pinning Array enhances the critical depinning current of the vortex lattices by effectively inducing more local disorder than the Poisson Random Pinning Array.

- Plasticity in moving vortex lattices is suppressed by Disordered Hyperuniform Pinning Array.

→ Provide insights for the study of plasticity in percolation theory.

Acknowledgments

- Xiaoyu Ma
- Yang Yang
- Nguyen Hong Duong
- Erik Skau

Thank You!

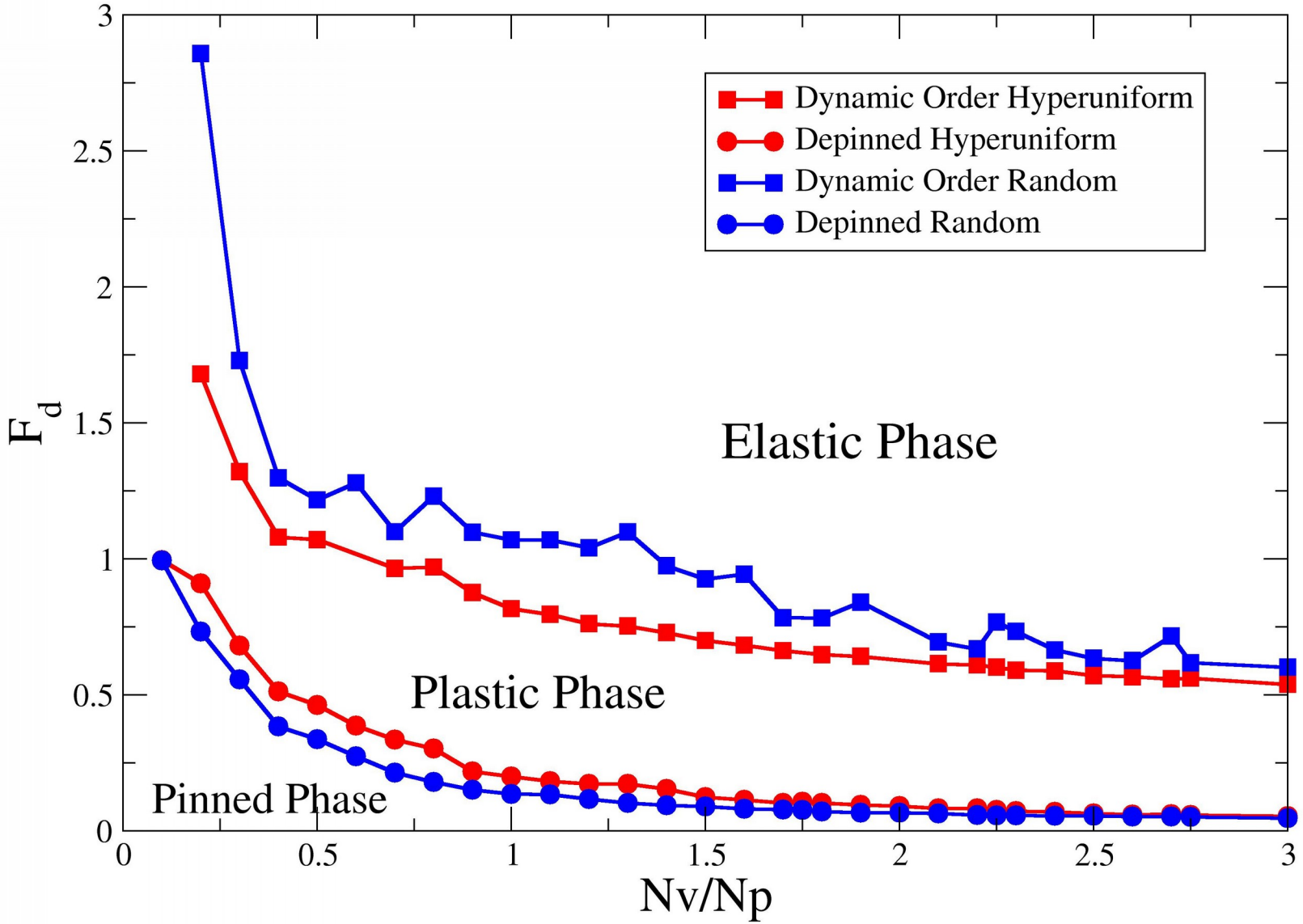
Dynamic Order Hyperuniform
Depinned Hyperuniform
Dynamic Order Random
Depinned Random
Elastic Phase
Plastic Phase
Pinned Phase
F_d
Nv/Np
0
0.5
1
1.5
2
2.5
3

New State of Matter: Disordered Hyperuniform

http://globe-views.com/dreams/eye.html

Random

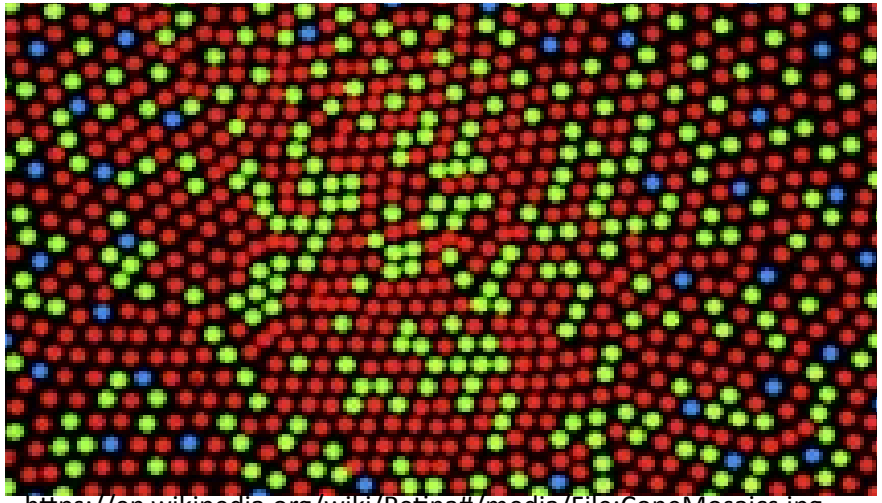

https://en.wikipedia.org/wiki/Retina#/media/File:ConeMosaics.jpg

http://www.backyardchickens.com/t/264409/chicken-eyes-let-me-see-your-pics

Disordered Hyperuniform

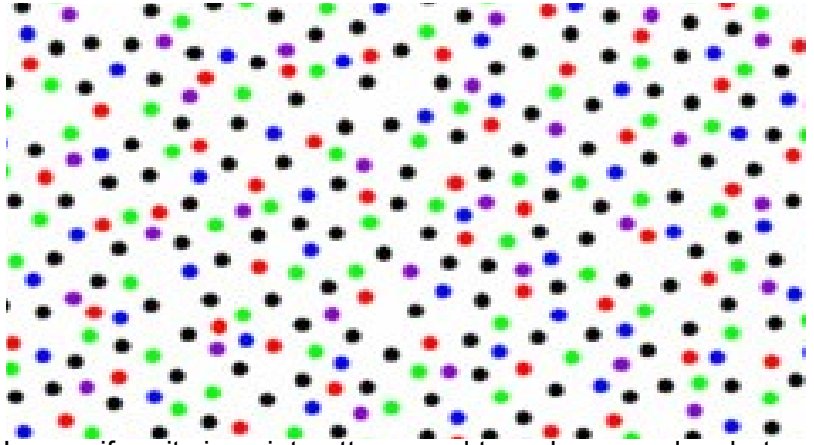

Hyperuniformity in point patterns and two-phase random heterogeneous media, Chase E Zachary and Salvatore Torquato, Journal of Statistical Mechanics: Theory and Experiment, Volume 2009, December 2009

Meissner Effect in type-II Superconductors

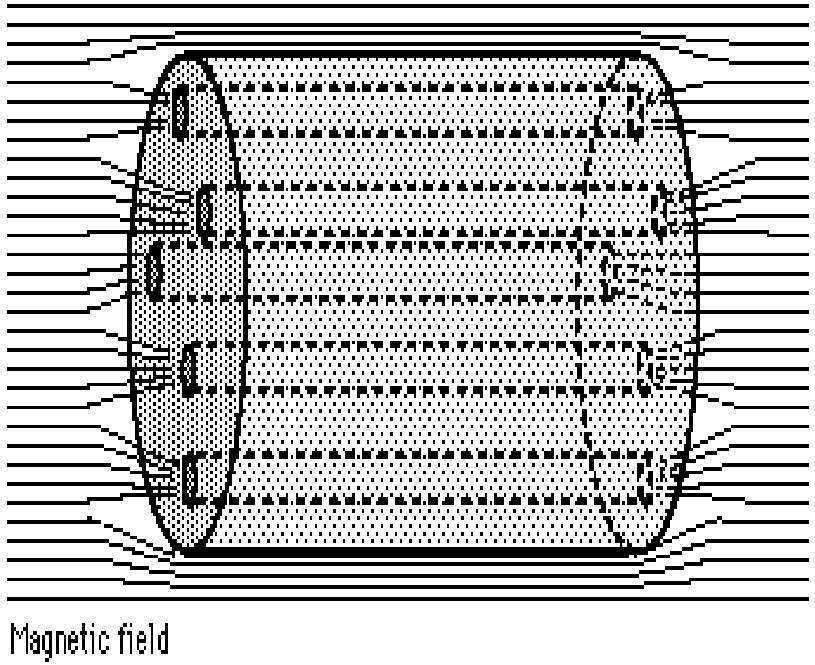

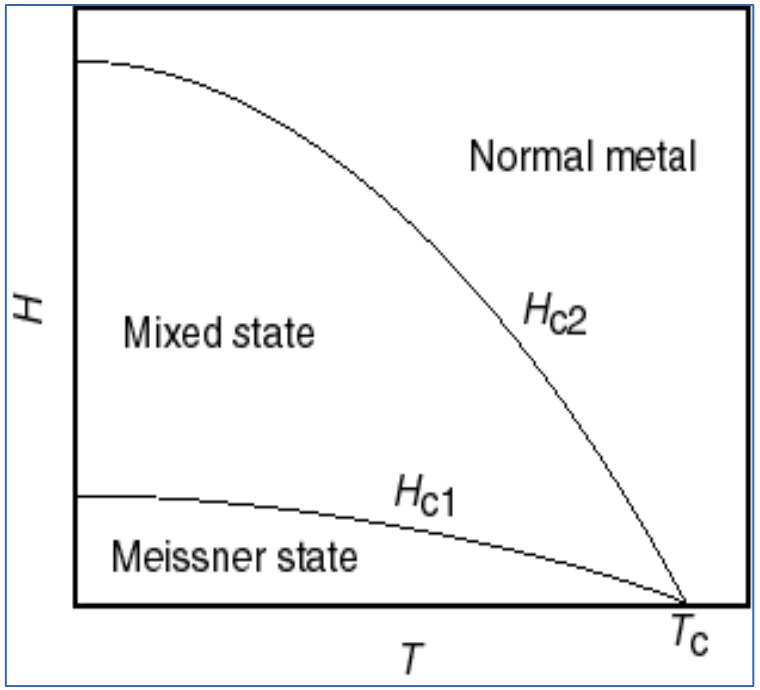

http://hyperphysics.phy-astr.gsu.edu/hbase/solids/meis.html

Clogging of bi-disperse disks driven through periodic landscape

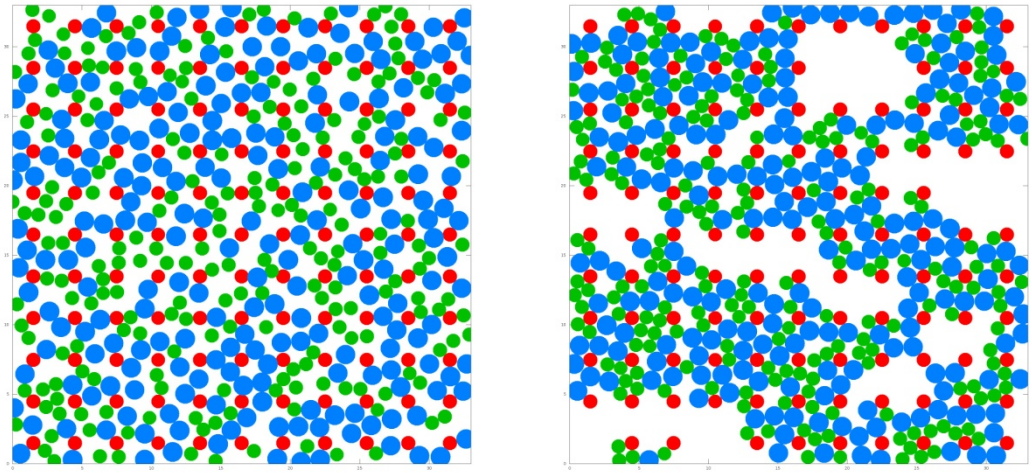

Hong Nguyen

University of South Florida

Charles Reichhardt

Cynthia Reichhardt

Theoretical Division, Los Alamos National Laboratory

Background

Jamming/Clogging: flowing -> stuck state

beans in funnel

Traffic flow

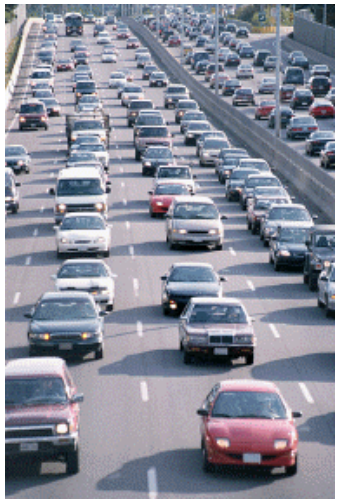

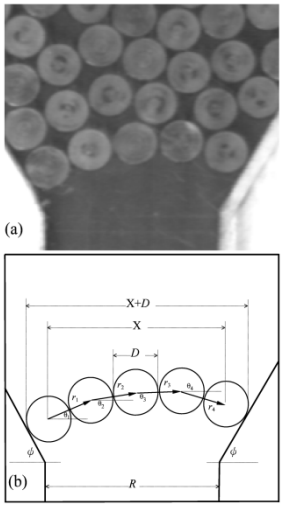

Hopper

(K. To, P. Lai, and H. Pak, PRL 01')

2D bi-disperse model

- **Presence of obstacles**
- **Role of particle density**

-> ability to predict clogging ?

Method

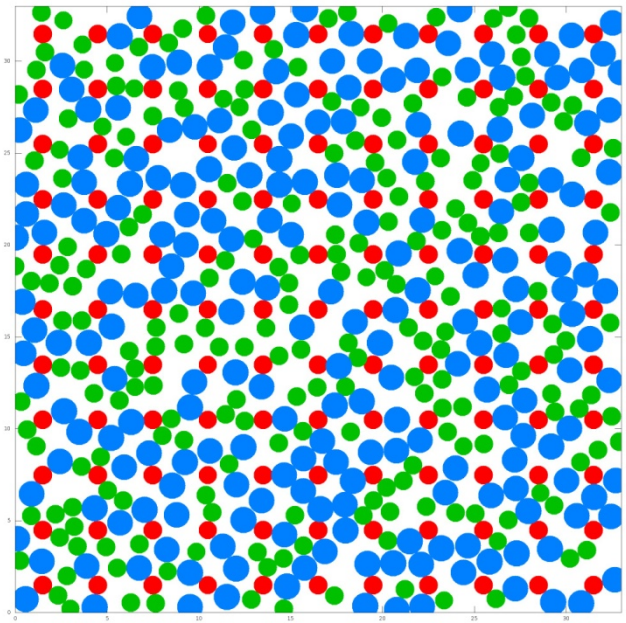

Red: pinned disks (obstacles)

Green, **Blue** : mobile disks

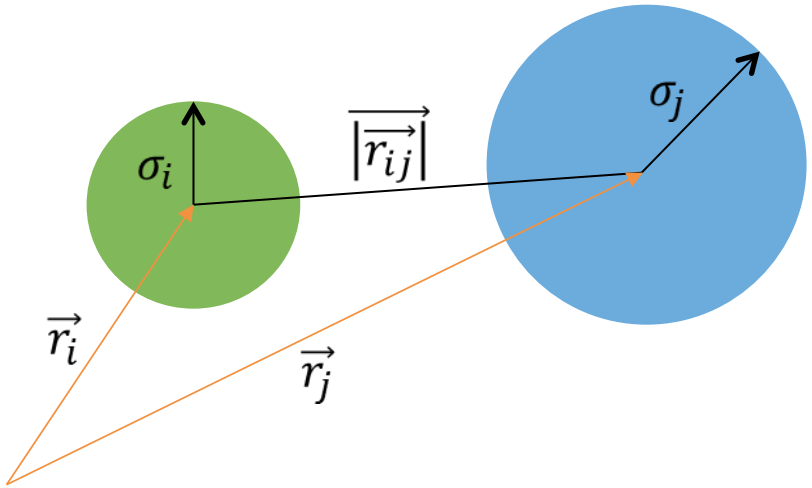

- N_m 50:50 bi-disperse mixture AB of disks $\sigma_A = 1.4\sigma_B$
- N_p obstacles; pinned small disks same as B
- $N = N_m + N_p$
- Grains interact when in physical contact
- $\overrightarrow{F_D}$ applied uniformly on every grains
- Over-damped equation, $\vec{r}_i$ is the position of disk i

$$\eta \frac{d\vec{r}_i}{dt} = \sum_{i \neq j}^{N} k\left(\sigma_{ij} - |\overrightarrow{r_{ij}}|\right)\Theta\left(\sigma_{ij} - |\overrightarrow{r_{ij}}|\right)\widehat{r_{ij}} + \overrightarrow{F_D} \quad (1)$$

$\sigma_{ij} = \sigma_i + \sigma_j$; $\overrightarrow{r_{ij}} = \vec{r}_i - \vec{r}_j$; Θ is Heaviside function

Characterization

- Average velocity $\langle V_{x,y} \rangle = \frac{1}{N_m} \sum_{i=1}^{N} \vec{v}_i \cdot \hat{x}(\hat{y})$
- The largest cluster during simulation
- Local density defined by Voronoi construction

$$\rho_i = \frac{1}{\phi_i}$$

Clogging & flowing states

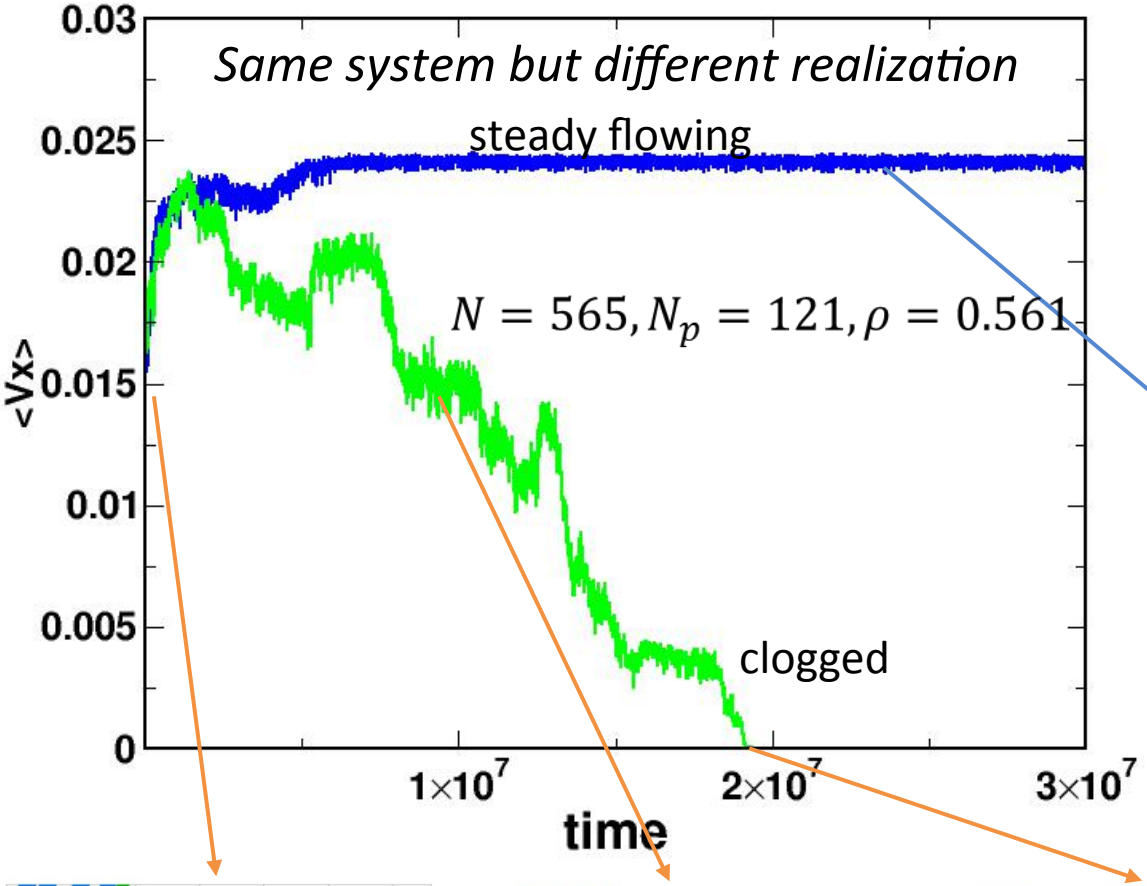

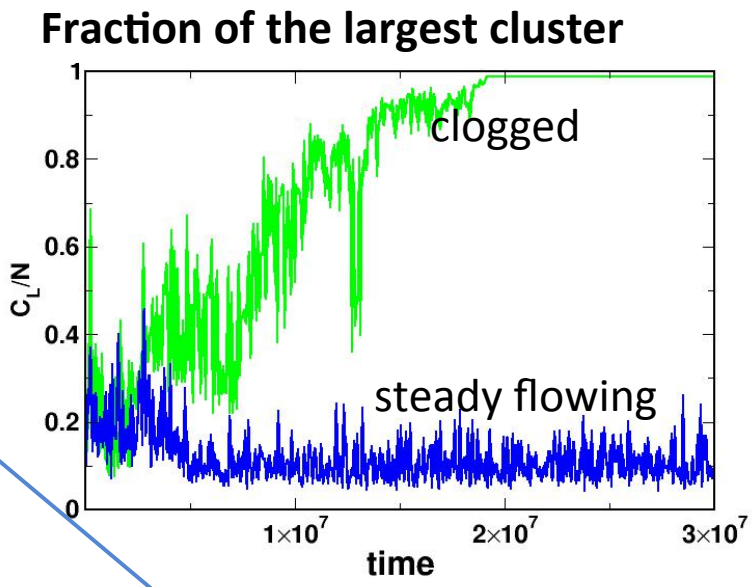

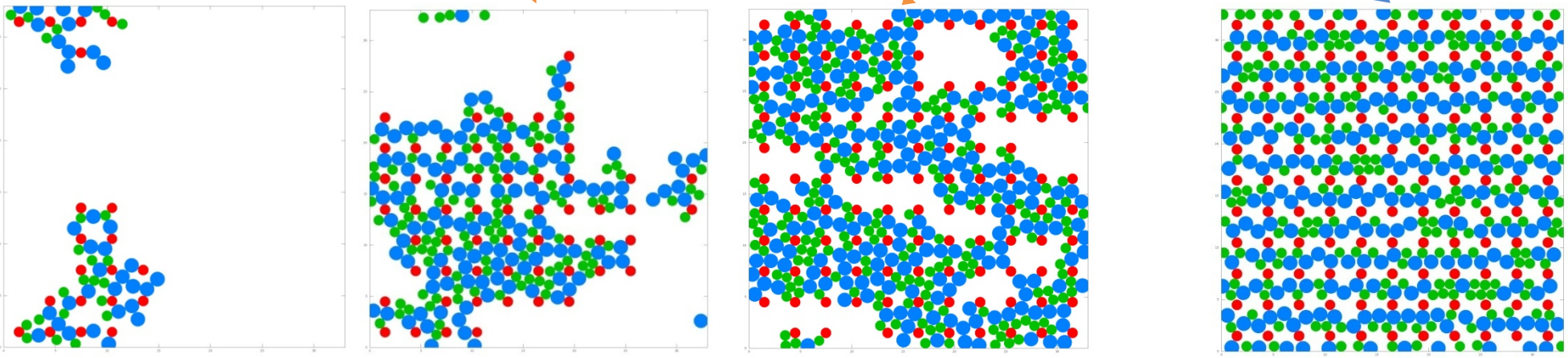

In 2D free-obstacle bi-disperse disks:

$Z = 4, \phi = 0.844$

(C. O'Hern, *et al* PRE 03')

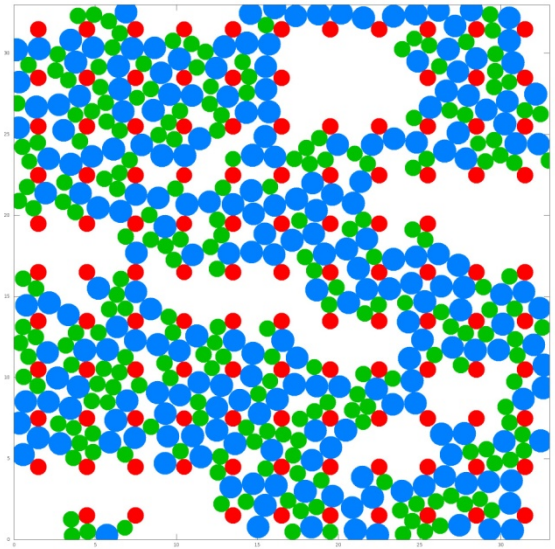

Packing fraction $\phi \ll 0.844$

Z number ~ 3

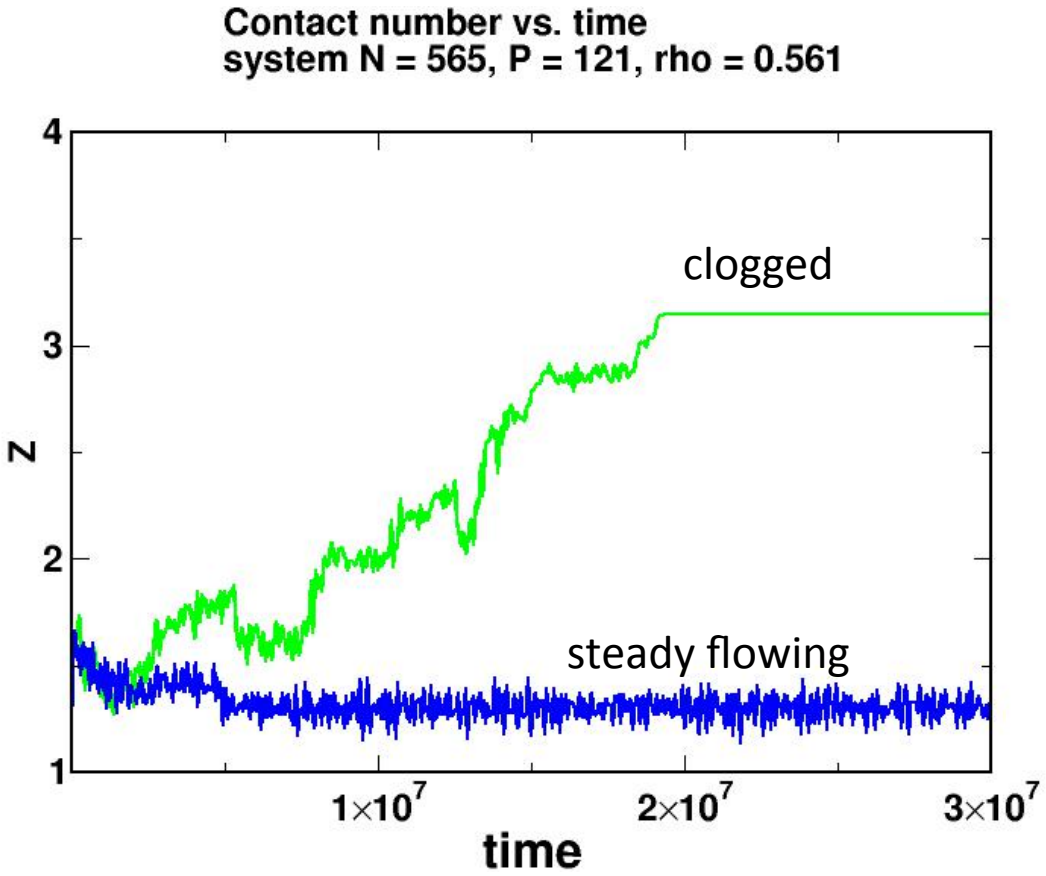

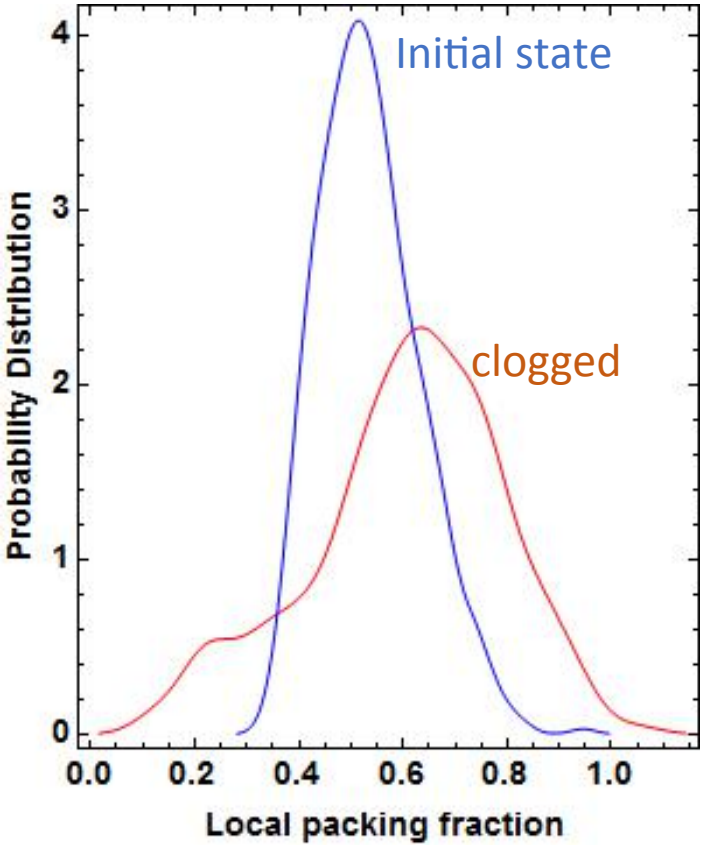

Effect of obstacle spacing

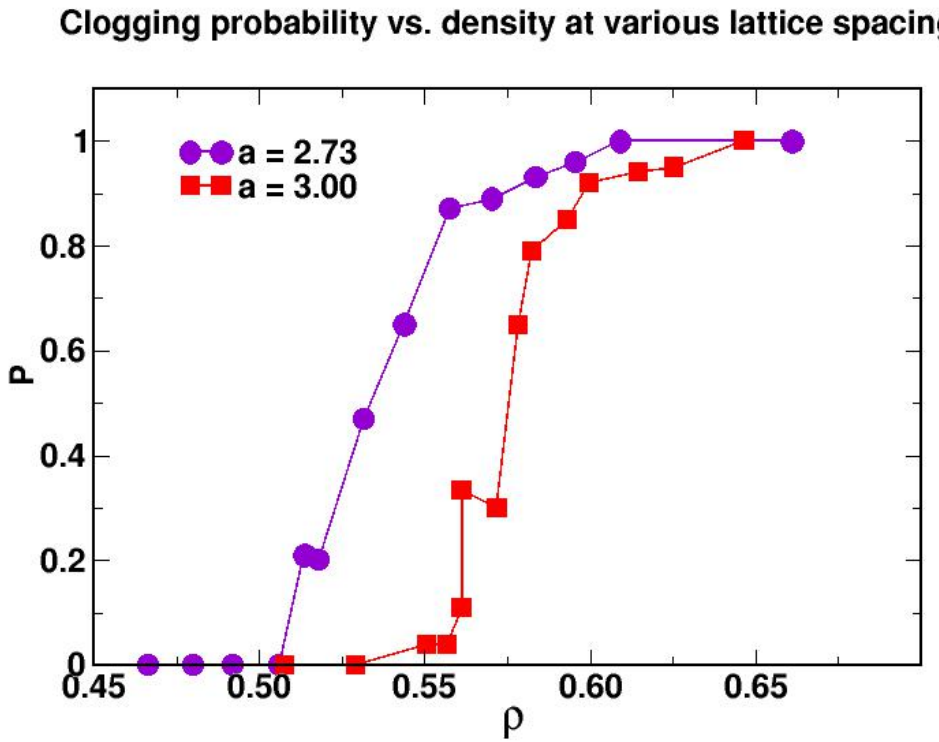

$N = 1600, N_p = 484, \rho = 0.47$

a : lattice constant of obstacle array

Particle density defined as area covered by all disks

$$\rho = [0.5N_m\pi\sigma_A^2 + (N_p{+}0.5N_m)\pi\sigma_B^2]/L^2$$

Hopper

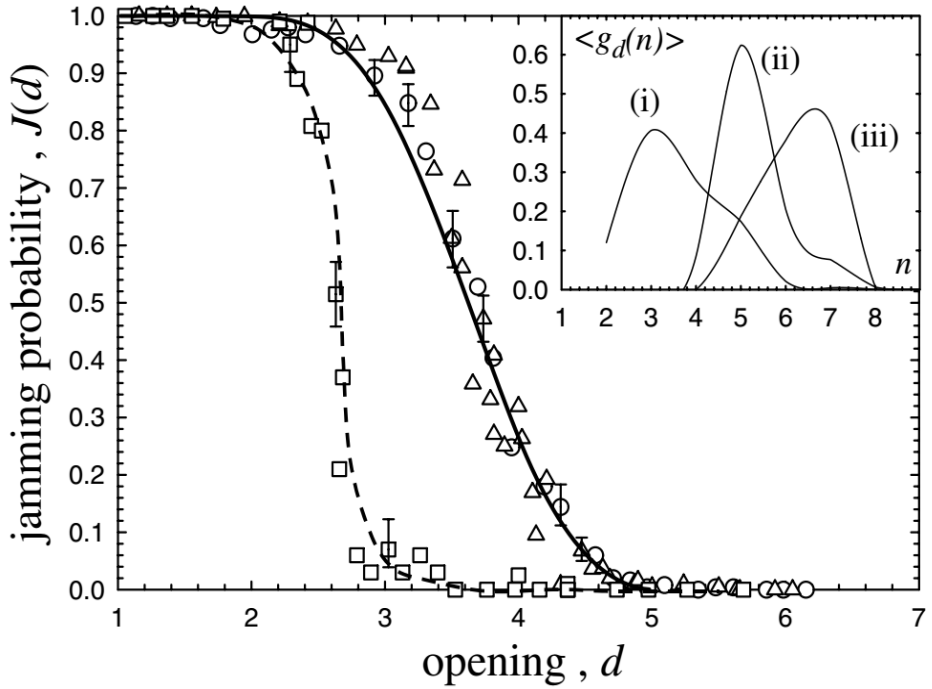

(K. To, P. Lai, and H. Pak, PRL 01')

Effect of the direction of the drive

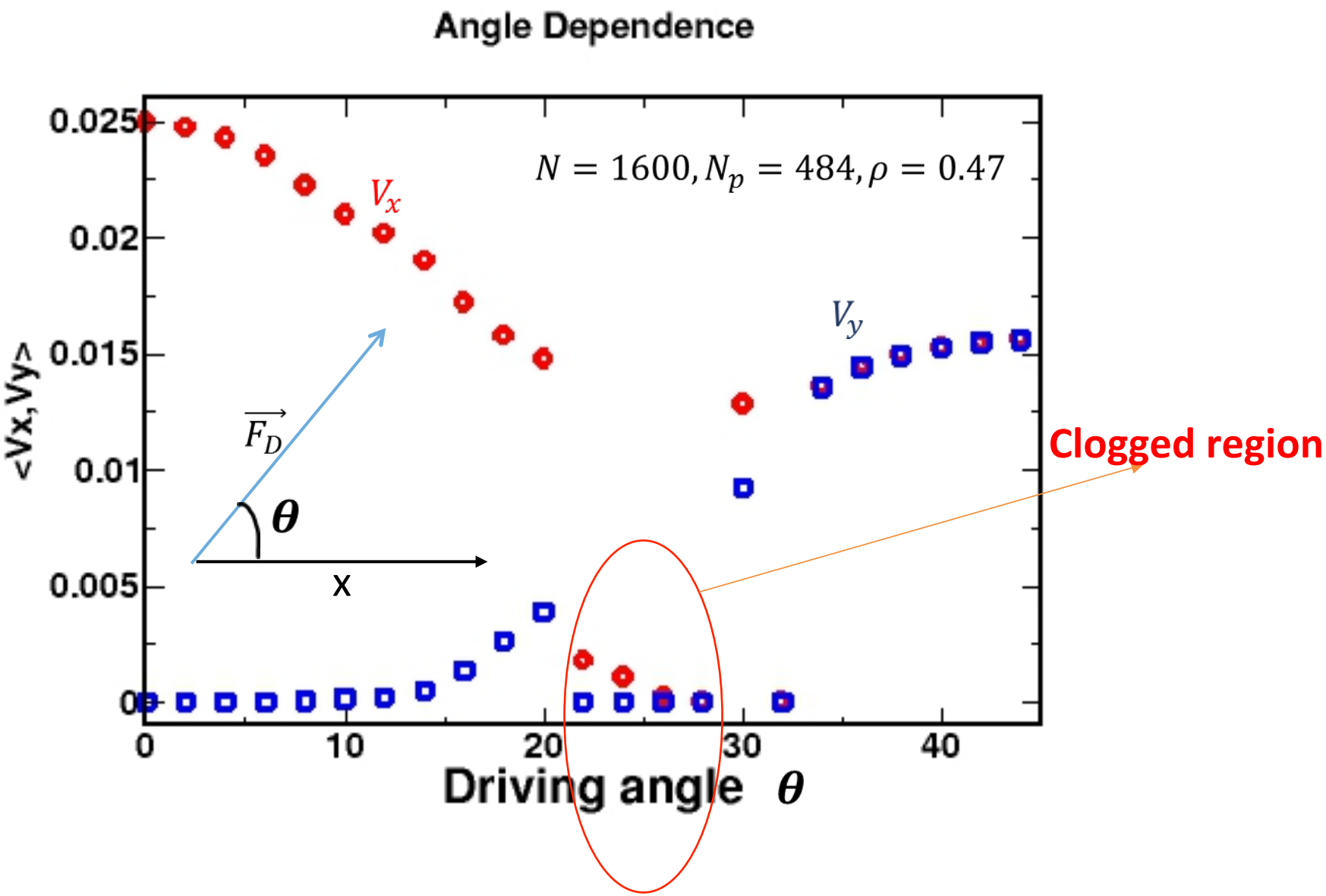

Conclusion

- Periodic array of obstacles reduces jamming density
- Contact number is significantly smaller than in the clean limit
- Clogging probability monotonically increases with the particle density
- Exhibit some features found in 2D jamming flowing through an aperture

THANKS!

Arctic Riverine CDOM and its Effects on the Polar Marine Light Field

Zoë Orandle

San Diego State University / Undergrad / Environmental Engineering / Mentors: Wilbert Weijer and Scott Elliott

OUTLINE

- The Importance of Phytoplankton and CDOM (Chromophoric Dissolved Organic Matter)
- Baseline Model
- Preliminary Conclusions
- Future improvements

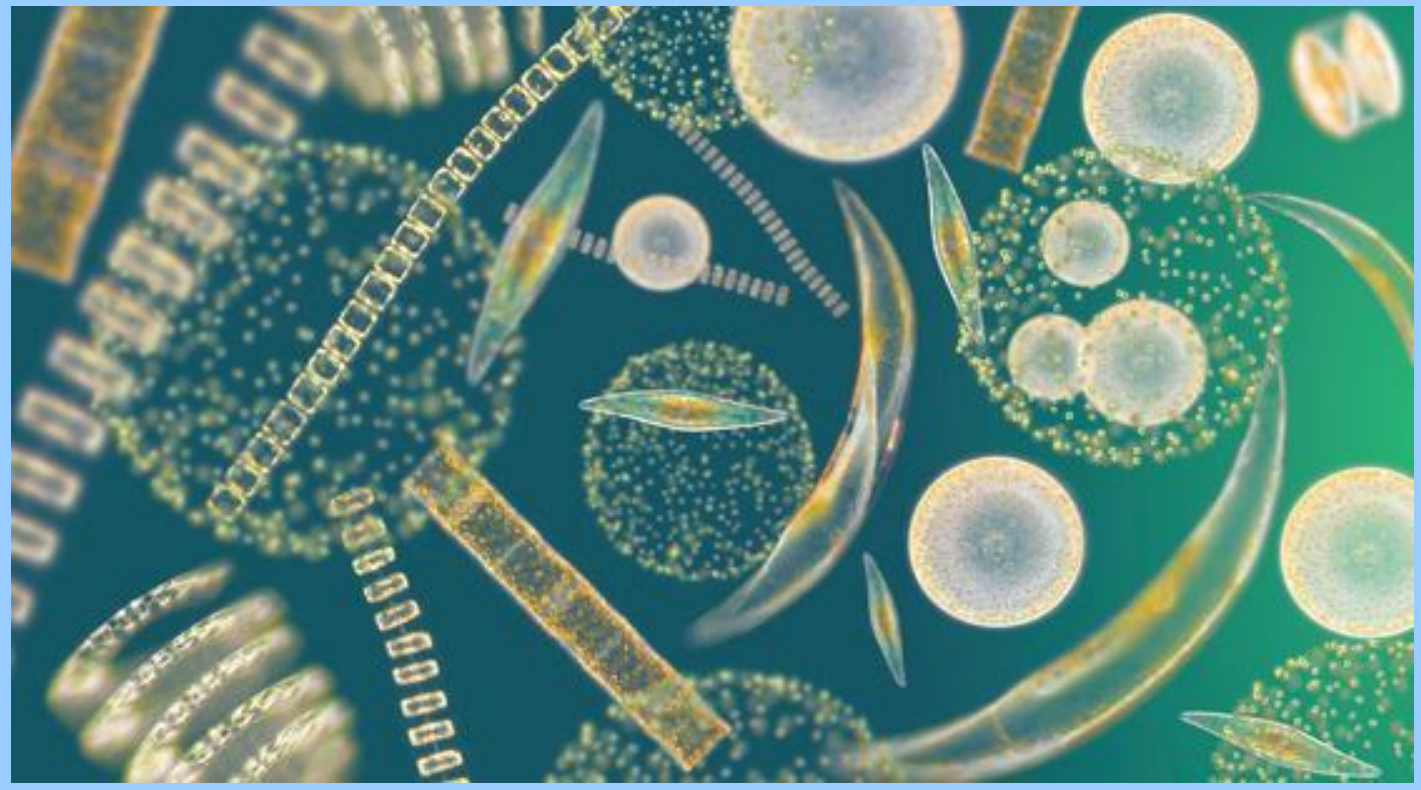

A map of the Arctic Region

Our model of the Arctic Region

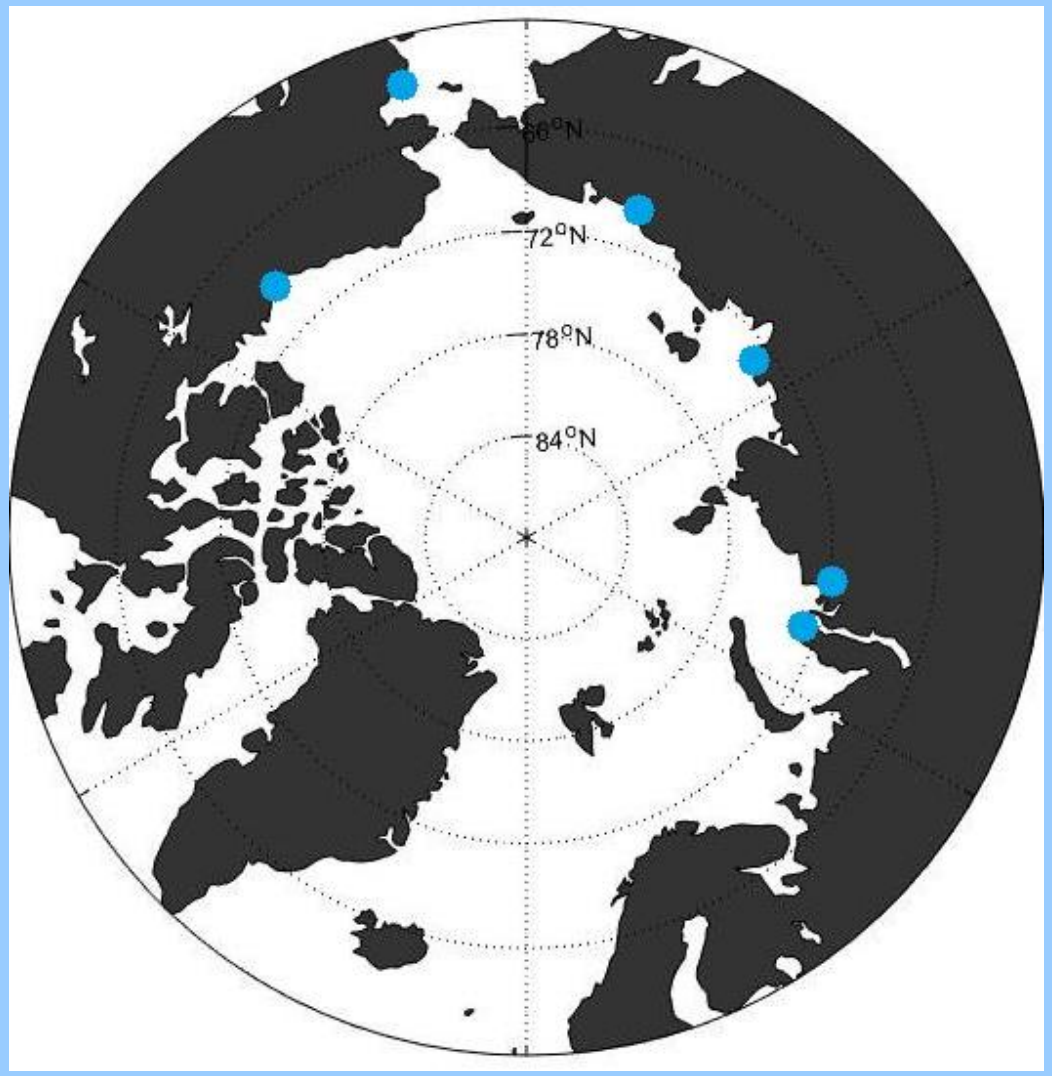

Phytoplankton

- Defined as microscopic, autotrophic organisms that inhabit the photic zone in oceans and fresh water.
- Obtain energy through photosynthesis
- Absorbs violet-blue and orange-red light best
- Foundation of food chain
- Open ocean

- Absorb same visible wavelengths of light
- Visible in high numbers

CDOM

- Defined as the optically measurable component of dissolved organic matter in water.
- Has a limiting effect on photosynthesis
- Can absorb UV radiation, absorbs best in blue and violet
- Dissolved detrital material
- Riverine inputs

NASA SATELLITE IMAGES OF PHYTOPLANKTON BLOOMS

July

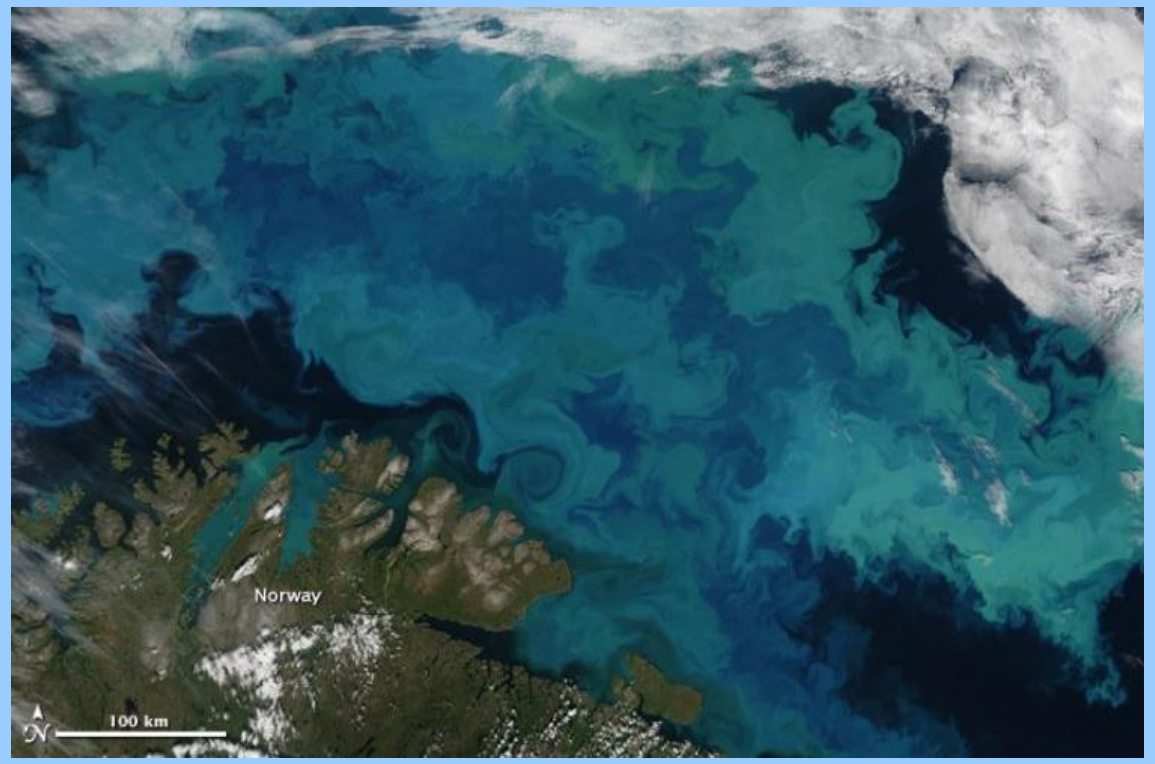

August

Although this bloom in the Barents Sea does not originate from a river, it complements our data quite nicely.

NASA SATELLITE IMAGE OF MACKENZIE RIVER PLUME

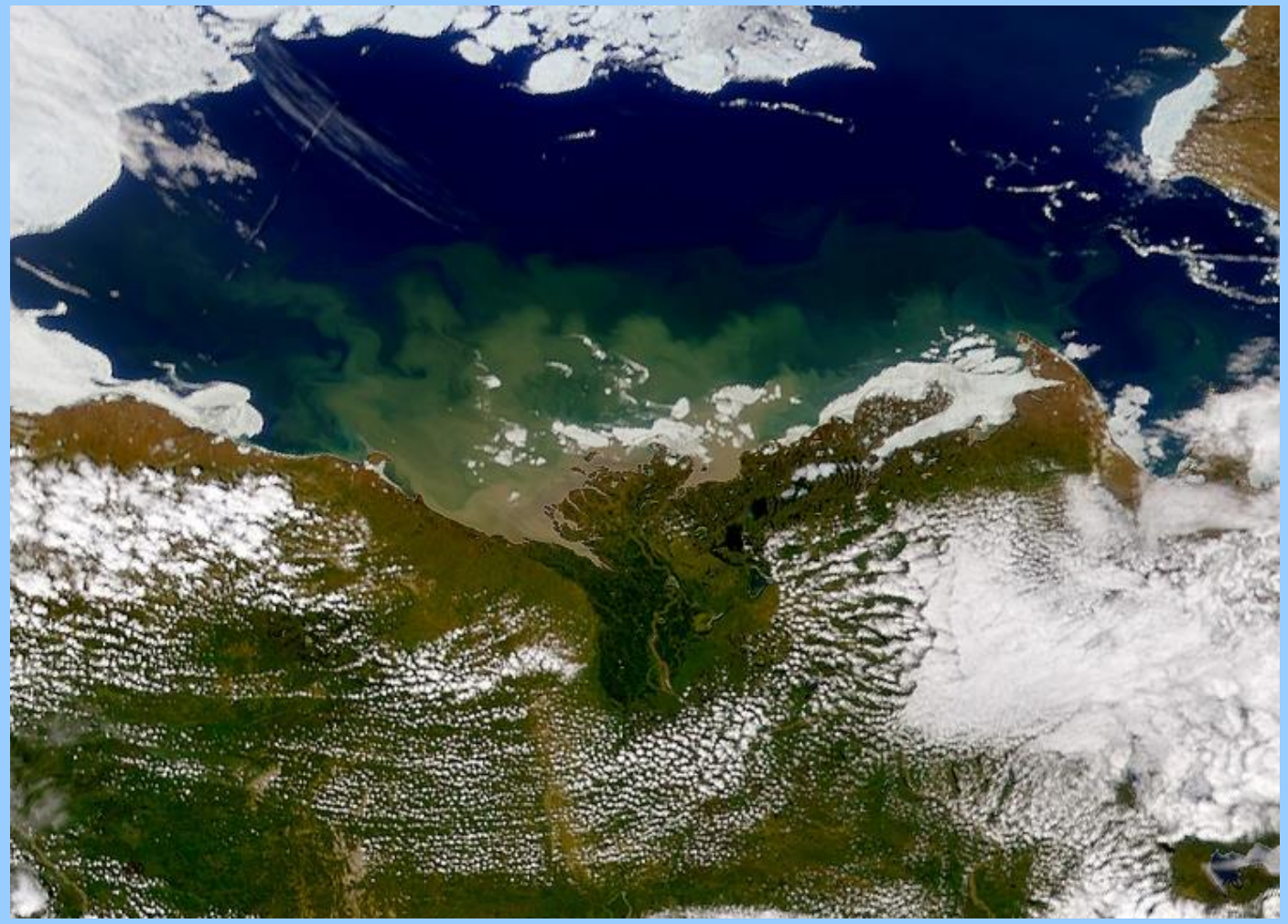

High concentrations of CDOM appear brown and then green as the plume spreads out.

PARAMETERS

Attenuation table

Months	CDOM (m^{-1})	DOC* (µM C)	CDOM / DOC* (m^{-1}) (µM C)	Sediment (m^{-1})	Clear sea water (m^{-1})
Jan	0.35	115.8	0.003022	0.05	0.017
Feb	0.7005	231.6	0.003025	0.05	0.017
Mar	1.401	463.2	0.003025	0.05	0.017
Apr	1.46	345.8	0.004222	0.05	0.017
May	8.33	1386	0.006010	0.05	0.017
Jun	5.5	932.75	0.005897	0.05	0.017
Jul	3.75	683.4	0.005487	0.05	0.017
Aug	2.6	632.8	0.004109	0.05	0.017
Sep	1.953	491.6	0.003973	0.05	0.017
Oct	3.47	708.83	0.004895	0.05	0.017
Nov	1.735	354.42	0.004895	0.05	0.017
Dec	0.35	177.21	0.004893	0.05	0.017

* = concentration, not attenuation value

- PAR (Photosynthetically Available Radiation W/m^2)
- Dynamic mixed layer depth (meters)
- Appropriate wavelength (443 nm)
- Attenuating factors (see left table)
- CDOM decay timescale (316 days)
- Concentrations and dilution factor (0.3)

These factors were used in calculating and plotting the average intensity in Watts per meter squared over the mixed layer of the Arctic Ocean.

BASELINE MODEL: JUNE

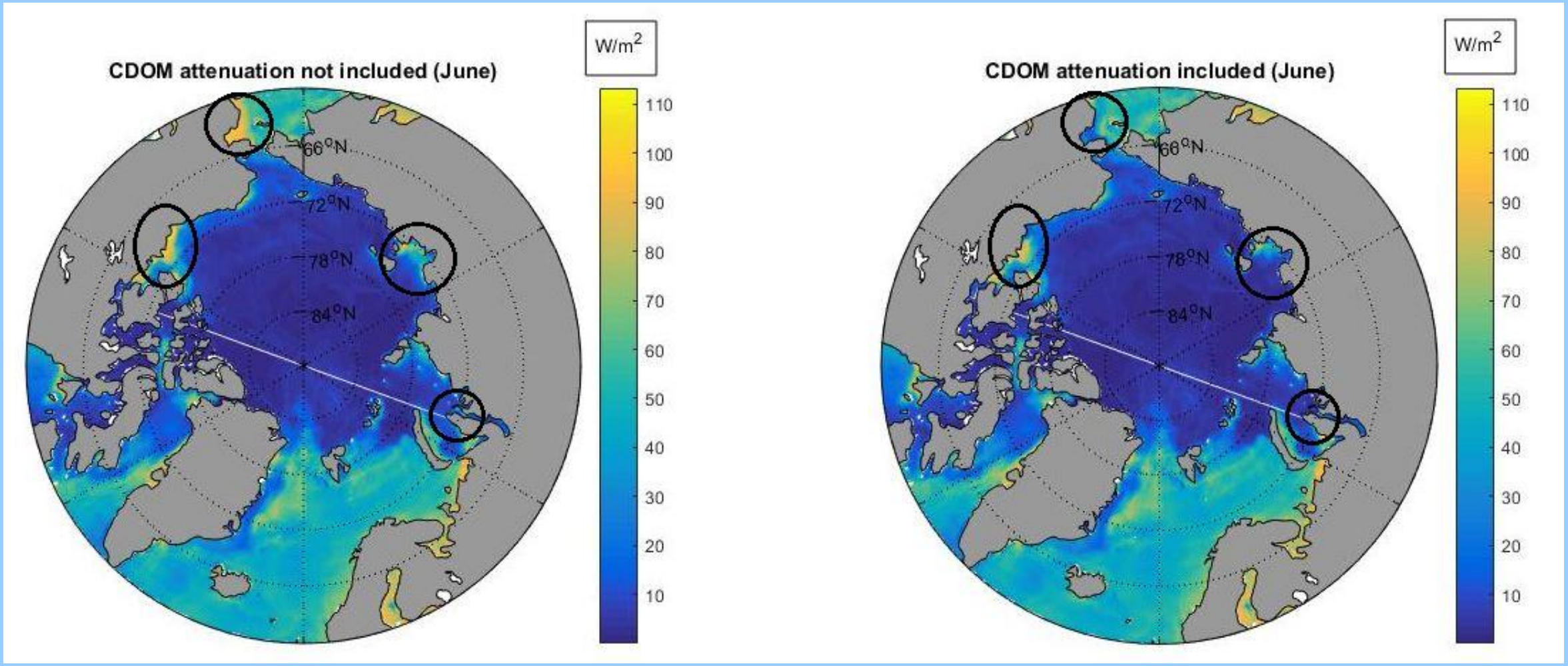

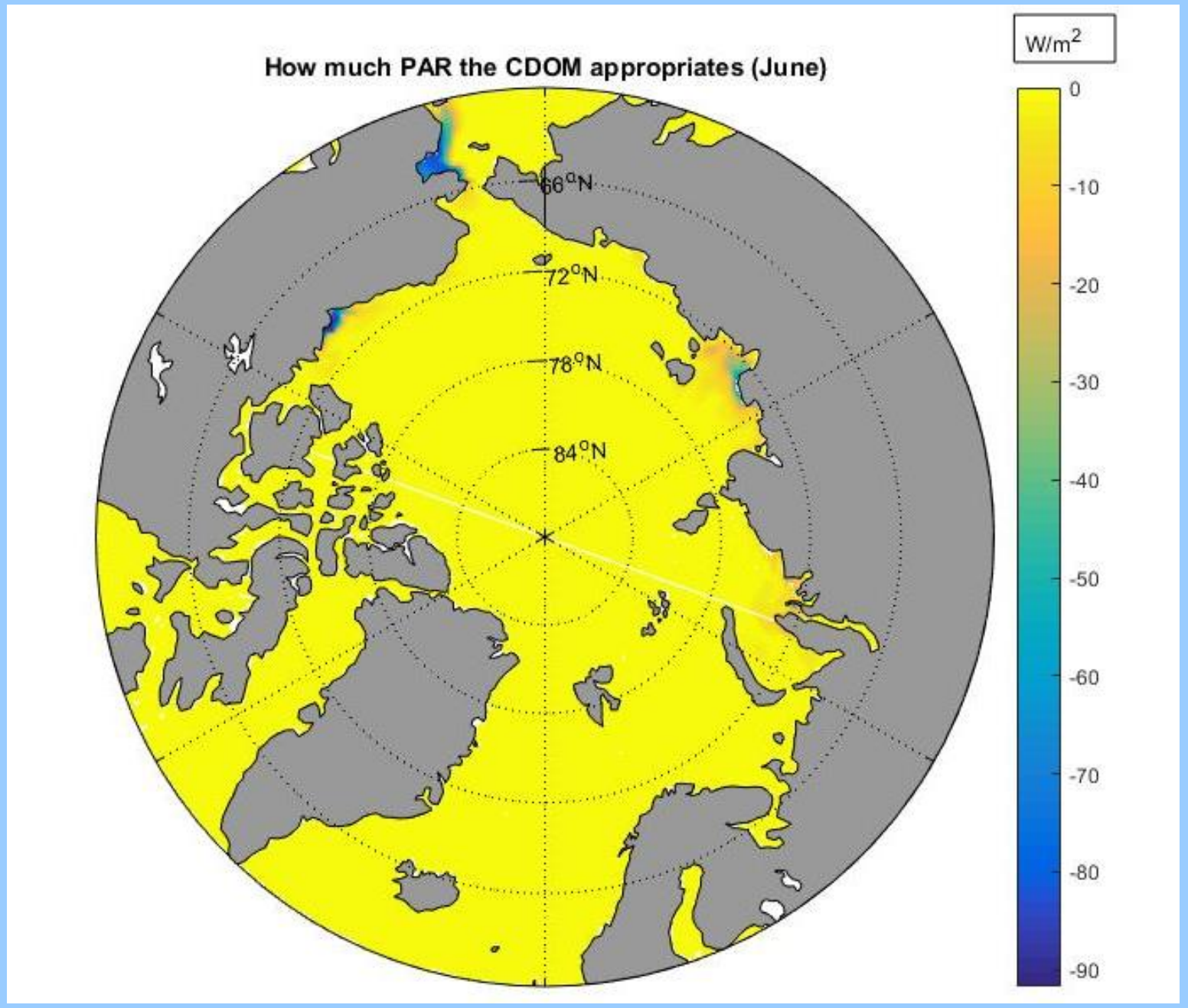
How much PAR the CDOM appropriates (June)
W/m2
0
-10
-20
-30
-40
-50
-60
-70
-80
-90
66°N
72°N
78°N
84°N

CONCLUSIONS

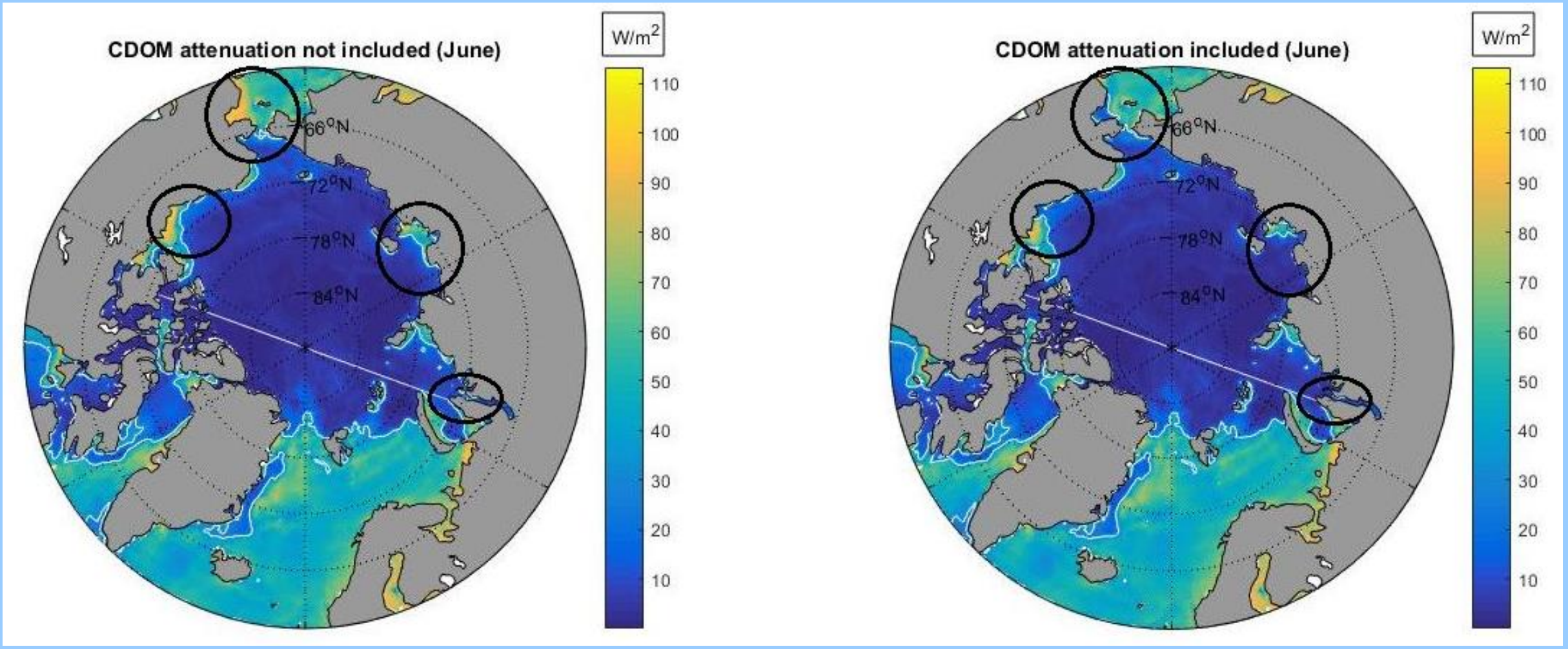

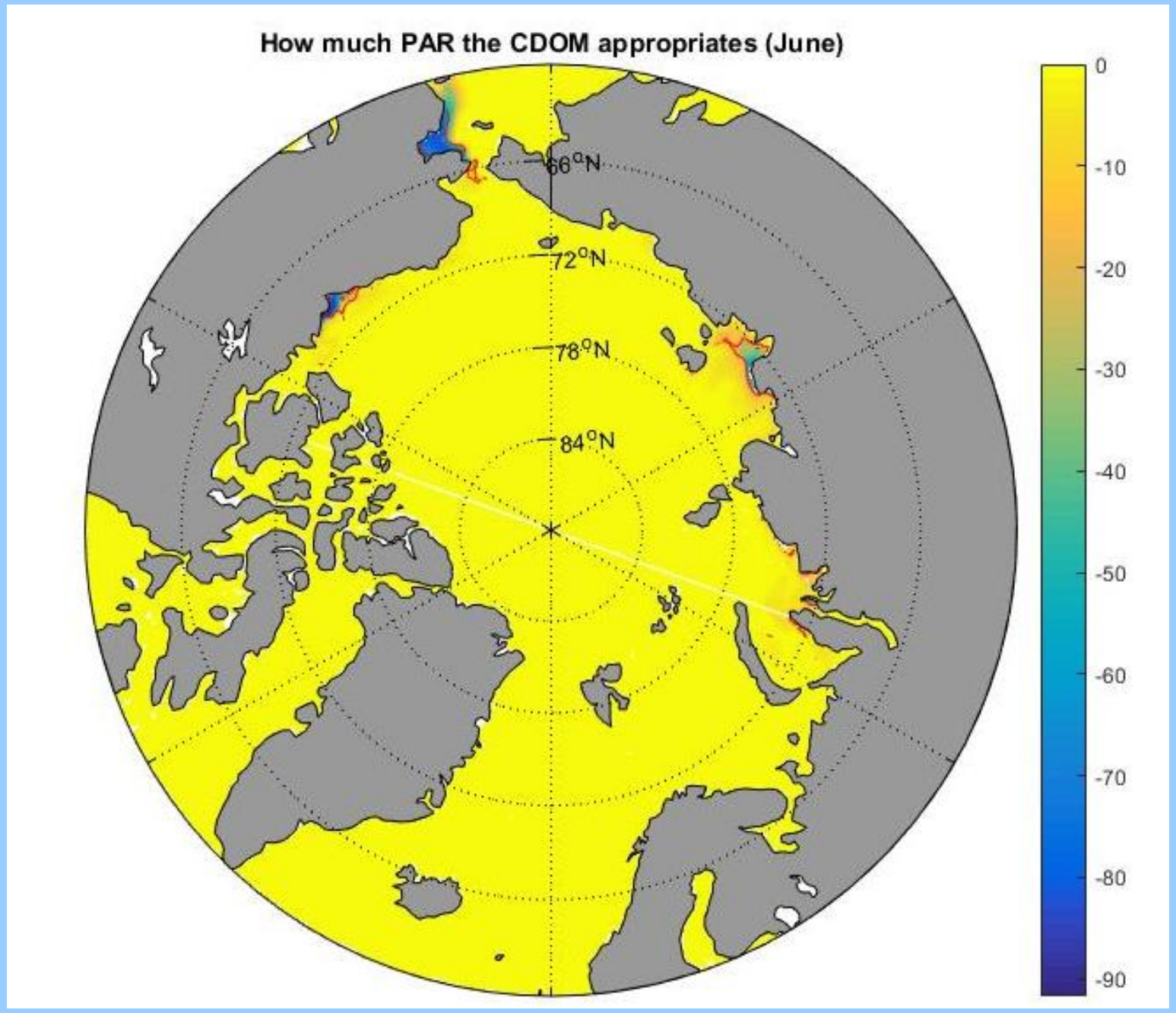
How much PAR the CDOM appropriates (June)
66°N
72°N
78°N
84°N
0
-10
-20
-30
-40
-50
-60
-70
-80
-90

FUTURE REFINEMENTS

Individual Rivers

Suspended Sediments

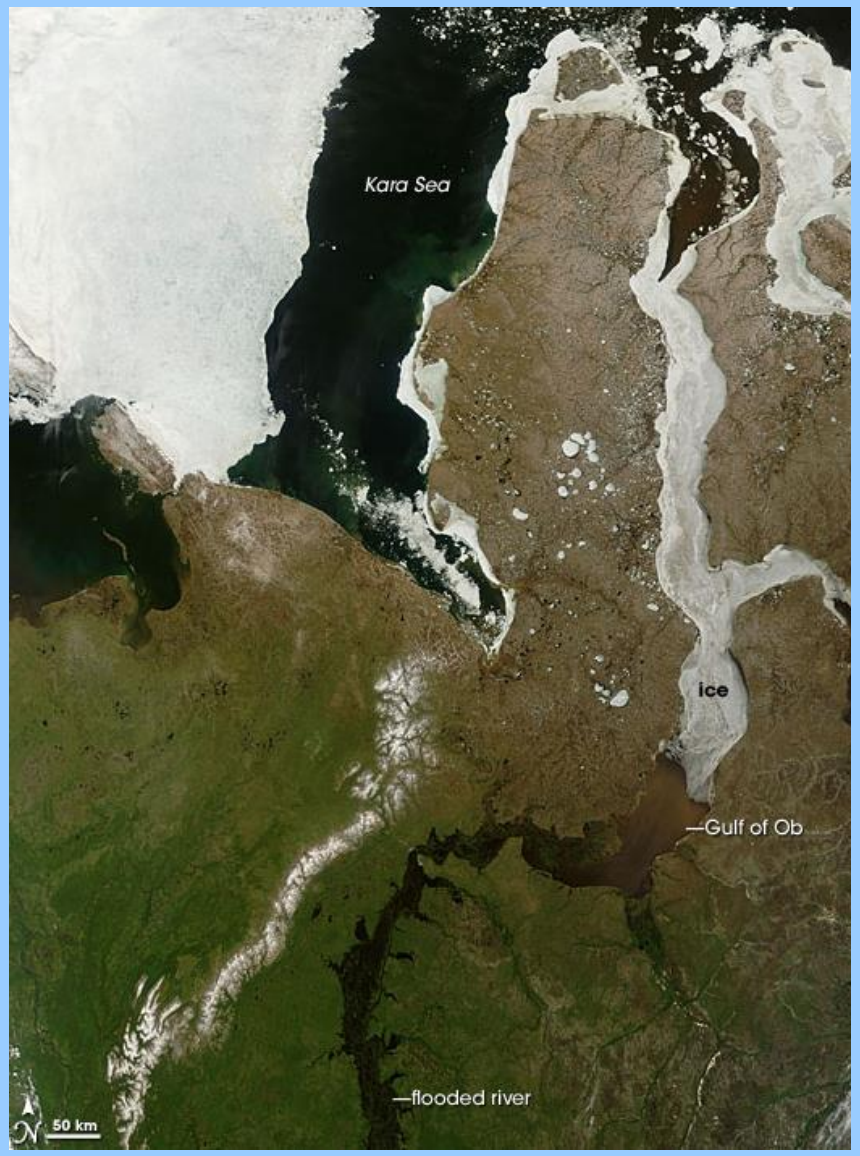

The Ob is completely blocked by ice in June unlike other major rivers

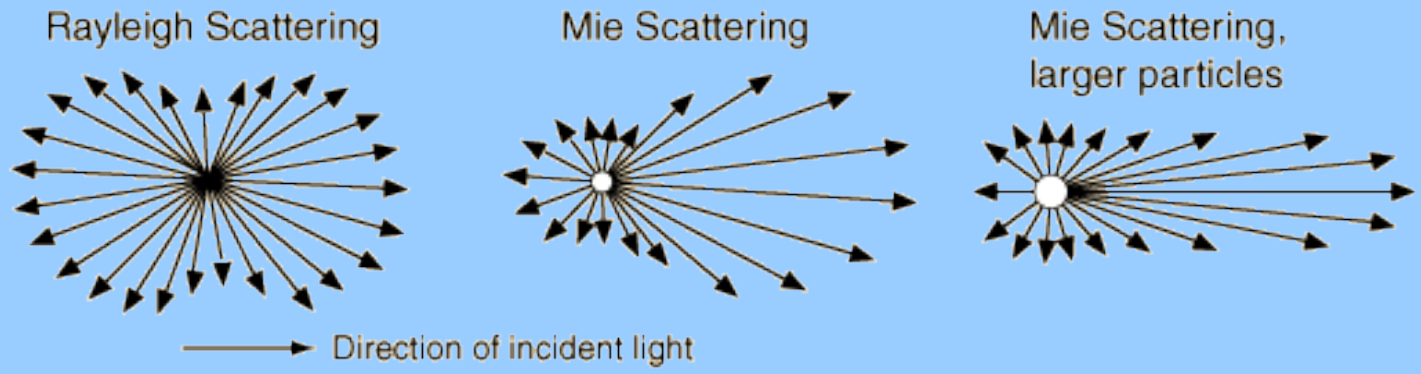

PICTURES CITED

In order of appearance

- http://sailorsforthesea.org/programs/ocean-watch/searching-phytoplankton (phytoplankton)
- https://nordpil.com/portfolio/mapsgraphics/arctic-topography/ (map of arctic)
- http://www.nasa.gov/feature/goddard/nasa-study-shows-oceanic-phytoplankton-declines-in-northern-hemisphere (July bloom 2014)
- http://earthobservatory.nasa.gov/NaturalHazards/view.php?id=51765 (August bloom 2011)
- http://visibleearth.nasa.gov/view.php?id=52586 (Ob river June)
- http://hyperphysics.phy-astr.gsu.edu/hbase/atmos/blusky.html (scattering types)

Improving the Parallel Scalability of BoxMG

Andrew Reisner[1]
David Moulton[2]
Luke Olson[1]

[1]Department of Computer Science, University of Illinois at Urbana-Champaign
[2]Applied Mathematics and Plasma Physics (T5), LANL

Dielectric Barrier Discharge Model Problem

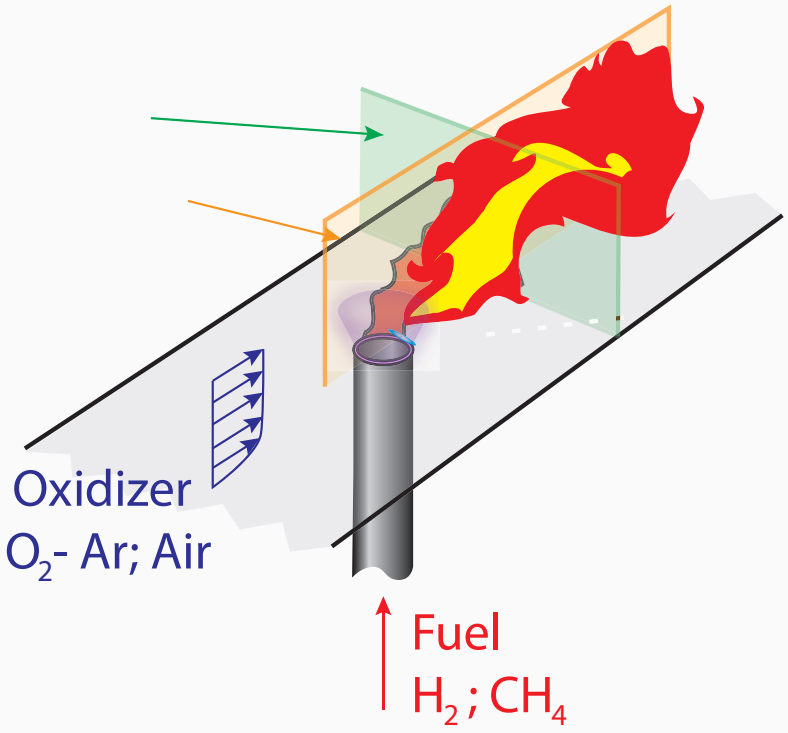

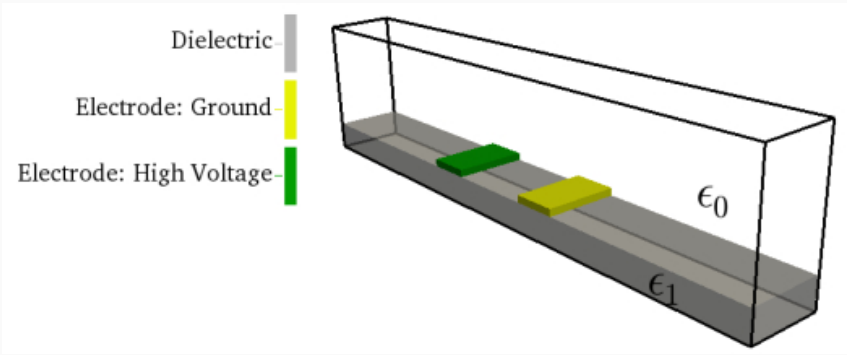

- **Goal:** Calculate electric field ($\nabla \cdot \epsilon \nabla \phi = f$) in dielectric barrier discharge
- **Application:** Electric field processed as body force on cross flow

Center for Exascale Simulation of Plasma-Coupled Combustion

E-field Calculation $\nabla \cdot \epsilon \nabla \phi = f$

- Accurate discretization leads to ill-conditioned S.P.D. matrix
- Efficient solution requires multilevel solvers

Multilevel Solver Design

- **Challenge:** Jump in diffusion coefficient (ϵ)
- **Approach:** Operator-induced interpolation

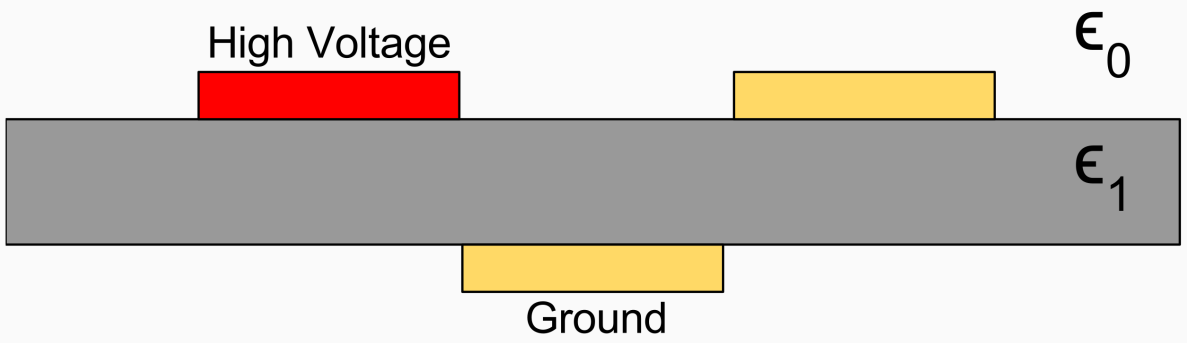

E-field Calculation $\nabla \cdot \epsilon \nabla \phi = f$

Multilevel Solver Design

- **Challenge:**
  - Electrodes at coarse levels
  - Applied potentials in domain

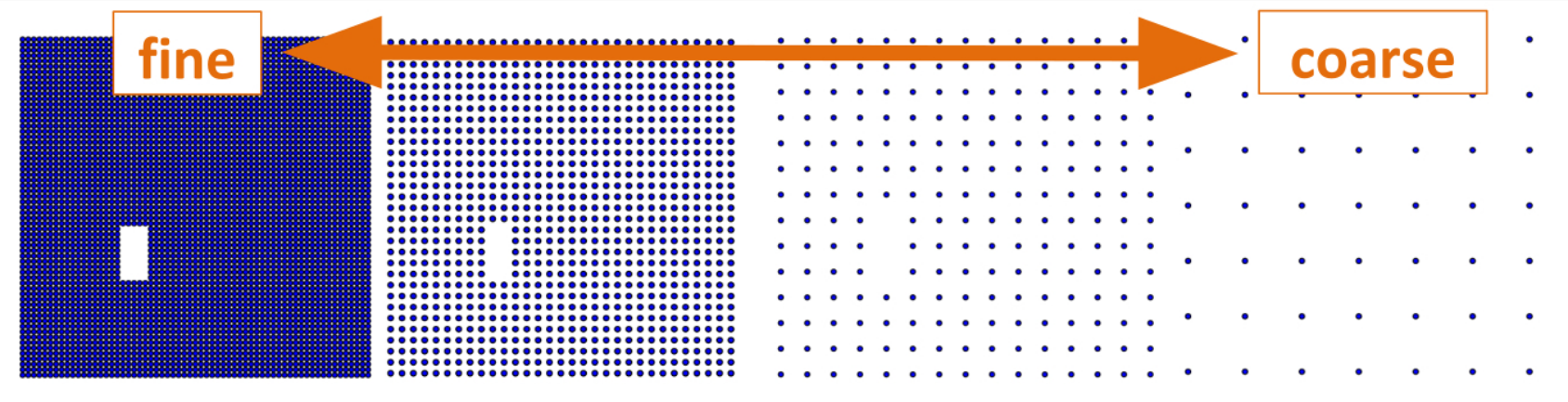

- **Approach:**
  - Operator-induced interpolation
  - Krylov solvers

E-field Calculation $\nabla \cdot \epsilon \nabla \phi = f$

Multilevel Solver Design

- **Challenge:**
  - Electrodes at coarse levels
  - Applied potentials in domain

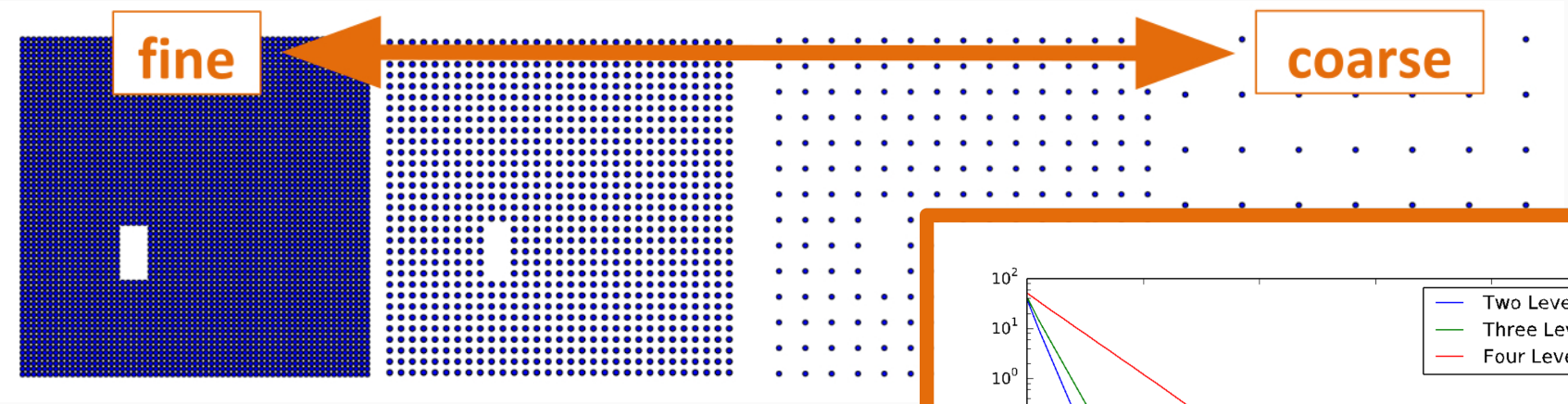

- **Approach:**
  - Operator-induced interpolation
  - Krylov solvers

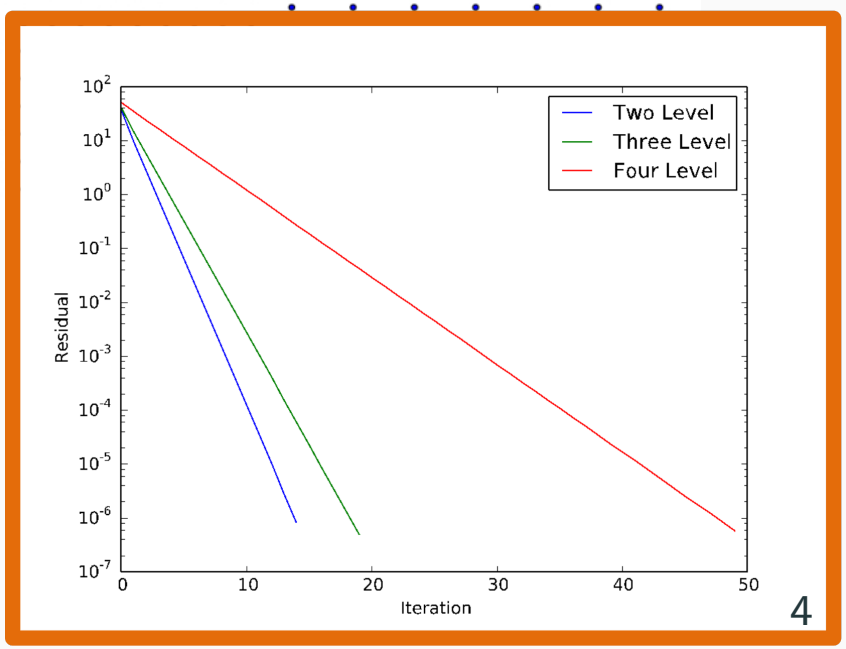

E-field Calculation $\nabla \cdot \epsilon \nabla \phi = f$

Multilevel Solver Design

- **Challenge:** Stretched meshes
- **Approach:** Line/plane relaxation with standard coarsening

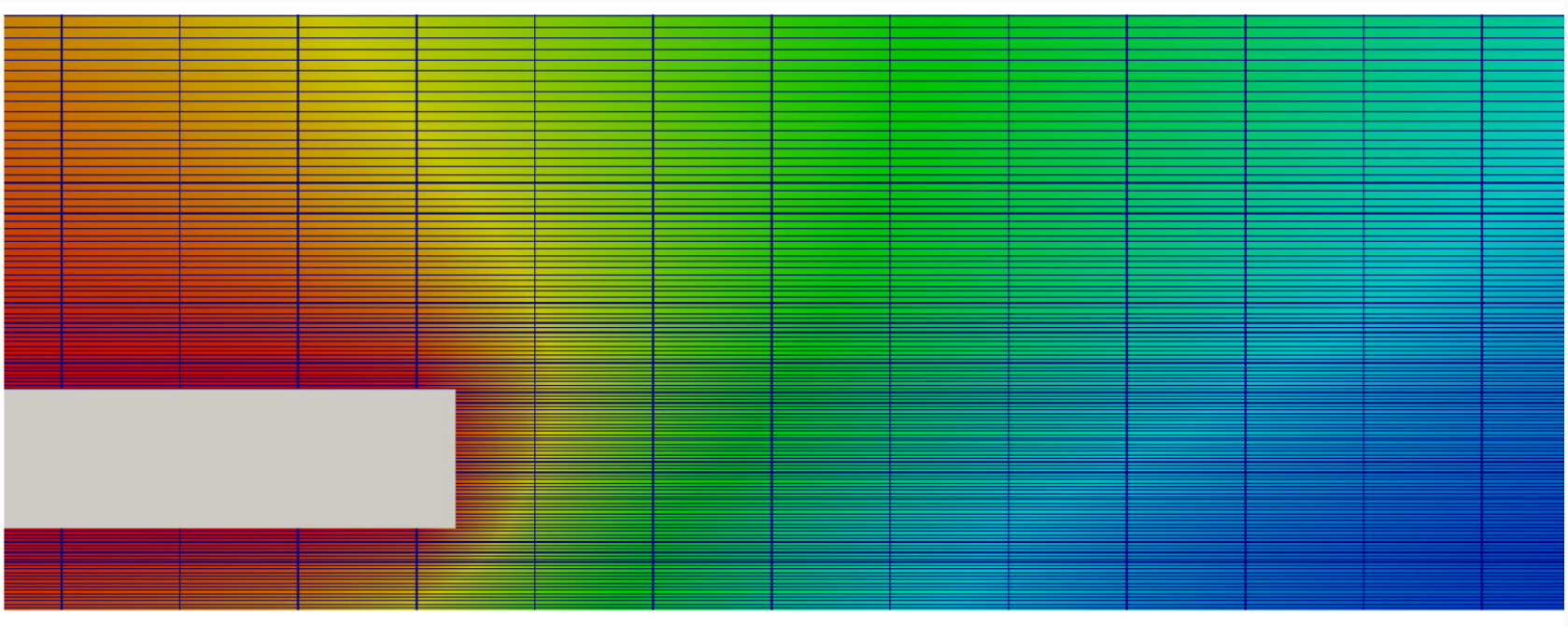

Black Box Multigrid (BoxMG)

Robust multigrid for discretizations on **structured grids**

Robust

- Operator-induced interpolation
  - Discontinuous coefficients
- Variational coarsening
  - Minimize CGC error in range of interpolation
- Line/Plane relaxation
  - Anisotropic problems

Structured Grids

- Fixed coarsening pattern
- Stencil operators on each level
- Direct memory access

Distributed BoxMG

- Point-relaxation and intergrid transfer use efficient stencil operators
- Coarse grid correction requires solve on coarsest level
- At some level in the coarsening we run out of local work
- Initial approach:
  - Gather data to one processor
  - Serial BoxMG cycle
  - Scatter solution and continue

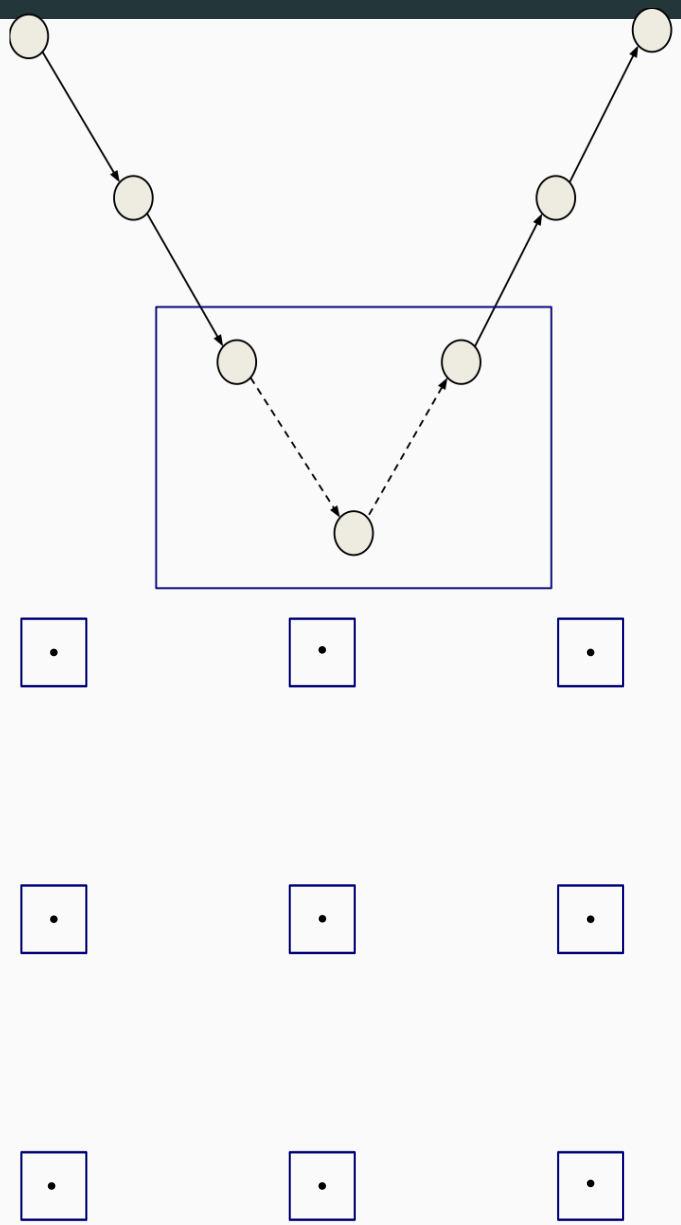

Distributed BoxMG

- Point-relaxation and intergrid transfer use efficient stencil operators
- Coarse grid correction requires solve on coarsest level
- At some level in the coarsening we run out of local work
- Initial approach:
  - **Gather data to one processor**
  - Serial BoxMG cycle
  - Scatter solution and continue

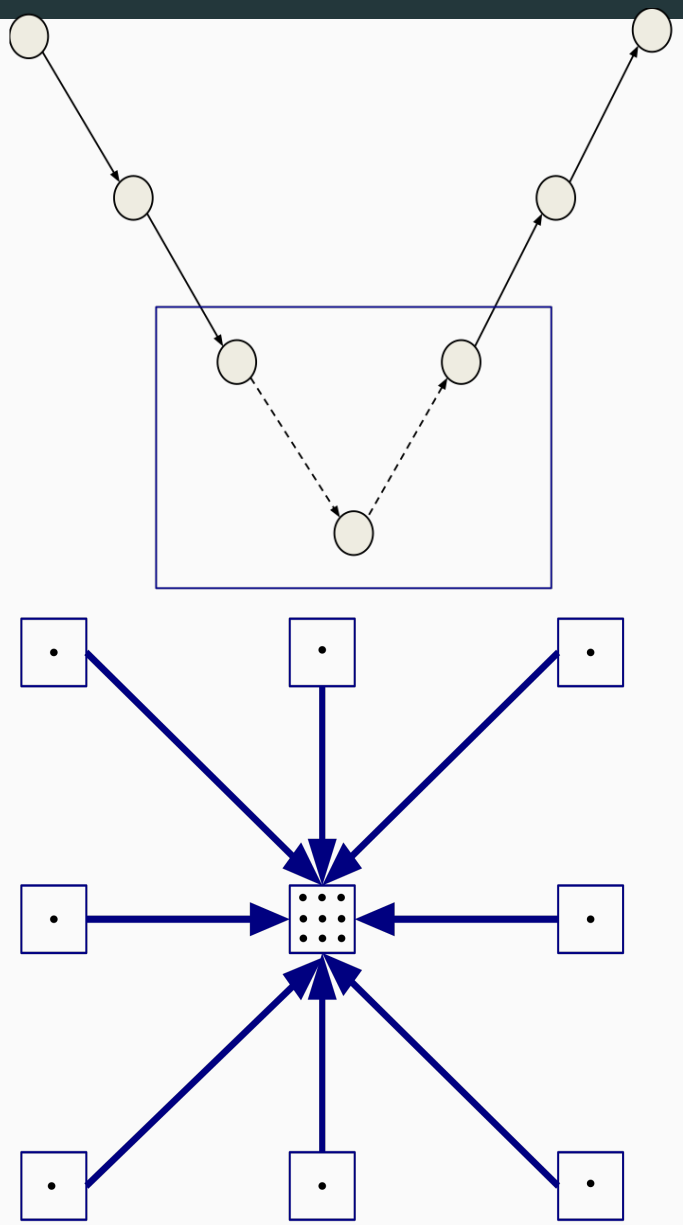

Distributed BoxMG

- Point-relaxation and intergrid transfer use efficient stencil operators
- Coarse grid correction requires solve on coarsest level
- At some level in the coarsening we run out of local work
- Initial approach:
  - Gather data to one processor
  - **Serial BoxMG cycle**
  - Scatter solution and continue

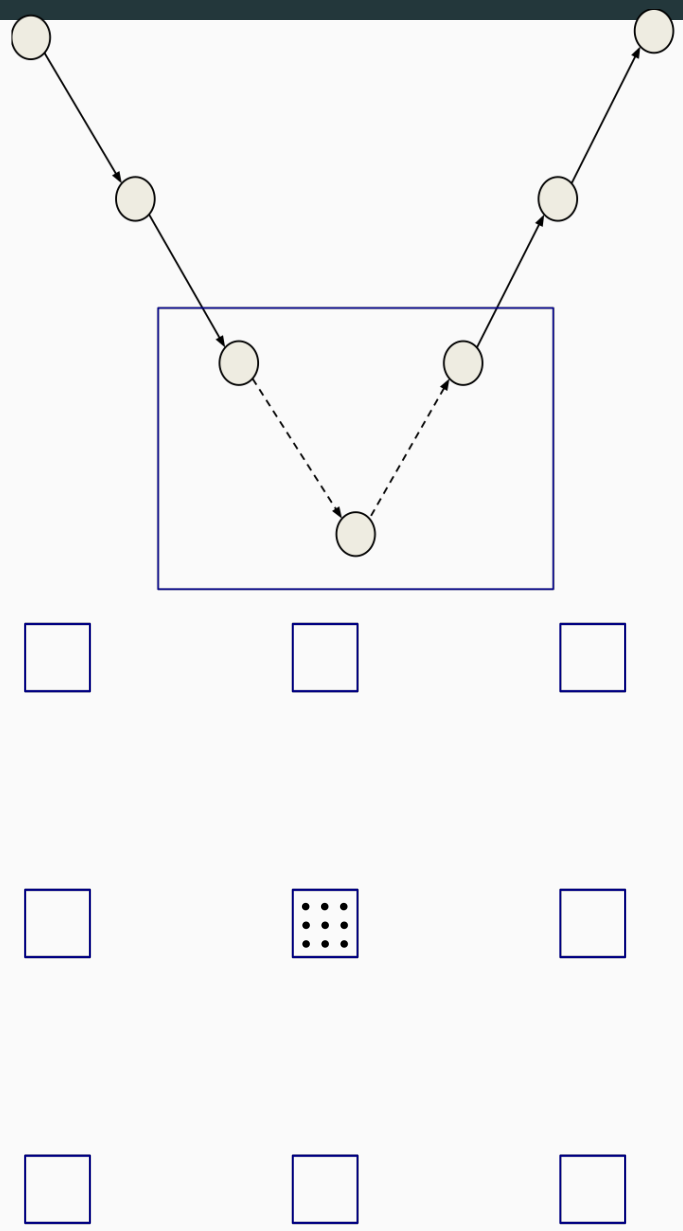

Distributed BoxMG

- Point-relaxation and intergrid transfer use efficient stencil operators
- Coarse grid correction requires solve on coarsest level
- At some level in the coarsening we run out of local work
- Initial approach:
  - Gather data to one processor
  - Serial BoxMG cycle
  - **Scatter solution and continue**

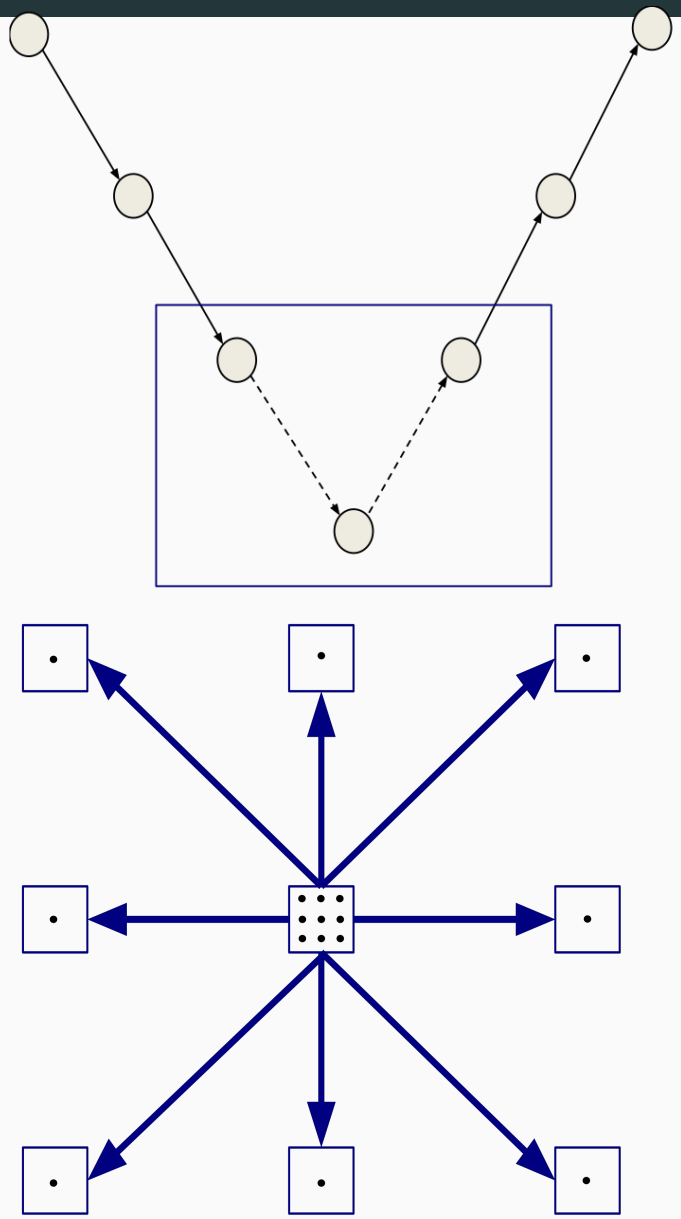

Redistribution

- Coarsest grid grows with number of processors
  - Best case: $3 \times 3 = 9$ or $3 \times 3 \times 3 = 27$ d.o.f. per core
- Redistribute problem on subset of processors
  - Using redundancy: opportunity for resilience

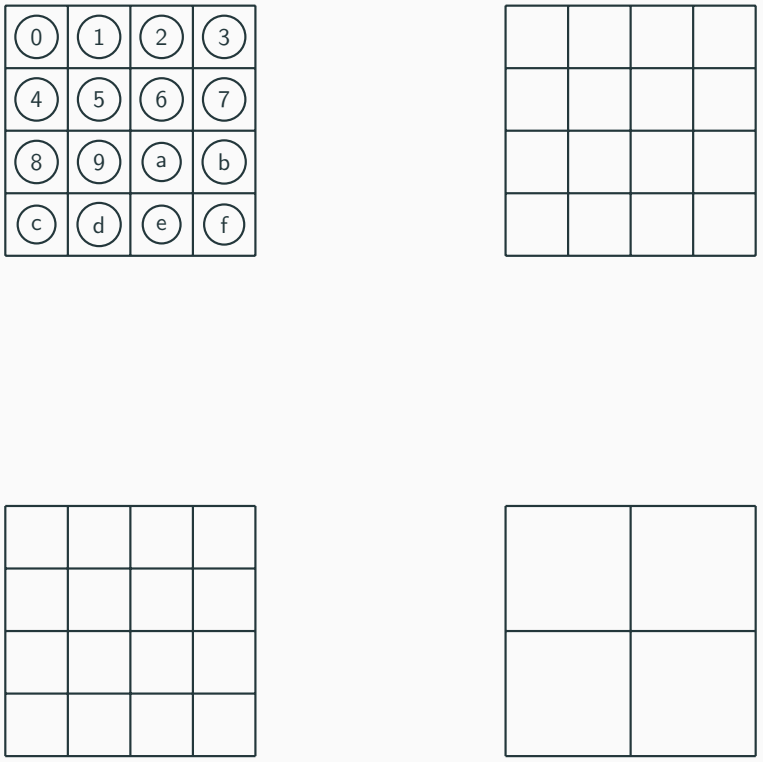

Redistribution

- Coarsest grid grows with number of processors
  - Best case: $3 \times 3 = 9$ or $3 \times 3 \times 3 = 27$ d.o.f. per core
- Redistribute problem on subset of processors
  - Using redundancy: opportunity for resilience

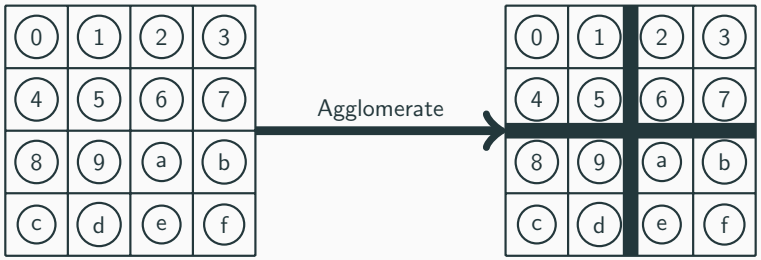

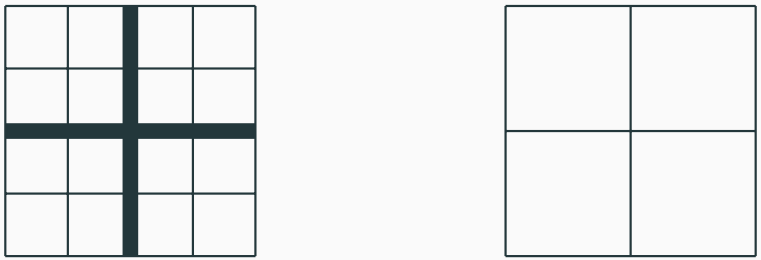

Redistribution

- Coarsest grid grows with number of processors
  - Best case: $3 \times 3 = 9$ or $3 \times 3 \times 3 = 27$ d.o.f. per core
- Redistribute problem on subset of processors
  - Using redundancy: opportunity for resilience

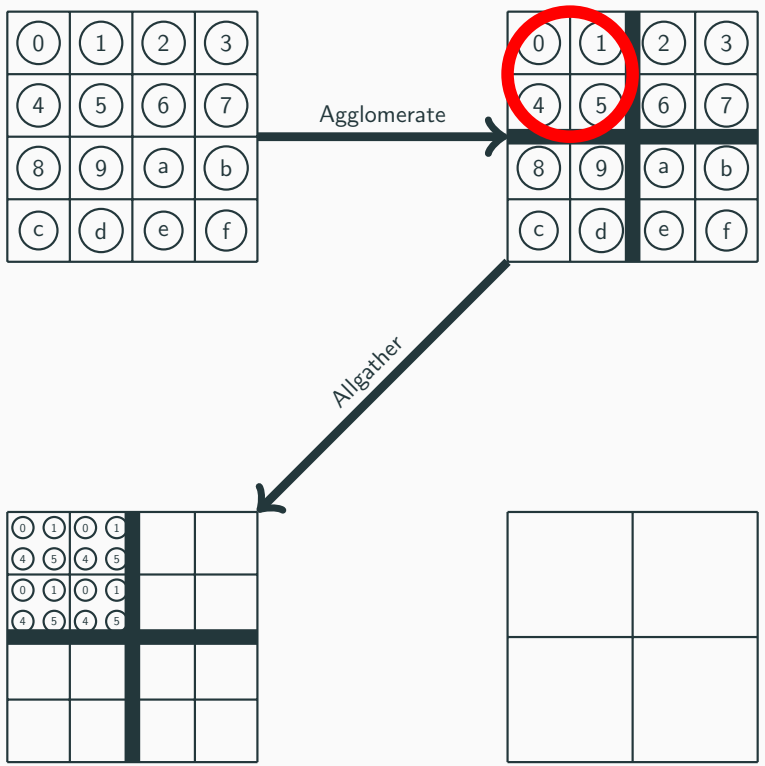

Redistribution

- Coarsest grid grows with number of processors
  - Best case: $3 \times 3 = 9$ or $3 \times 3 \times 3 = 27$ d.o.f. per core
- Redistribute problem on subset of processors
  - Using redundancy: opportunity for resilience

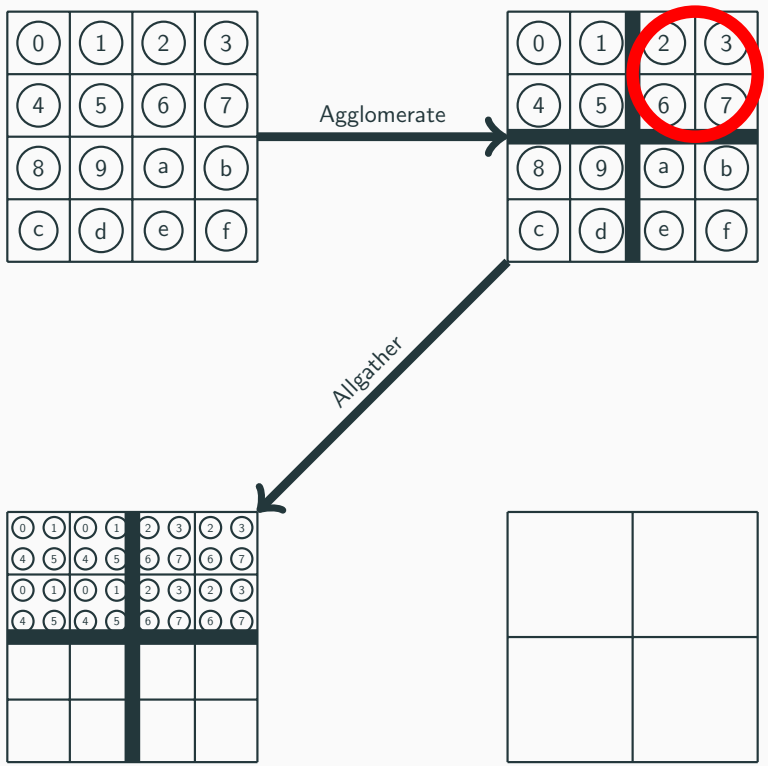

Redistribution

- Coarsest grid grows with number of processors
  - Best case: $3 \times 3 = 9$ or $3 \times 3 \times 3 = 27$ d.o.f. per core
- Redistribute problem on subset of processors
  - Using redundancy: opportunity for resilience

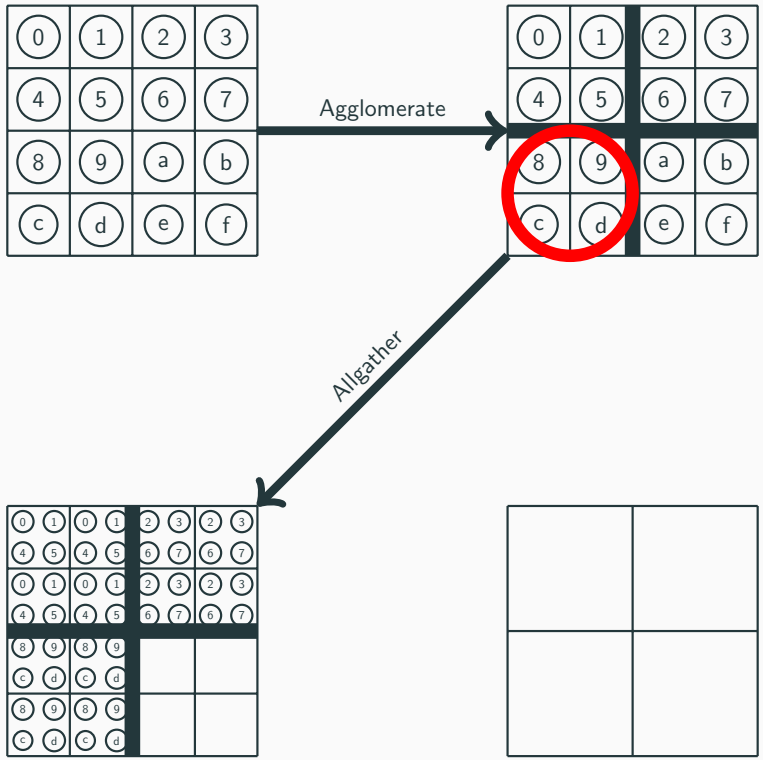

Redistribution

- Coarsest grid grows with number of processors
  - Best case: $3 \times 3 = 9$ or $3 \times 3 \times 3 = 27$ d.o.f. per core
- Redistribute problem on subset of processors
  - Using redundancy: opportunity for resilience

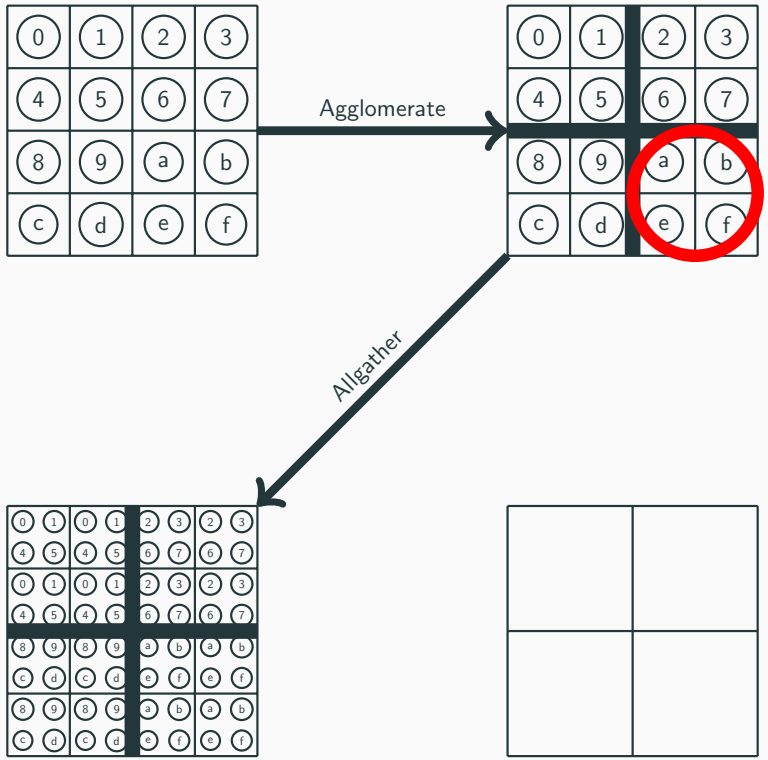

Redistribution

- Coarsest grid grows with number of processors
  - Best case: $3 \times 3 = 9$ or $3 \times 3 \times 3 = 27$ d.o.f. per core
- Redistribute problem on subset of processors
  - Using redundancy: opportunity for resilience

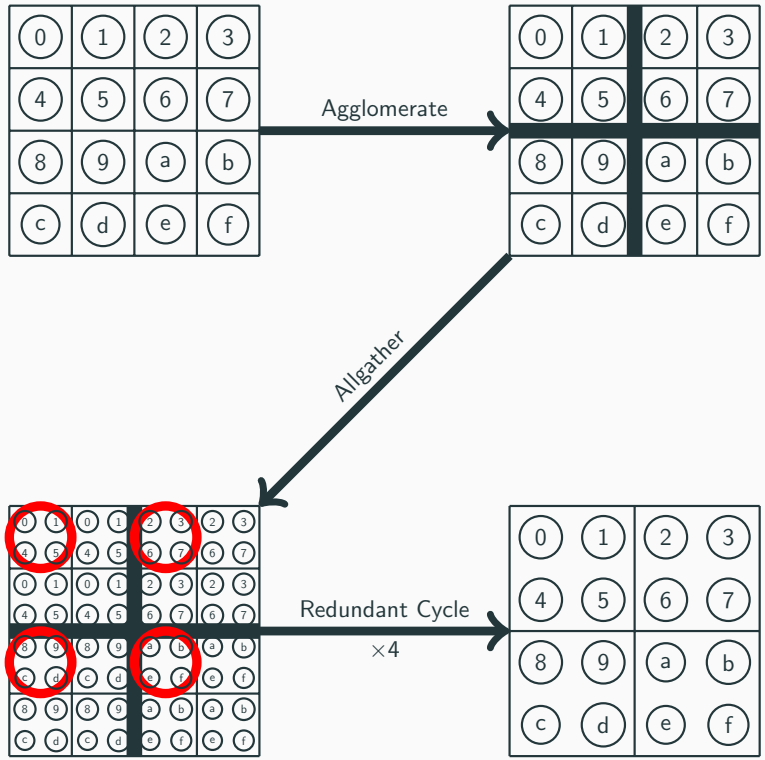

Algorithm

- Subset enumeration
  - Group processors into blocks that will share the same data
  - Start with one agglomerate and refine greedily by dimension
- Redistribution search
  - Known structure of coarse-grid operators enables global search over recursive redistribution
  - Path cost given by predictive performance model

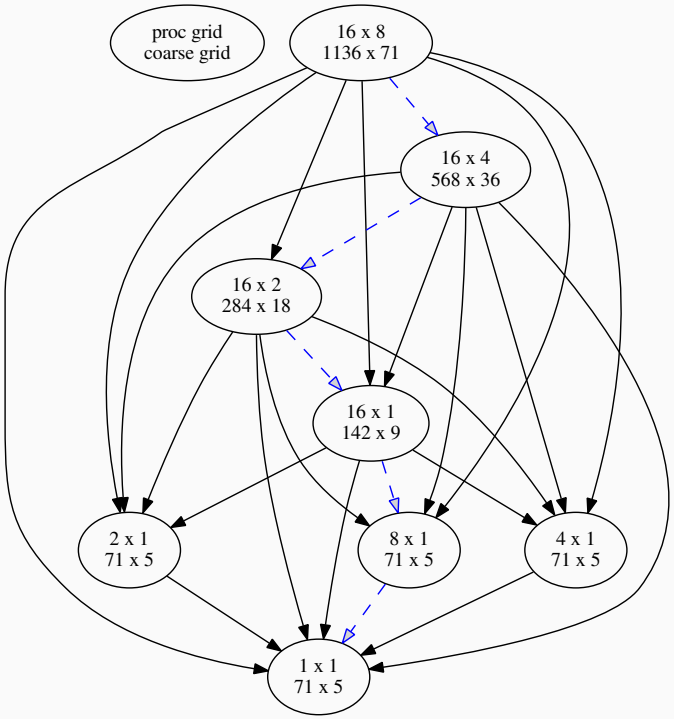

Weak Scaling on BlueWaters[1]

- Local problem: $568 \times 71 \approx 40,000$ d.o.f. per core
- Processor grid ratio: 2×1

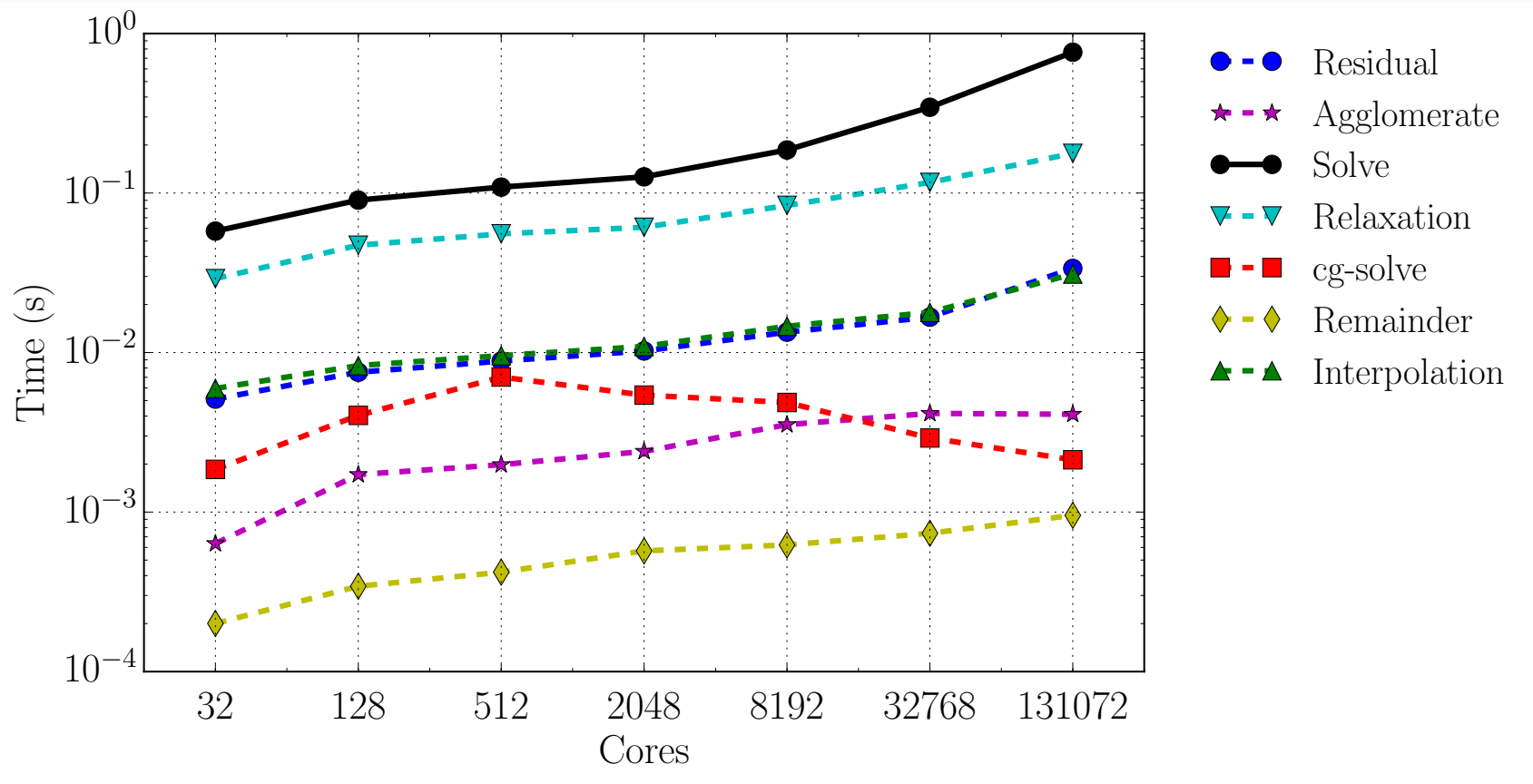

[1] Cray XE/XK hybrid with 22,640 XE compute nodes with two AMD "Interlagos" processors (NCSA) `https://bluewaters.ncsa.illinois.edu`

Weak Scaling on Mira[2]

- Local problem: $568 \times 71 \approx 40,000$ d.o.f. per core
- Processor grid ratio: 2×1

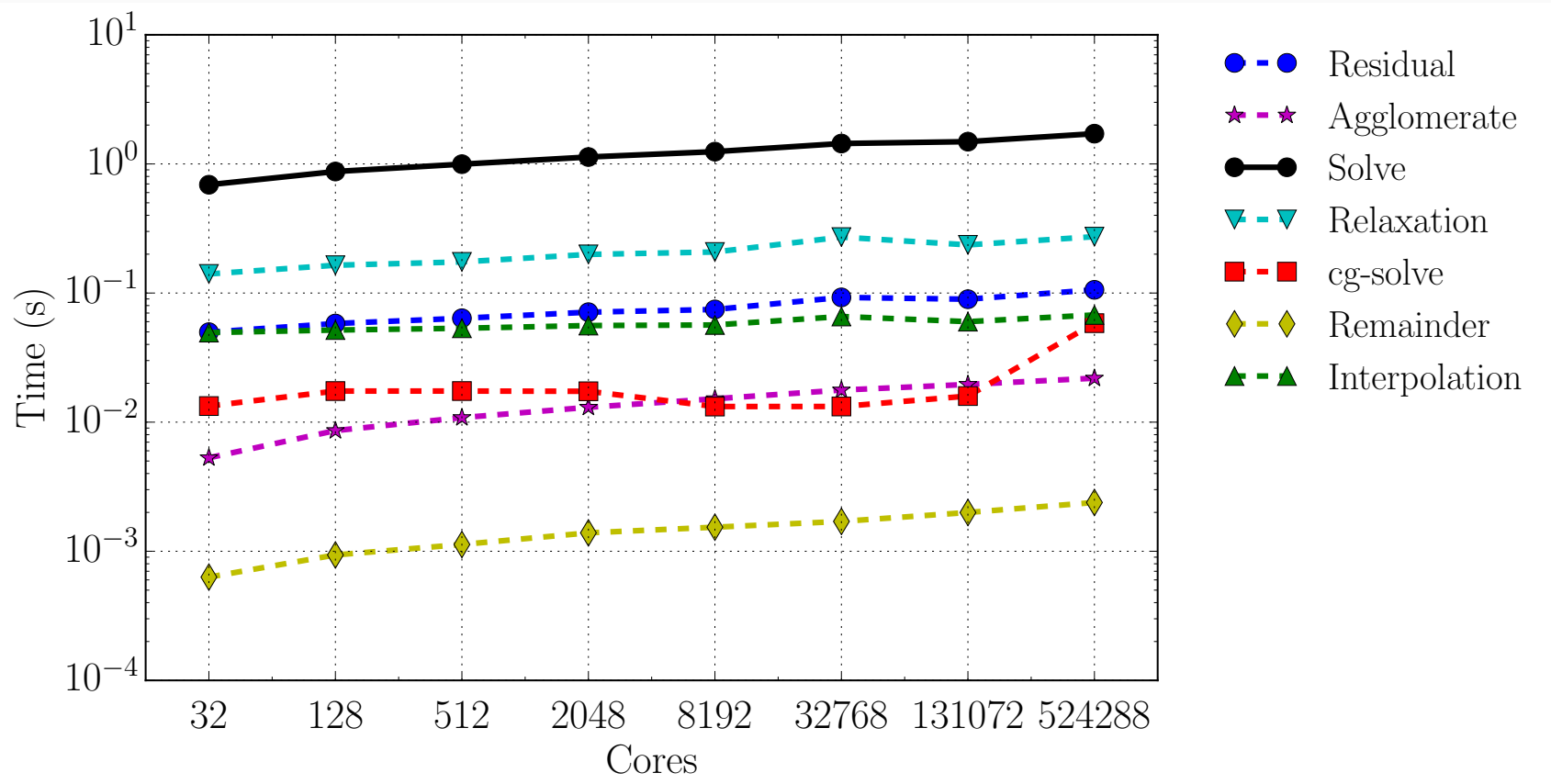

[2]IBM BlueGene/Q with 49,152 compute nodes with PowerPC A2 processors (Argonne) `https://www.alcf.anl.gov/mira`

Conclusions & Future Work

Conclusions

- Redistribution extends the scalability of BoxMG
- Global search guided by performance model templates robust/flexible redistribution
- Logarithmic setup cost can be avoided by local search and heuristics

Future Work

- Line/plane relaxation
- Study accuracy of performance estimation
- Improve baseline performance model

Questions

This material is based in part upon work supported by the Department of Energy, National Nuclear Security Administration, under Award Number DE-NA0002374

Predicting the Crystal Structures of Layered Materials with an Evolutionary Algorithm

Benjamin Revard, Sven Rudin

- Evolutionary algorithm
  - How it works
- Layered materials
  - Island approach to layered structure prediction
- Preliminary results
  - SnSe – VSe_2 layered system
- Future work
  - Variable composition search

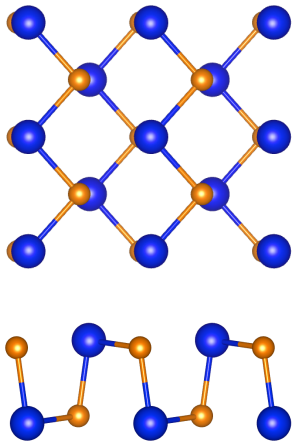

top view

side view

G.A.S.P.

Genetic Algorithm for Structure Prediction

http://gasp.mse.ufl.edu

https://github.com/henniggroup/gasp

Los Alamos NATIONAL LABORATORY EST. 1943

Cornell University

UF UNIVERSITY of FLORIDA

NSF

Evolutionary Algorithm: How it works

1. Make random initial structures and evaluate their energies with VASP
2. Select two relaxed structures to act as parents
3. Combine parent structures together to form offspring structure
4. Repeat step 2 and 3

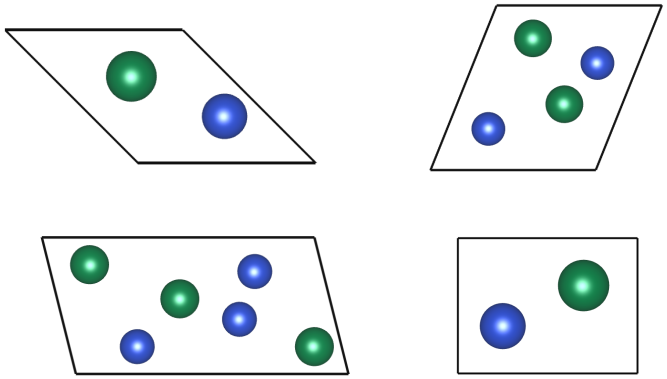

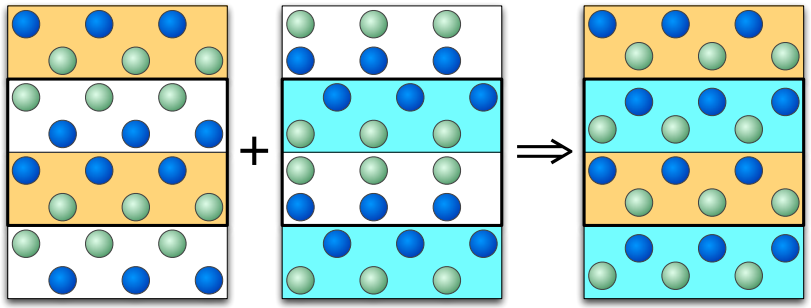

G.A.S.P.

Genetic Algorithm for Structure Prediction

http://gasp.mse.ufl.edu

Los Alamos NATIONAL LABORATORY EST. 1943

W. W. Tipton & R. G. Hennig. J. Phys.: Cond. Matter 25, 495401 (2013)
B. C. Revard, W. W. Tipton, and R. G. Hennig. Topics in Current Chemistry (2014)

NSF

Island Approach to Layered Structure Prediction

- Layered materials have unique properties, can be precisely synthesized
- Approximate one layer with a finite island, leave the other infinite

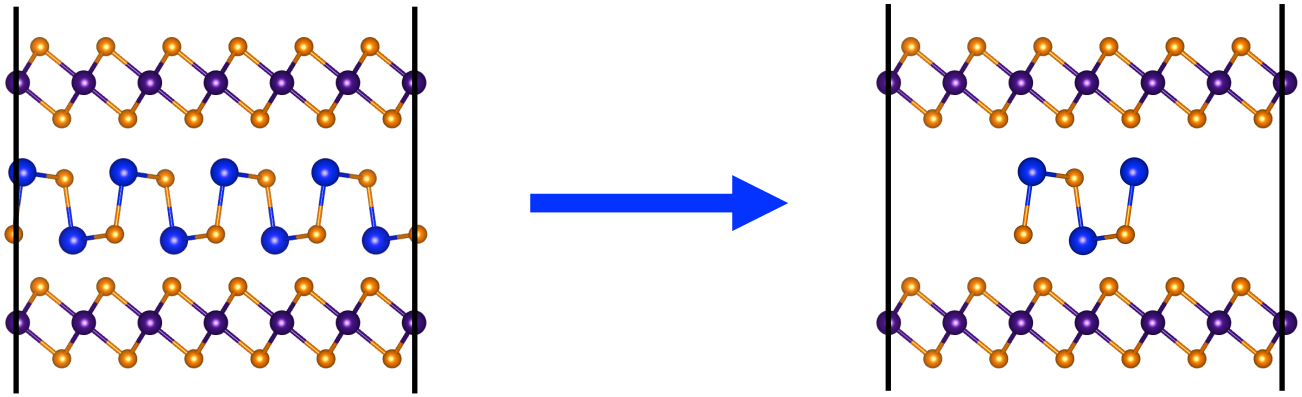

Advantages:

- Exploring new systems
  - -> No constraints on relative orientations of the layers
  - -> Identify energetically favorable ion positions
- Computationally less expensive
- Provides guidance to experimentalists
  - -> Applied to $[(SnSe)_{1+y}]_m(VSe_2)_n$ layered system

Los Alamos NATIONAL LABORATORY EST. 1943

S. P. Rudin and D. C. Johnson. Physical Review B 91.14, 144203 (2015)

NSF

SnSe Islands between VSe_2 Sheets

- SnSe – VSe_2 layered materials have recently been synthesized
- Island approach previously used to elucidate layers' orientation
- Good test case for evolutionary algorithm island search

Bulk structures

VSe_2

SnSe

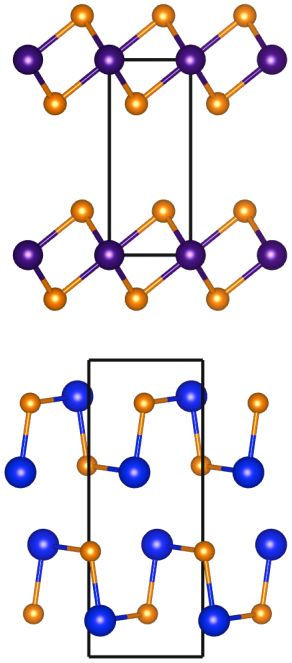

Lowest energy island structure found by the algorithm so far…

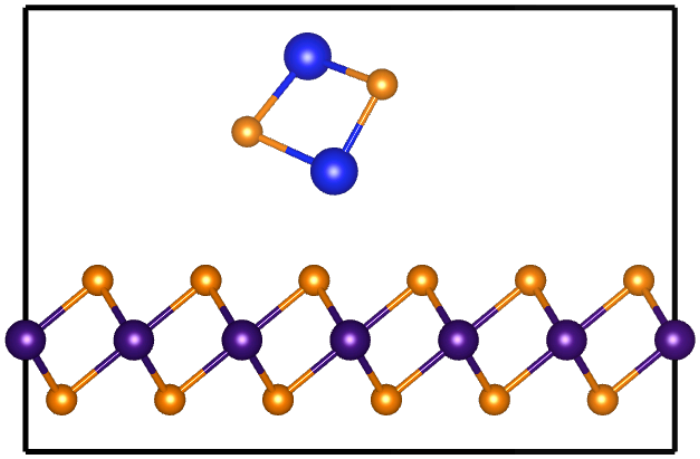

Promising start!

Los Alamos NATIONAL LABORATORY EST. 1943

R. Atkins *et al*. Chemistry of Materials 26.9, 2862-2872 (2014)
S. P. Rudin and D. C. Johnson. Physical Review B 91.14, 144203 (2015)

NSF

Predicting the Crystal Structures of Layered Materials with an Evolutionary Algorithm

Benjamin Revard, Sven Rudin

- Evolutionary algorithm
  - How it works
- Layered materials
  - Island approach to layered structure prediction
- Preliminary results
  - SnSe – VSe_2 layered system
- Future work
  - Variable composition search

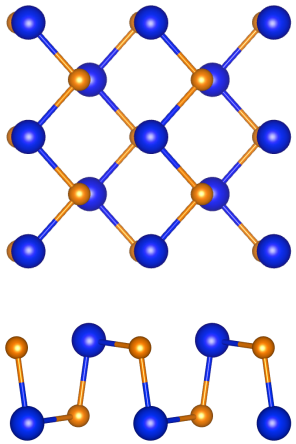

top view

side view

G.A.S.P.

Genetic Algorithm for Structure Prediction

http://gasp.mse.ufl.edu

https://github.com/henniggroup/gasp

Los Alamos NATIONAL LABORATORY EST. 1943

Cornell University

UF UNIVERSITY of FLORIDA

NSF

Evolutionary Algorithm: Why it works

Cast structure prediction as a global optimization problem

Minimize the enthalpy (per atom) as a function of the structural parameters

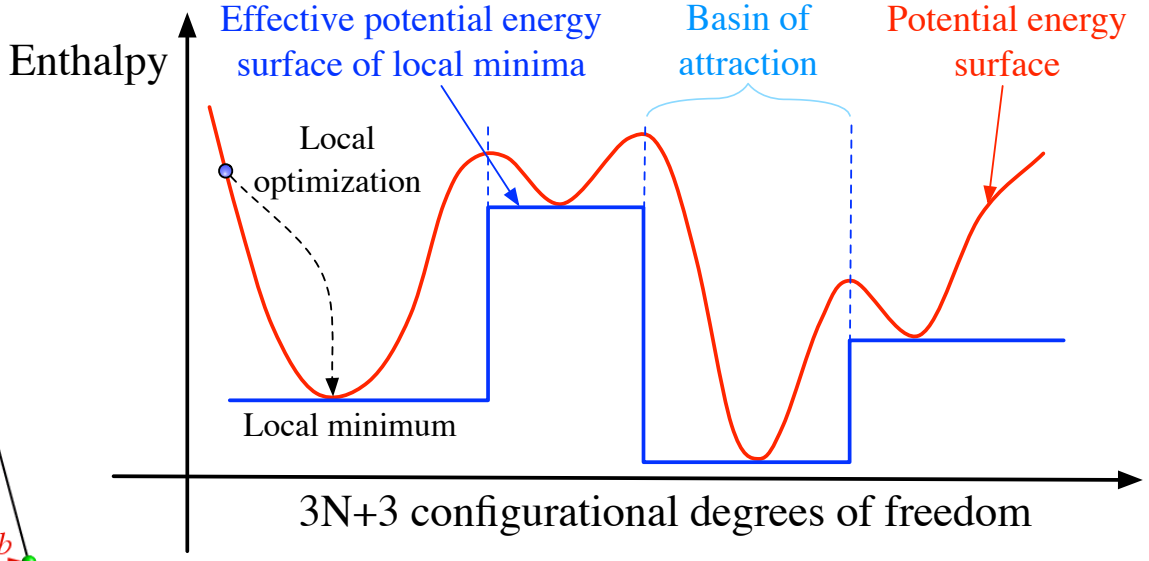

lattice vectors
&
atomic locations

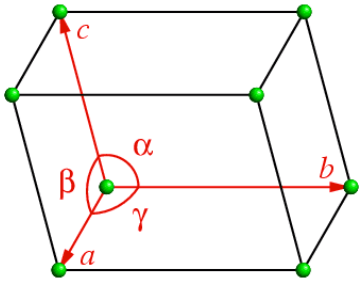

Exploit features of the potential energy surface

- Potential energy surface divided into basins of attraction
- Hypervolume increases with the basin depth
- Physical constraints reduce size of search space
- Short-range interactions contribute most to energy

Los Alamos NATIONAL LABORATORY EST. 1943

C. P. Massen & J. P. Doye (2007), W. W. Tipton & R. G. Hennig (2013),
B. C. Revard, W. W. Tipton, and R. G. Hennig (2014), J. K. Cockcroft (1995)

NSF

Modifications for Layered Crystal Structure Prediction

Once a structure has been generated…

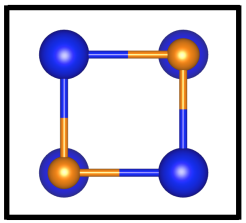

Sandwich it between sheets to create an island

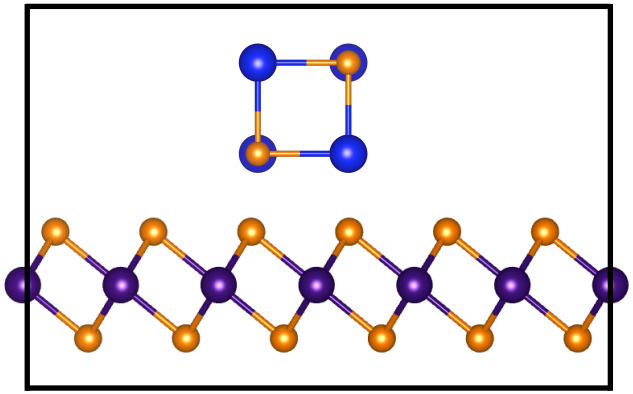

Pass to energy code

VASP
PAW-PBE

Remove sandwiching sheets

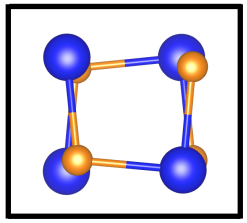

Los Alamos NATIONAL LABORATORY EST. 1943

NSF

Texture completion using a pre-trained convolutional neural network

By : Julien Roy, Nicholas Lubbers,
Kipton Barros & Brendt Wohlberg

POLYTECHNIQUE
MONTRÉAL

Center for
Nonlinear Studies

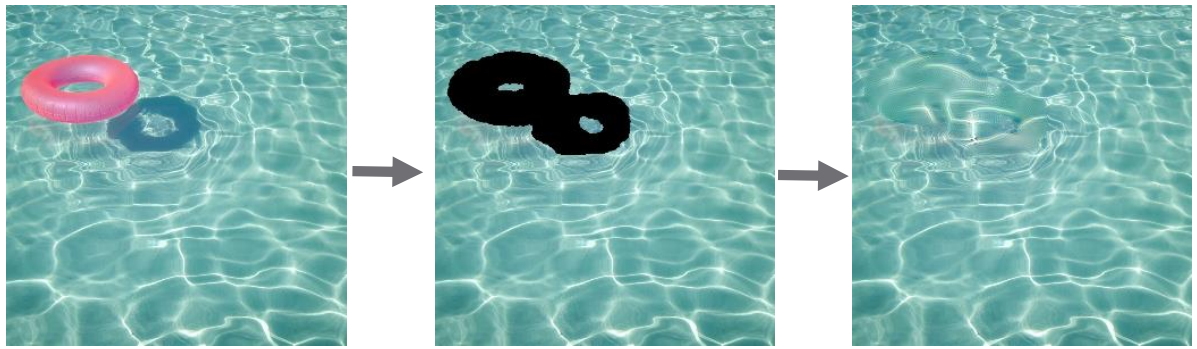

Introduction

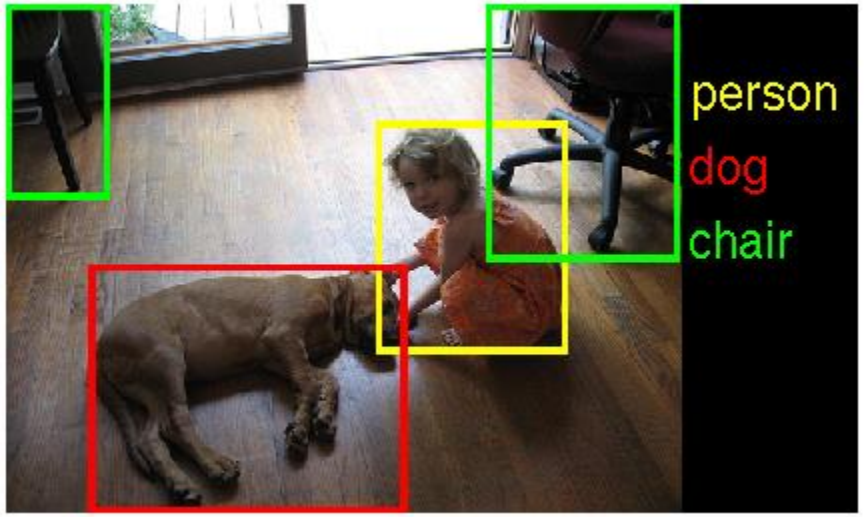

Convolutional Neural Networks : The stars of computer vision

-> Perform tasks like : classification, localization, segmentation, etc.

-> Recently exceeded human-level performance

-> Can be used for new tasks beyond the scope of their training (*transfer learning*)

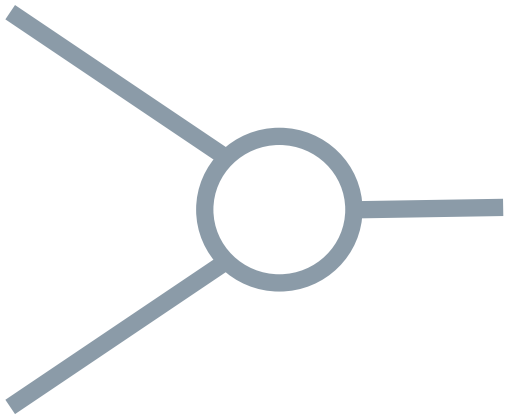

CNNs

Texture model

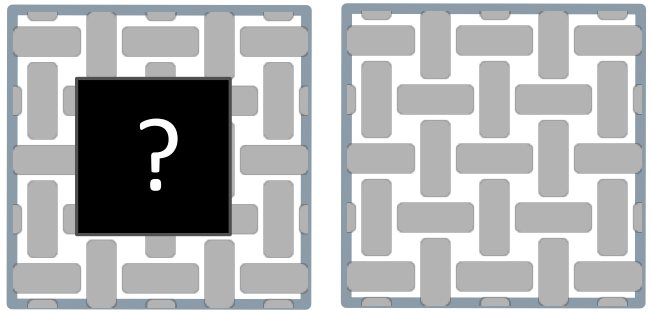

Texture completion

Outline

Artificial Neural Networks (ANN)

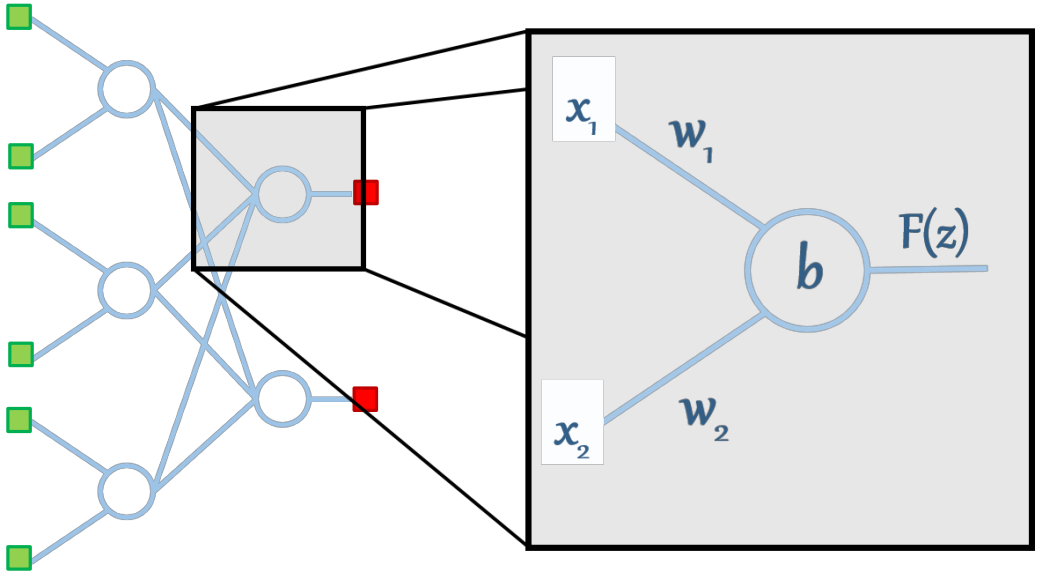

: inputs

: outputs

$$z = \sum w_i x_i + b$$

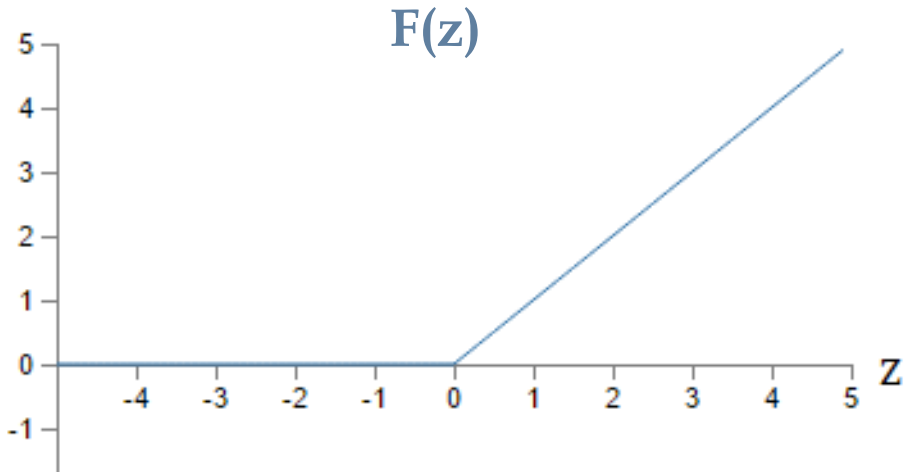

Convolutional neural networks (CNNs)

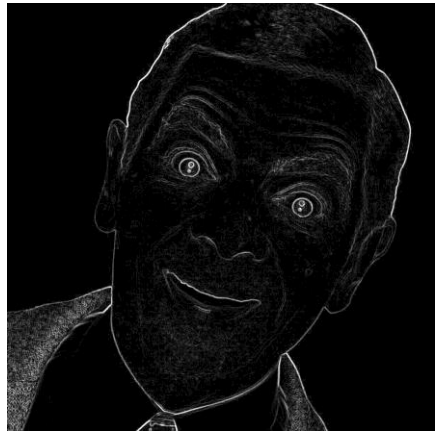

Input image

Convolutional layer (Filtering)

Pooling layer (Step back)

Convolutional neural networks (CNNs)

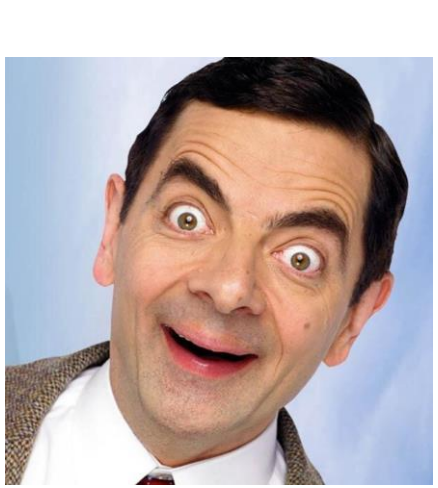

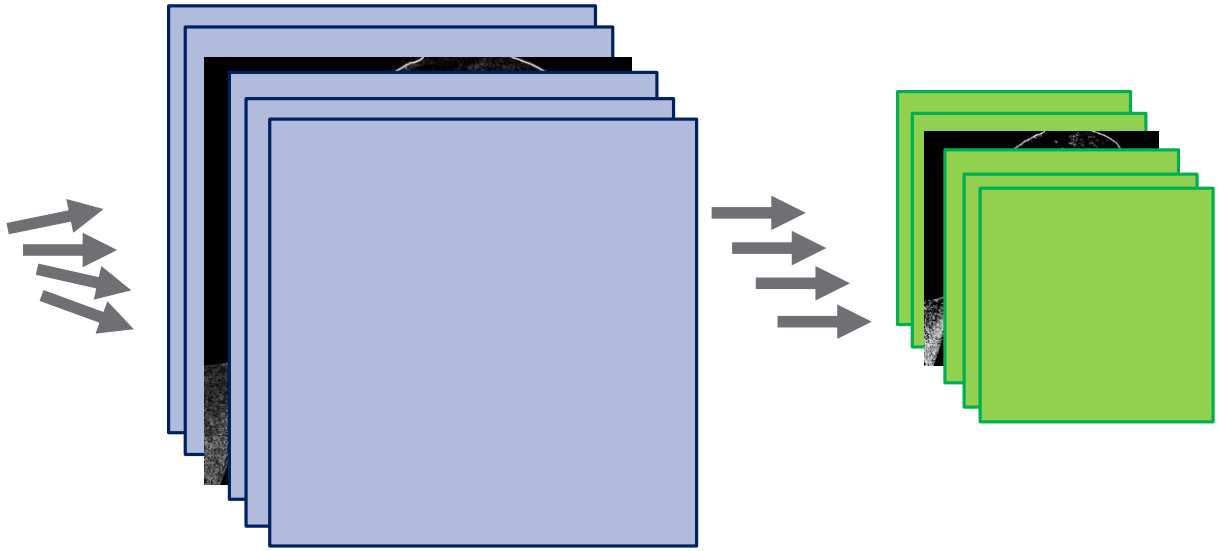

Input image

Convolutional layer (Filtering)

Pooling layer (Step back)

Convolutional neural networks (CNNs)

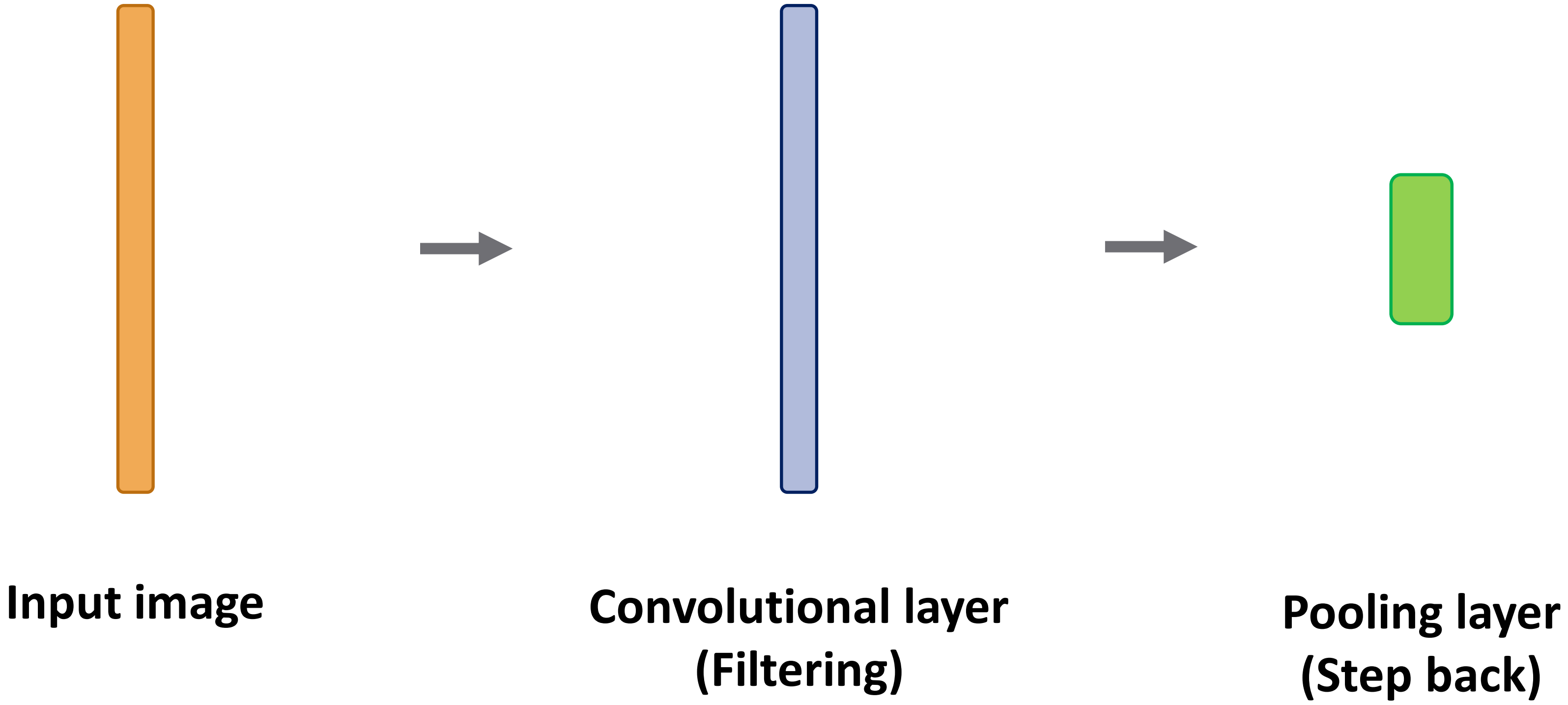

Gatys' texture representation

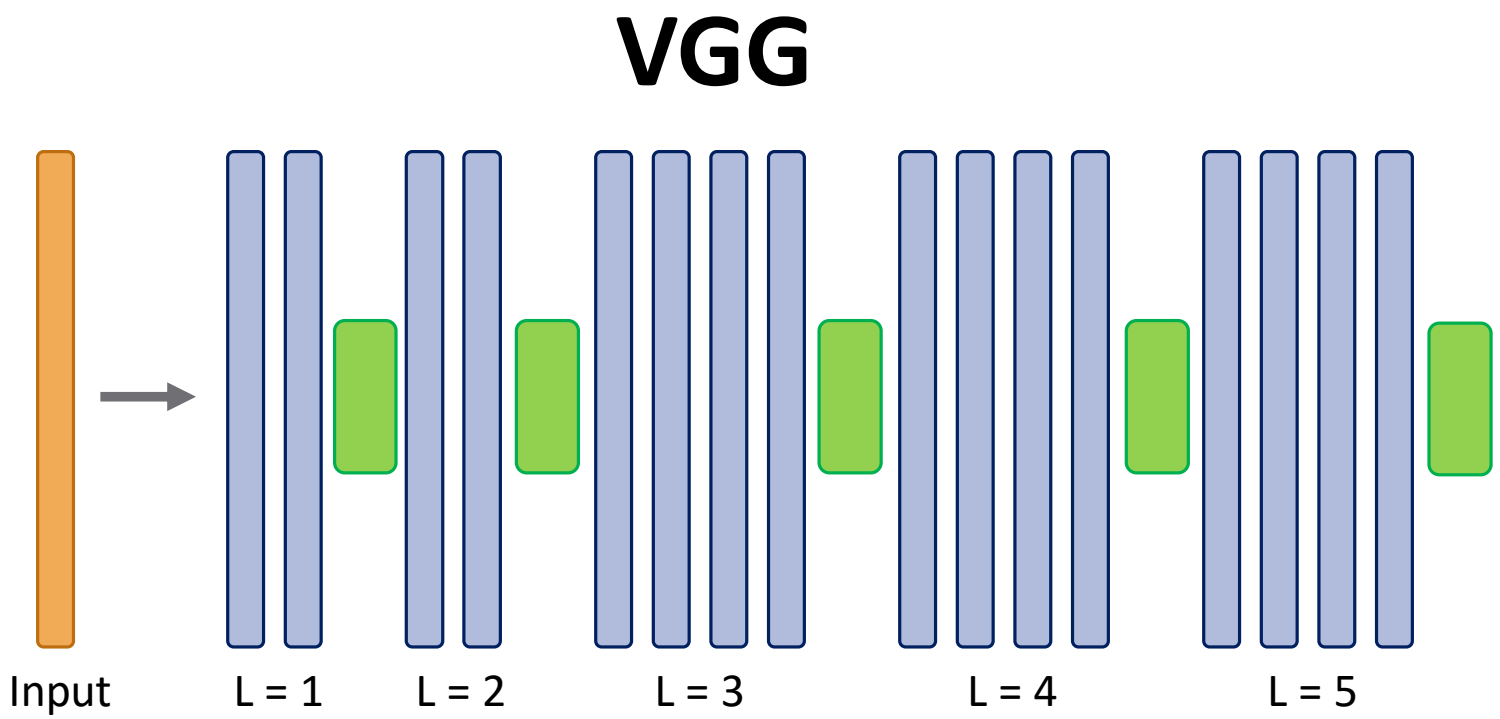

Gatys' texture representation

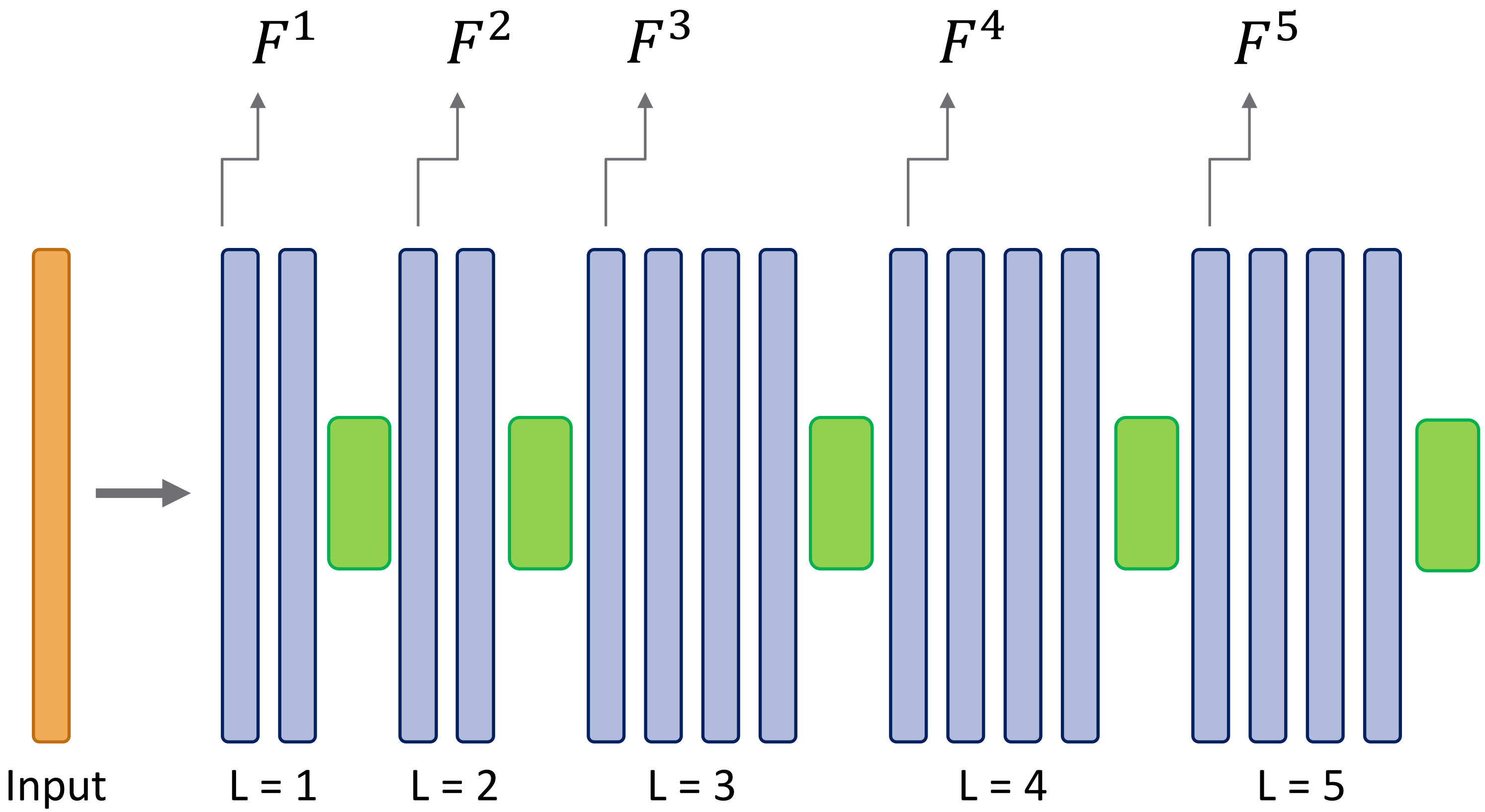

Gram Matrix :

$$G^L_{i,j} = \sum_x F^L_{i,x} F^L_{j,x}$$

Loss Function :

$$E = \left\| G - \hat{G} \right\|^2_{l^2}$$

Reference   Target

Texture synthesis

Reference

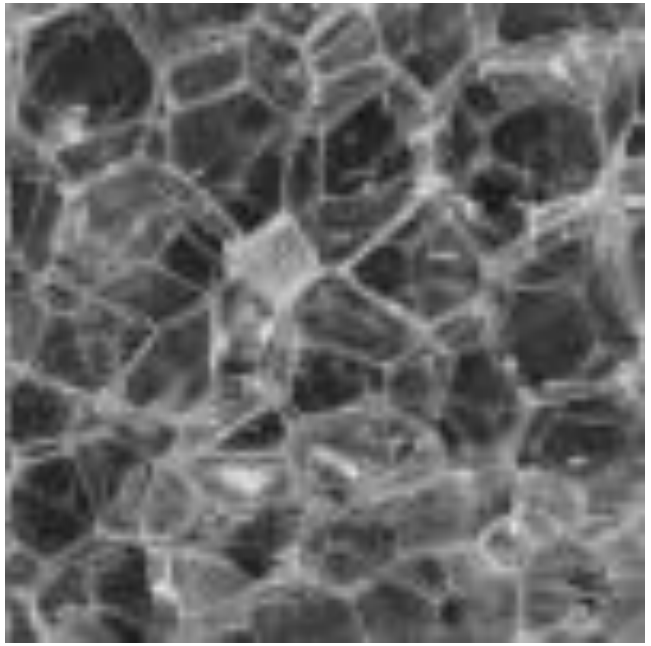

Target

Texture synthesis

Reference

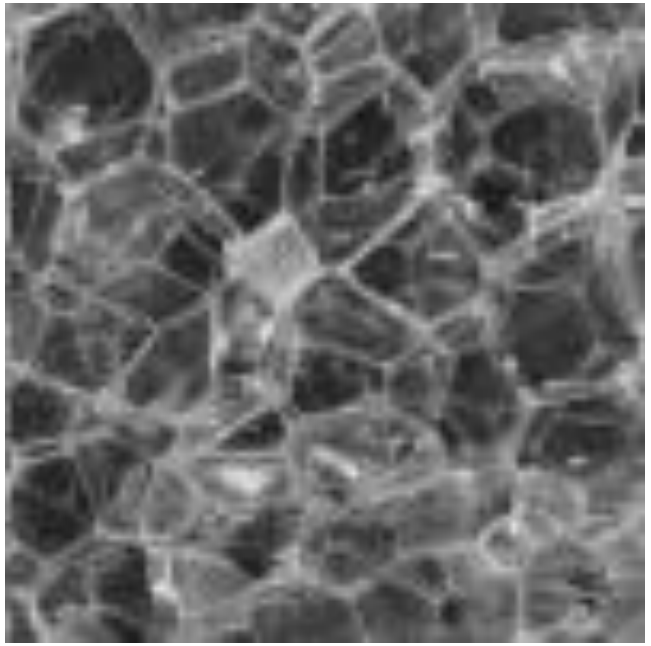

Target

Texture synthesis

Reference

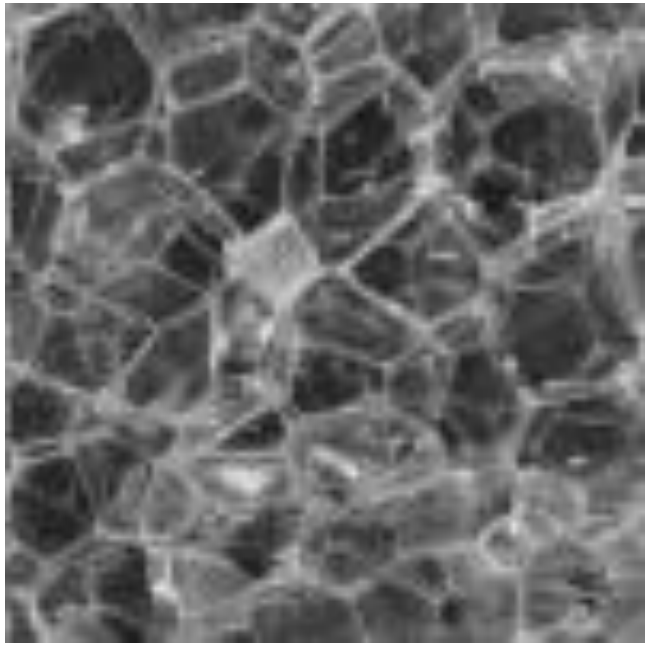

Target

Texture synthesis

Reference

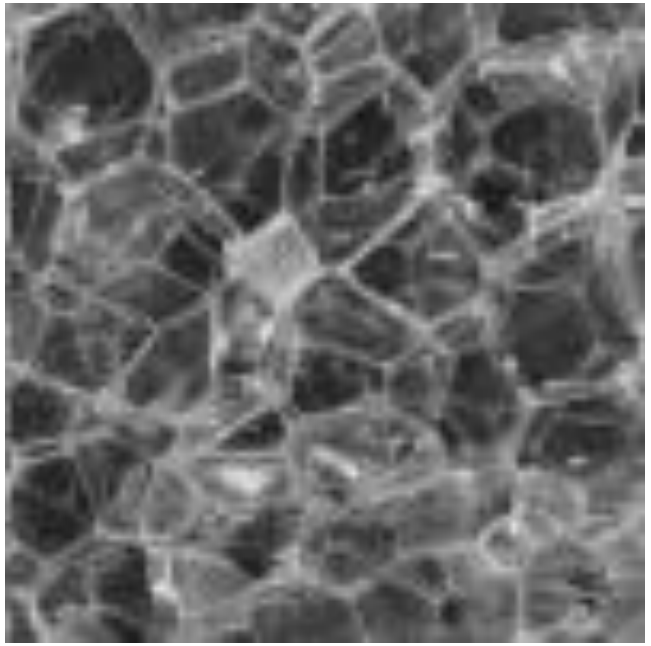

Target

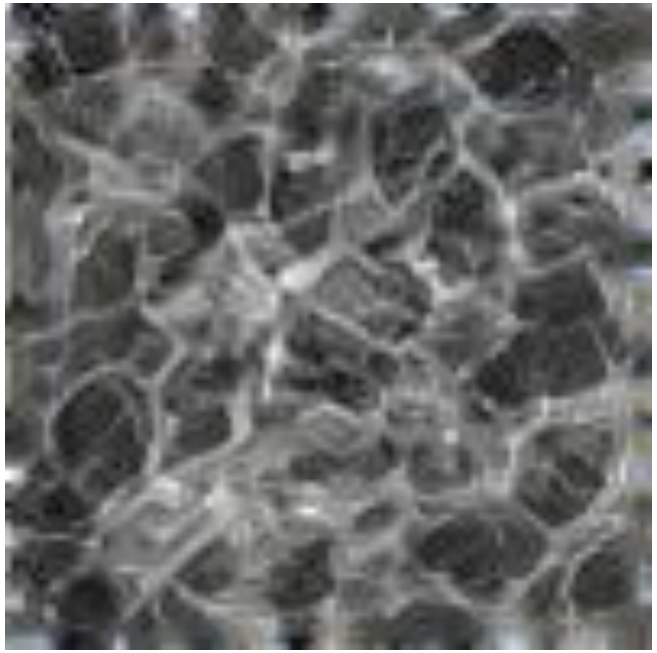

Texture completion

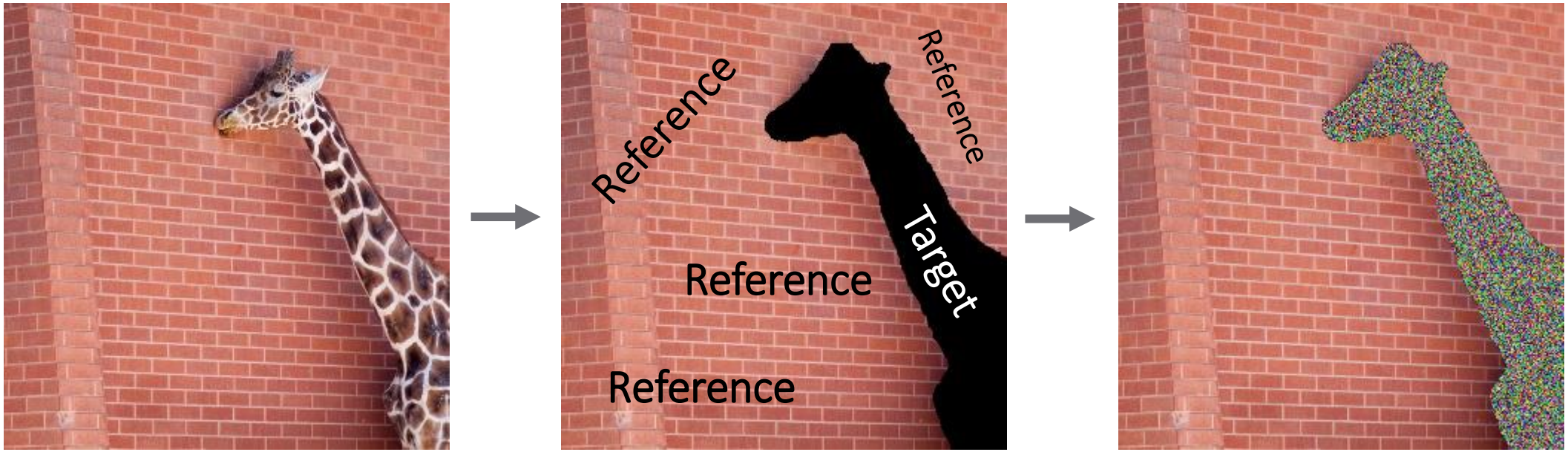

Texture completion

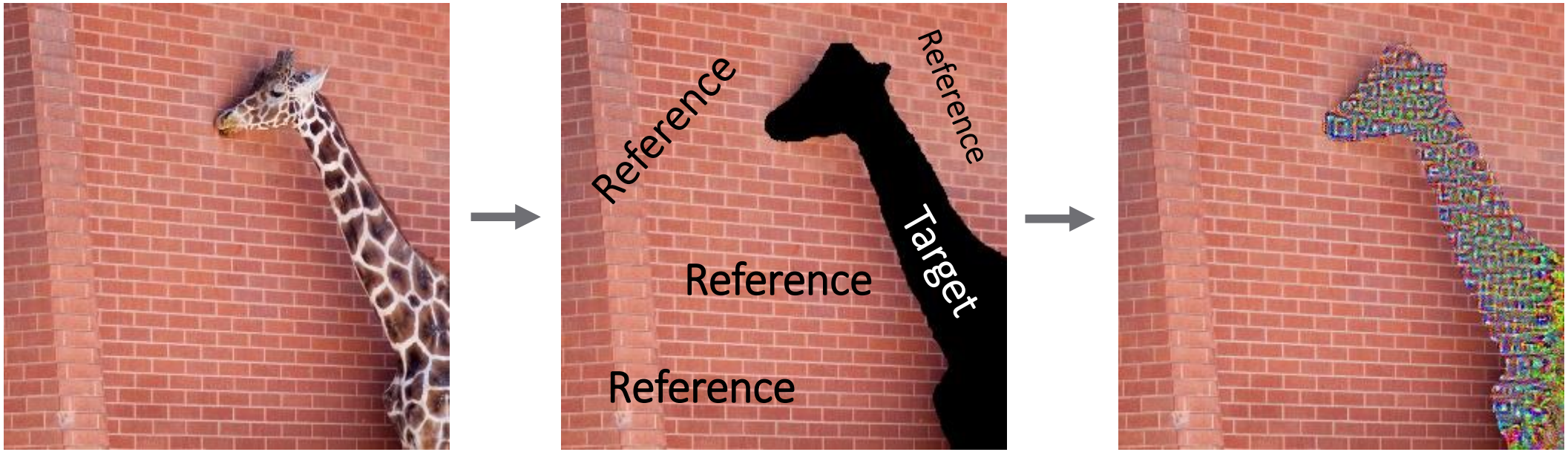

Texture completion

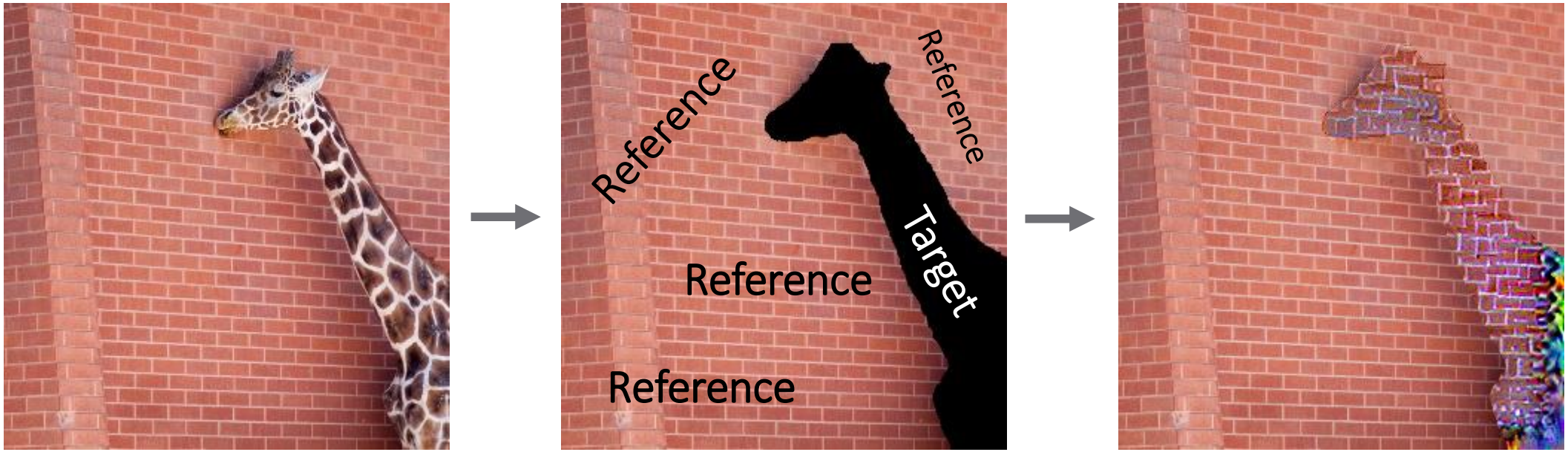

Texture completion

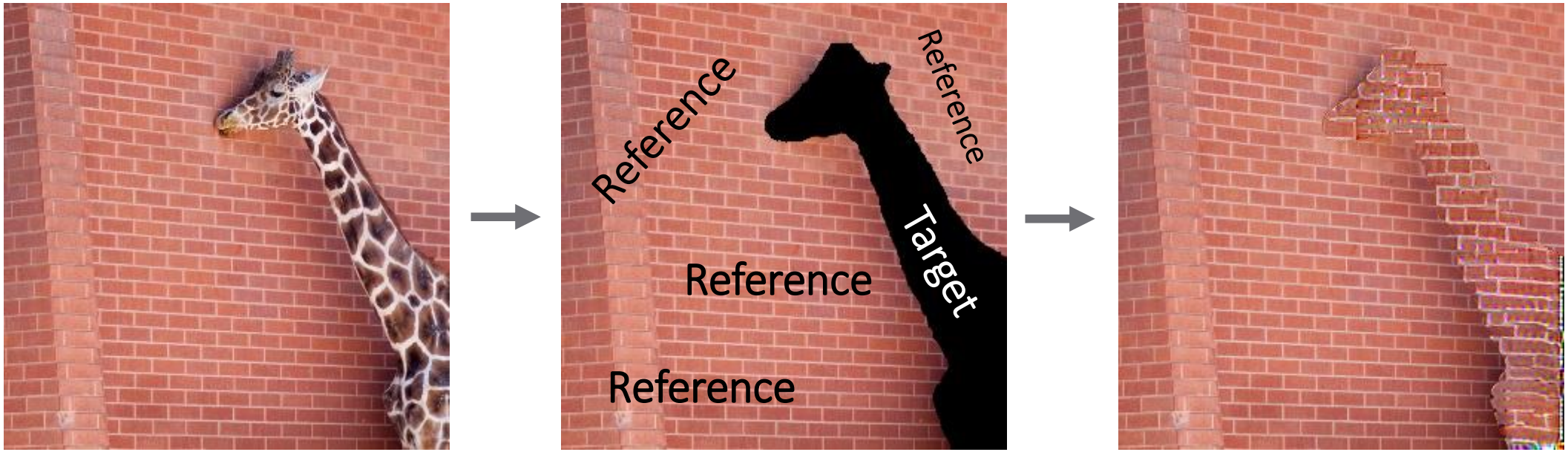

Texture completion

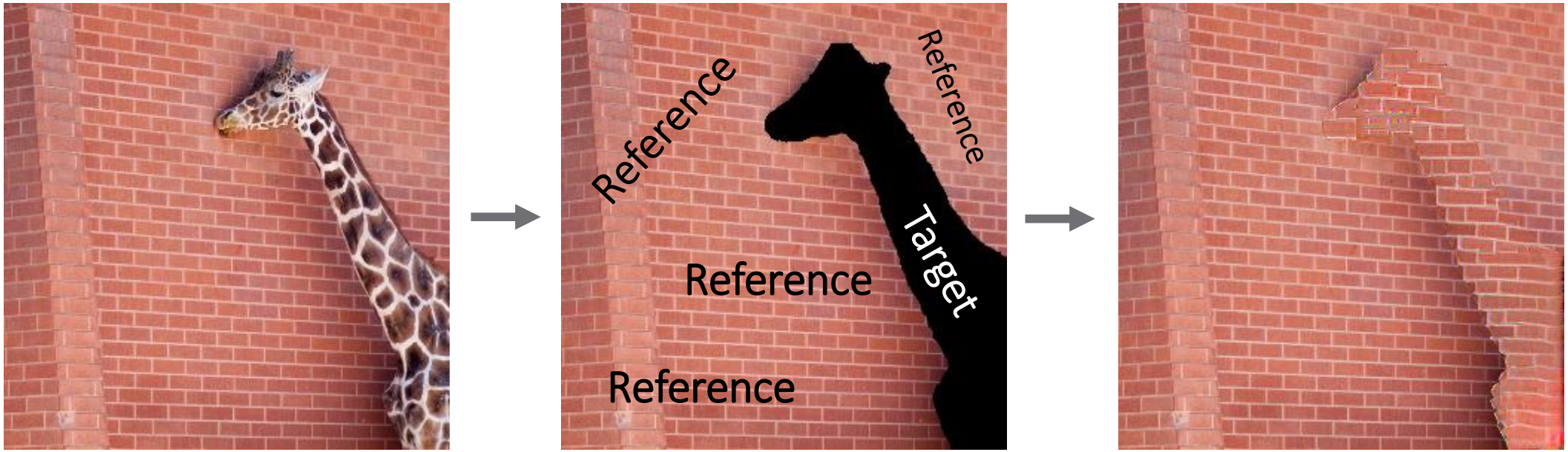

Masking

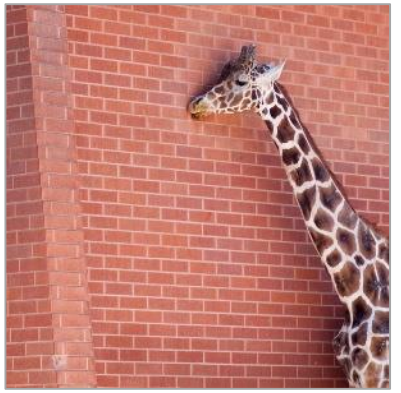

A way of keeping track of :

- ❑ neurons that have only seen the reference
- ❑ neurons that are looking at the target

Input mask

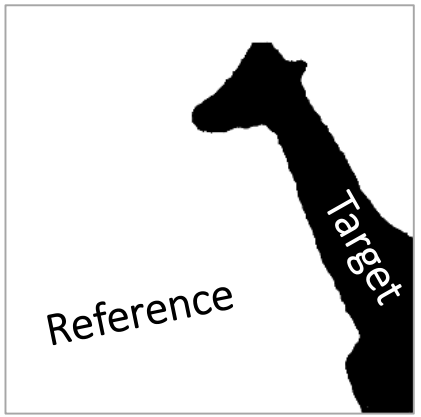

Conv 1

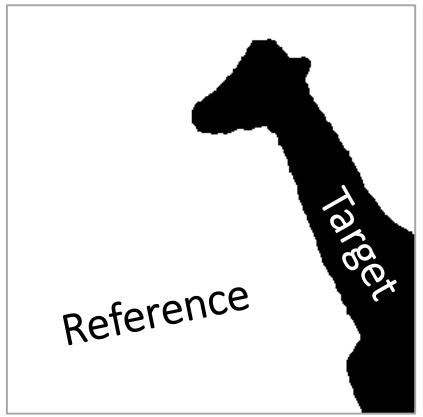

Conv 2

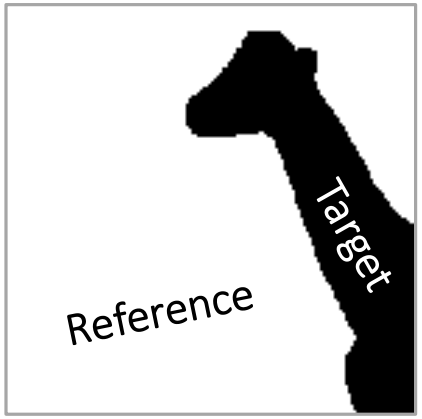

Conv 3

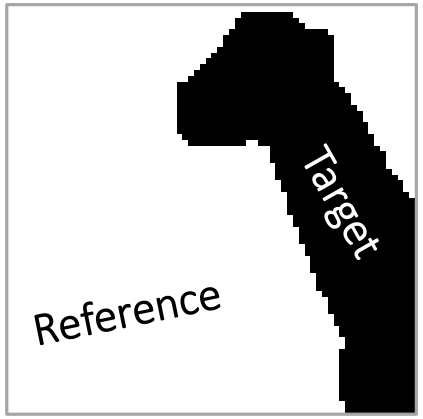

Conv 4

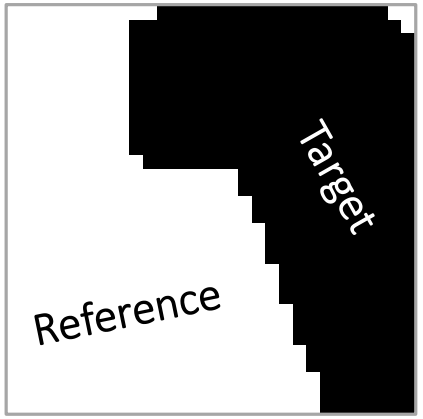

Results

Source | Initialization | Reconstruction

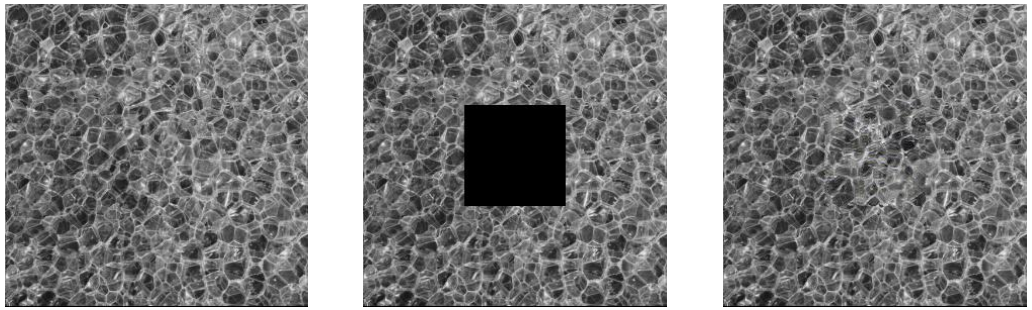

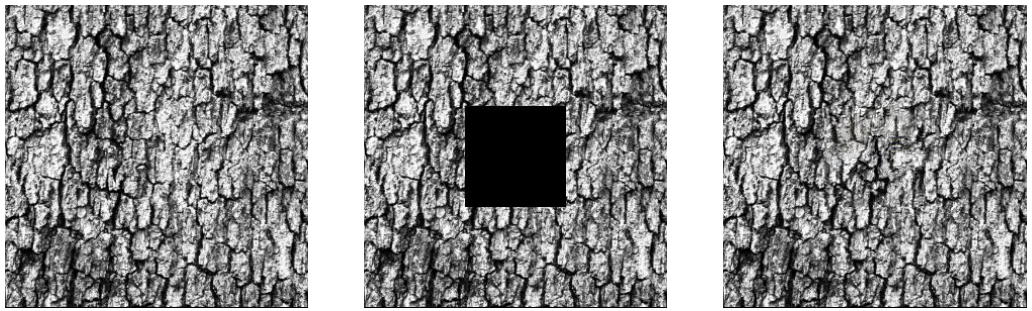

Source | Initialization | Reconstruction

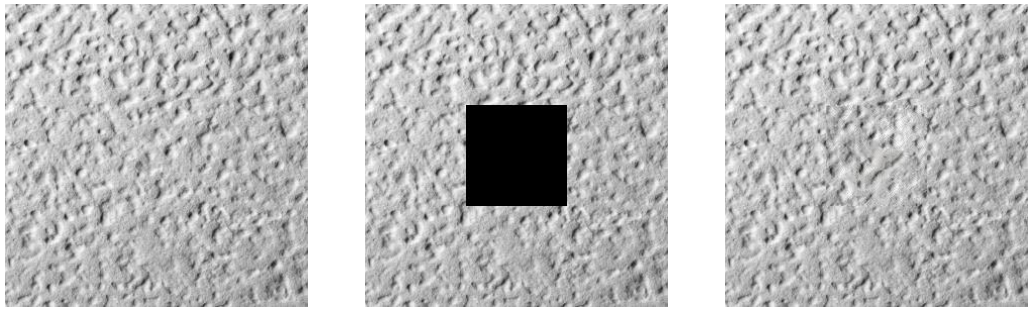

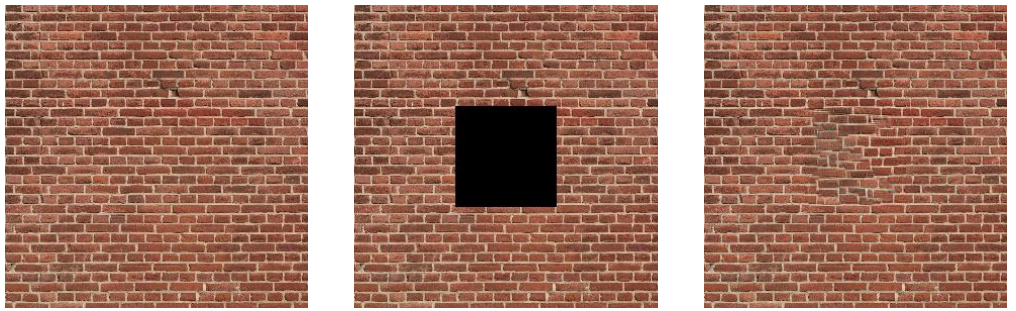

Successes

Source

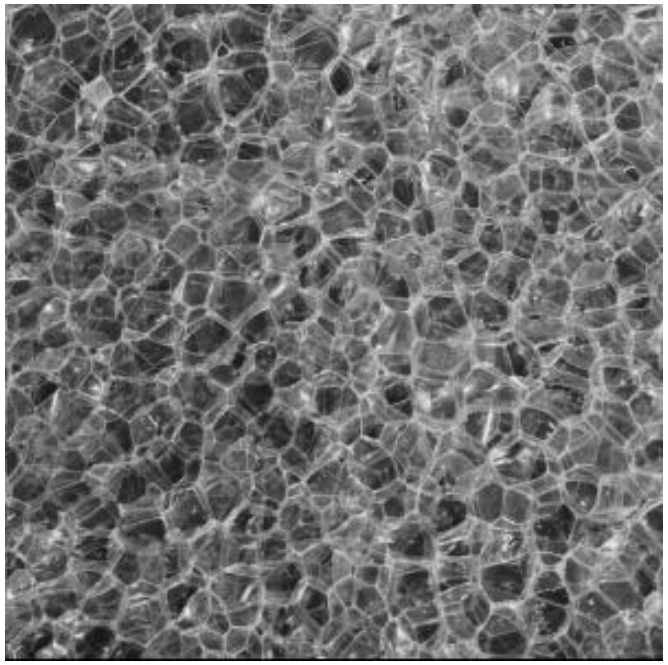

Initialization

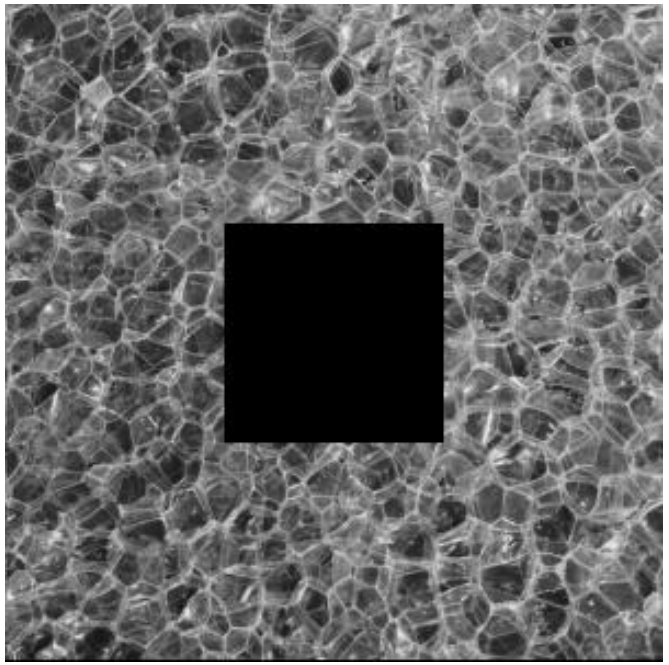

Reconstruction

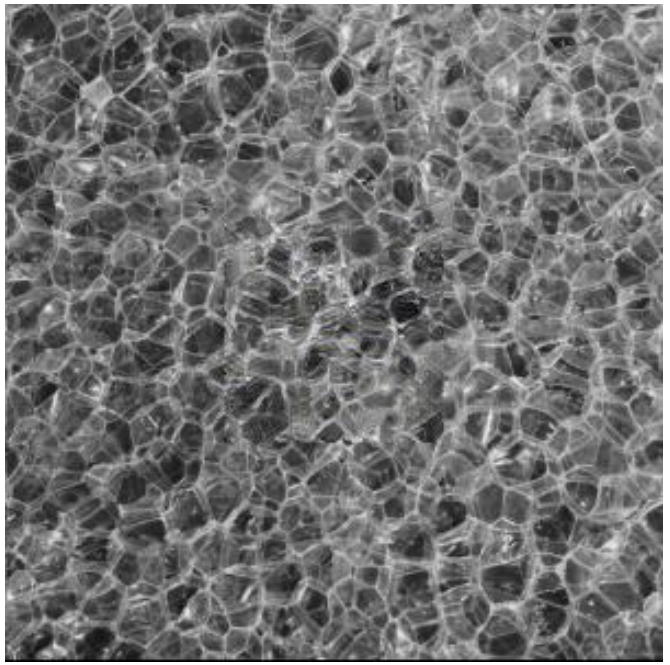

Successes

Source

Initialization

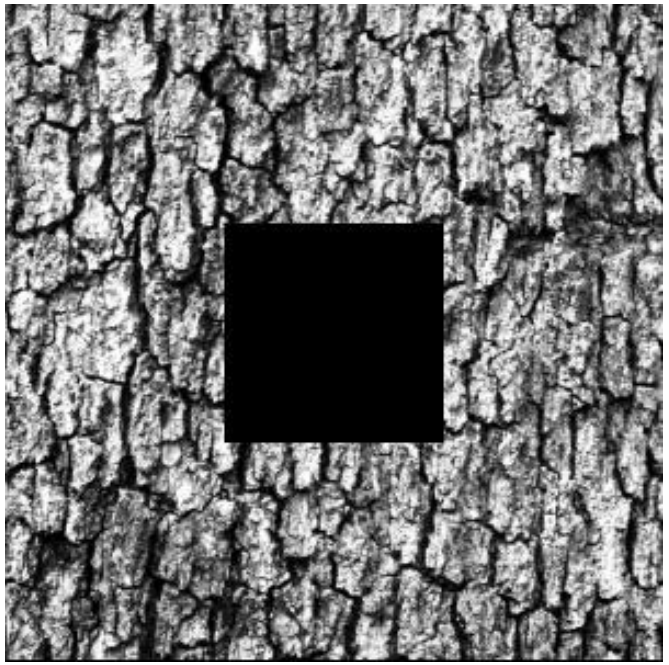

Reconstruction

Failure modes : Highly constrainted patterns

Source

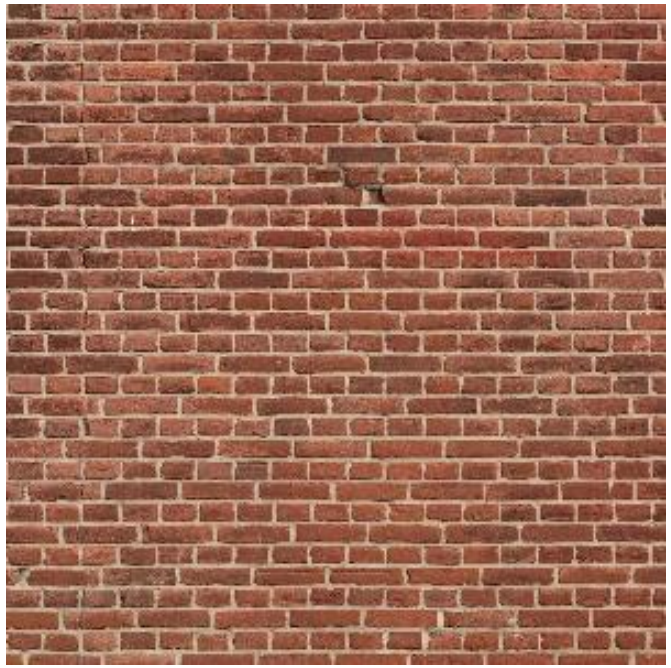

Initialization

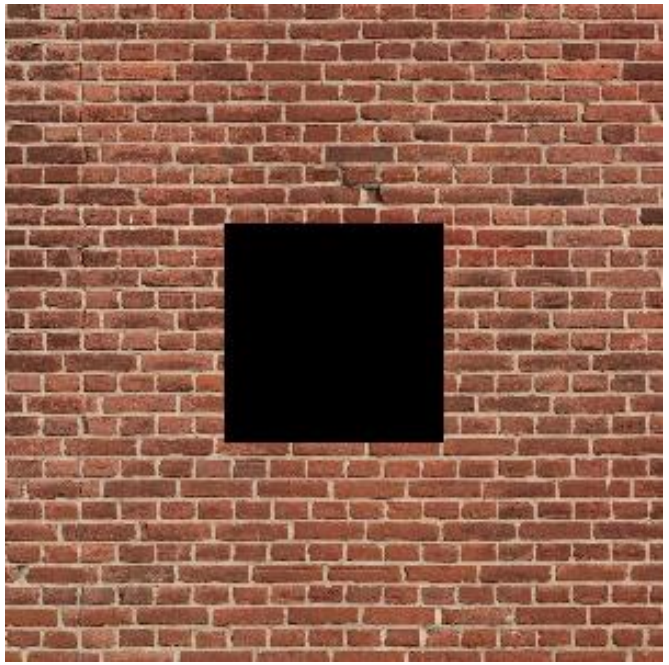

Reconstruction

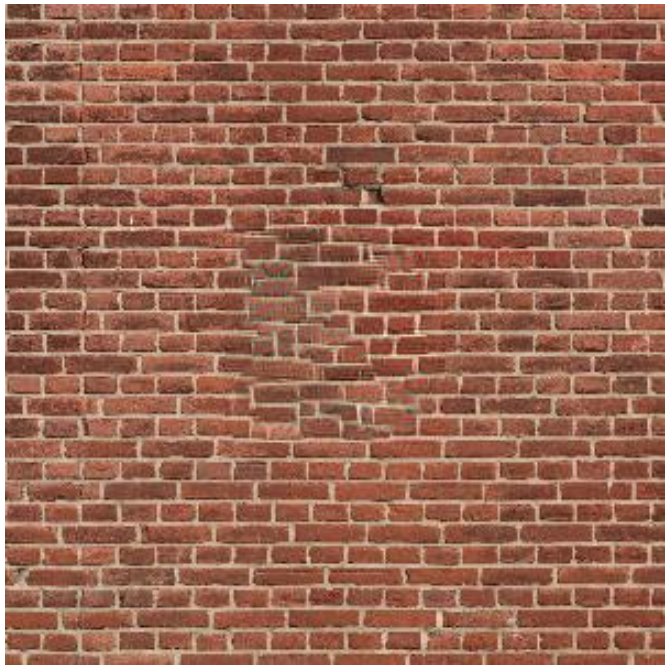

Failure modes : Critically degraded images

Source

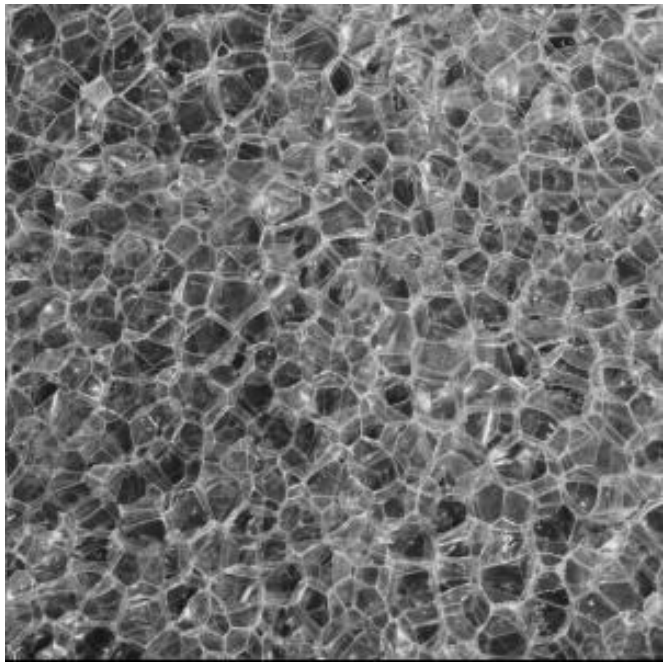

Initialization

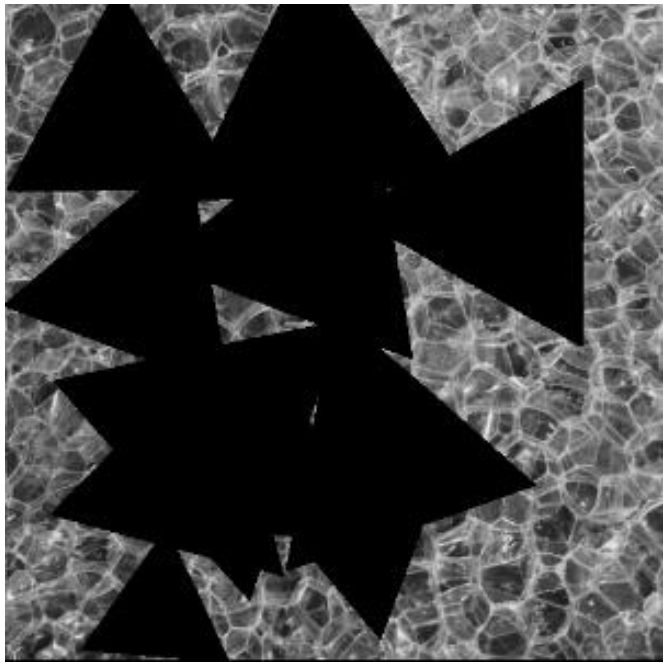

Reconstruction

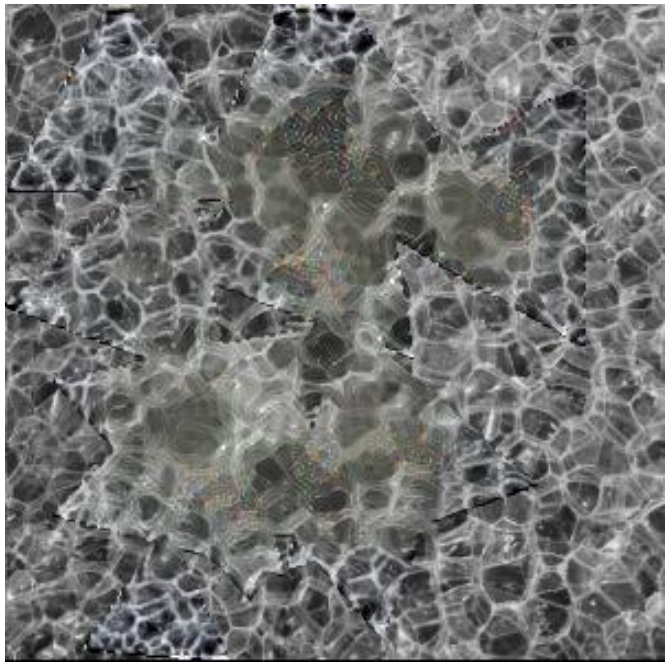

Thank you from the bottom of our hearts !

(pun)

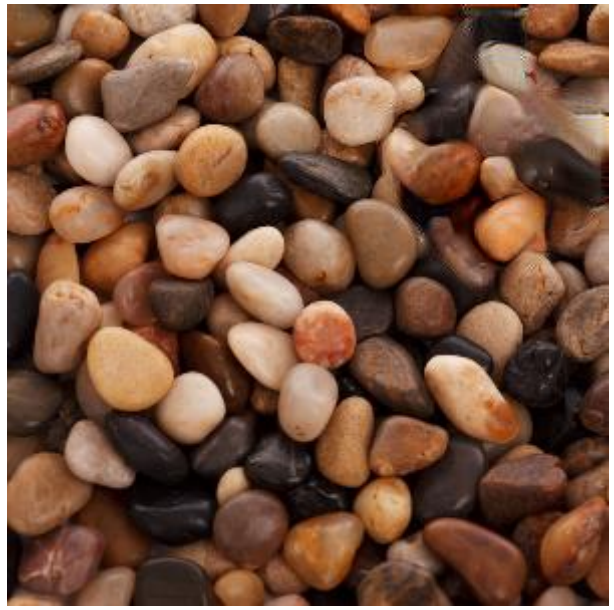

Rule-based modelling of autophagy with dynamic compartments allows incorporation of effects of Influenza A infection

Kalina Slavkova
advised by Dr. Bill Hlavacek and Dr. Ruy Ribeiro

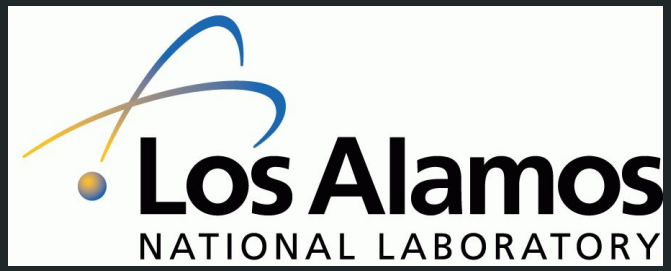

Background

↳ Problems

↳ Approaches

↳ Results

↳ Future Directions

What is autophagy?

Autophagy = "self-eating"

Macroautophagy = "Macroautophagy is a process in which cellular contents are degraded by lysosomes or vacuoles and recycled."
Starvation-induced(http://www.nature.com/subjects/macroautophagy)

Microautophagy = Direct engulfment of small particles by the lysosome

Important in viral and cancer pathways

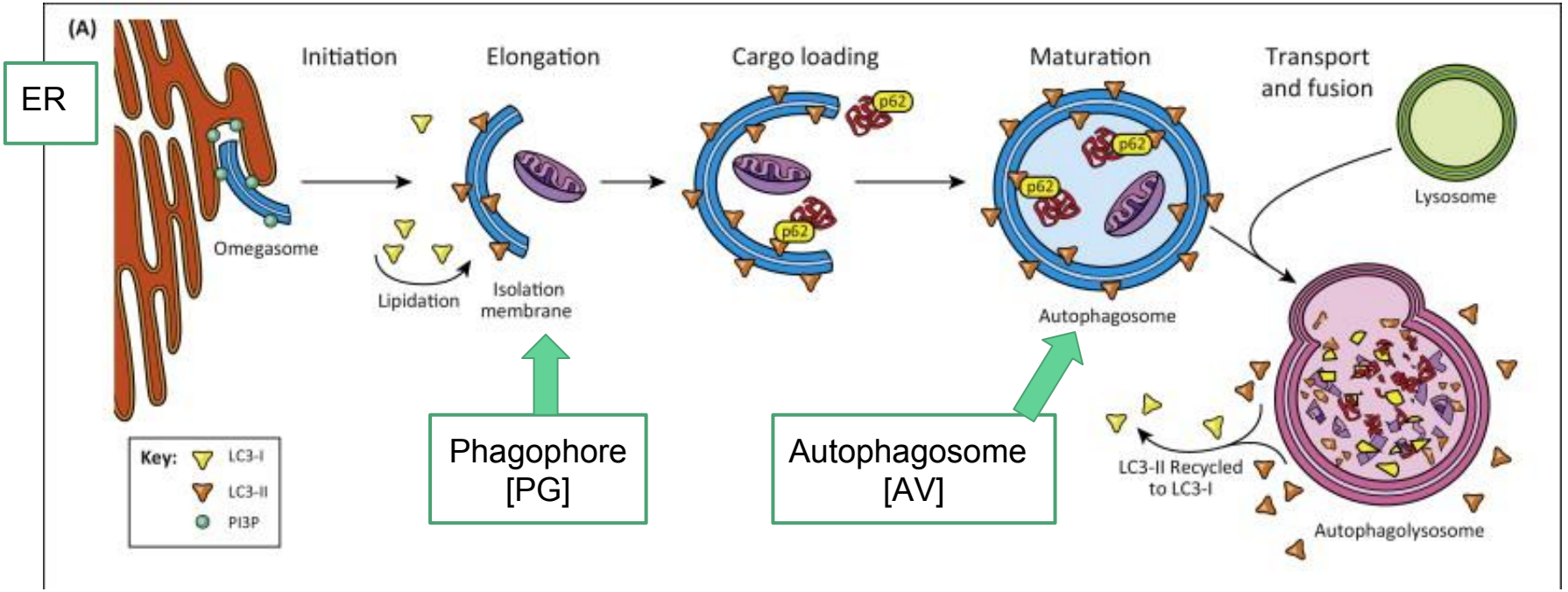

Fig. 1: Trends in Neurosciences, Vol. 28, Issue 1, p26–35

What is rule-based modelling?

➡ Implicitly describe mathematics of reactions with a set of rules

Languages

- **RuleBender**

```
#association/dissociation of WIPI and PtdIns(3,5)P2
R16: WIPI(l,l) + PIns(t~PP,f~PP,l,l) <-> WIPI(l!1,l).PIns(t~PP,f~PP,l!1,l) k_cap, k_rel2
```

- **ML-Rules**

```
MemSrc[PtdIns35P2:pip2 + pm?] + WIPI:w -> MemSrc[WIPI_PtdIns35P2+pm?] @ k_a2*#pip2*#w; //forward ass
MemSrc[WIPI_PtdIns35P2:wpt2+pm?] -> MemSrc[PtdIns35P2 +pm?]+ WIPI  @k_d2_2*#wpt2;//dissociation, eq
```

Key Publications

Martin, K. R., Barua, D., Kauffman, A. L., Westrate, L. M., Posner, R. G., Hlavacek, W. S., & MacKeigan, J. P. (2013). Computational model for autophagic vesicle dynamics in single cells. *Autophagy*, *9*(1), 74-92.

- Count AV's via GFP labelled LC3-II
- Computational model of autophagy under different conditions
- AZD8055 - stimulates autophagy
- BafA1 - inhibits autophagy

Zhirnov, O. P., & Klenk, H. D. (2013). Influenza A virus proteins NS1 and hemagglutinin along with M2 are involved in stimulation of autophagy in infected cells. *Journal of virology*, *87*(24), 13107-13114.

- NS1 and M2 stimulate autophagy
- NS1 may downregulate apoptosis

Deterministic Model of Autophagy (Martin et al.)

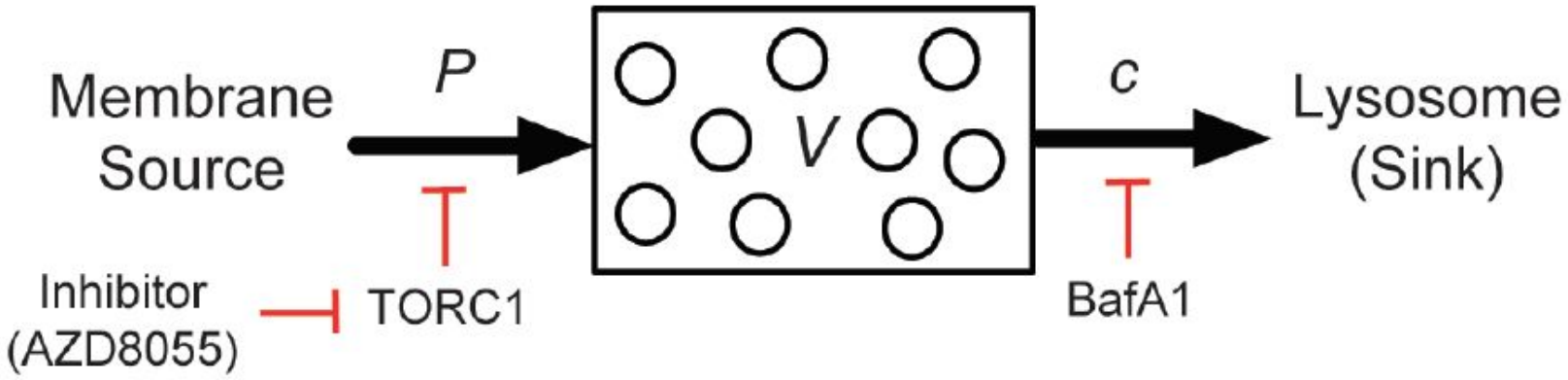

Fig. 2: Simple deterministic model of autophagy, modelled by one ODE (Fig. 3 A in Martin et al.)

$$\frac{dV}{dt} = (1+\delta_a k)P - (1-\delta_b)cV,$$

P = initiation rate = 0.18 min
k = augmentation of P = 2.94
c = degradation rate = 0.037
δ_a = presence of AZD8055 = 0 or 1
δ_b = presence of BafA1 = 0 or 1

[Background]

Mechanistic model of autophagy (Martin et al.)

Fig. 3: Mechanistic model of autophagy, stochastically simulated as reactions (Fig. 5 in Martin et al.)

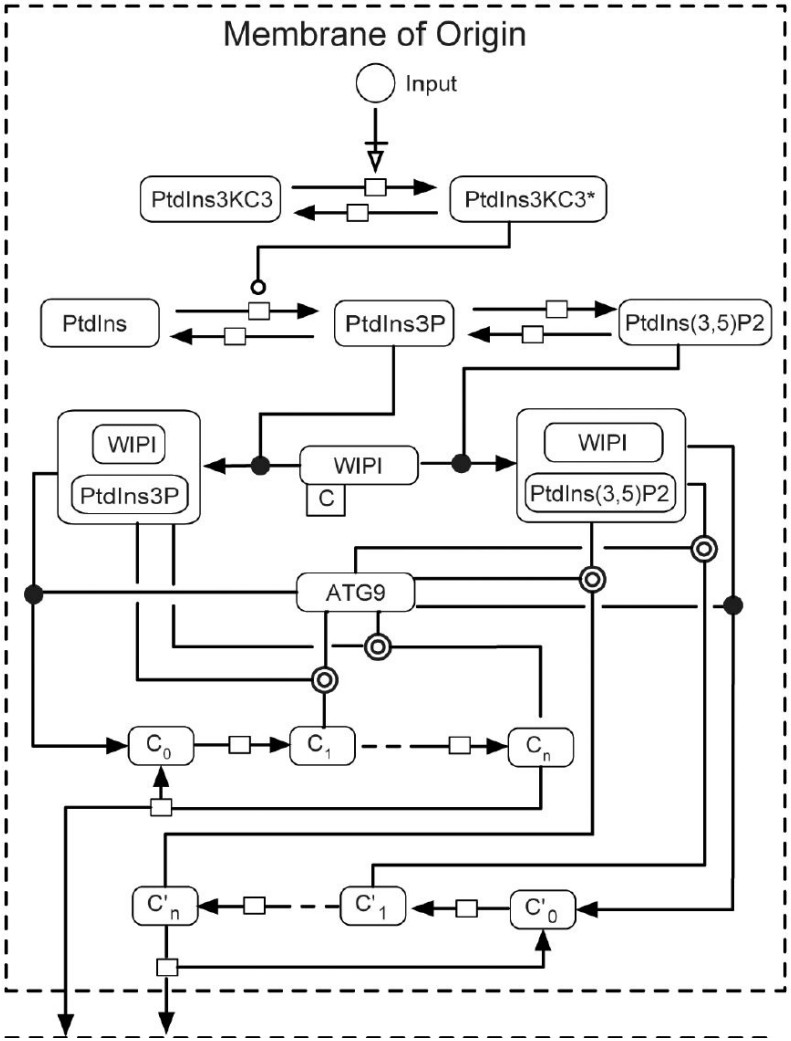

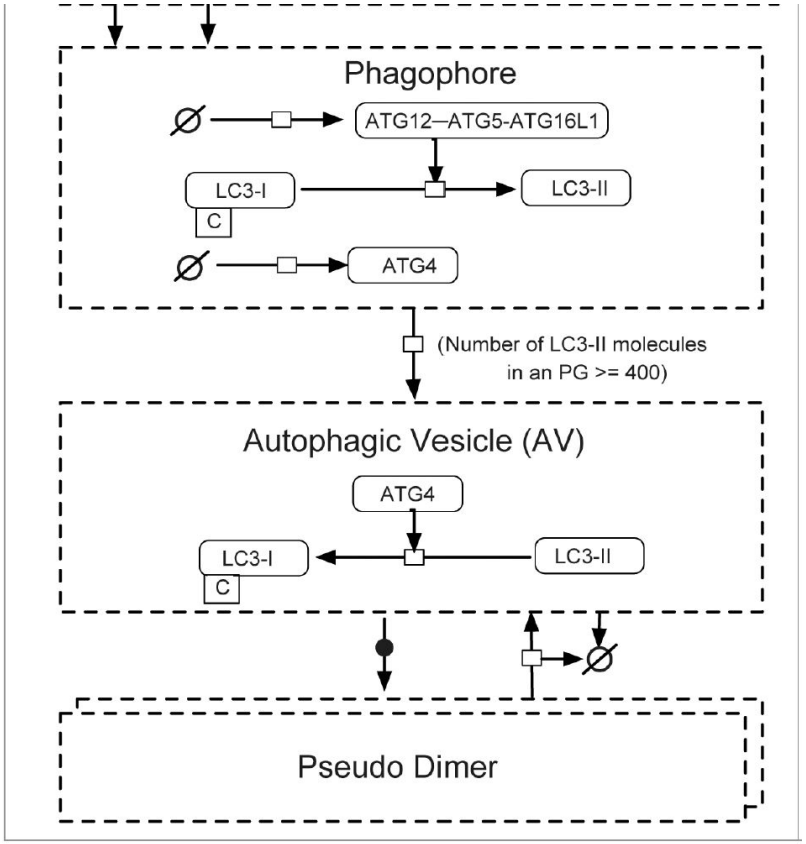

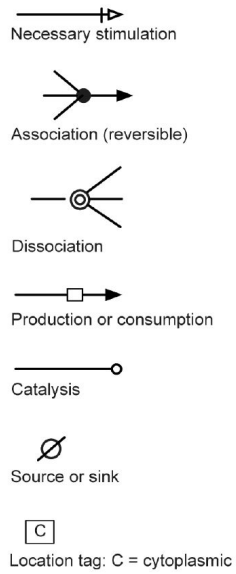

Key Players:

*PI3KC3: Class III phosphatidylinositol 3-kinase

*PtdIns3P: **Phosphatidylinositol 3-phosphate**

*LC3-I: Microtubule-associated protein 1A/1B-light chain 3

*LC3-II: phosphatidylethanolamine conjugated LC3

*ATG Proteins: Autophagy related proteins

Effects of IA Proteins on Autophagy (Zhirnov et al.) [**influenza model**]

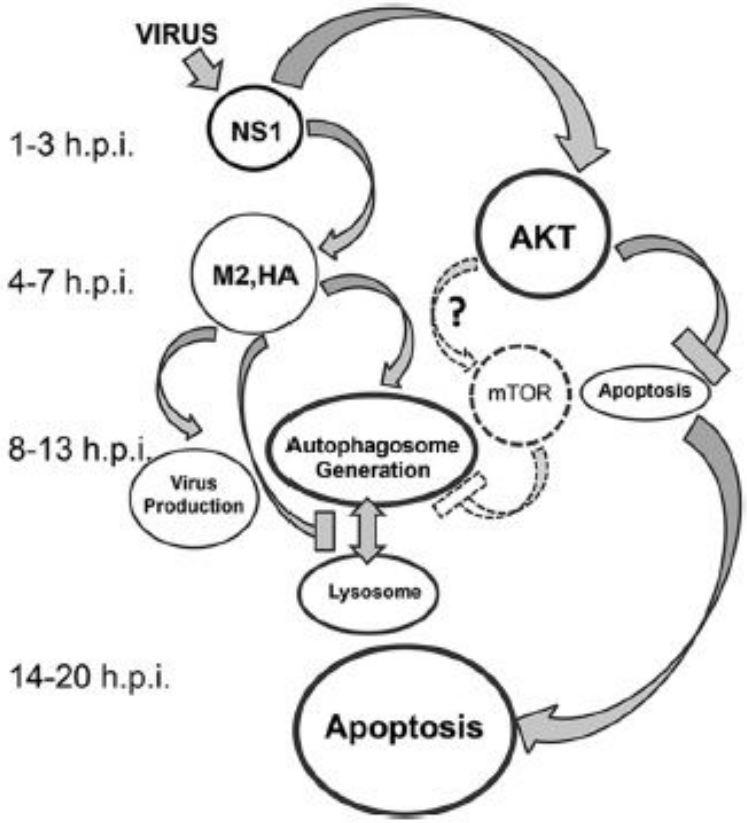

Fig 4. Autophagy pathway under IA infection. NS1 stimulates amplified production of M2 and HA, which in turn block fusion of autophagosome with lysosome. ***M2 recruits LC3 to the plasma membrane, effectively redistributing phospholipids*** (Fig. 7 Zhirnov et al.)

Key Players:
*NS1: Nonstructural Protein 1
*HA: Hemagglutinin
*M2 Microtubule-associated protein 1A/1B-light chain 3

Problems of Interest

1.) Martin et al. models not executed with a system capable of dynamic compartments; hard-coded in C instead. We want an easily expandable model

Solution: ML-Rules rule-based language with dynamic compartments

2. Deterministic model in Martin et al. is very simples; not many degrees of freedom to explore

Solution: create an expanded model with four stages of autophagy

3.) Martin et al. models do not explicitly describe effects of Influenza A proteins

Solution: add relevant parameters/rules to expanded model

Main Motivation: Develop ML-Rules as useful tool in this context, get some results on IAV infection

Approach to P#1: Modelling with ML-Rules

1. Convert SBML of simple and mechanistic models to **ML-Rules** syntax
2. Run and average many simulations using **SESSL** modelling package
   a. Simple model will serve as control
3. Plot autophagosome count averages and compare to published data

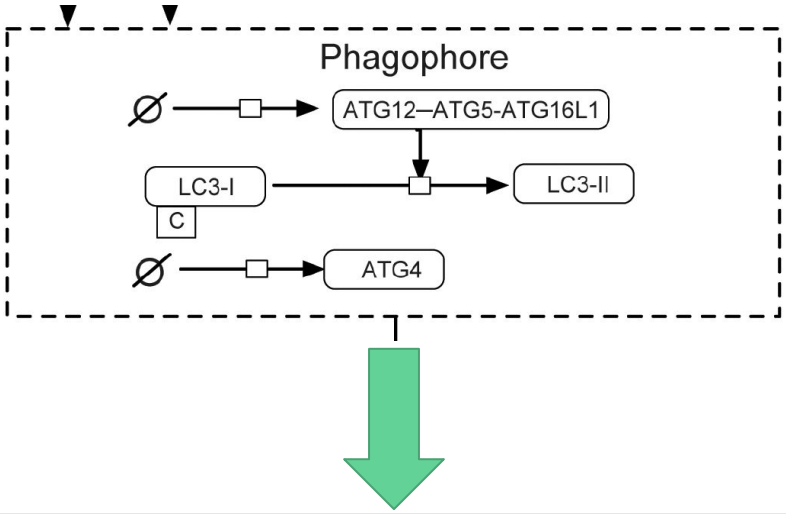


```
LC3I:lc3i + PG[ATGComp+ sol?]:pg ->  PG[LC3I_ATGComp + sol?]@ k_a4*#pg*#lc3i; //association, eq 19
PG[LC3I_ATGComp:la + sol?]:pg -> LC3I + PG[ATGComp + sol?] @k_d4*#la*#pg; //dissociation, eq 19
PG[LC3I_ATGComp:la + sol?]:pg -> PG[LC3II + ATGComp + sol?] @k_cat3*#la*#pg; //LC3II production, eq 19
PG[LC3II:lc3ii + sol?]:pg -> (1)AV[LC3II +sol?] @ if (#lc3ii > thrsh) then k_av*#lc3ii*#pg else 0; //thre
```

Fig 5. Screen shot from Martin et al mechanistic model and corresponding ML-Rules syntax

Translate Simple Model (Martin et al.) into ML-Rules

Editor

```
1 //PARAMETERS
2 p:0.18;              //initiation rate
3 p_azd:0.71;          //stimulated initiation rate
4 c: 0.037;            //degradtion rate
5
6
7
8 //SPECIES
9 I();
10
11AV()[];
12AV_azd()[];
13AV_baf()[];
14AV_both()[];
15
16//INITIAL SOLUTION
17>>INIT[(infinity())I];
18
19//REACTION RULES
20//production and degradation
21I -> AV @p;
22AV:av -> @c*#av;
23
24I -> AV_azd @p_azd;
25AV_azd:azd -> @c*#azd;
26
27I -> AV_baf @p;
28I -> AV_both @p_azd;
29
```

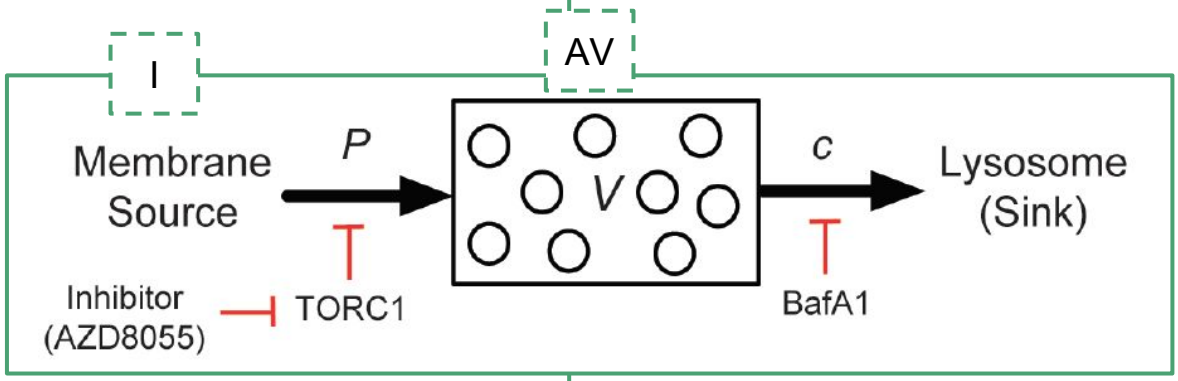

Translate Mechanistic Model (Martin et al.) into ML-Rules

Editor

```
1  //no cytoplasm
2  //Constants
3  i:4.48*1e-6; //stimulus
4  k_d:0.1; //deactivation rate of PtdIns3KC3; sece-1
5  k_a1:1e-6;  // association rate of PtdIns3KC3* and PtdIns; (molecule/cell)e-1*s
6  k_d1:0.1;  // dissociation rate of PtdIns3KC3* and PtdIns; sece-1
7  k_cat: 1;  // phosphorylation rate of PtdIns to PtdIns3P; sece-1
8  k_dep: 1;  // dephosphorylatoin rate of PtdIns3P; sece-1
9  k_cat2: 1; // rate of catalytic conversino of PtdIns3P to PtdIns(3, 5)P2; sece-
10 k_dep2: 1; //rate of dephosphorylation of PtdIns(3,5)P2 to PtdIns3P; sece-1
11 k_a2: 1e-6; // rate of association of  of WIPI and Ptdins3P or PtdIns(3,5)P2;
12 k_d2_1:0.1; // rate of dissociation of WIPI and PtdIns3P; sece-1
13 k_d2_2:1; //rate of dissociation of WIPI and PtdIns(3,5)P2; sece-1
14 k_a3:1e-6; //rate of association of ATG9 and WIPI.PtdIns3P or WIPI.PtdIns(3,5)P
15 k_d3:0.1; //rate of dissociation of ATG9.WIPI.PtdIns3P or ATG9.WIPI.PtdIns(3,5
16 k_mod: 0.1; // rate of activation step of ATG9.WIPI.PtdIns3P or ATG9.WIPI.PtdI
17 k_nuc:0.01; //rate of nucleation of phagophore, requires fully activated ATG9
18 k_flux:0.1; // rate at which ATGComp is added into PG
19 k_atg:0.1; //rate at which ATG4 is recruited into PG
20 k_a4:1e-6; //rate at which ATGComp and LC3I associate
21 k_d4:0.1; //rate at which ATGComp and LC3I dissociate
22 k_cat3:1; //rate of conversion of LC3I to LC3II
23 k_av:0.05; //rate of AG formation
24 k_rel: 1e-6; //rate of release of LCII from autophagosome
25 k_dim:5*(1e-4); //rate of pseudo-dimerization of autophagosomes
26 k_splt:0.15; //rate of splitting of pseudo dimers of autophagosomes
27 k_degr:4.5e-4;//rate of degradation of autophagosome
28 thrsh:400; //threshold of LC3II needed for AV formation
29 //Species
30 //compartments
31 MemSrc()[]; //membrane source, ER primarily
32 PG()[]; //phagophore, switch to IM
33 AV()[]; //autophagosome
34 AVDim()[]; //autophagosome pseudo-dimer, dimer
35 //components
36 PtdIns3KC3(bool); //PI3KC3
37 PtdIns();
38 PtdIns3P();
39 PtdIns35P2();
40 PtdIns3KC3_PtdIns();
41 WIPI();
42 WIPI_PtdIns3P();
43 WIPI_PtdIns35P2();
44 ATG9();
45 C0(); C1(); C2(); C3();
```

Editor

```
46 C0_1(); C1_1(); C2_1(); C3_1();
47 LC3I();
48 LC3II();
49 ATG4();
50 ATGComp(); //write out the name
51 LC3I_ATGComp();
52
53 //Initial solution
54 >>INIT[(1)MemSrc[(1e5)PtdIns3KC3(false) + (1e6)PtdIns +(1e5)ATG9 ]
55           +(infinity())ATGComp + (infinity())ATG4 + (1e5)LC3I+(1e5)WIPI ];
56
57 //Rules
58 //Plasma membrane
59 MemSrc[PtdIns3KC3(false):pi3kc3d +pm?]  -> MemSrc[PtdIns3KC3(true)+pm?] @i*#pi3kc3d; //activated, eq 1
60 MemSrc[PtdIns3KC3(true):pi3kc3a+pm?] -> MemSrc[PtdIns3KC3(false)+pm?] @k_d*#pi3kc3a; //disactivated, eq 2
61
62 MemSrc[PtdIns3KC3(true):pi3kc3a + PtdIns:pi +pm?] -> MemSrc[PtdIns3KC3_PtdIns +pm?] @k_a1*#pi3kc3a*#pi; //association, e
63 MemSrc[PtdIns3KC3_PtdIns:pkpi+pm?] -> MemSrc[PtdIns3KC3(true) + PtdIns +pm?]@k_d1*#pkpi; //dissociation, eq 3
64
65 MemSrc[PtdIns3KC3_PtdIns:pkpi +pm?] -> MemSrc[PtdIns3KC3(true) + PtdIns3P+pm?] @k_cat*#pkpi; //phosphorylation, eq 3
66 MemSrc[PtdIns3P:pi +pm?] -> MemSrc[PtdIns+pm?] @ k_dep*#pi; //dephosphorylation, eq 4
67
68 MemSrc[PtdIns3P:pip + pm?] -> MemSrc[PtdIns35P2+pm?] @k_cat2*#pip; //phosphorylation, eq 10
69 MemSrc[PtdIns35P2:pip2 +pm?] -> MemSrc[PtdIns3P+pm?] @k_dep2*#pip2; //dephosphorylation eq 11
70
71 MemSrc[PtdIns3P:pip+pm?]+ WIPI:w -> MemSrc[WIPI_PtdIns3P +pm?] @ k_a2*#pip*#w; //association, eq 5
72 MemSrc[WIPI_PtdIns3P:wpt +pm?] ->MemSrc[PtdIns3P + pm?]+ WIPI @ k_d2_1*#wpt; //dissociation, eq 8
73
74 MemSrc[PtdIns35P2:pip2 + pm?] + WIPI:w -> MemSrc[WIPI_PtdIns35P2+pm?] @ k_a2*#pip2*#w; //forward association, eq 12
75 MemSrc[WIPI_PtdIns35P2:wpt2+pm?] -> MemSrc[PtdIns35P2 +pm?]+ WIPI  @k_d2_2*#wpt2;//dissociation, eq 12
76
77 MemSrc[WIPI_PtdIns3P:wpt + ATG9:atg + pm?]-> MemSrc[C0+pm?] @k_a3*#wpt*#atg; //forward association, eq 6
78 MemSrc[C0:c0+pm?]-> MemSrc[WIPI_PtdIns3P + ATG9 + pm?] @ k_d3*#c0; //dissociation, eq 6
79
80 MemSrc[WIPI_PtdIns35P2:wpt2 + ATG9:atg +pm?]-> MemSrc[C0_1+pm?] @ k_a3*#wpt2*#atg; //forward association, eq 13
81 MemSrc[C0_1:c01 +pm?]-> MemSrc[WIPI_PtdIns35P2 + ATG9+pm?] @ k_d3*#c01;//dissociation, eq 15
82
83 //activation of complexes in series (C0 to C3 and C0_1 to C3_1)
84 MemSrc[C0:c0 + pm?] -> MemSrc[C1 + pm?] @ k_mod*#c0; //activation of C0 to C1, eq 7
85 MemSrc[C1:c1 + pm?] -> MemSrc[WIPI_PtdIns3P + ATG9+pm?] @k_d3*#c1; //deactivation of C1 with dissociation of ATG9 from c
86 MemSrc[C1:c1 + pm?] -> MemSrc[C2 + pm?] @ k_mod*#c1; //activation of C1 to C2, eq 7
87 MemSrc[C2:c2 + pm?] -> MemSrc[WIPI_PtdIns3P + ATG9+pm?] @k_d3*#c2; //deactivation of C2 with dissociation of ATG9 from c
88 MemSrc[C2:c2 + pm?] -> MemSrc[C3 + pm?] @ k_mod*#c2; //activation of C2 to C3, eq 7
89 MemSrc[C3:c3 + pm?] -> MemSrc[WIPI_PtdIns3P + ATG9+pm?] @k_d3*#c3; //deactivation of C3 with dissociation of ATG9 from c
90 MemSrc[C0_1:c0_1 + pm?] -> MemSrc[C1_1 + pm?] @ k_mod*#c0_1; //activation of C0_1 to C1_1 eq 14
91 MemSrc[C1_1:c1_1 + pm?] -> MemSrc[WIPI_PtdIns35P2 + ATG9 + pm?] @k_d3*#c1_1; //deactivation of C1_1 with dissociation of ATG9 from complex, eq 15
92 MemSrc[C1_1:c1_1 + pm?] -> MemSrc[C2_1 + pm?] @ k_mod*#c1_1; //activation of C1_1 to C2_2 eq 14
93 MemSrc[C2_1:c2_1 + pm?] -> MemSrc[WIPI_PtdIns35P2 + ATG9 + pm?] @k_d3*#c2_1; //deactivation of C2_2 with dissociation of ATG9 from complex, eq 15
94 MemSrc[C2_1:c2_1 + pm?] -> MemSrc[C3_1 + pm?] @ k_mod*#c2_1; //activation of C2_2 to C3_3 eq 14
95 MemSrc[C3_1:c3_1 + pm?] -> MemSrc[WIPI_PtdIns35P2 + ATG9 + pm?] @k_d3*#c3_1; //deactivation of C3_3 with dissociation of ATG9 from complex, eq 15
96
97 //phagophore formation
98 MemSrc[C3:c3 + pm?] -> (1)PG + MemSrc[C0 + pm?] @k_nuc*#c3; // PG formation eq 9
99 MemSrc[C3_1:c3_1 + pm?] -> (1)PG + MemSrc[C0_1 + pm?] @k_nuc*#c3_1; // PG formation eq 16
100
101//Phagophore compartment
102ATGComp + PG[sol?]:pg ->  PG[ATGComp+sol?] @ k_flux*#pg; //recruit ATGComp (enzyme X) from cytoplasm to phagophore, eq 17
103ATG4 + PG[sol?]:pg -> PG[ATG4 + sol?]  @k_atg*#pg; //recruit ATG4 from cytoplasm to phagophore, eq 18
104
105//lipidation of LC3I to LC3II
106LC3I:lc3i + PG[ATGComp+ sol?]:pg ->  PG[LC3I_ATGComp + sol?]@ k_a4*#pg*#lc3i; //association, eq 19
107PG[LC3I_ATGComp:la + sol?]:pg -> LC3I + PG[ATGComp + sol?] @k_d4*#la*#pg; //dissociation, eq 19
108PG[LC3I_ATGComp:la + sol?]:pg -> PG[LC3II + ATGComp + sol?] @k_cat3*#la*#pg; //LC3II production, eq 19
109PG[LC3II:lc3ii + sol?]:pg -> (1)AV[LC3II +sol?] @ if (#lc3ii > thrsh) then k_av*#lc3ii*#pg else 0; //threshold level of LC3II needed for formation of autophagosomes, eq 20
110
111//Autophagosome compartment
112AV[ATG4 + LC3II:lc3ii +sol?] -> AV[ATG4 +sol?] +  LC3I @k_rel*#lc3ii; //ATG4 mediated conversion and release of LC3II -> LC3I on an AV, eq 21
113AV[sol?]:av + AV[sol?]:av -> AVDim[sol?] @ k_dim*#av*#av; //pseudo-dimerization eq 22
114AVDim[sol?]:avd -> AV[sol?] + AV[sol?] @k_splt*#avd; //splitting of pseudo-dimer eq 22
115AVDim[sol?]:avd -> AV[sol?] @2*k_degr*#avd; //account for potential for degradation of pseudo-dimer components
116AV[sol?]:av -> @ k_degr*#av; //degradation, eq 23
117
```

[Approaches]

Control: Test ML-Rules language by simulating ***simple model*** using SESSL and comparing against published data.

SESSL: Simulation Experiment Specification via a Scala Layer

SampleExperiment.scala

```
import sessl._
import sessl.mlrules._

object SampleExperiment extends App {

  execute {
    new Experiment with Observation with ParallelExecution with CSVOutput {
      model = "./simple_modelDIM.mlrules"
      simulator = StandardSimulator()

      replications = 10
      parallelThreads = -1

      stopTime = 300

      //scan("k_extraction" <~ range(0.02, 0.01, 0.08))

      observe("AV" ~ "*/AV")
      observe("AV_baf" ~ "*/AV_baf")
      observe("AV_azd" ~ "*/AV_azd")
      observe("AV_both" ~ "*/AV_both")

      observe("Dimer" ~ "*/Dimer")
      observe("Dimer_azd" ~ "*/Dimer_azd")
      observe("Dimer_baf" ~ "*/Dimer_baf")
      observe("Dimer_both" ~ "*/Dimer_both")

      observeAt(range(0.0, 1.0, 300))

      withExperimentResult(r => {
        // this overwrites existing files
        writeToCSVFile(r, "./results", append = false)
      })
    }
  }
```

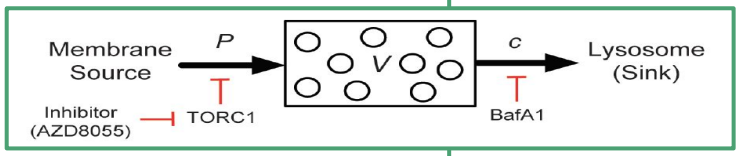

RunSampleExperiment.sh

```
#!/usr/bin/env bash

rm -rf SampleExperiment.jar results
scalac -classpath "../*:../libs/*" SampleExperiment.scala -d SampleExperiment.jar
java -classpath "*:../*:../libs/*" SampleExperiment
```

Control matches published data

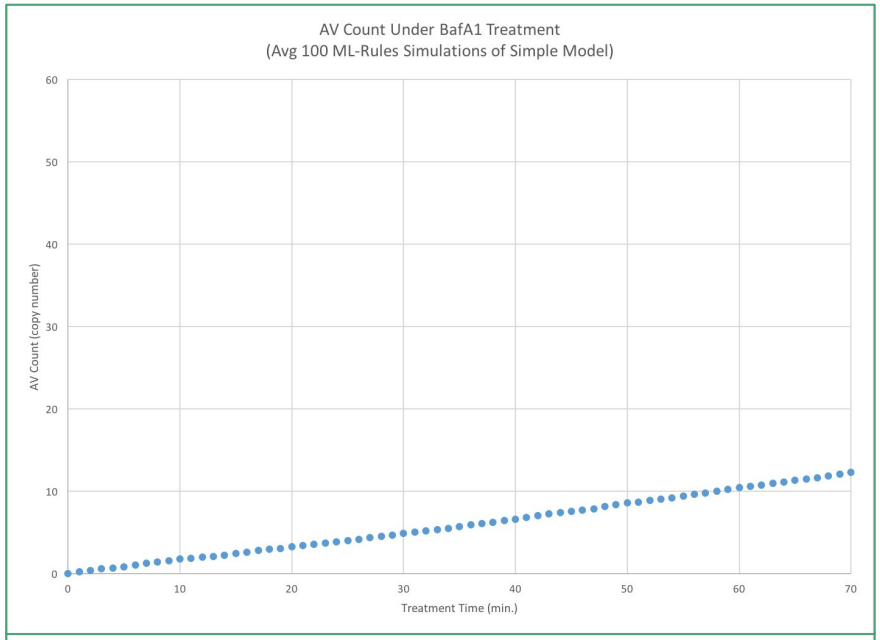

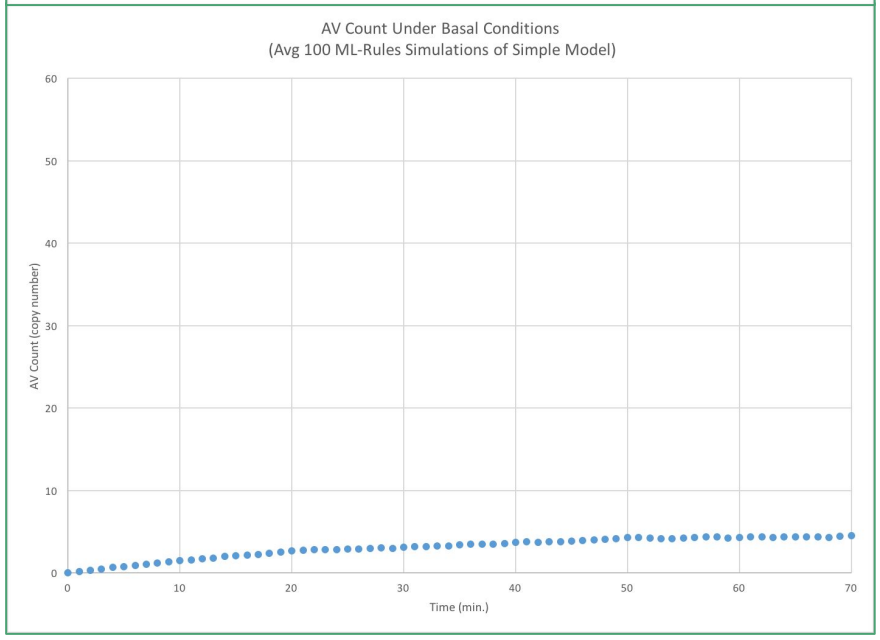

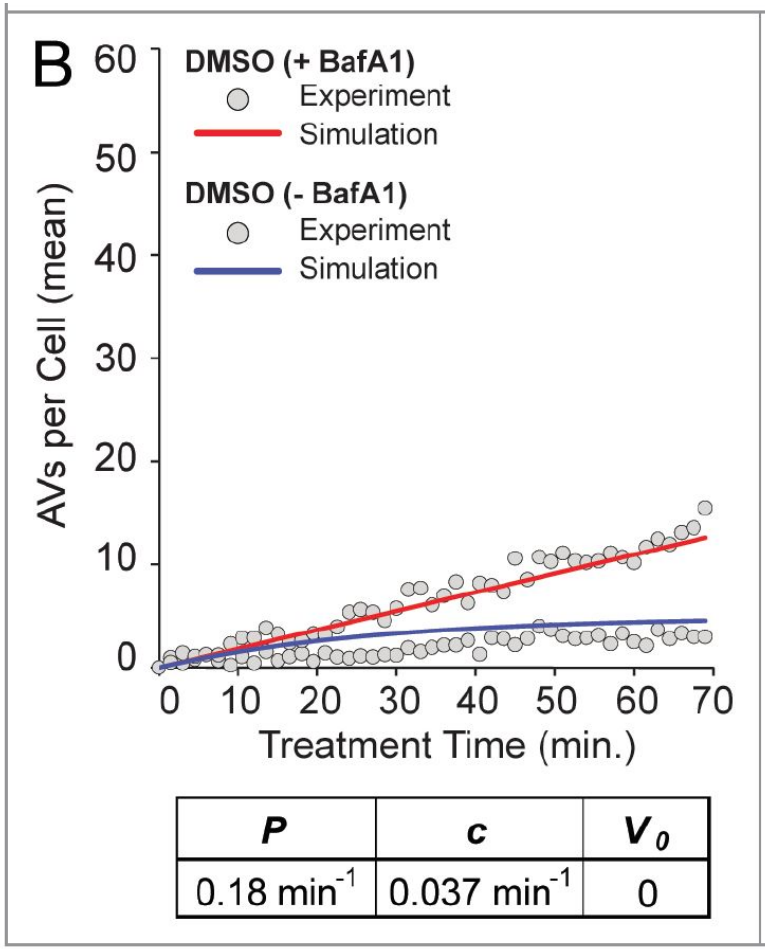

P	c	V_0
0.18 min^{-1}	0.037 min^{-1}	0

Published data Martin et al.

Control matches published data

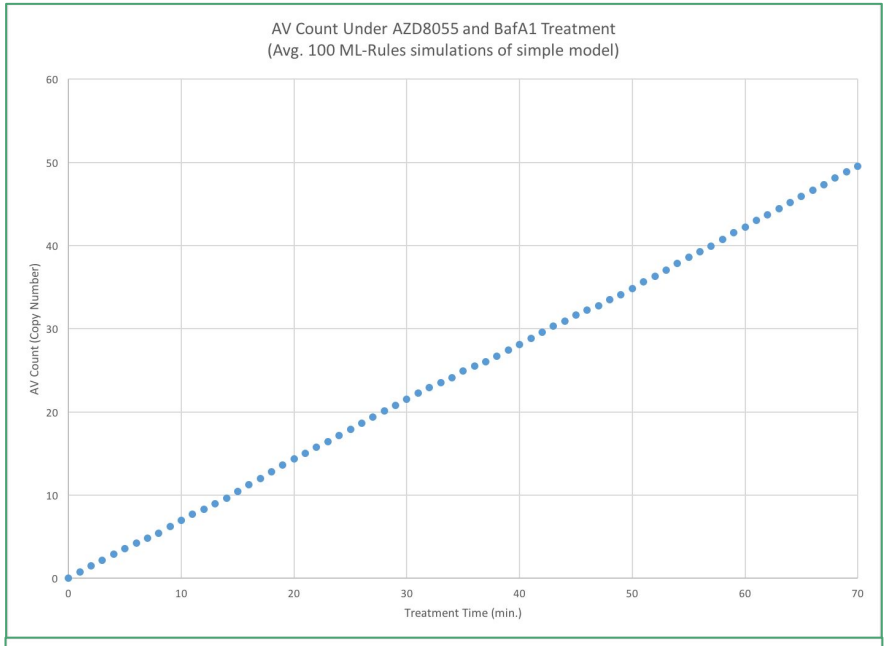

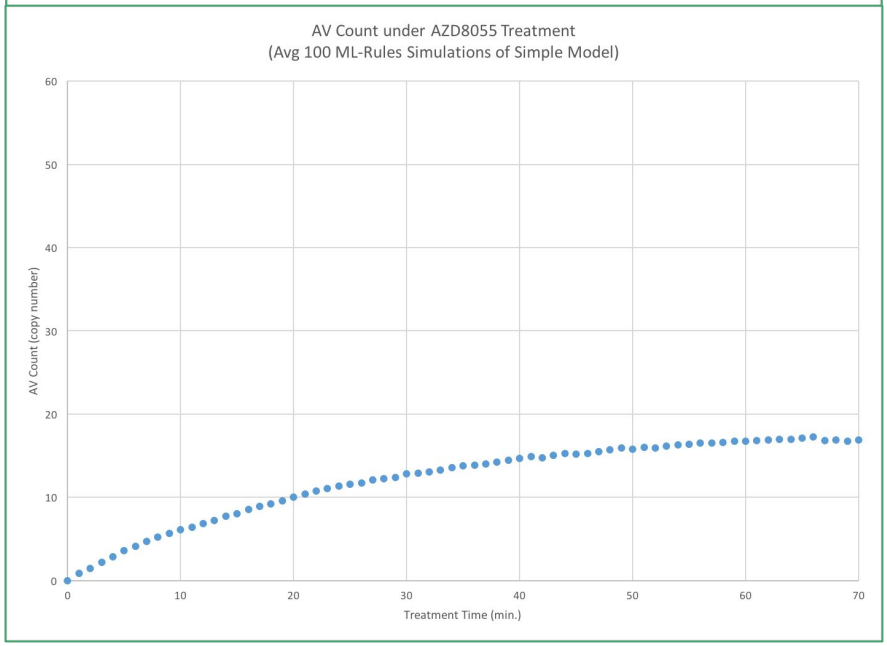

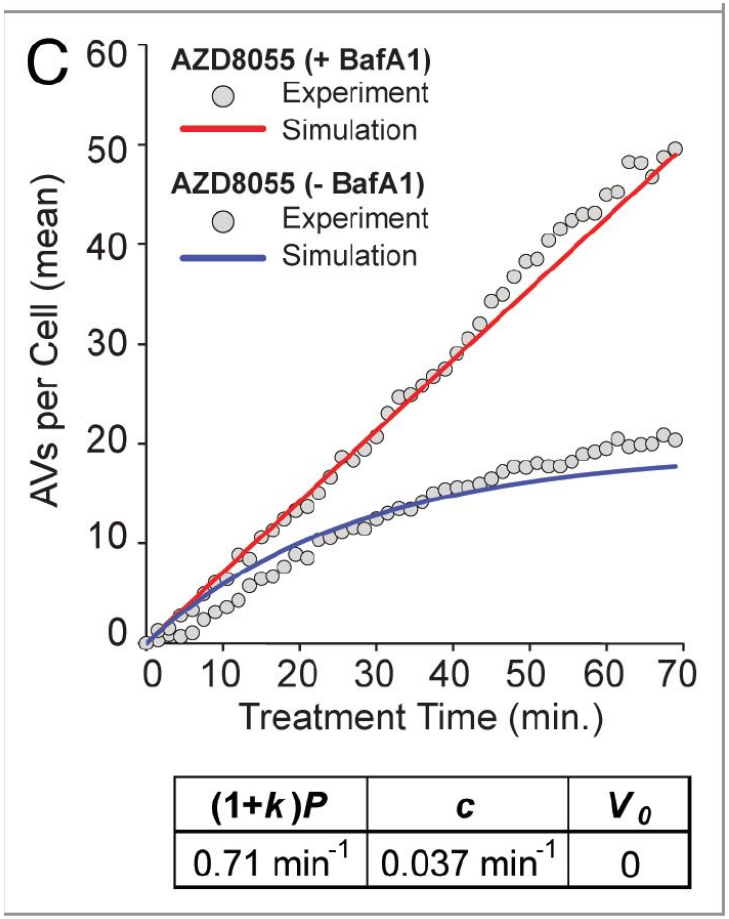

$(1+k)P$	c	V_0
0.71 min^{-1}	0.037 min^{-1}	0

Published data Martin et al.

Control matches published data

Basal conditions

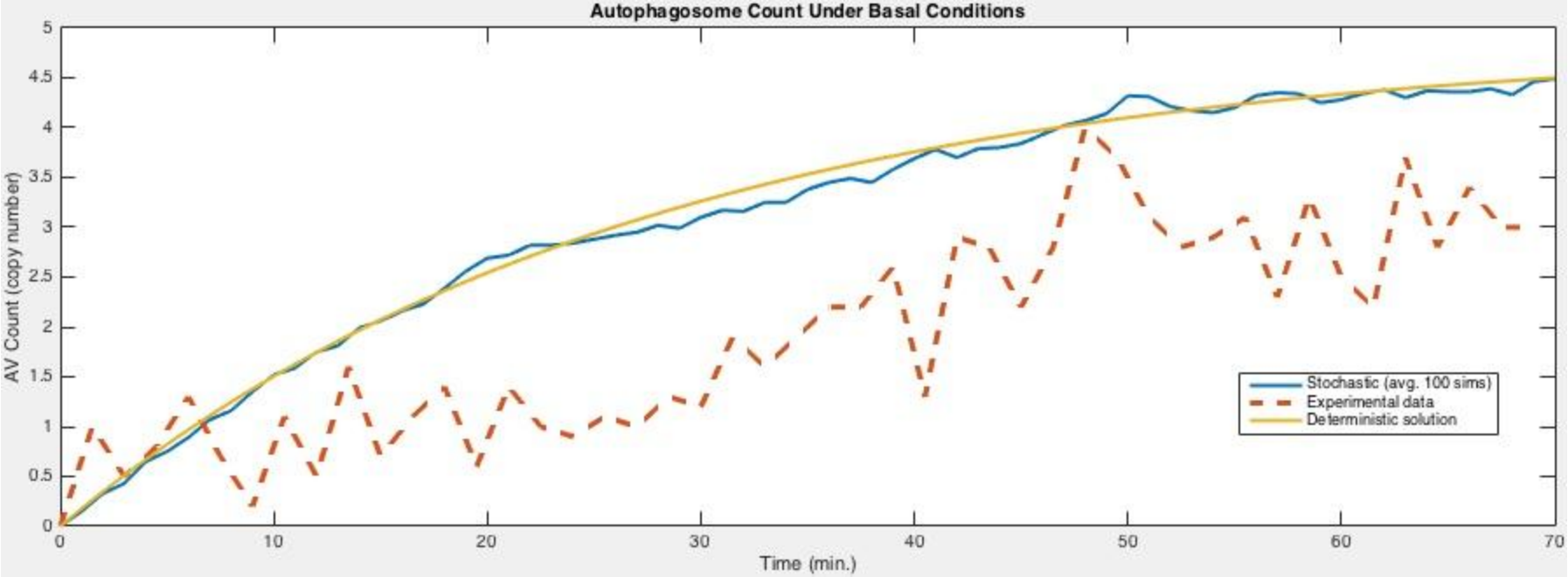

Control matches published data

AZD8055 Treatment

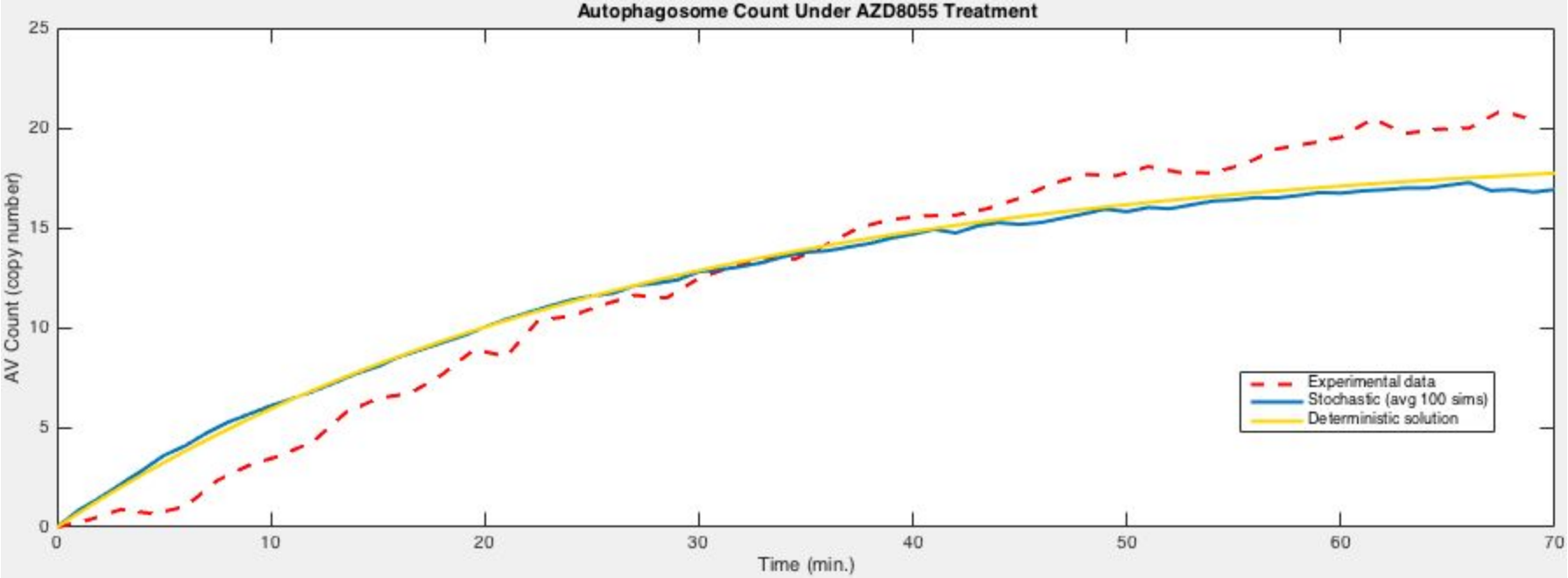

Control matches published data

BafA1 Treatment

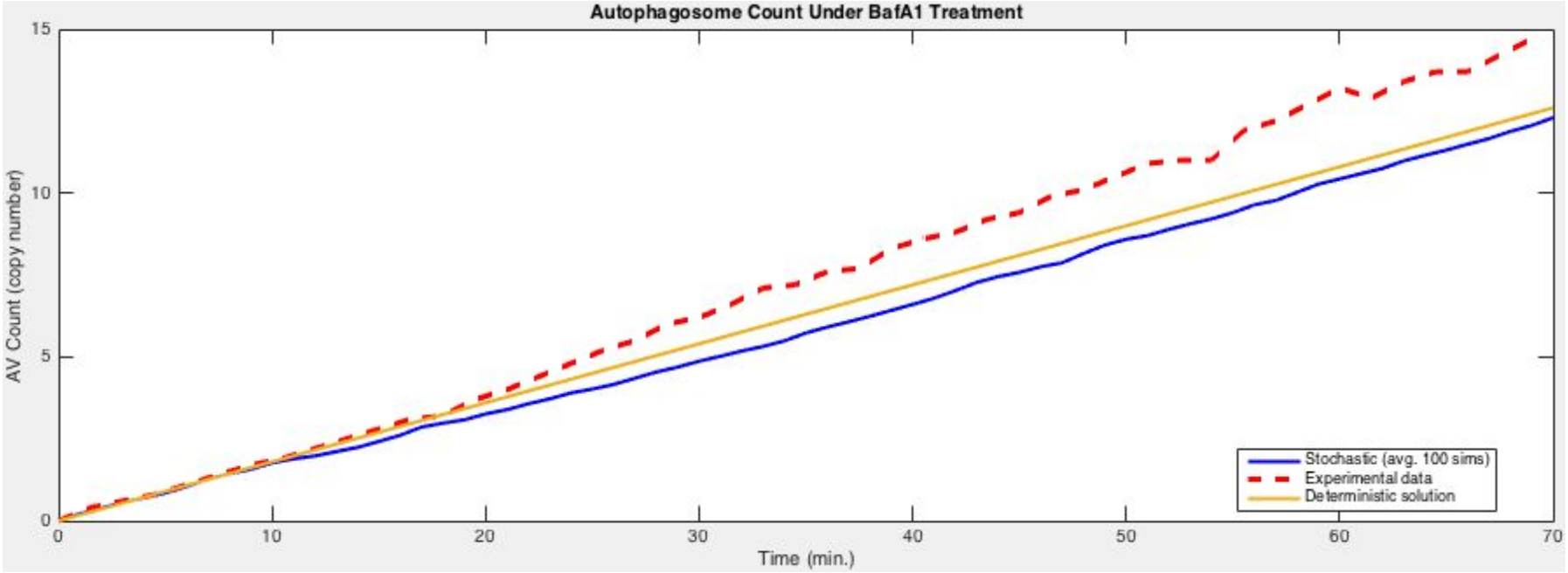

Control matches published data

AZD8055 and BafA1 Treatment

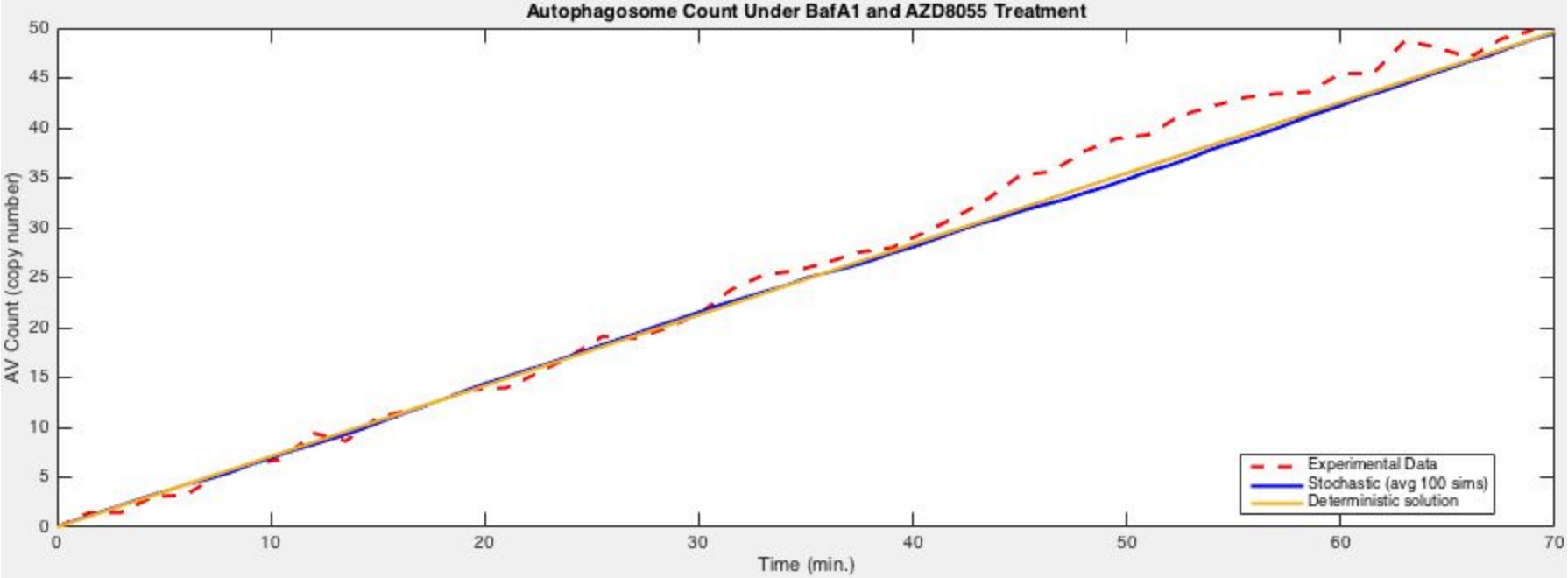

Next, simulate mechanistic model

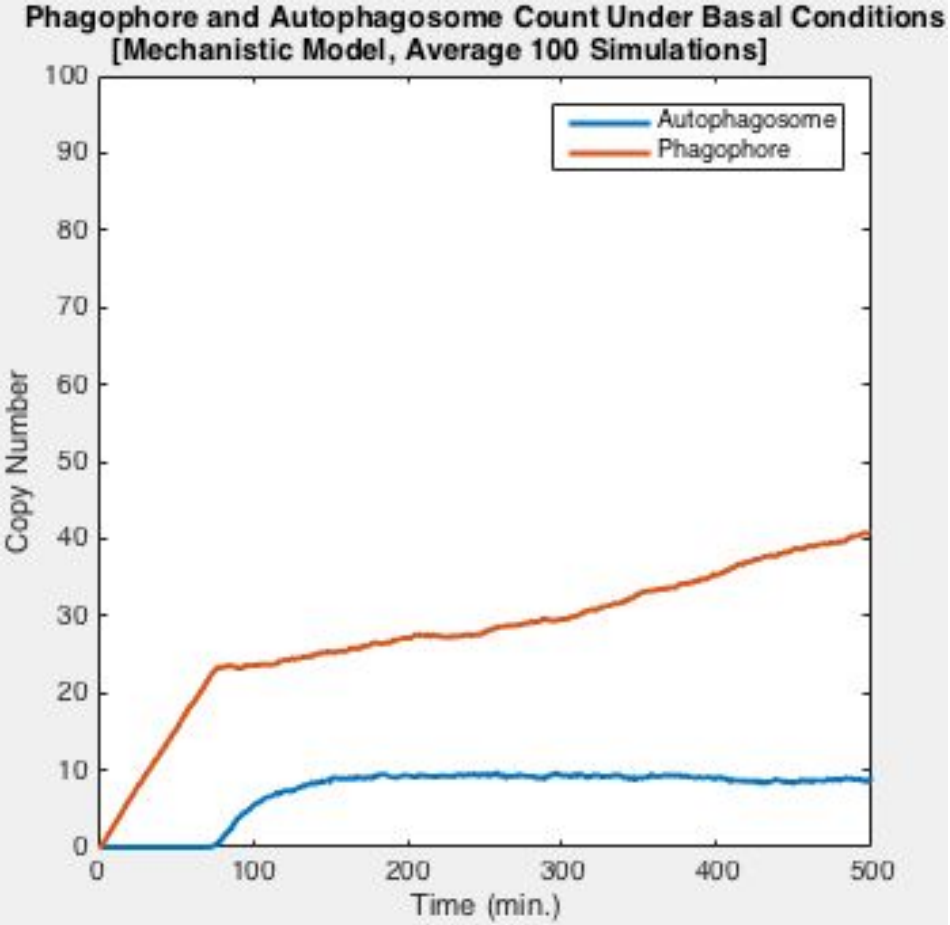

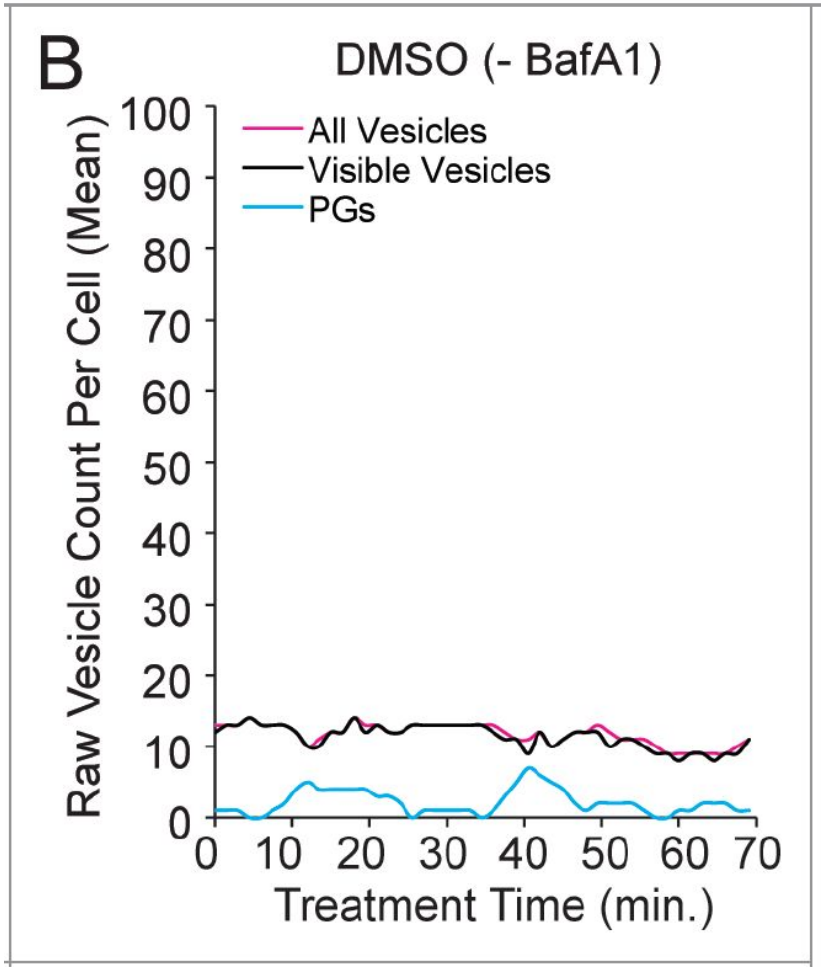

Published data Martin et al.

Approach to P#2: Expanding Simple Model

1. Expanded Model: four stages of autophagy

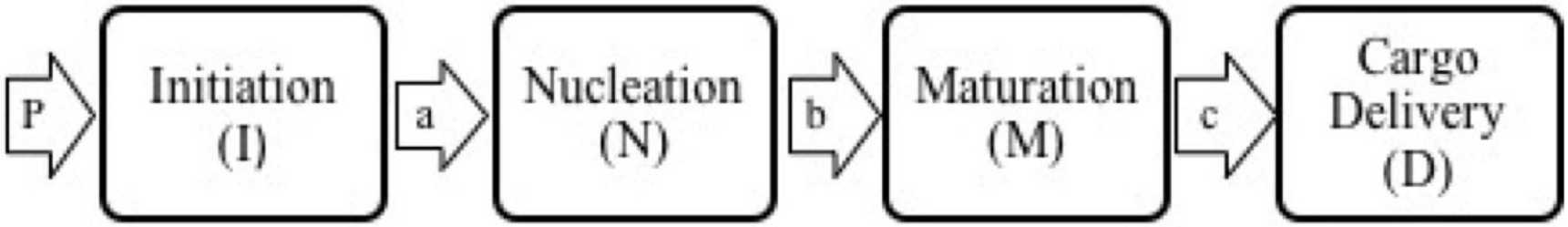

2. Solve ODEs and fit parameters a and b using MATLAB and Data2Dynamics [D2D]

$$\underset{A}{\begin{pmatrix} -a & 0 & 0 & 0 \\ a & -b & 0 & 0 \\ 0 & b & -c & 0 \\ 0 & 0 & c & 0 \end{pmatrix}} * \underset{X}{\begin{pmatrix} I \\ N \\ M \\ D \end{pmatrix}} + \underset{B}{\begin{pmatrix} P \\ 0 \\ 0 \\ 0 \end{pmatrix}} = \underset{diff(X)}{\begin{pmatrix} I' \\ N' \\ M' \\ D' \end{pmatrix}}, \qquad C = \begin{pmatrix} 0 \\ 0 \\ 0 \\ 0 \end{pmatrix}$$

```
eqn = diff(X) == A*X + B;  dsolve(eqn, C);
```

[Approaches]

Data2 Dynamics Overview

autophagy_simple_model.def

```
% Load models & data
clear all;
arInit

arLoadModel('simple_model2');
arLoadData('autophagy_model_data');
arLoadData('autophagy_model_data_baf');
arLoadData('autophagy_model_data_azd');
arLoadData('autophagy_model_data_both');
arCompileAll();

arSetPars('sd_M_count',[],2);
arSetPars('sd_M_count_baf',[],2);
arSetPars('sd_M_count_azd',[],2);
arSetPars('sd_M_count_both',[],2)

arFit();
arPrint();
arPLECalc([1, 2], 100);
figure
arPlotPLE([1, 2], false);
arPlot(false, true);
arTuner();
```

```
DESCRIPTION
"Autophagy model with four compartments"

PREDICTOR
t          T  min      time     0    69

COMPARTMENTS

STATES
M_state          C  "units/cell"    "conc."
M_state_baf      C  "units/cell"    "conc."
M_state_azd      C    "units/cell"  "conc."
M_state_both     C    "units/cell"  "conc."


INPUTS

ODES
"P-c*M_state"
"P"
"(1+2.9)*P - c*M_state_azd"
"(1+2.9)*P"


DERIVED

OBSERVABLES
M_count   C    "units"    "amount"  0    0    "M_state"
M_count_baf   C    "units"    "amount"  0    0    "M_state_baf"
M_count_azd   C    "units"    "amount"  0    0    "M_state_azd"
M_count_both  C    "units"    "amount"  0    0    "M_state_both"


ERRORS
M_count          "sd_M_count"
M_count_baf      "sd_M_count_baf"
M_count_azd      "sd_M_count_azd"
M_count_both     "sd_M_count_both"


CONDITIONS
init_M_state     "0"
init_M_state_baf      "0"
init_M_state_azd      "0"
init_M_state_both     "0"
```

Control: test D2D on simple model; recover published parameter estimations [P = 0.18 min^{-1} and c = 0.037 min^{-1}]

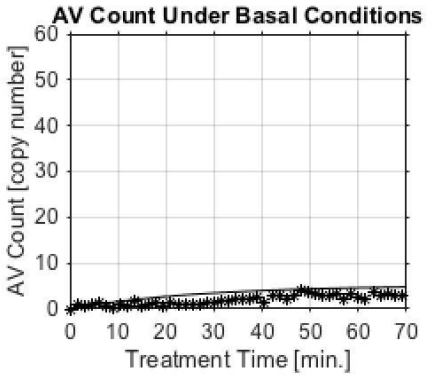

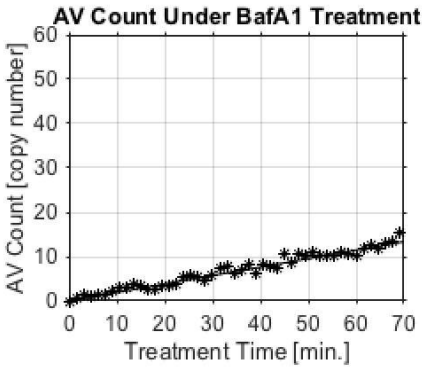

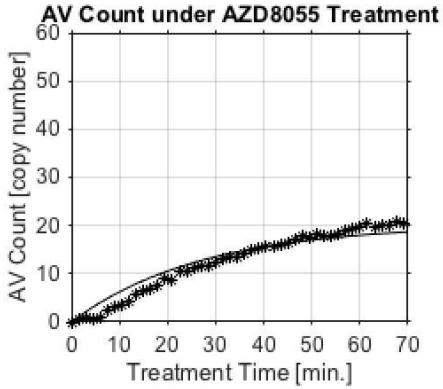

P = 0.19 min^{-1}
c = 0.037 min^{-1}

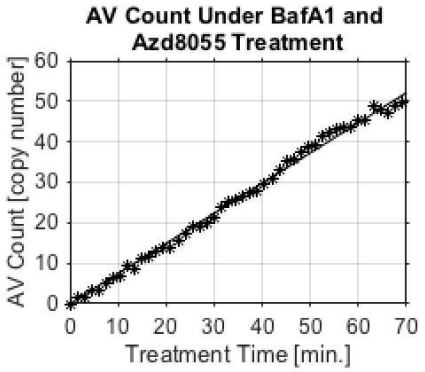

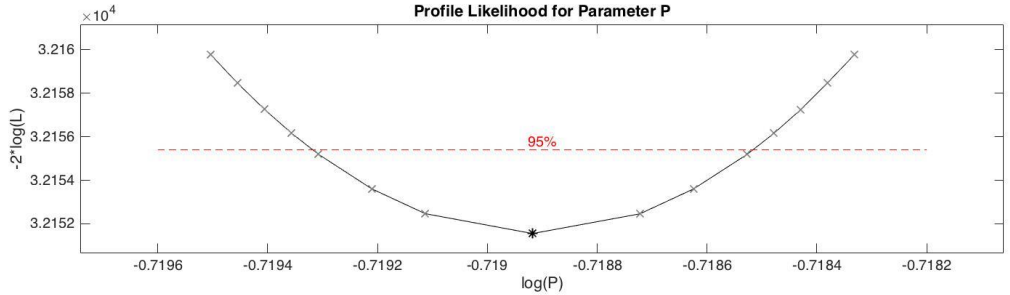

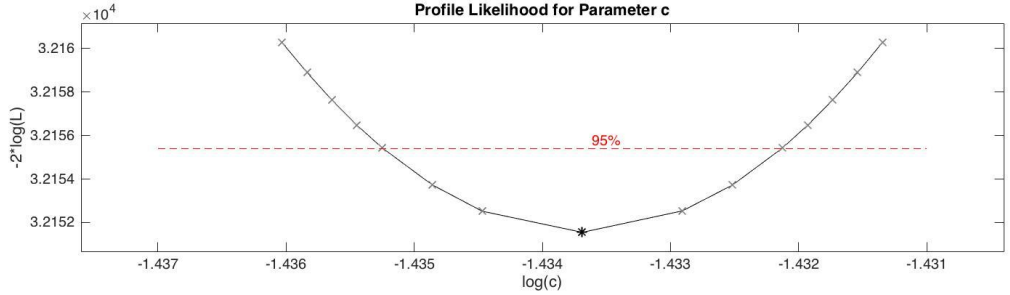

Estimate parameters a and b in expanded model

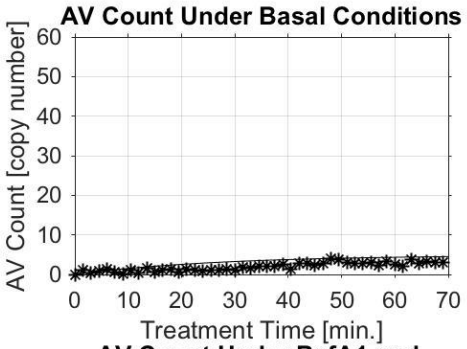

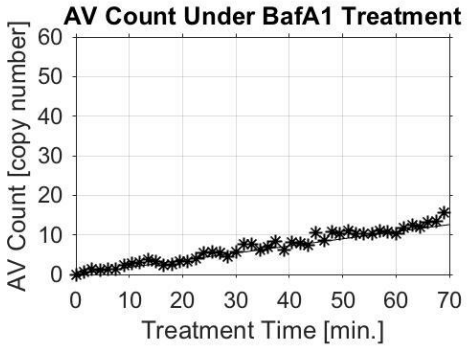

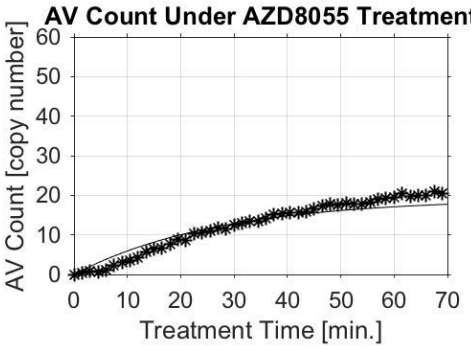

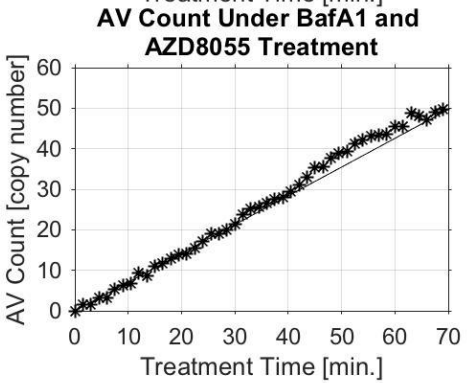

$a = 1000\ min^{-1}$
$b = 1000\ min^{-1}$

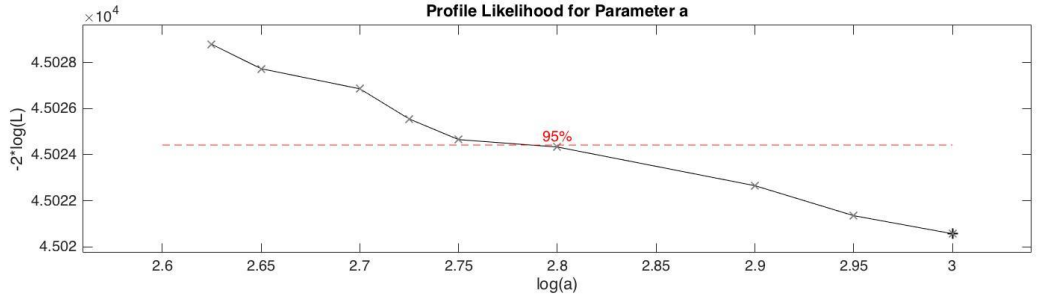

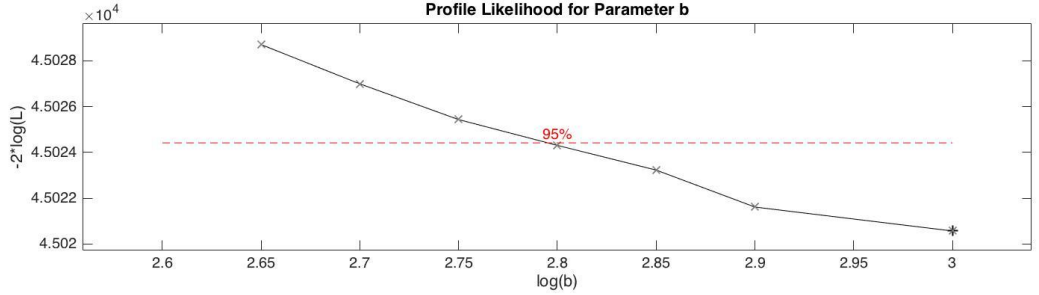

Approach to P#3: Incorporating Effects of IAV Proteins

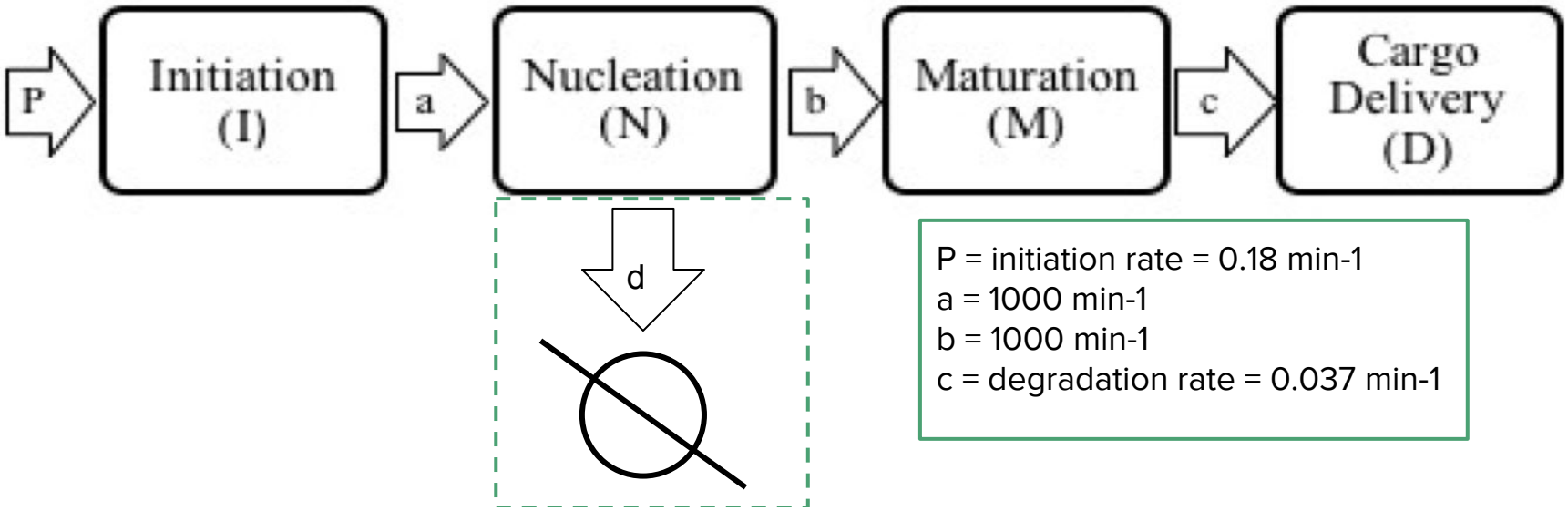

P = initiation rate = 0.18 min-1
a = 1000 min-1
b = 1000 min-1
c = degradation rate = 0.037 min-1

B.)

$$\underset{A}{\begin{pmatrix} -a & 0 & 0 & 0 \\ a & -b-d & 0 & 0 \\ 0 & b & -c & 0 \\ 0 & 0 & c & 0 \end{pmatrix}} * \underset{X}{\begin{pmatrix} I \\ N \\ M \\ D \end{pmatrix}} + \underset{B}{\begin{pmatrix} P \\ 0 \\ 0 \\ 0 \end{pmatrix}} = \underset{diff(X)}{\begin{pmatrix} I' \\ N' \\ M' \\ D' \end{pmatrix}}, \quad C = \begin{pmatrix} 0 \\ 0 \\ 0 \\ 0 \end{pmatrix}$$

```
eqn = diff(X) == A*X + B;   dsolve(eqn, C);
```

Results for P#3: parameter scan of d (avg. 10 simulations)

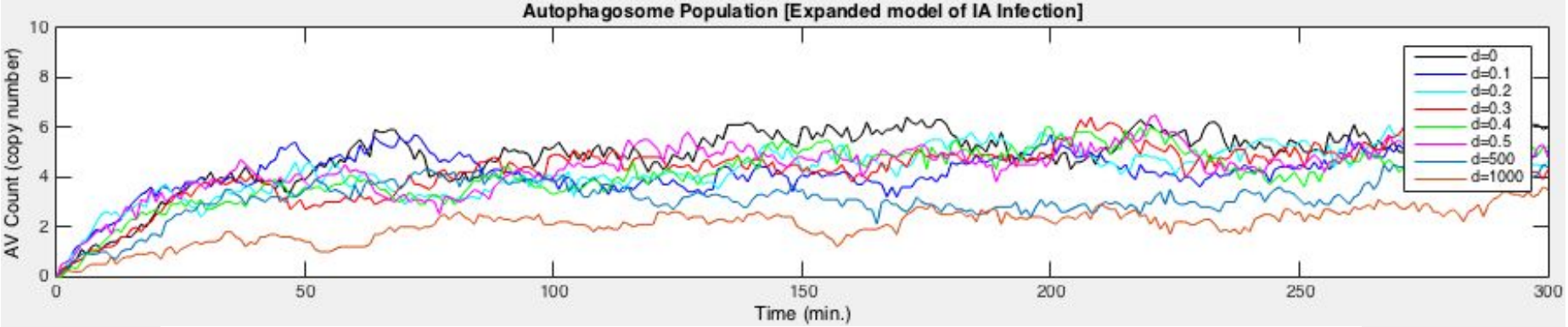

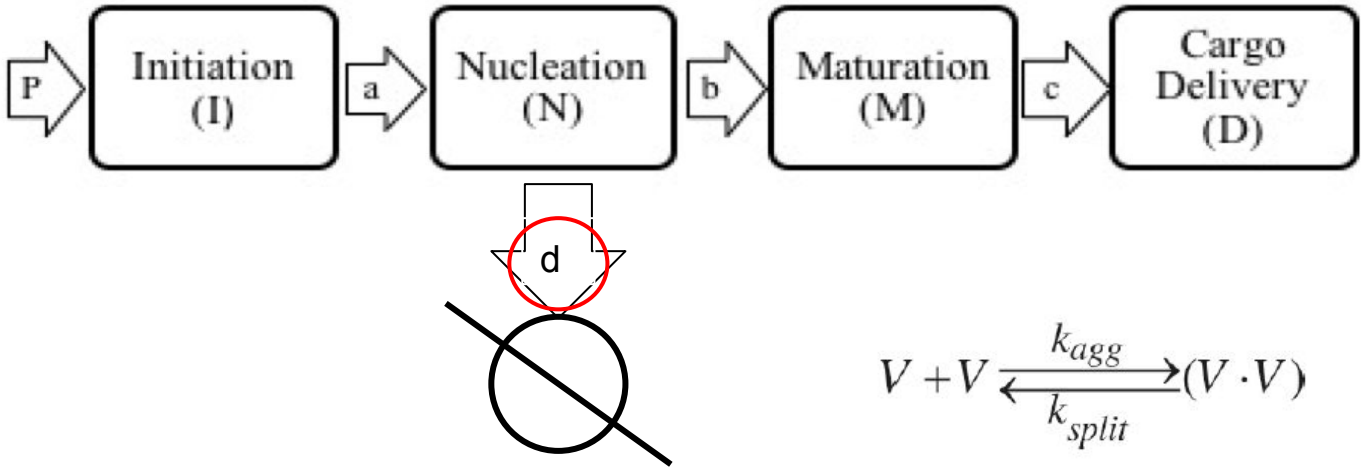

$$V + V \underset{k_{split}}{\overset{k_{agg}}{\rightleftarrows}} (V \cdot V)$$

[Results]

d=0.1

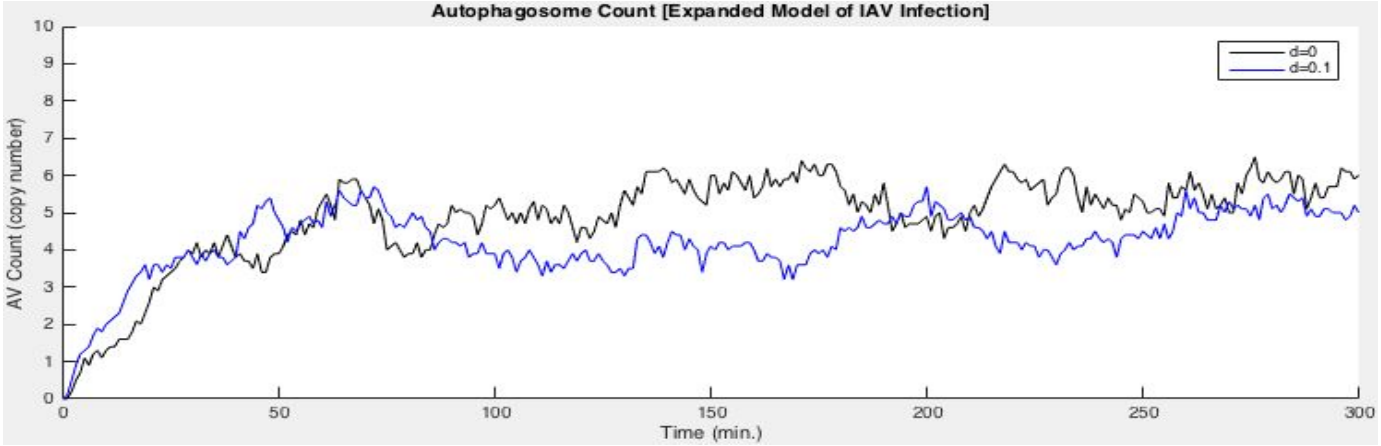

d=0.2

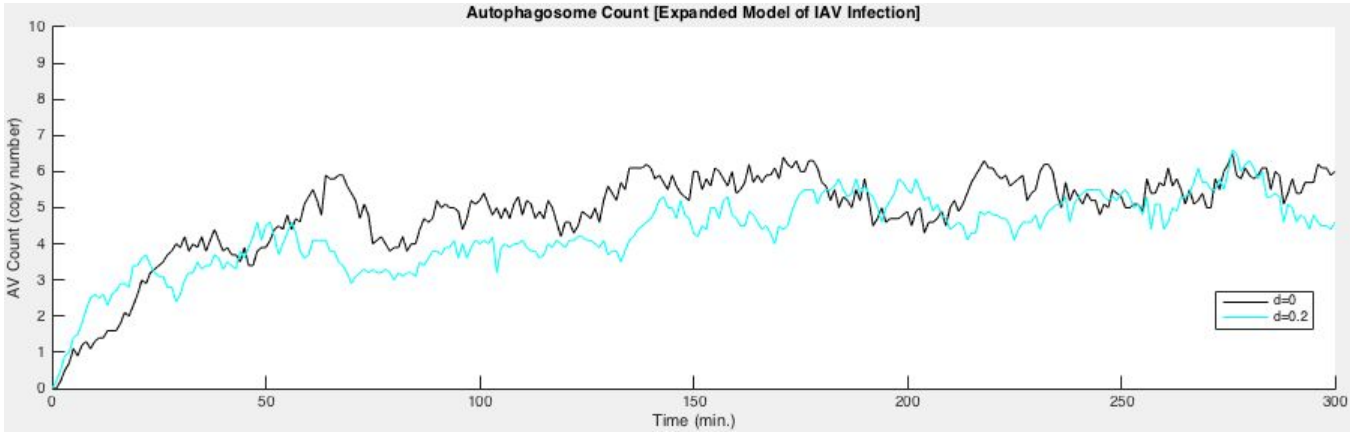

d=0.3

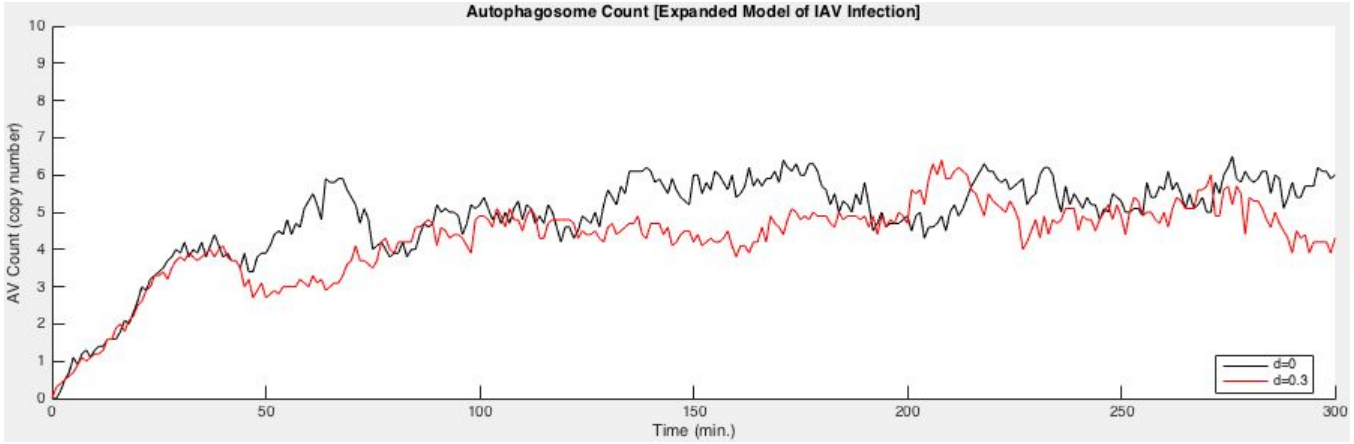

d=0.4

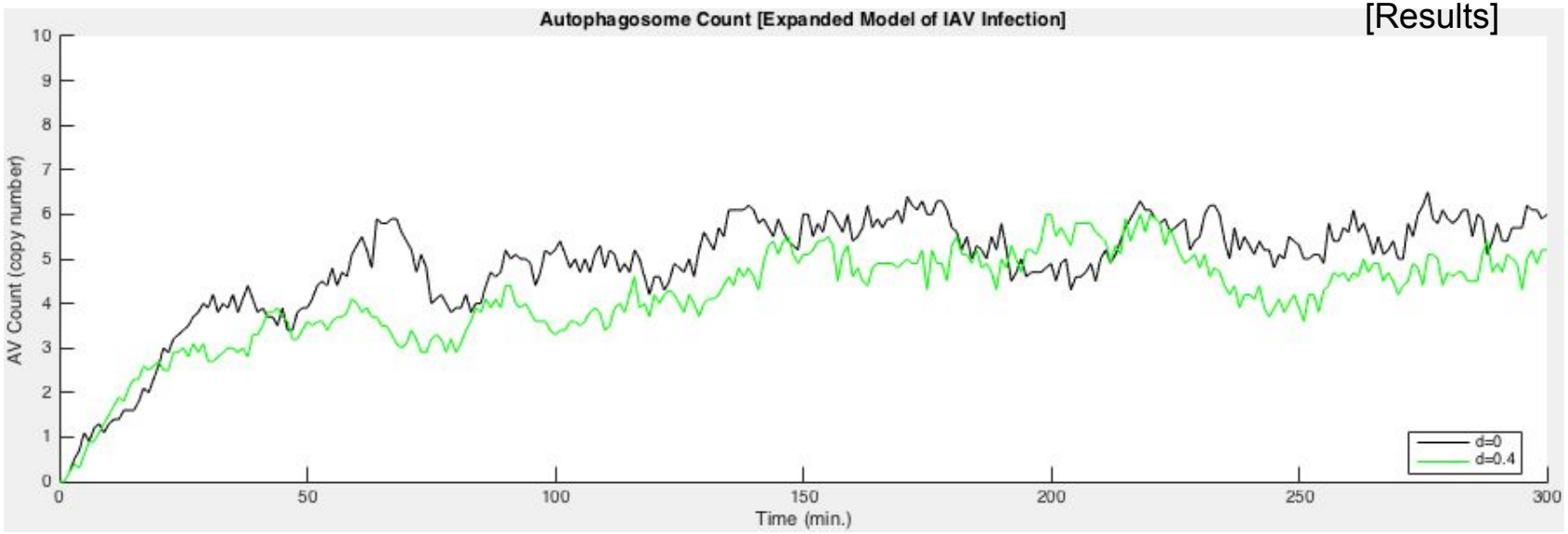
Autophagosome Count [Expanded Model of IAV Infection]
AV Count (copy number)
Time (min.)
d=0
d=0.4

d=0.5

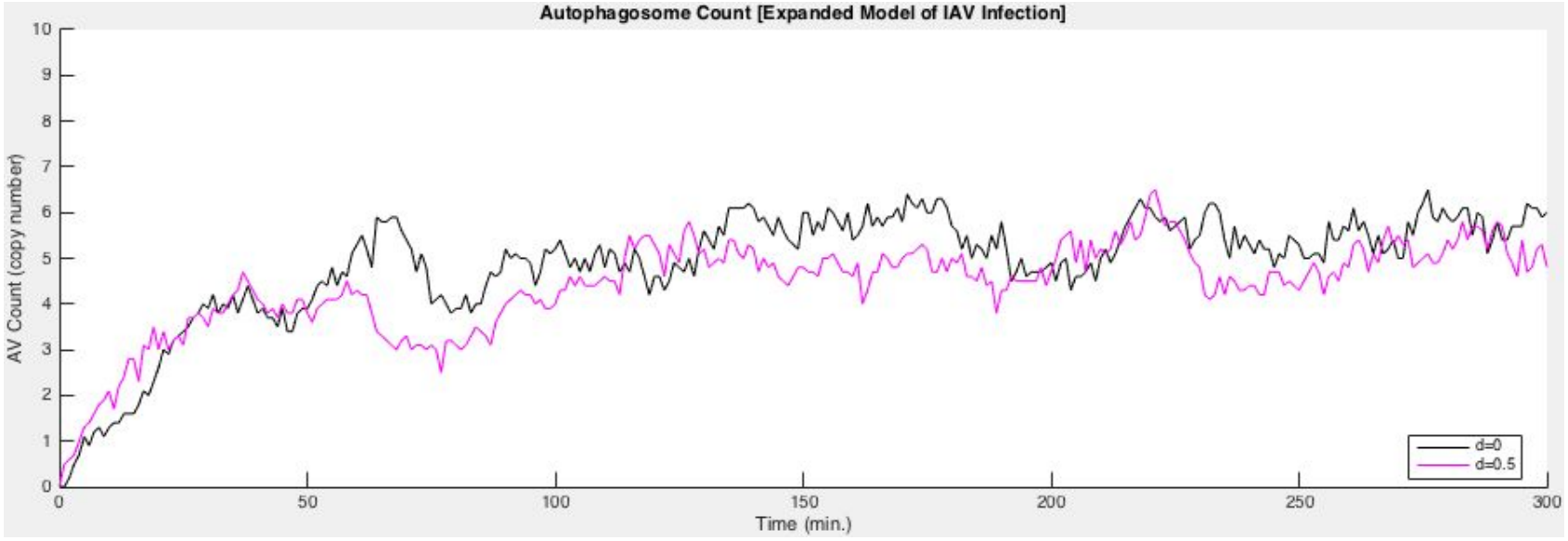
Autophagosome Count [Expanded Model of IAV Infection]
AV Count (copy number)
Time (min.)
d=0
d=0.5

d=500

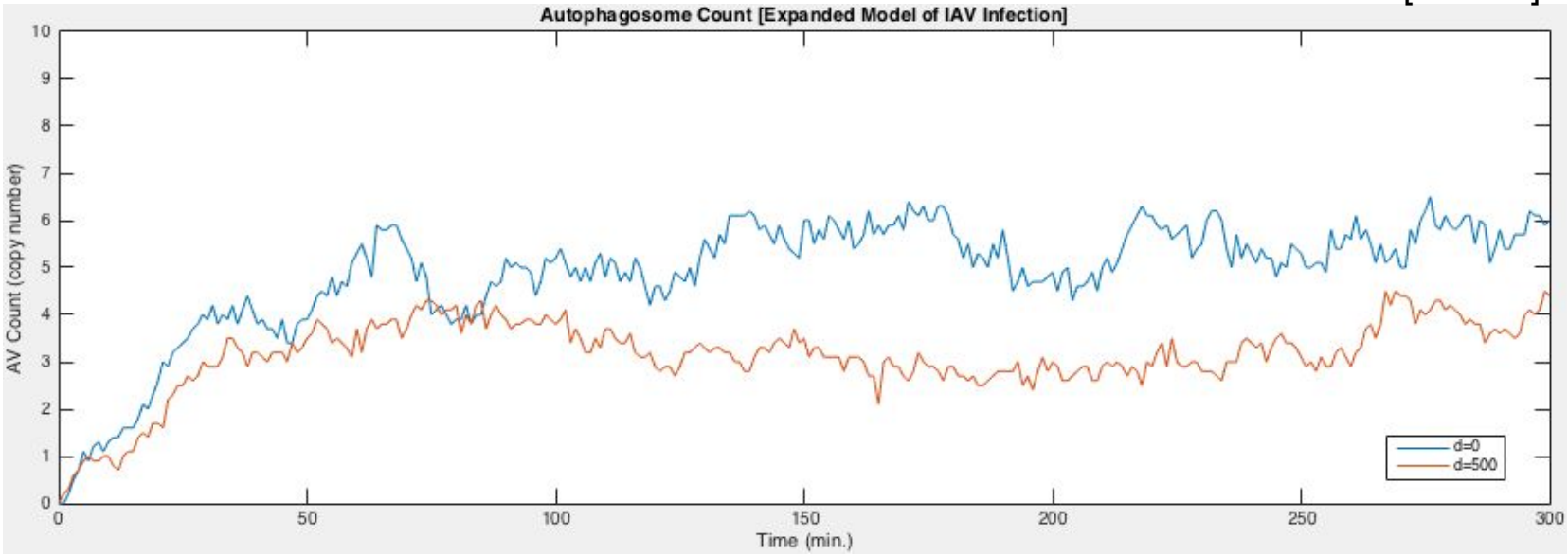
Autophagosome Count [Expanded Model of IAV Infection]
AV Count (copy number)
Time (min.)
d=0
d=500

d=1000

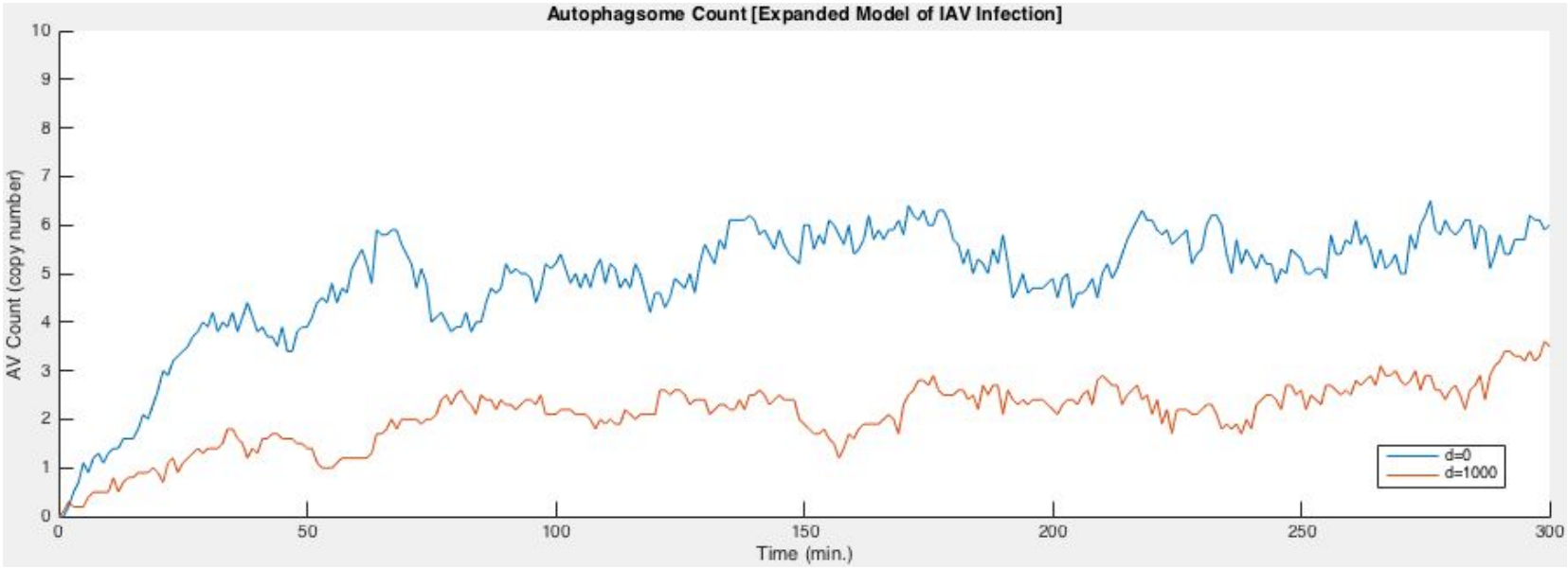
Autophagsome Count [Expanded Model of IAV Infection]
AV Count (copy number)
Time (min.)
d=0
d=1000

Now tune P and c in conjunction with d

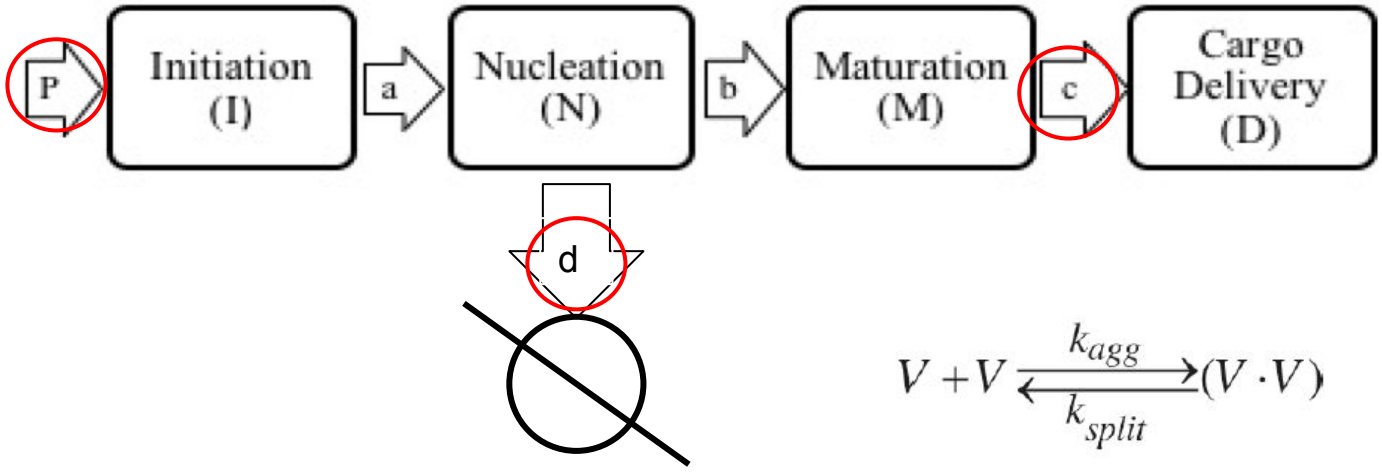

P = initiation rate = 0.18 min-1
a = 1000 min-1
b = 1000 min-1
c = degradation rate = 0 min-1

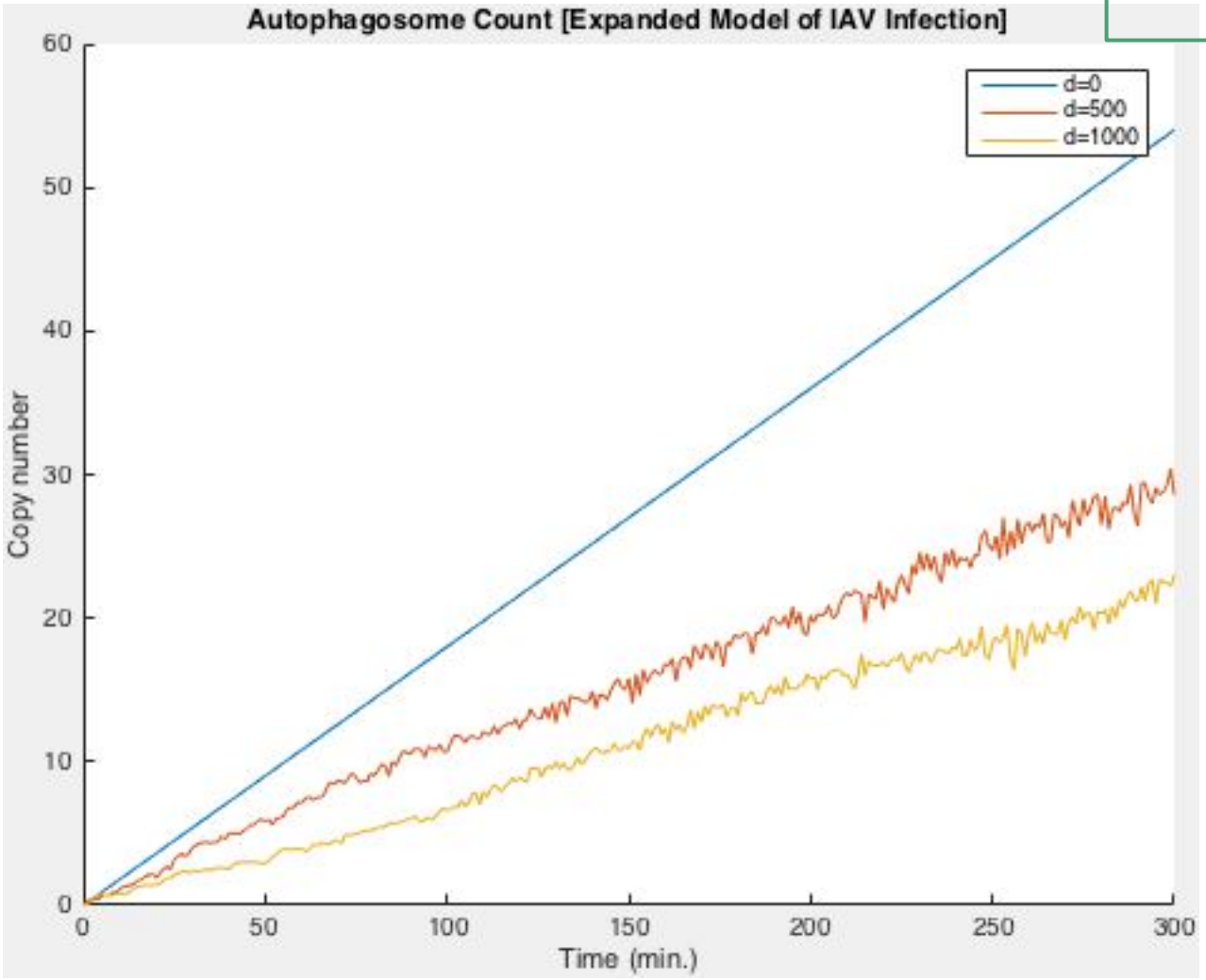

P = initiation rate = 0.71 min-1
a = 1000 min-1
b = 1000 min-1
c = degradation rate = 0.037 min-1

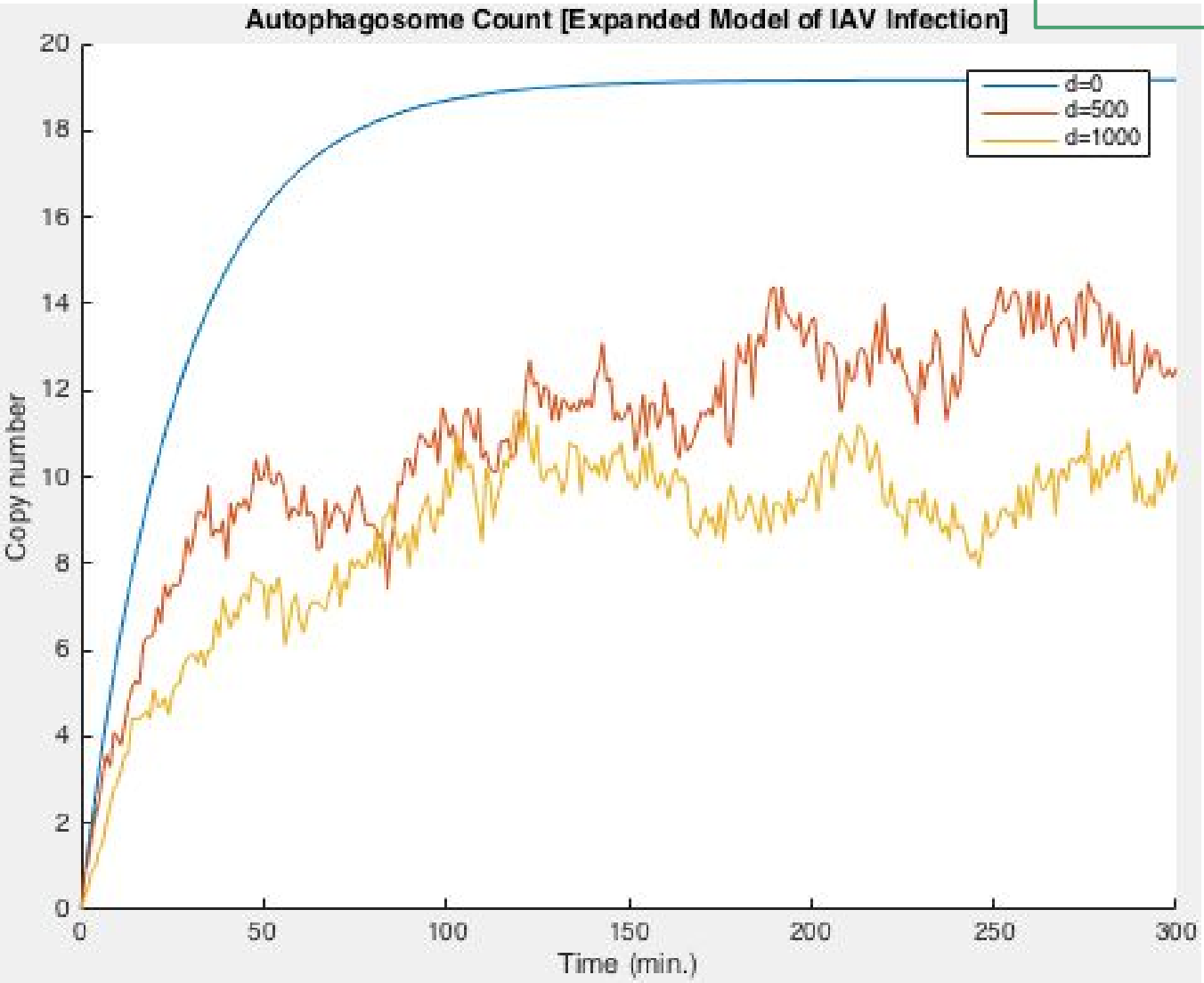

P = initiation rate = 0.71 min-1
a = 1000 min-1
b = 1000 min-1
c = degradation rate = 0 min-1

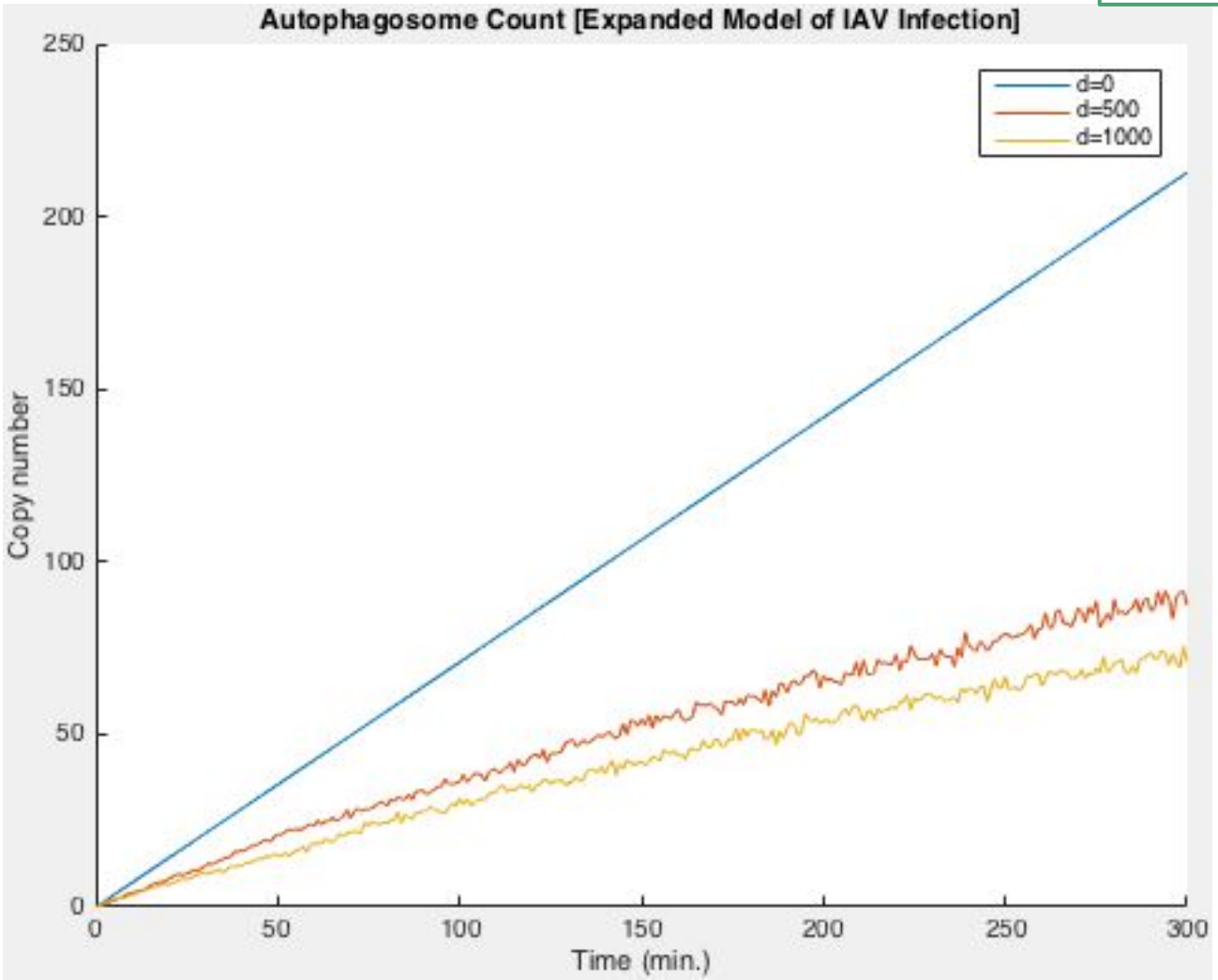

Are a and b really that large?

P = initiation rate = 0.18 min-1
a = 5 min-1
b = 5 min-1
c = degradation rate = 0.037 min-1

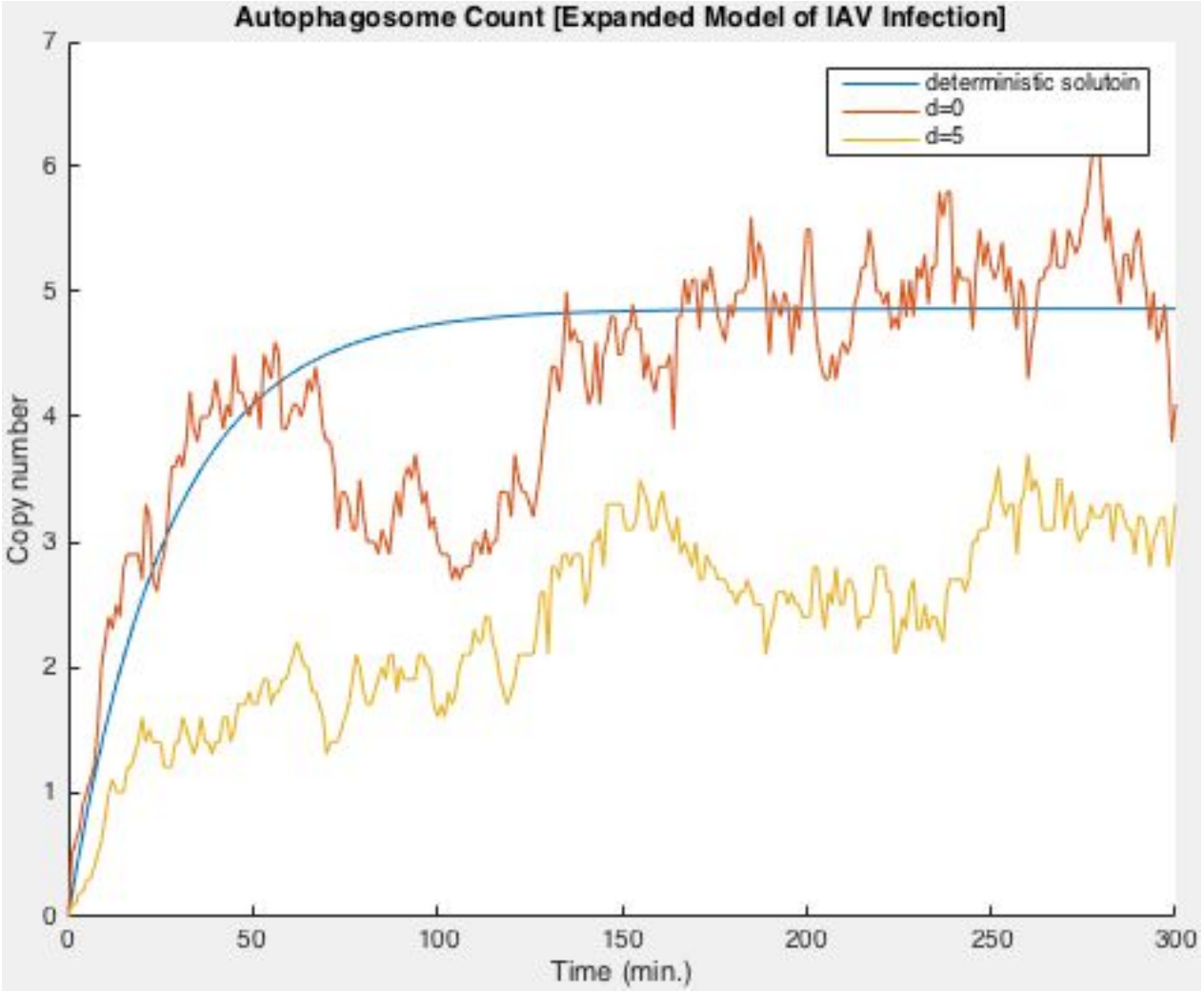

Conclusions

- Mechanistic model closely fits autophagosome count data from Martin et al.;
- ML-Rules and D2D are reliable packages for further analytical work
- No conclusive values for a and b parameters in expanded model of IAV infection. They need not be on the order of 1e3!
- Need experimental data of IAV infection to better understand IA model

Future Directions

- Simulate mechanistic model in ML-Rules with effects of AZD8055 & BafA1 and to longer times
- Determine precise initial conditions in mechanistic model in ML-Rules during time span before steady state
- ***Continue adding more details of influenza A infection to expanded model***
  - ***Compare against data once available***
  - ***Collaboration with experimentalists***
- Add more chemical species to mechanistic model for a more complete model of autophagy

What I learned

- How to model
  - Heuristic -> computational
  - Approaches
    - Rule based modeling
    - Deterministic
    - Stochastic
  - Tools
    - RuleBender
    - ML-Rules
    - D2D
    - SESSL
    - Loads more MATLAB in a different context
- Molecular mechanisms of autophagy
- Influenza A Viral dynamics & mechanisms of infection

Experiences

- 10th annual q-Bio Summer School;
  University of New Mexico, Albuquerque
  - Lectures on computational biology tools
  - Introduction to ongoing investigations
- 10th annual q-bio Conference;
  Vanderbilt University, Nashville, TN
  - Keynote speakers:
    Jim Collins, MIT
    Terry Sejnowski, Salk Institute

Acknowledgements

Dr. Bill Hlavacek

Dr. Ruy Ribeiro

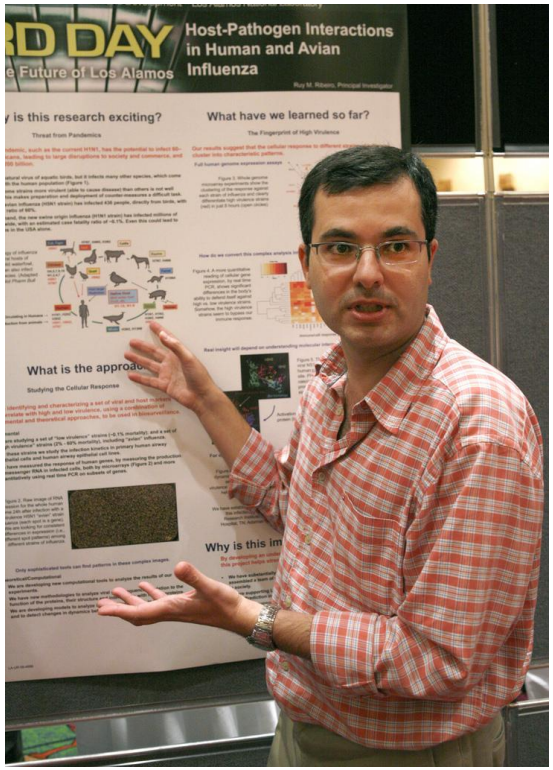

Dr. Ryan Suderman

Los Alamos
NATIONAL LABORATORY
EST. 1943

DOE - SULI Program

DEPARTMENT OF ENERGY · UNITED STATES OF AMERICA ·

Plasma treatment of cancer:
Selective electrostatic disruption of cancer cells

Kathleen Weichman[1], Gian Luca Delzanno[2], Kim Rasmussen[2] and Marlene Rosenberg[3]

[1]University of Texas at Austin
[2]Los Alamos National Laboratory
[3]University of California San Diego

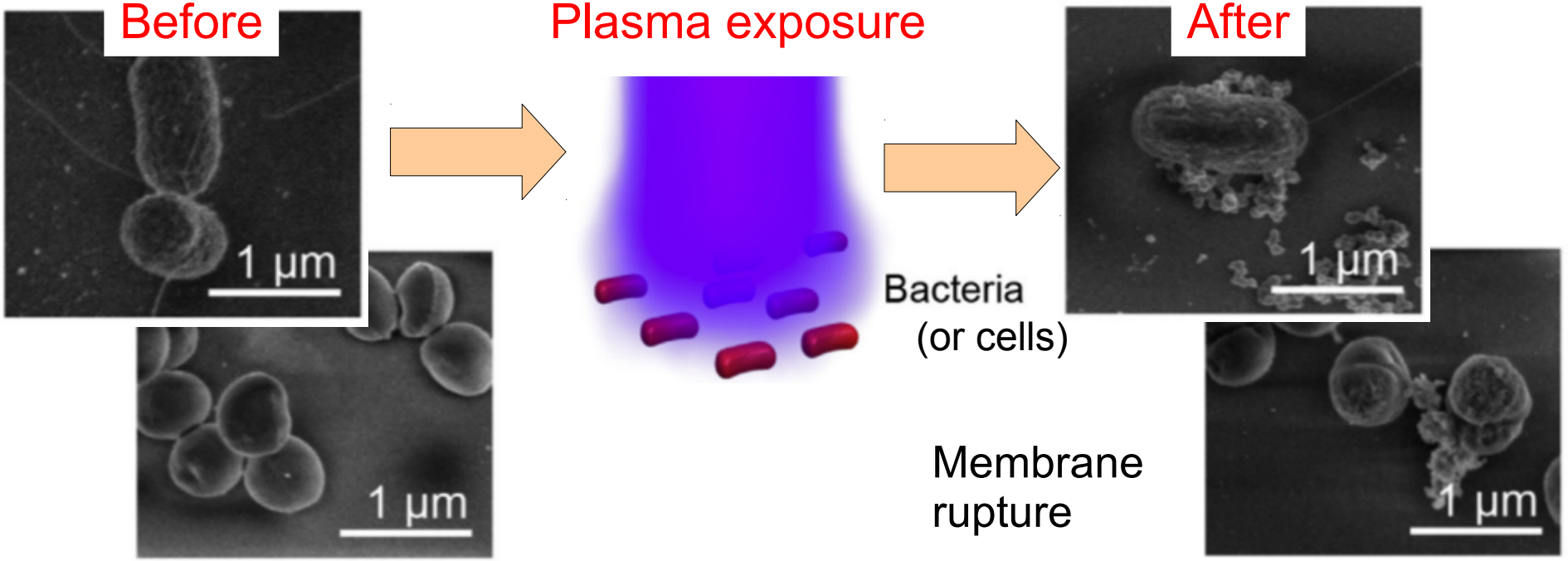

O. Lunov et al., Biomaterials 82, 71 (2016)

Outline

- What is plasma medicine? What does it hope to accomplish?
- Mechanisms of interaction between plasma and cells
  - Chemistry
  - Electric fields and plasma physics
- Electrostatic disruption
  - Plasma charging
  - No electrostatic disruption predicted for healthy cells
  - Selective disruption of cancer cells
- Future work

Plasma medicine

- Motivations
  - Resistance to conventional therapies
  - Enhanced selectivity and fewer side effects
- Cold atmospheric (non-thermal) plasma (CAP)

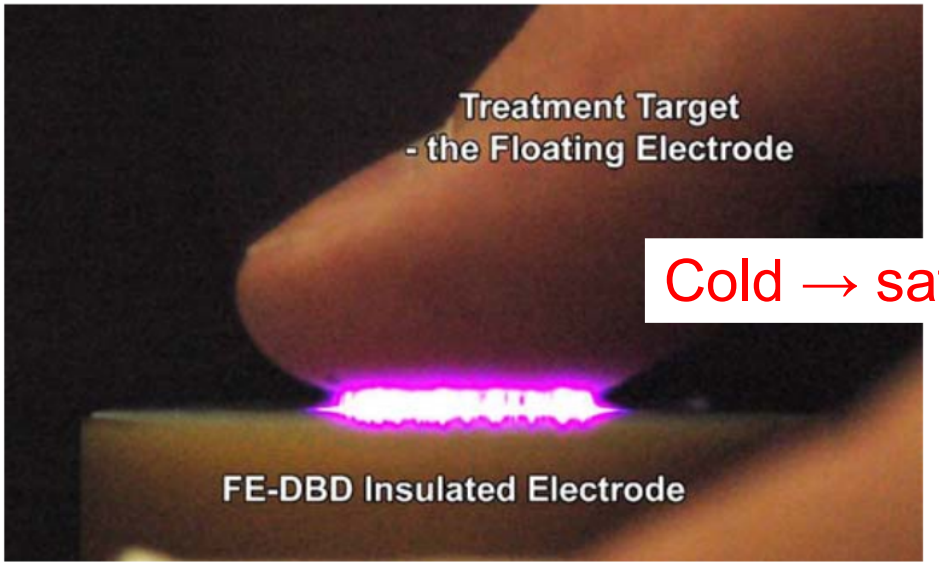

Cold → safe for healthy tissue

G. Fridman et al., Plasma Chem Plasma Process 26, 425 (2006)

R. Guerrero-Preston et al., Int J Mol Med 43, 941 (2014)

Plasma medicine

- Motivations
  - Resistance to conventional therapies
  - Enhanced selectivity and fewer side effects
- Cold atmospheric (non-thermal) plasma (CAP)

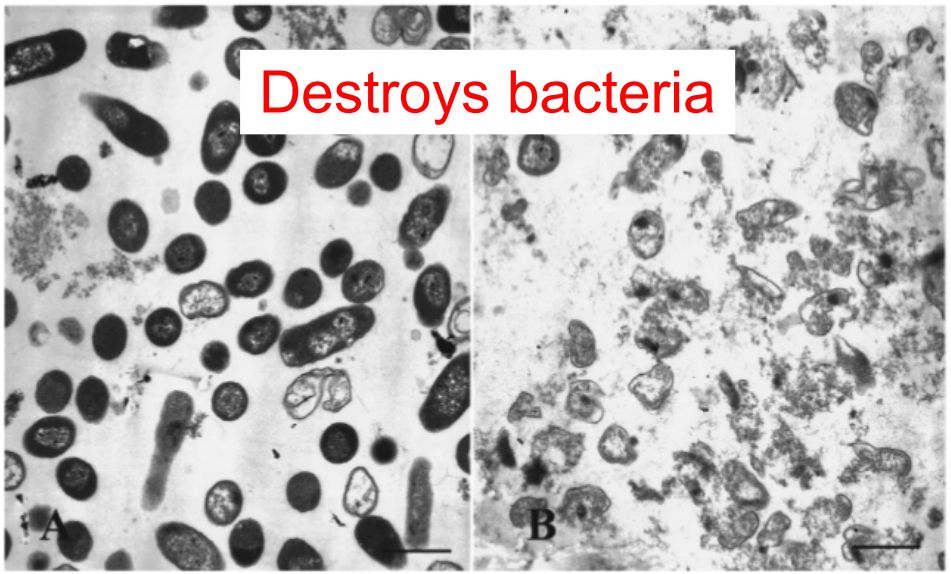

K. Kelly-Wintenberg et al., JVST A 17, 1539 (1999)

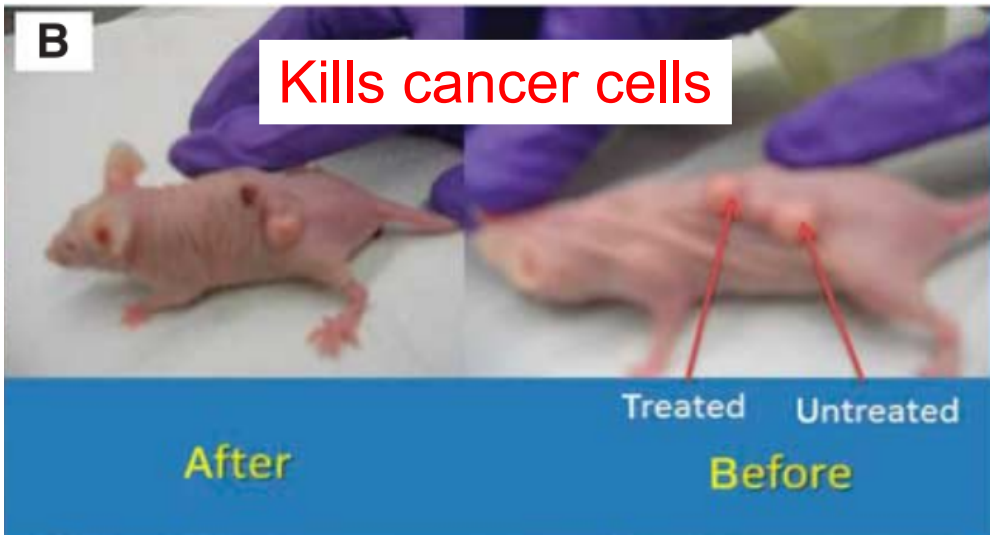

M. Keidar et al., Brit J Cancer 105, 1295 (2011)

Chemical and physical effects of cold atmospheric plasma

Plasma → water

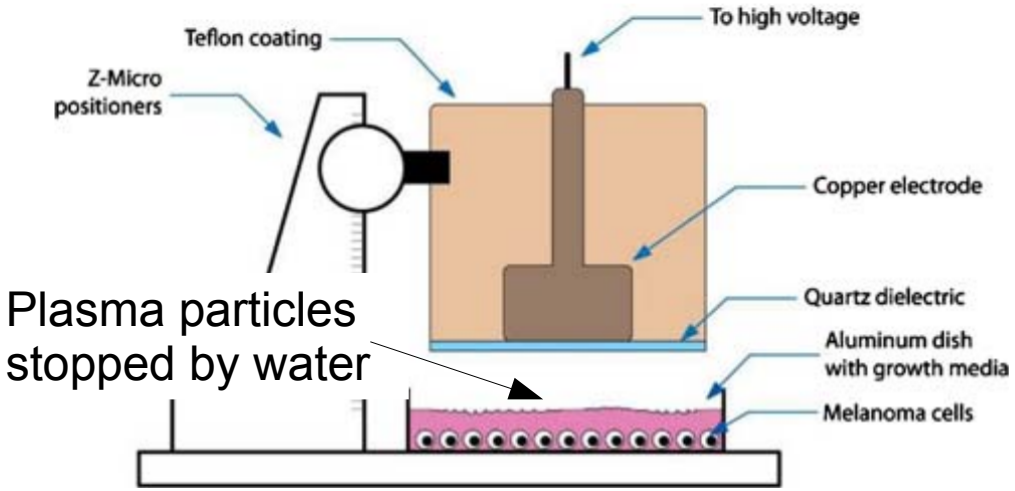

G. Fridman et al., Plasma Chem Plasma Process 27, 163 (2007)

Plasma-water interface

- Chemistry: reactive oxygen and nitrogen species (ROS, RNS)
  - Device electric fields

Explanation of plasma medicine community for cancer cell killing and selectivity

(ROS/RNS generation also a feature of conventional treatments)

Chemical and physical effects of cold atmospheric plasma

Plasma → water

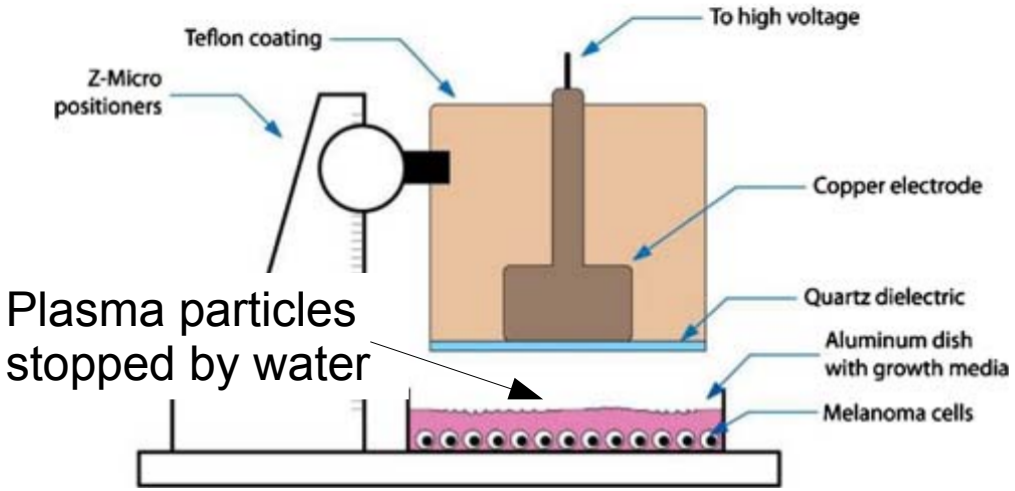

G. Fridman et al., Plasma Chem Plasma Process 27, 163 (2007)

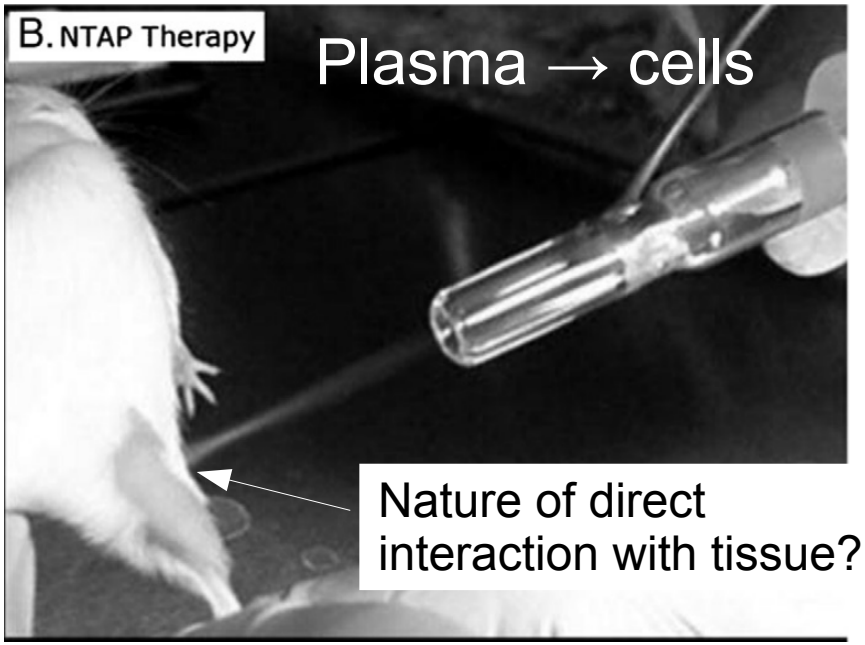

R. Walk et al., J Pediatr Surg 48, 67 (2013)

Plasma-water interface

- Chemistry: reactive oxygen and nitrogen species (ROS, RNS)
  - Device electric fields

Plasma contacts tissue

- Plasma physics effects: charging and plasma-mediated electric fields

Could plasma charging lead to cell death?

Electrostatic disruption due to plasma charging

1. Plasma charging → surface potential

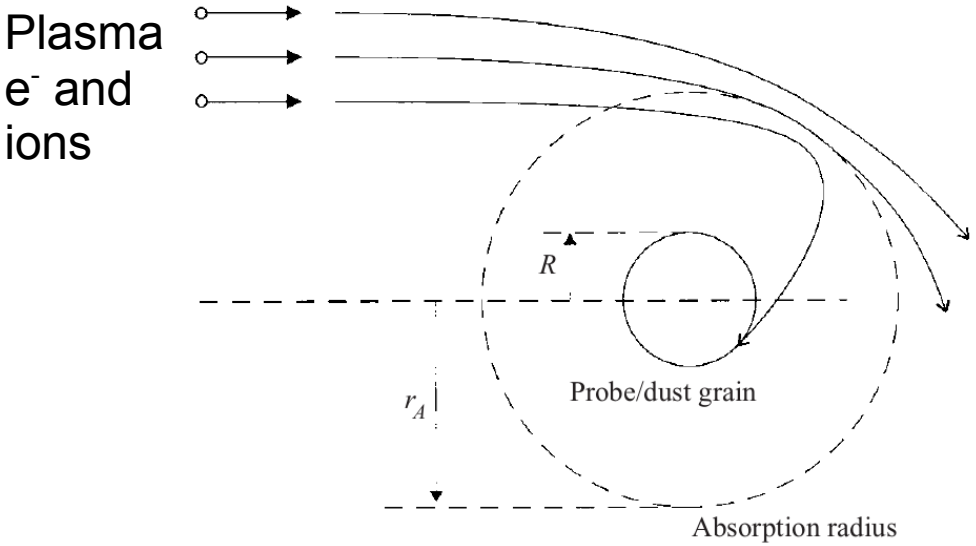

Surface charge

$$Q = C\phi$$

Electrostatic pressure

Electric field

R.V. Kennedy and J.E. Allen, J. Plasma Physics 69, 485 (2003)

2. Failure

- Electrostatic pressure > cohesive force (F_{max})
- Plasma charging → critical potential for disruption

$C_{plasma} \neq C_{vacuum}$

$$|\phi_{crit}| \geq \sqrt{\frac{2}{\pi}} \sqrt{F_{max}/\epsilon_0} \frac{C_{vac}}{C} \cdot \text{shape factor}$$

elongated cells disrupt more easily

Is disruption of cells possible?

- Expected surface potential: - 4 to - 20 V
- Critical potential with vacuum capacitance: - 270 V (based on bursting force given in [1,2])

Typical CAP device parameters

Electron density	$n_e \sim 10^{13} cm^{-3}$
Neutral gas density	$n_n = 2x10^{19} cm^{-3}$
Electron temperature	T_e = 1-5 eV
Ion temperature	T_i = 1/40 eV
Electron mean free path	l_e =0.5 μm
Ion mean free path	l_i =0.125 μm

[1] Z. Zhang et al., Appl Microbiol Biot 36, 208 (1991)
[2] V. Lulevich, et al., Langmuir 22, 815 (2006)
[3] G.-L. Delzanno and X.-Z. Tang, Phys Plasmas 22, 113703 (2015)

Is disruption of cells possible?

- Expected surface potential: - 4 to - 20 V
- Critical potential with vacuum capacitance: - 270 V
- C_{plasma}/C_{vacuum} ~ 5 – 10 [Ref. 3]

Neglected by plasma medicine community!

- Critical potential with capacitance correction: - 27 to - 55 V

Healthy cells are not expected to disrupt!

Typical CAP device parameters

Electron density	$n_e \sim 10^{13} cm^{-3}$
Neutral gas density	$n_n = 2x10^{19} cm^{-3}$
Electron temperature	T_e = 1-5 eV
Ion temperature	T_i = 1/40 eV
Electron mean free path	l_e =0.5 μm
Ion mean free path	l_i =0.125 μm

[1] Z. Zhang et al., Appl Microbiol Biot 36, 208 (1991)
[2] V. Lulevich, et al., Langmuir 22, 815 (2006)
[3] G.-L. Delzanno and X.-Z. Tang, Phys Plasmas 22, 113703 (2015)

Physical selectivity of CAP treatment to cancer cells

Cancerous cells are:

- Less stiff
- More elongated/irregular
  - Spindle-shaped cells are especially invasive
  - Also especially favorable for disruption!

Surface potential: - 4 to - 20 V

Critical potential for a cancer cell: - 3 to - 18 V

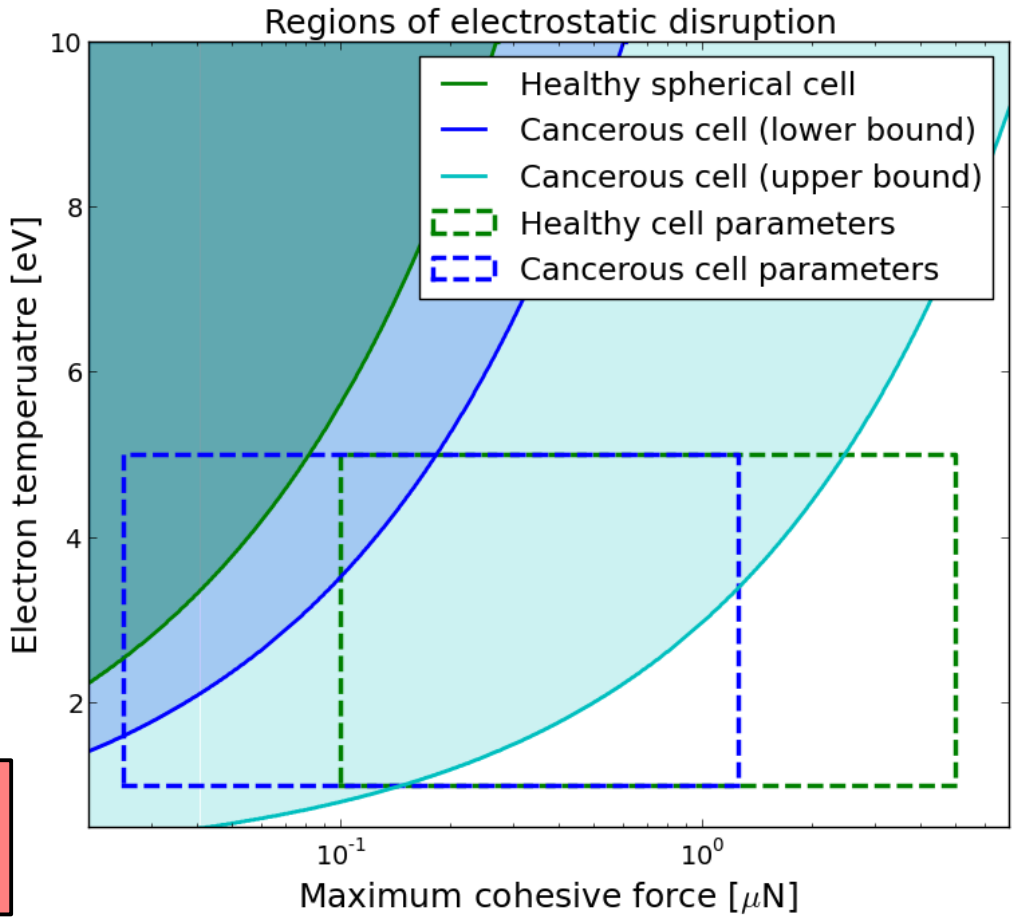

Selective electrostatic disruption of cancer cells is possible!

Future work

- Verify plasma capacitance by simulation
- Effect of higher order shape and surface roughness
- How does the device electric field contribute?
  - (Irreversible) electroporation?
- Can deformation lead to failure (such as occurs for water droplets)?

Conclusions

- Cold atmospheric plasma treatment destroys bacteria and kills cancer cells
  - Chemical effects are typically implicated in cancer cell death
  - Plasma charging can also selectively kill cancer cells
- Future work focuses on shape and surface roughness effects and the role of device electric fields

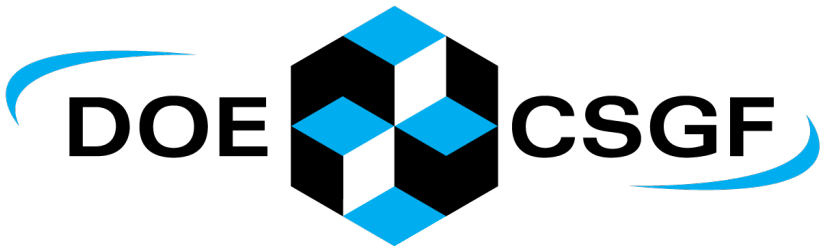

KW is supported by the DOE CSGF under Grant No. DE-FG02-97ER25308

A STOCHASTIC OPTIMIZATION MODEL FOR ELECTRIC VEHICLE FAST-CHARGING STATION

FEI WU

THE OHIO STATE UNIVERSITY

THE OHIO STATE UNIVERSITY

Agenda

THE OHIO STATE UNIVERSITY

1. Motivation

2. Stochastic Optimization Model

3. Case Study and Analysis

EV PENETRATION

THE OHIO STATE UNIVERSITY

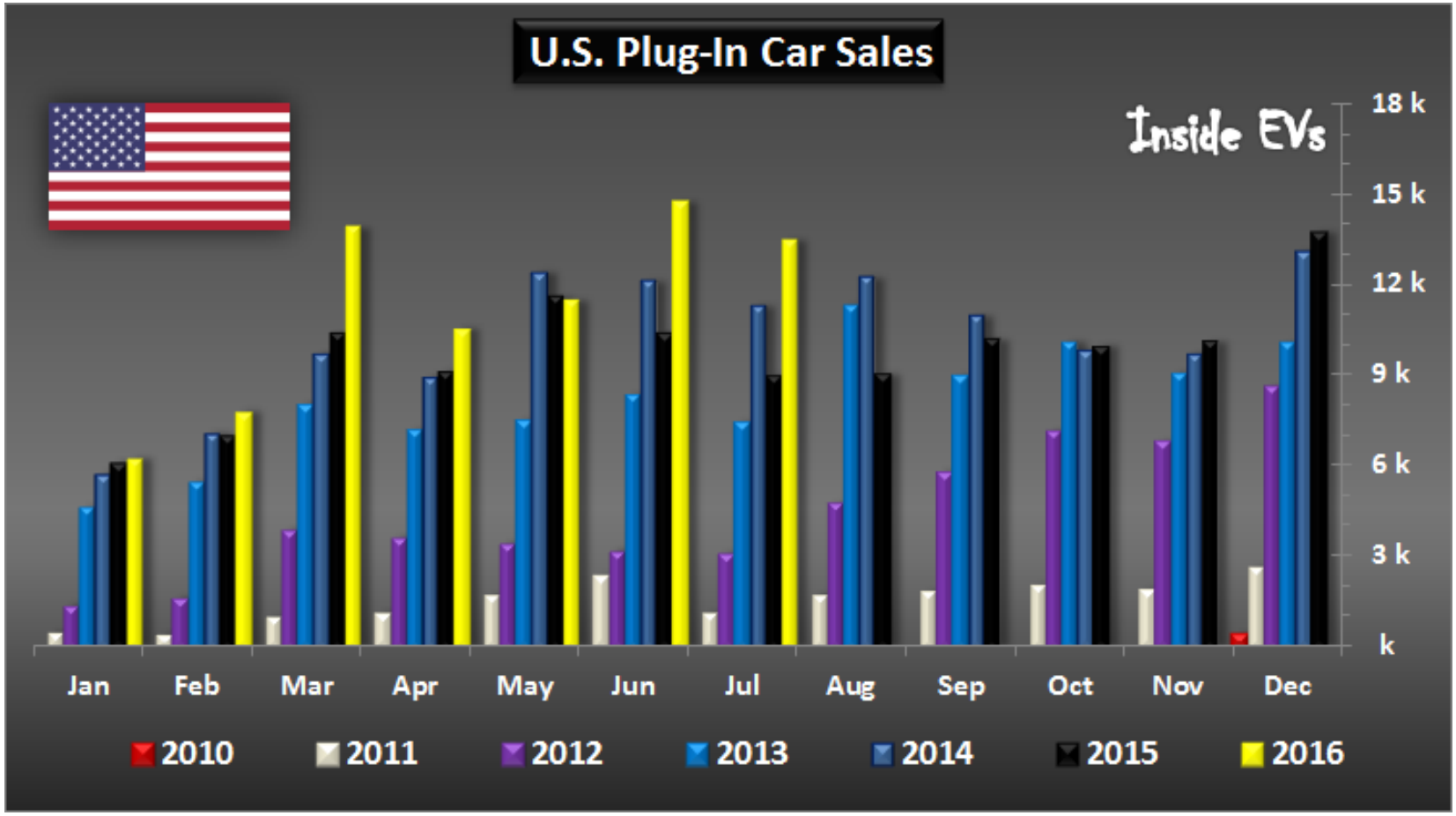

Source: InsideEVs(http://insideevs.com/monthly-plug-in-sales-scorecard/)

EV RANGE AND CHARGING STANDARD

THE OHIO STATE UNIVERSITY

EV Ranges

EV Brand	Range (miles)
Tesla Models	265
Toyota RAV4 EV	103
FIAT 500e	87
Nissan Leaf	84
Chev. Spark EV	82
Ford Focus Electric	76
Smart fortwo electric drive	68
Mitsubishi i-MiEV	62
Scion iQ EV	48

AC/DC charging levels from SAE J1772-2011

Power level types	Voltage level(v)	Power cap.(kW)	Times
AC L1	120 VAC	1.4/1.9	17 h
AC L2	240 VAC	19.2	7 h/3.5 h
AC L3	-	-	-
DC L1	200-500 VDC	up to 40 kW	1.2 h
DC L2	200-500 VDC	up to 100 kW	20 min
DC L3	200-600 VDC	up to 240 kW	-

TRANSFORMER LOAD PROFILE WITH EVS

THE OHIO STATE UNIVERSITY

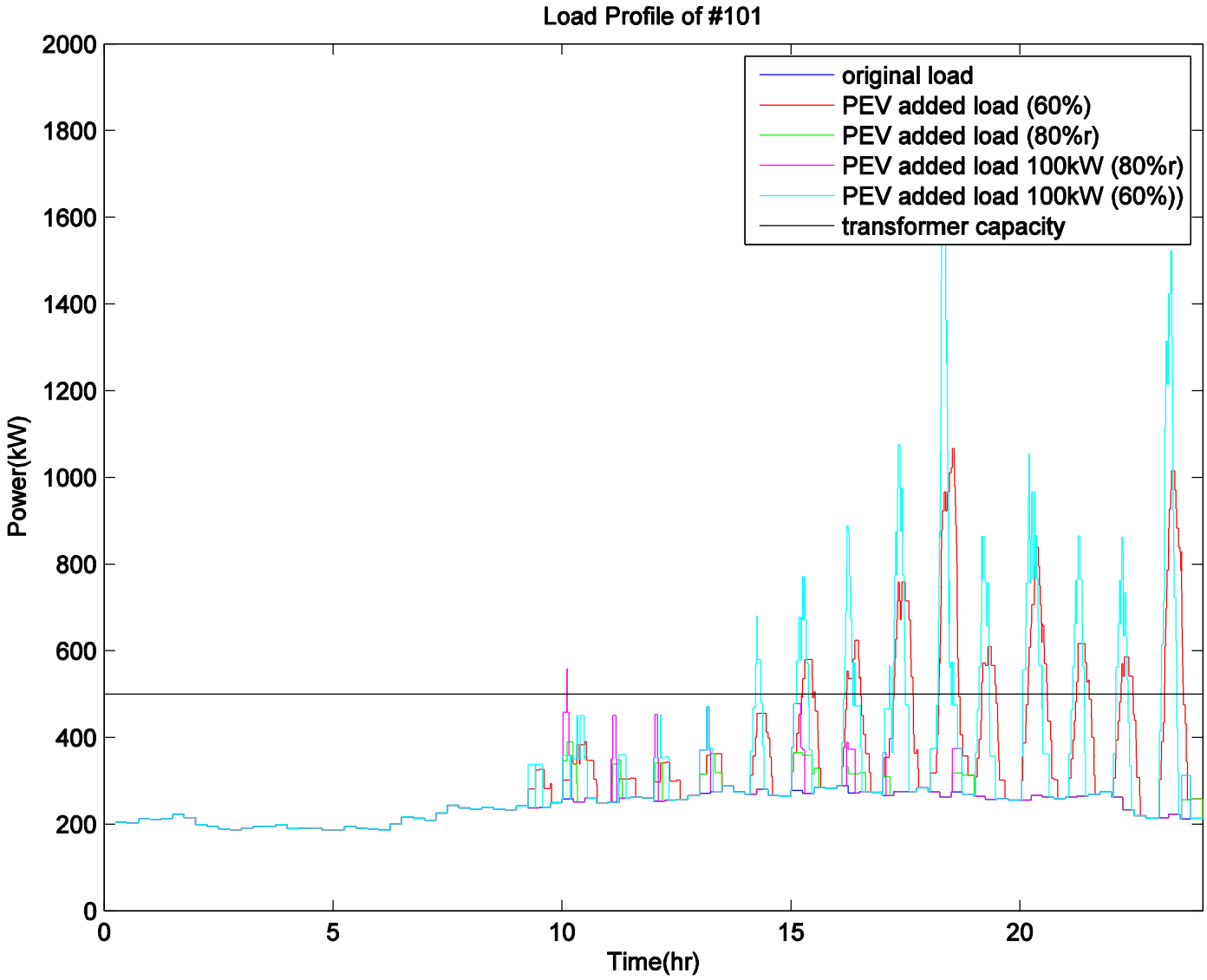

Charing Effect on Current Transmission System

THE OHIO STATE UNIVERSITY

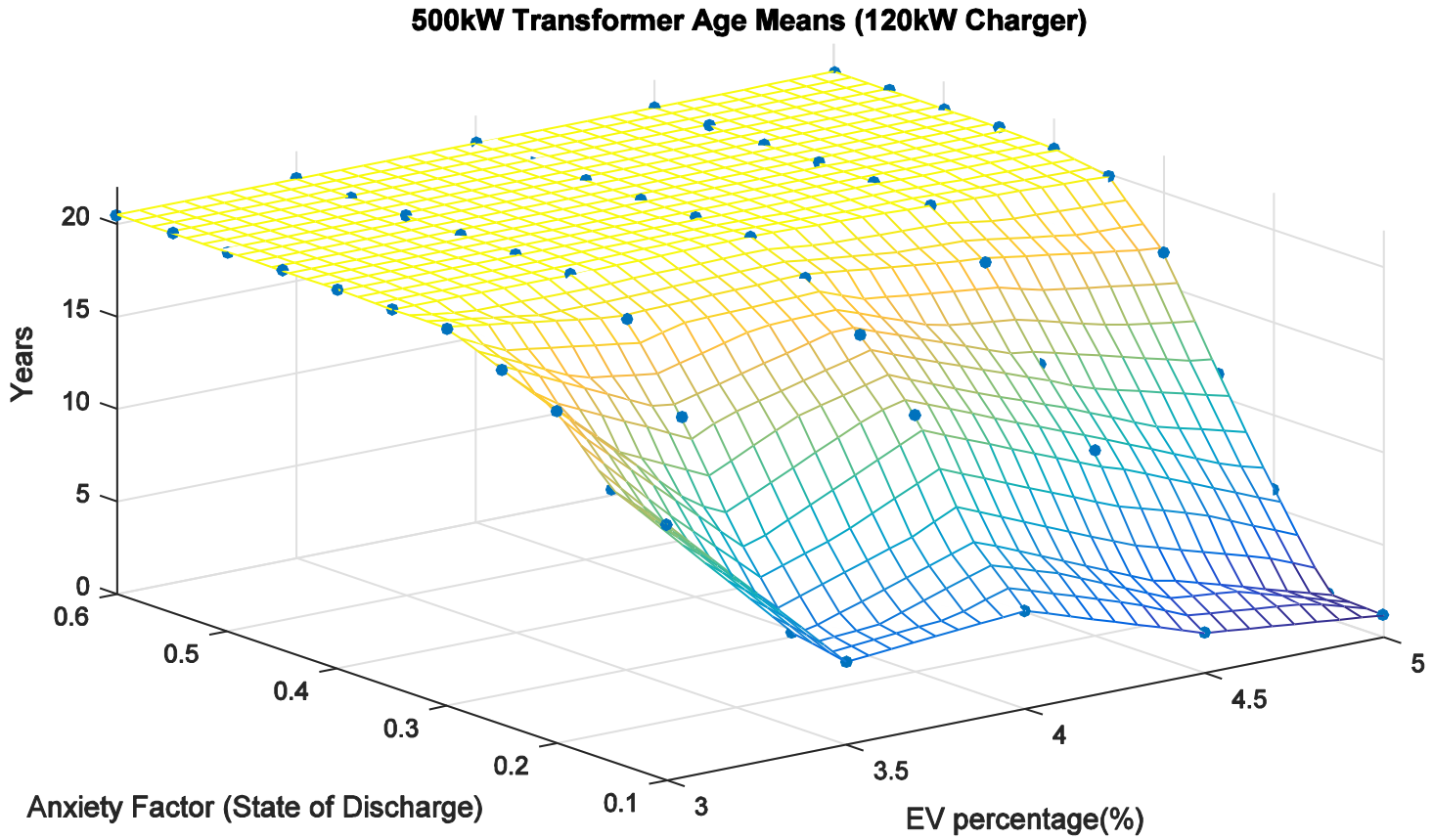

Relief Transformer Capacity Constraints

THE OHIO STATE UNIVERSITY

- ✓Distributed energy resources
  1. Photovoltaic solar panels
  2. Energy storage
- ✓Reschedule EV charging load
  1. EV charging strategies
  2. Energy storage charging/discharging strategies
- ✓Challenges
  1. Uncertain EV arrival
  2. Stochastic solar generator output

2-Stage Stochastic Optimization Model

THE OHIO STATE UNIVERSITY

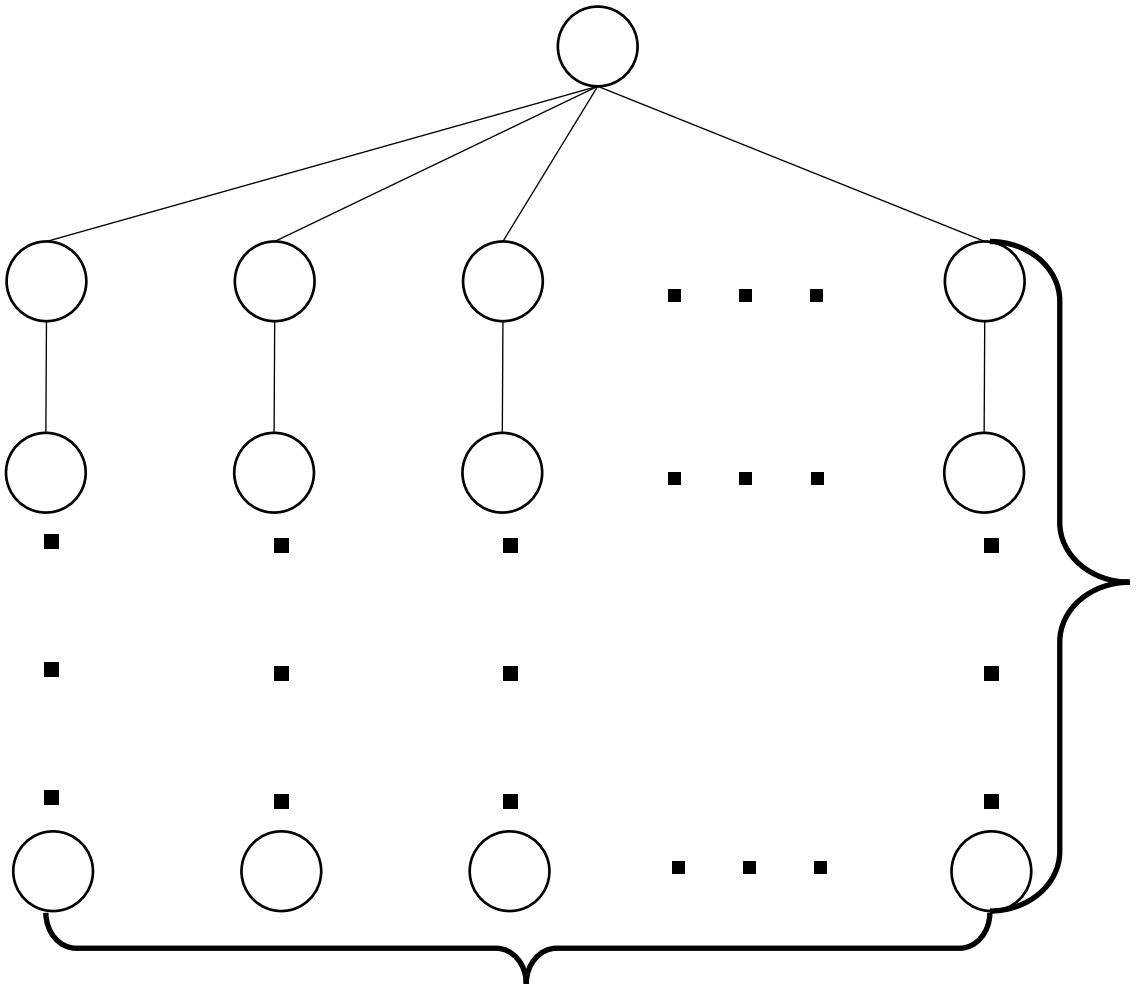

Stage 1: Current Problem
- Station Status is realized
- The optimal solution is implemented immediately

Stage 2: Sample Paths
- From the next time unit to the end of optimization horizon
- Based on forecasting:
  - Solar output
  - EV arrival
  - Non-EV load
  - Electricity price

Infinite Sample Paths/Scenarios:
- Forecast parameter vectors is infinite support

SAA and Sequential Approximation

THE OHIO STATE UNIVERSITY

- ✓Sample Average Approximation
  - original large-scale problem ← a smaller problem with randomly generated scenario samples
- ✓Sequential Approximation
  - Use a different sample to evaluate the SAA solution quality
  - Create optimality gap confidence interval
  - Decide a sample size of the next iteration

Case Study

THE OHIO STATE UNIVERSITY

A medium EV-flow-density station

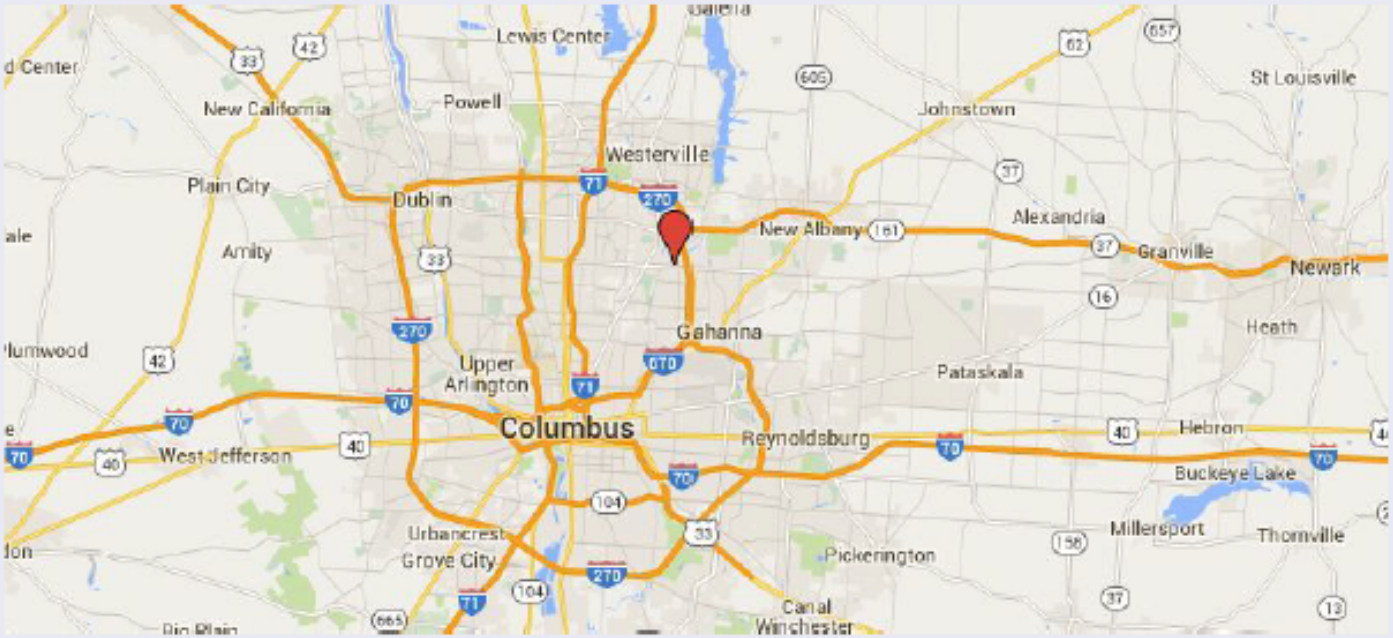

Operation Performance

THE OHIO STATE UNIVERSITY

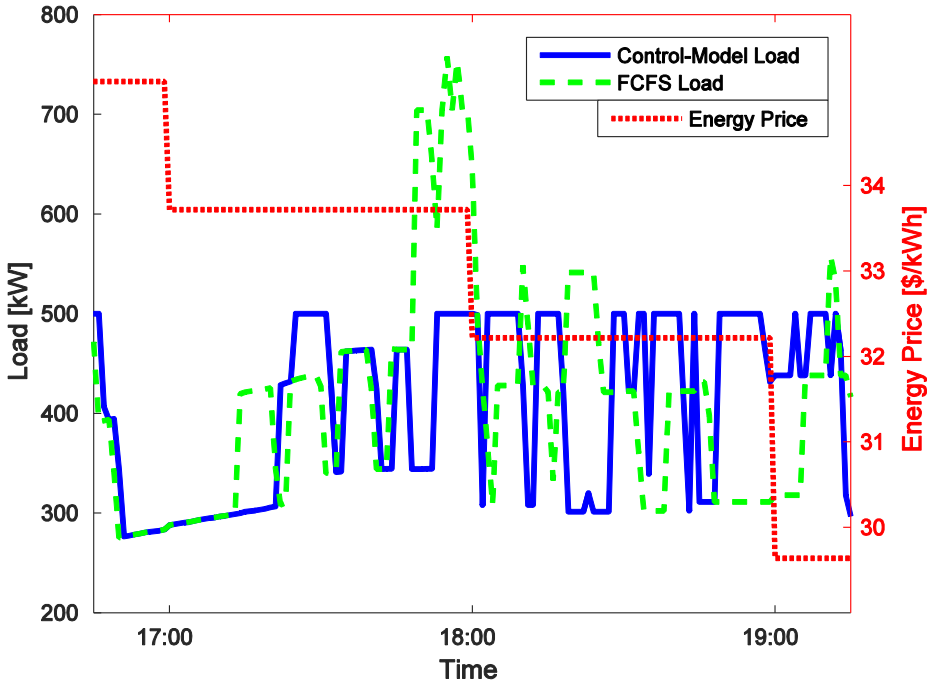

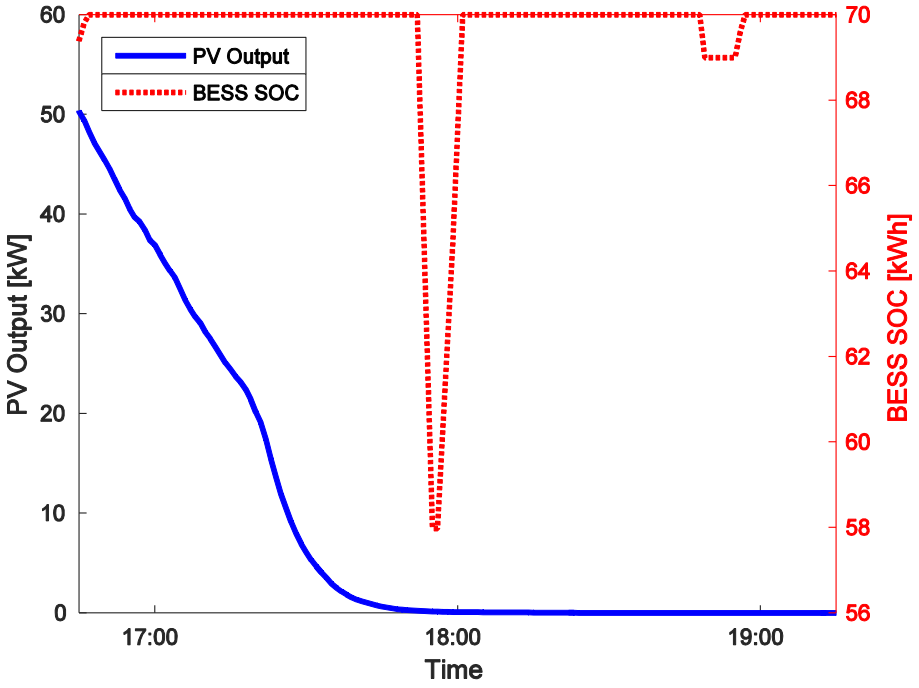

Compare with other heuristic methods

THE OHIO STATE UNIVERSITY

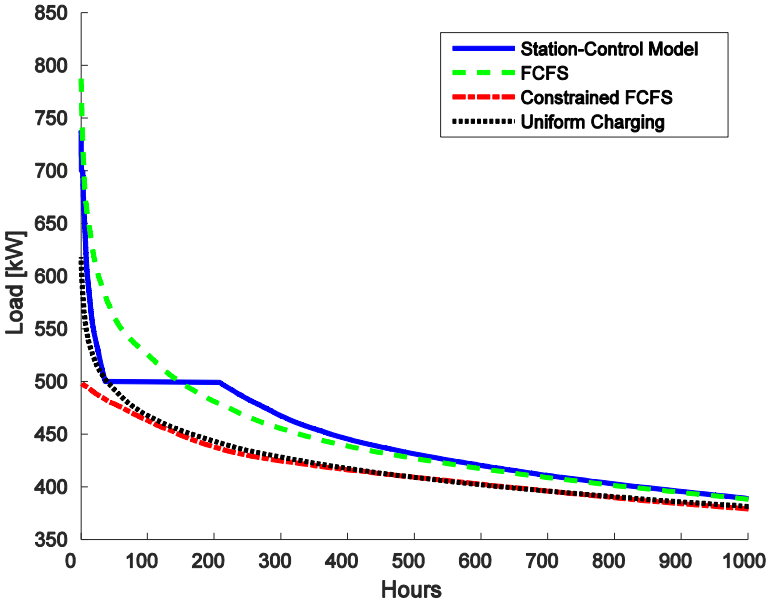

30 mins

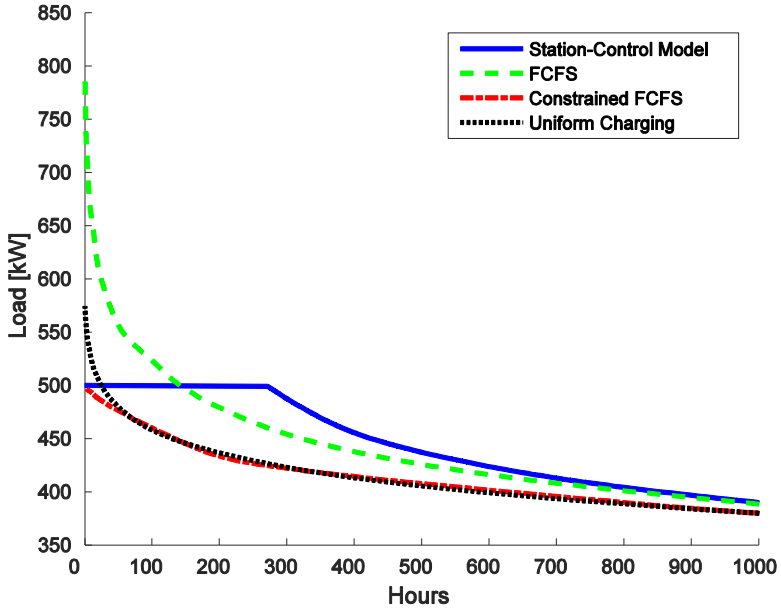

40 mins

The minimum time length a EV in the station

Sensitivity analysis

THE OHIO STATE UNIVERSITY

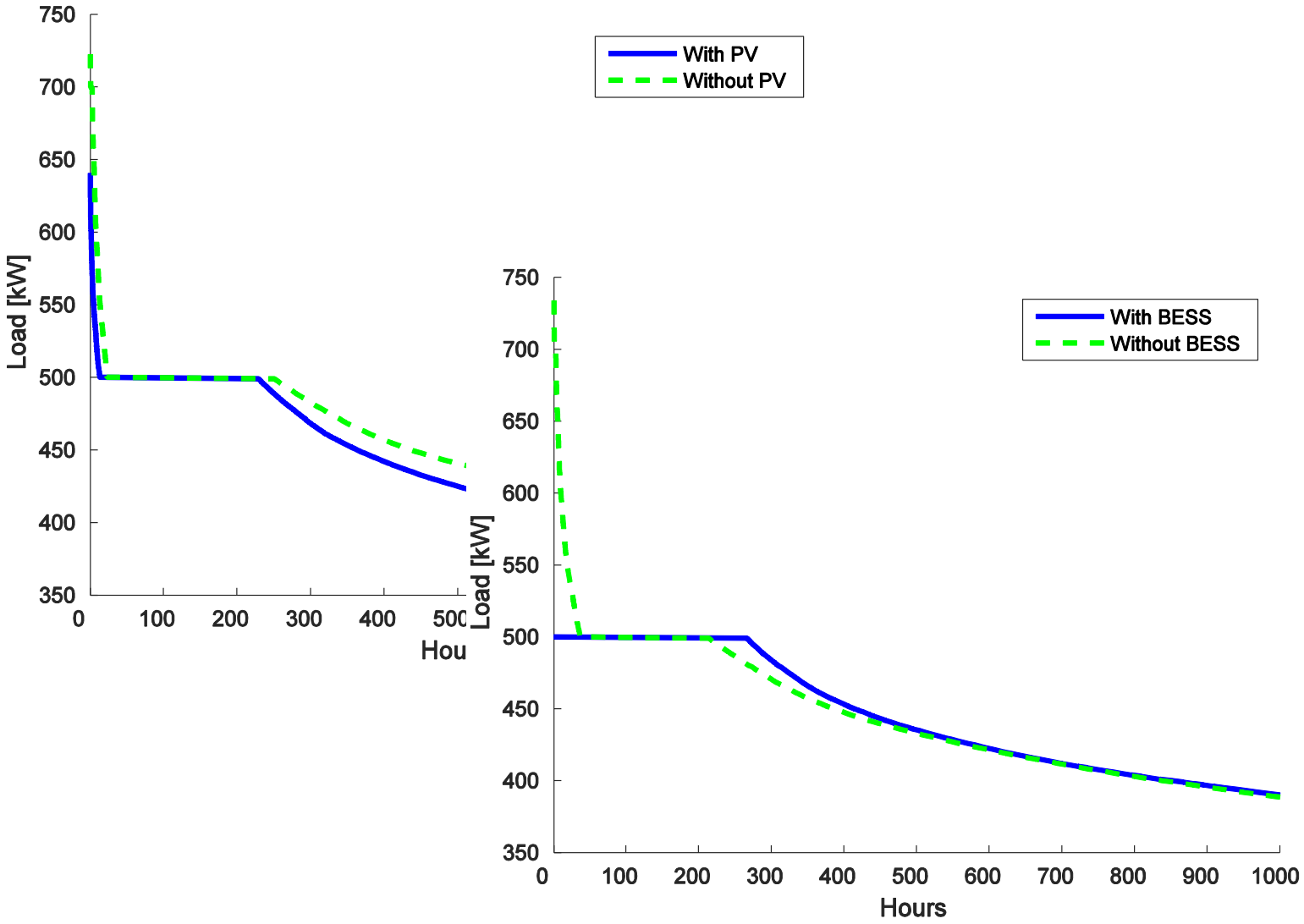

Questions?

THE OHIO STATE UNIVERSITY

- References
  - F. Wu and R. Sioshansi, "A Two-Stage Stochastic Optimization Model for Scheduling Electric Vehicle Charging Loads to Relieve Distribution-System Constraints," submitted to *Transportation Research Part B: Methodological*.

- Acknowledgments
  - This materials of this research is based upon work financially supported by the U.S. Department of Energy under Award Number DEPI0000012 and by the National Science Foundation through Grant Number 1029337.

Pinning Effects on Granular Particles

Yang Yang
(Wabash College)
Mentors:
Dr. Cynthia J. Olson Reichhardt and Dr. Charles Reichhardt
(T-1 Group)

07/14/2016

Granular Materials

Properties

- Repulsive Short-Range Interaction
- Energy Dissipation
- Unusual Phase State

Applications to Studying Granular Materials

- Landslide and Erosion
- Industrial Transport

Interacting with Substrate

images from: http://guernseydonkey.com (top)
http://www.marshallnews.com (bottom)

Approach to Simulation

Initialization

- System Size: 60×60 Particle Diameters
- Placing Particles on Square Lattice
- Randomly Placing Pinning Sites

Tuning Parameters

- Density of Particles/Packing Fraction Φ
- Number of Pinning Sites
- Driving Force $\vec{F}_D$

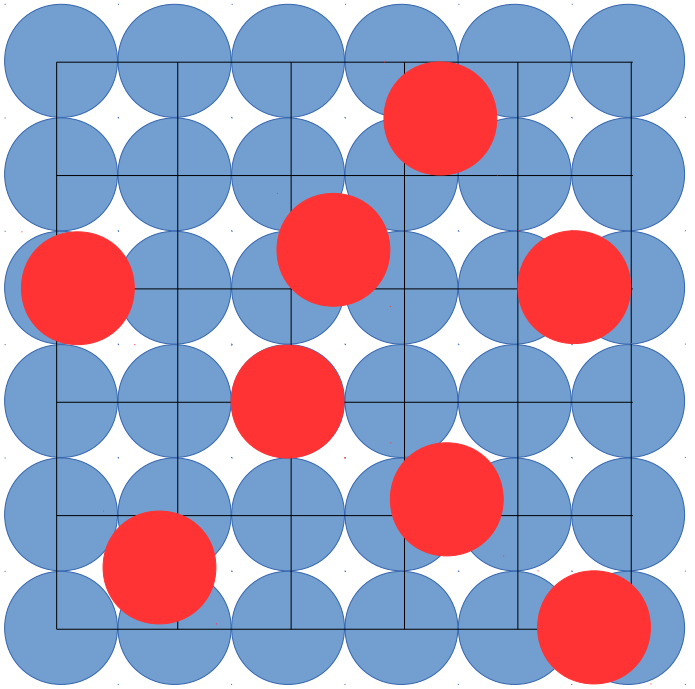

6×6 Particle-Diameter System
$\Phi = 0.785$

Approach to Simulation

Initialization

- System Size: 60×60 Particle Diameters
- Placing Particles on Square Lattice
- Randomly Placing Pinning Sites

Tuning Parameters

- Density of Particles/Packing Fraction Φ
- Number of Pinning Sites
- Driving Force $\vec{F}_D$

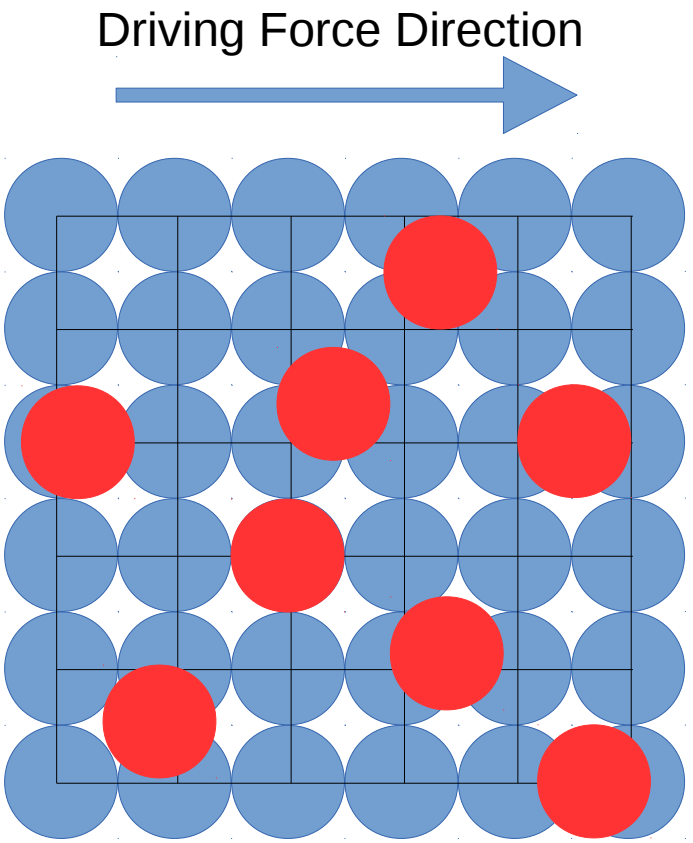

6×6 Particle-Diameter System
$\Phi = 0.785$

Simulation Model

Overdamped Langevin Dynamics

$$\eta \frac{d\vec{R}_i}{dt} = \vec{F}_i^{particle} + \vec{F}_i^{pinning} + \vec{F}_i^{drive}$$

Particle-Particle Interaction:

Spring Interaction

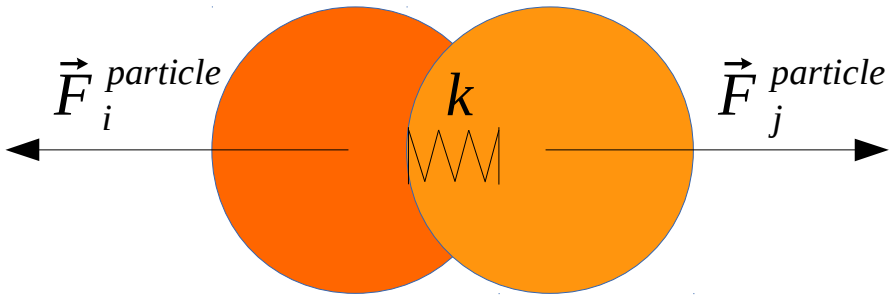

Particle-Pinning Interaction:

Harmonic Potential Wells

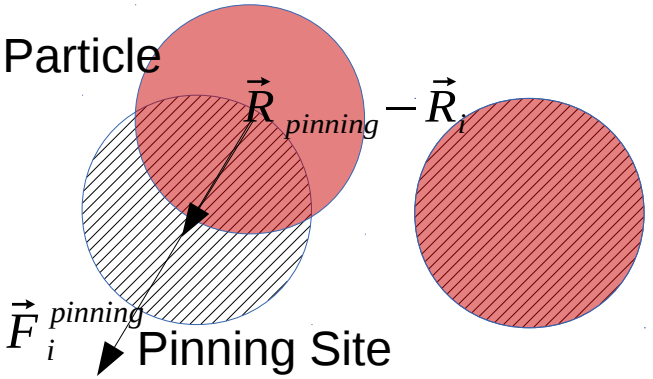

Driving Force $\vec{F}_D$

Jamming VS Flowing at Low Particle Density

- Packing Fraction: $\Phi = 0.3$

$\vec{F}_D$

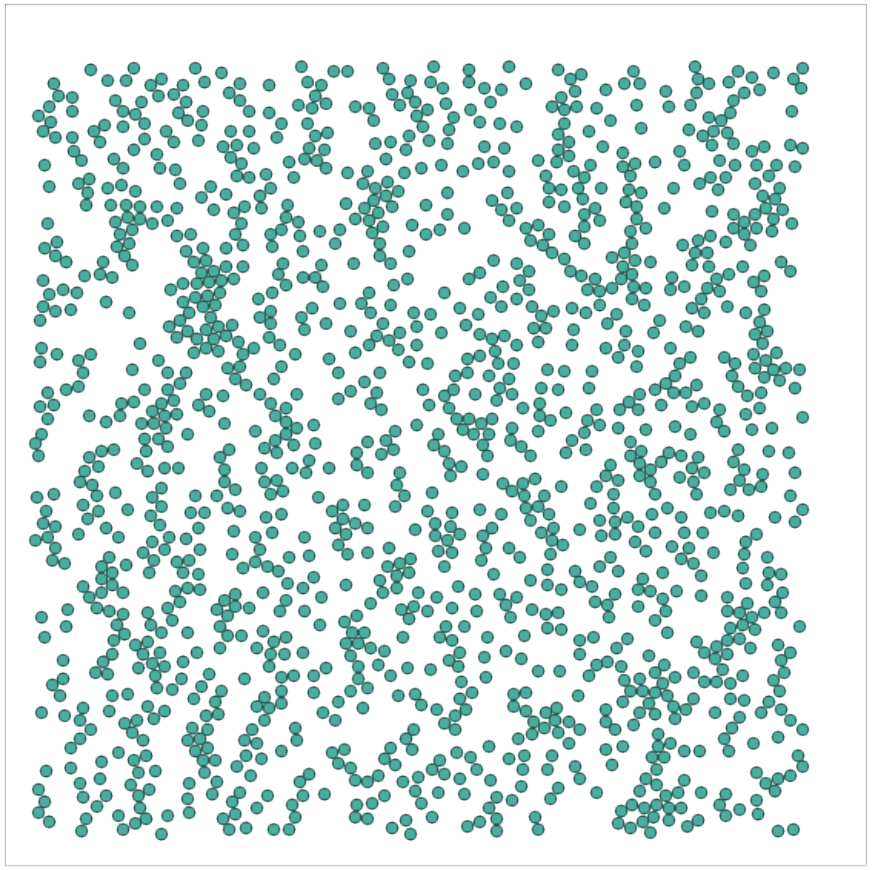

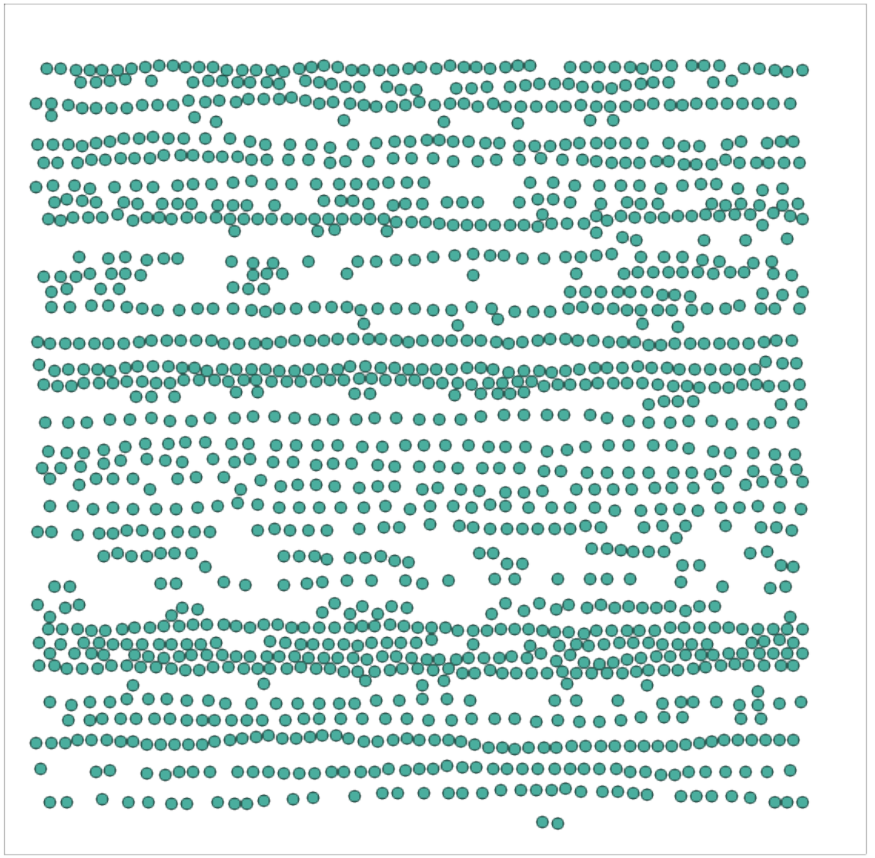

$F_D = 0.15$

$F_D = 2.00$

Jamming VS Flowing at High Particle Density

- Packing Fraction: $\Phi = 0.61$

$\vec{F}_D$

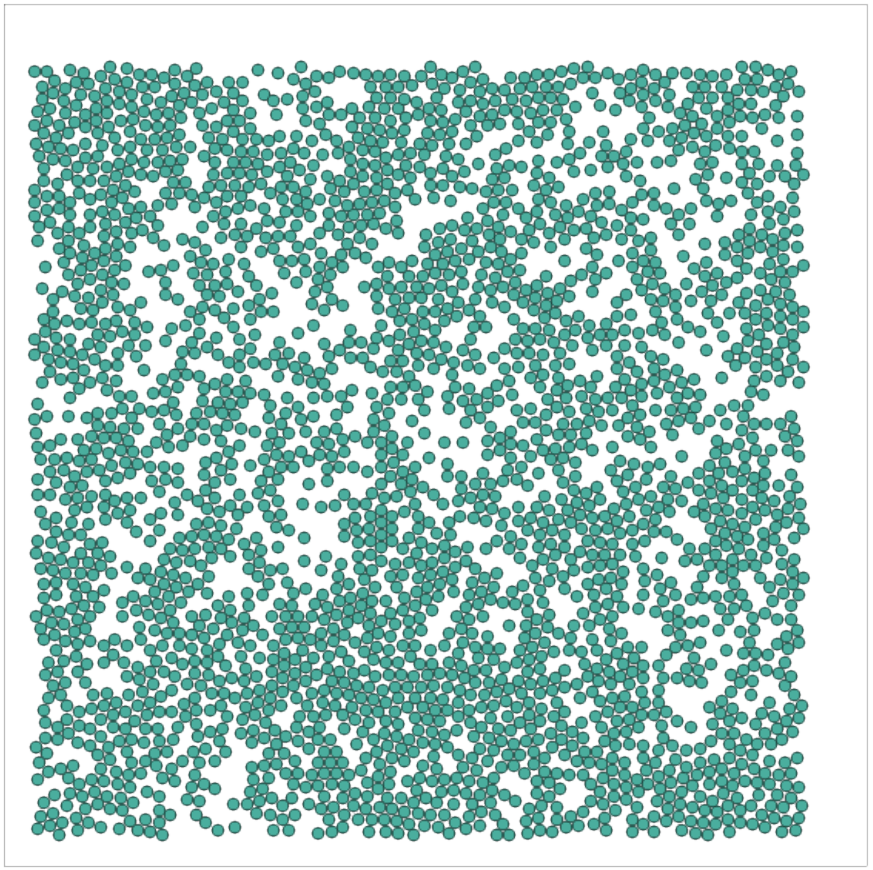

$F_D = 0.2$

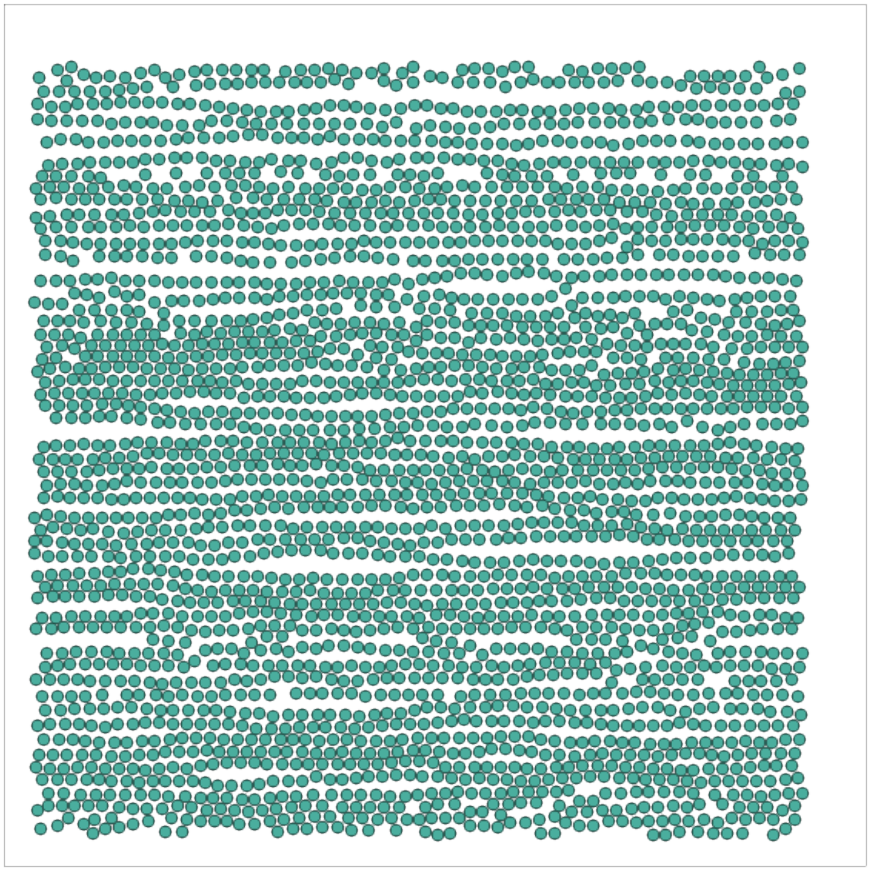

$F_D = 2.00$

Phase-Separation at Depinning Phase

- Driving Force: $F_D = 1.05$

$\vec{F}_D$

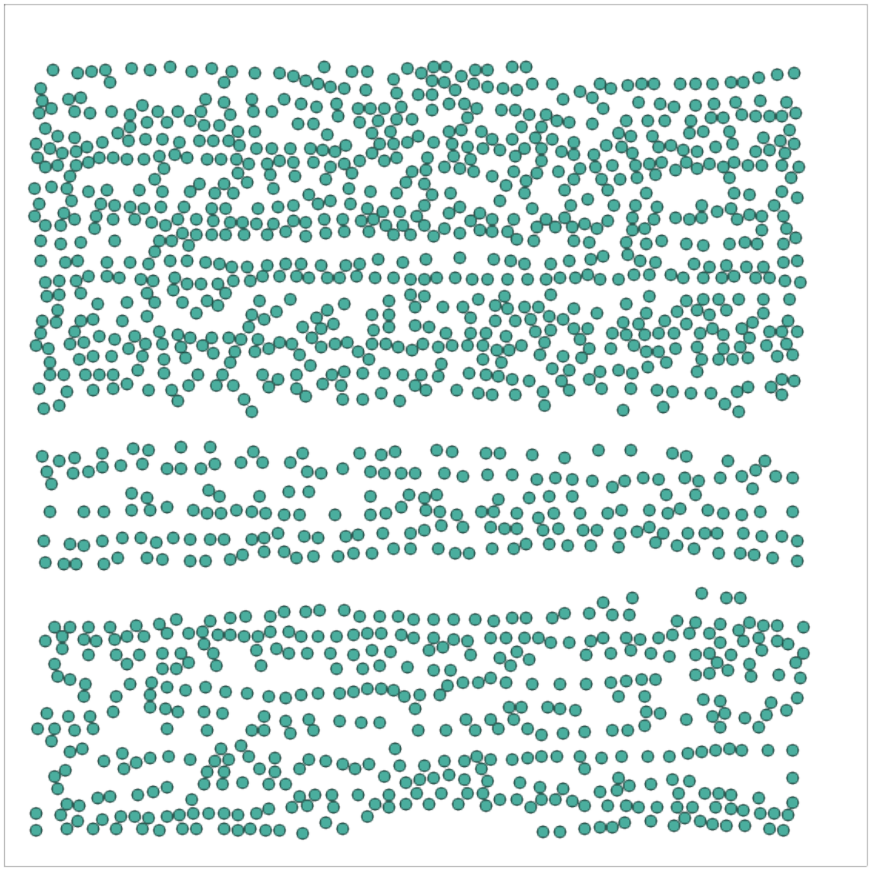

Packing Fraction $\Phi = 0.3$

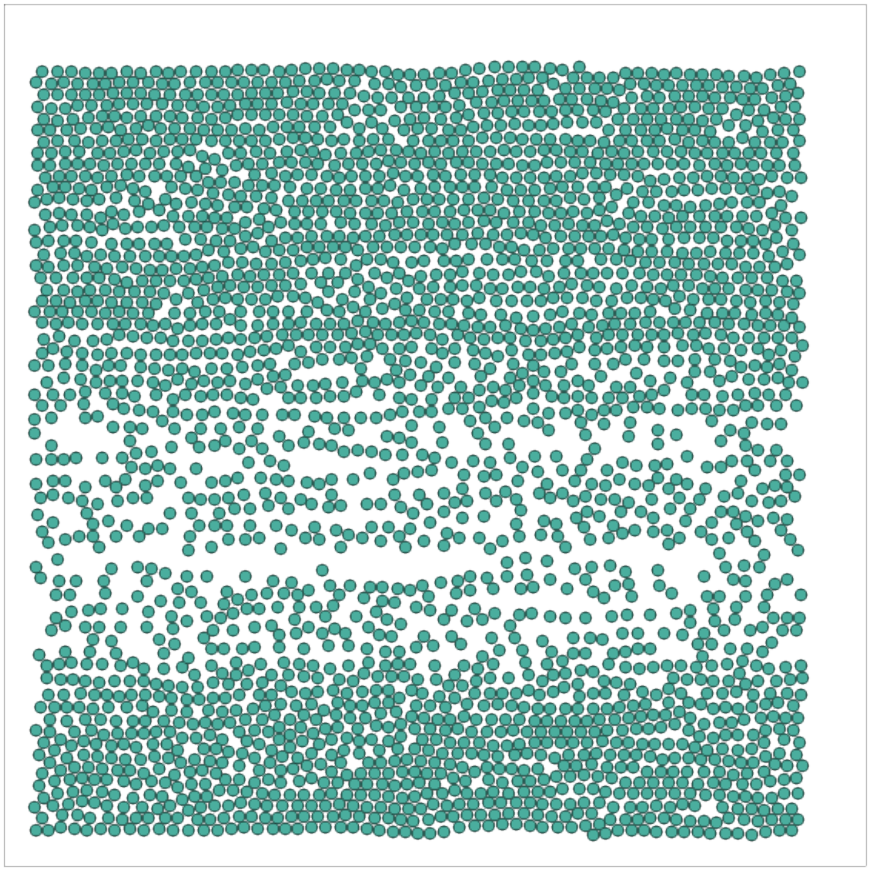

Packing Fraction $\Phi = 0.61$

Depinning and Clustering Phases

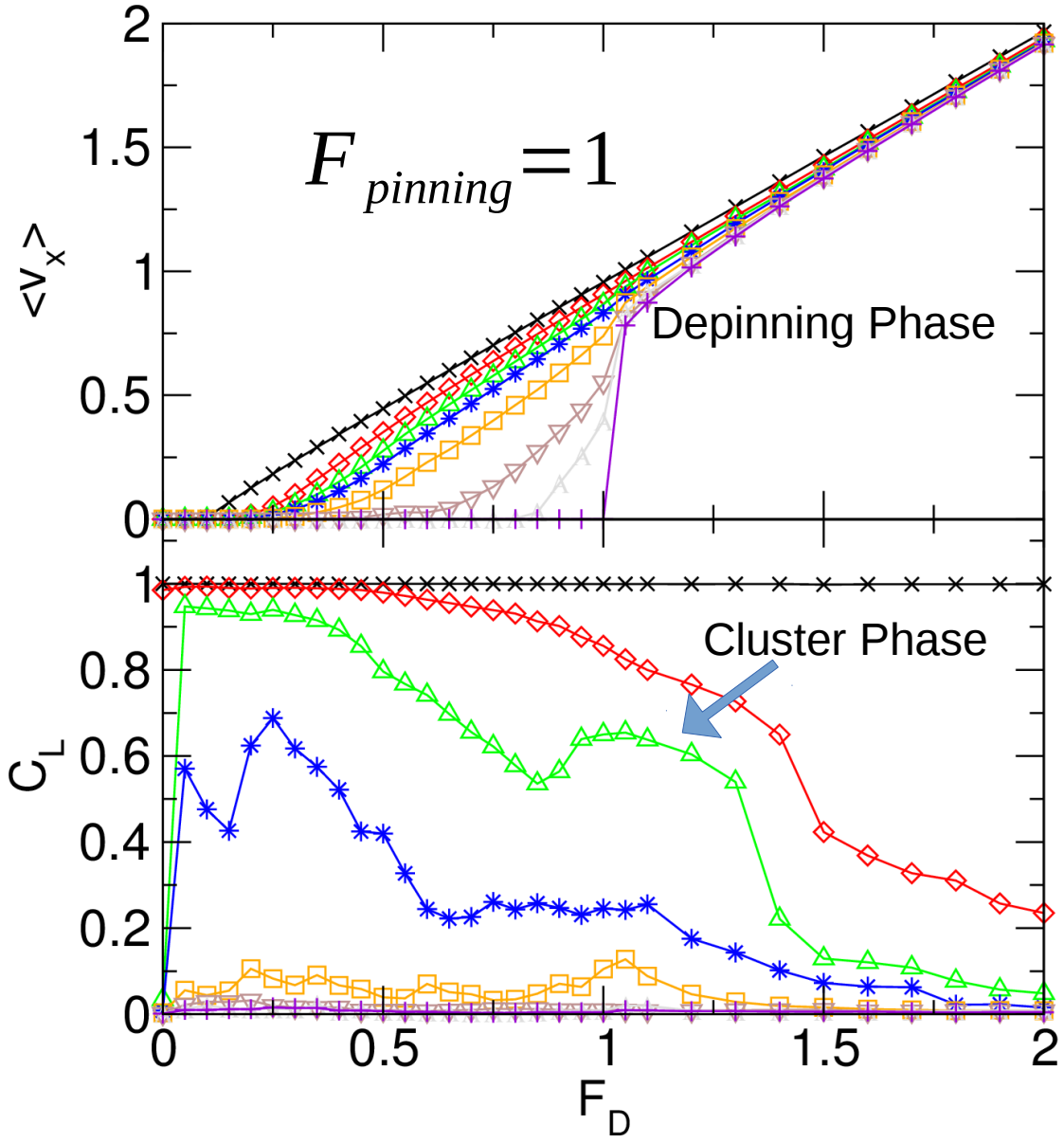

$\langle V_x \rangle$ Average Horizontal Velocity

C_L Largest Cluster Size

F_D Driving Force

Packing Fraction Φ

- 0.85
- 0.71
- 0.61
- 0.55
- 0.43
- 0.3
- 0.25
- 0.15

Super-Diffusion

Diffusion Fit Coefficient: α is defined as $\langle \Delta y^2 \rangle \propto t^{\alpha}$

- Normal Diffusion: $\alpha = 1$
- Super-Diffusion: $\alpha > 1$
- Sub-Diffusion: $\alpha < 1$

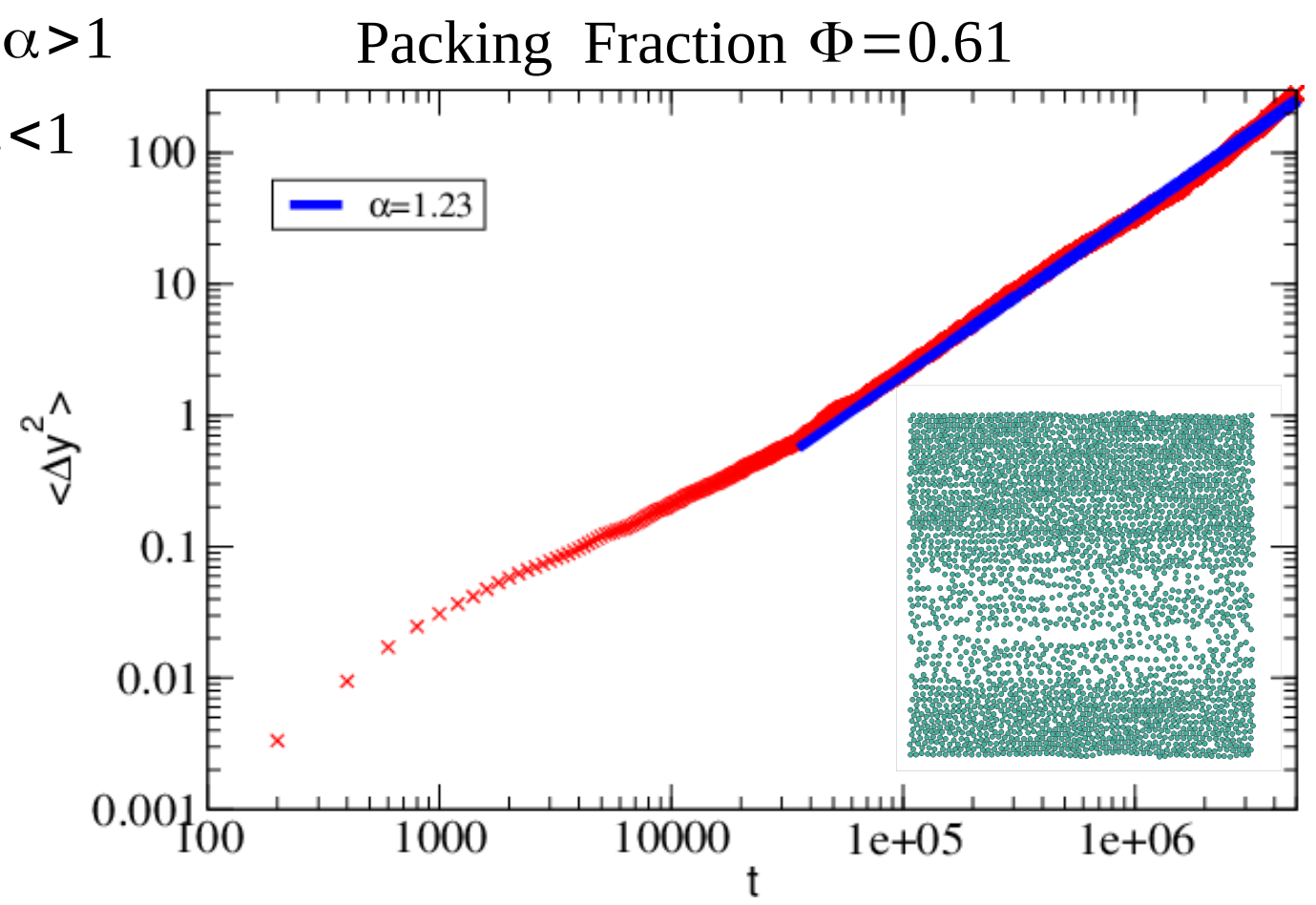

Super-Diffusion

Diffusion Fit Coefficient: α is defined as $\langle \Delta y^2 \rangle \propto t^{\alpha}$

- Normal Diffusion: $\alpha = 1$
- Super-Diffusion: $\alpha > 1$
- Sub-Diffusion: $\alpha < 1$

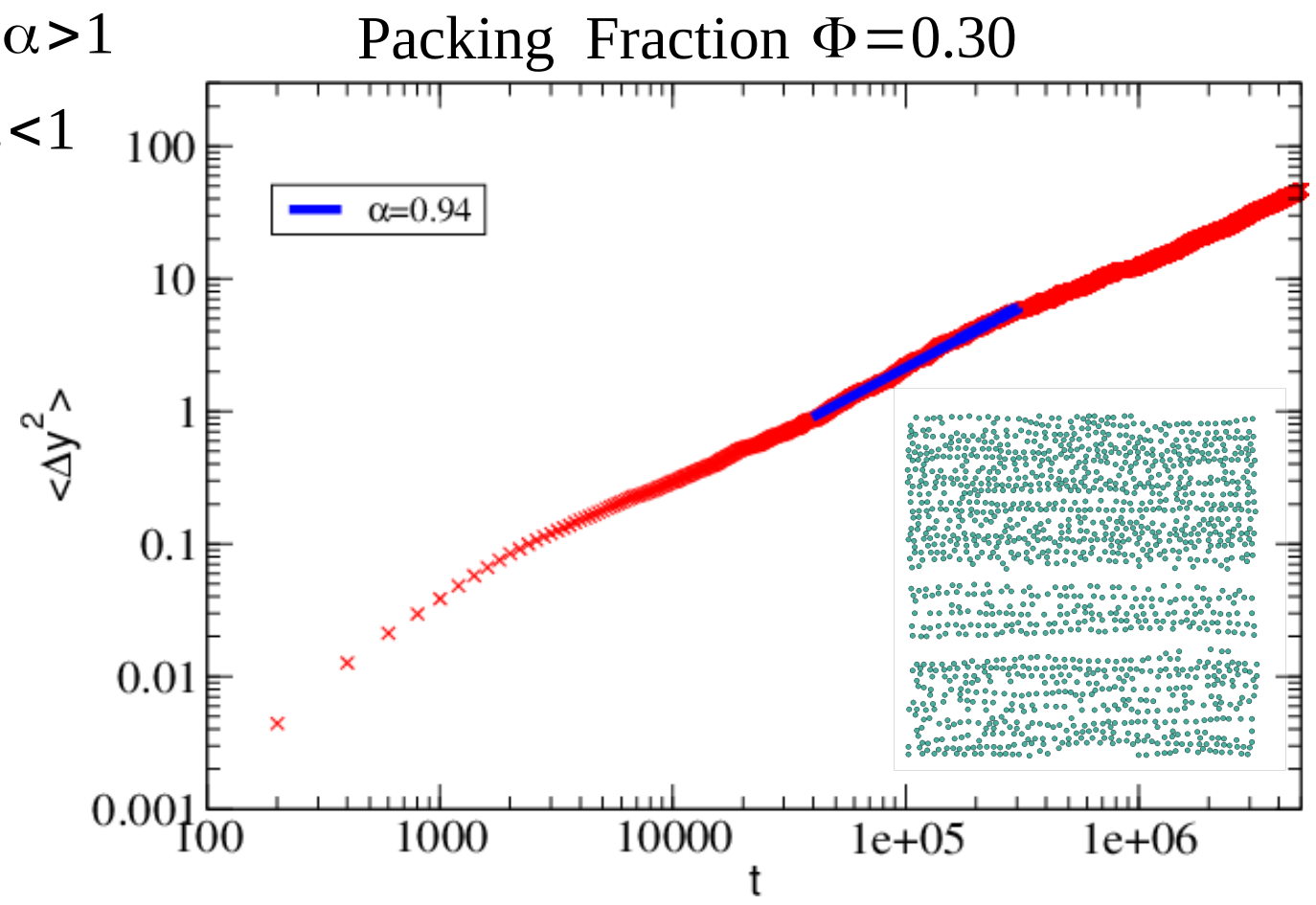

Summary

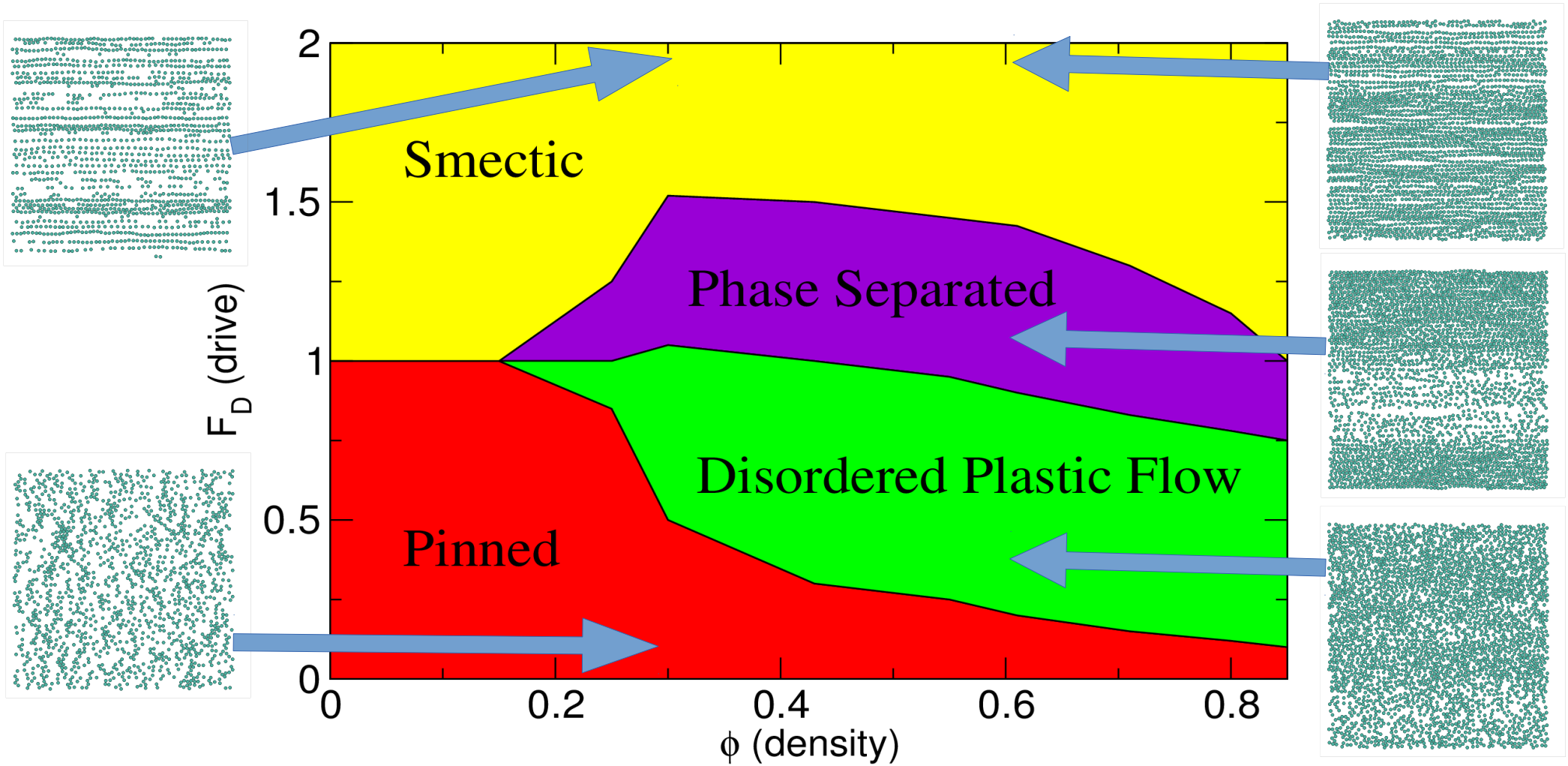
Smectic
Phase Separated
Disordered Plastic Flow
Pinned
2
1.5
1
0.5
0
0
0.2
0.4
0.6
0.8
F_D (drive)
ϕ (density)

Acknowledgment

- I would like to thank:
    - *Dr. Cynthia J. Olson Reichhardt* and *Dr. Charles Reichhardt* for mentoring this project
    - *Dr. Danielle McDermott* for helping with the preparation of this project
    - *Xiaoyu Ma*, *Hong Nguyen* and *Minh Quan Le Thien* for some useful discussion on this project

References

H.M. Jaeger, S.R. Nagel, R.P. Behringer, Phys. Today **49** (4), 32 (1996)

C. Reichhardt, C.J.O. Reichhardt, arXiv:1602.03798 [cond-mat.supr-con]

C. Reichhardt, C.J.O. Reichhardt, Phys. Rev. E**90**, 012701 (2014)

Y. Fily, E. Olive, N. Di Scala, J.C. Soret, Phys. Rev. B**82**, 134519 (2010)

Diffusion Coefficients under Different Particle Densities

- Diffusion Fit Coefficient: $\alpha = 1$ corresponds to normal diffusion $\langle \Delta y^2 \rangle \propto t$

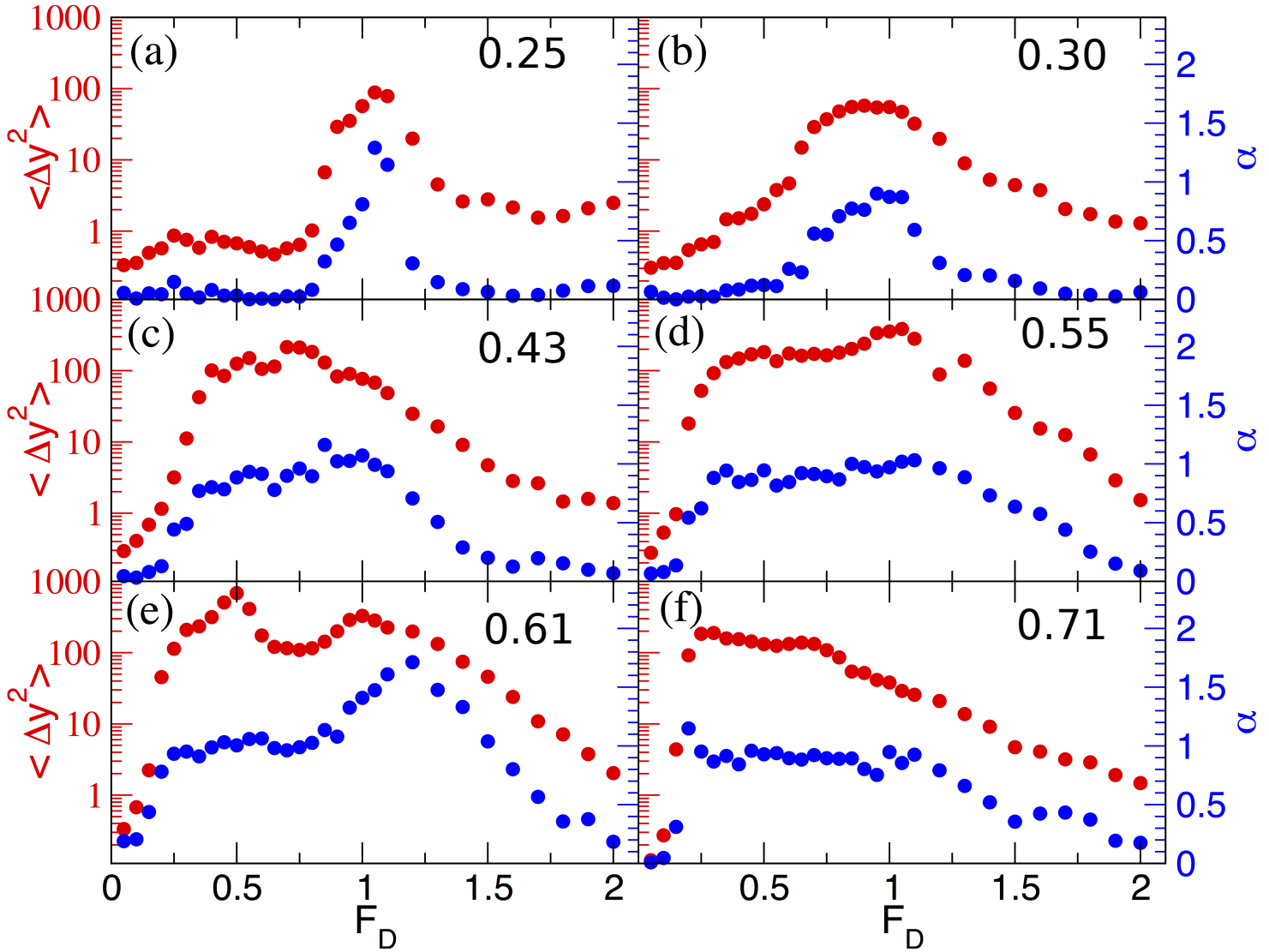

Correlation between Grain Boundary Anisotropy and Nanovoid Nucleation under Shock Loading

Sabine Pogue Zentgraf
University of Colorado, Colorado Springs
Mentor: Curt Bronkhorst

Grain Boundaries

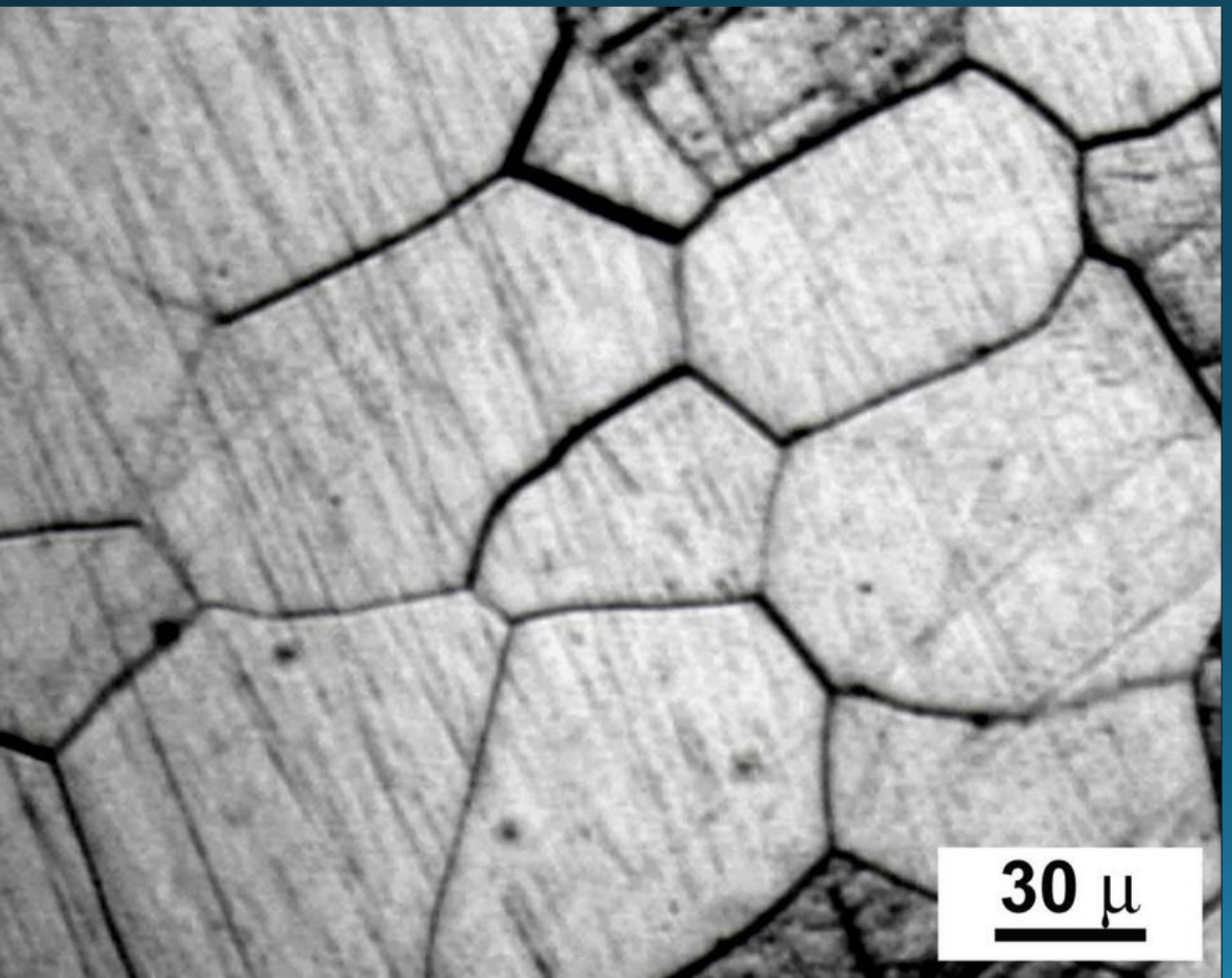

- Order of perfect lattice disrupted during recrystallization
- Usually only 1-2 atoms wide
- Determine performance and integrity of material
  - Limit dislocation migration
- Lattice mismatch causes broken bonds between the atmos.
  - Large excess free energy
- **Nucleation sites for voids**

Some Traditional Approaches to Describe Grain Boundaries

Geometric

- Coincidence Site Lattice (CSL)
  - Source of commonly used **Σ**-values.
- **Σ** assignment according to 2D structure, no information about boundary inclination
- Does not provide information on energy

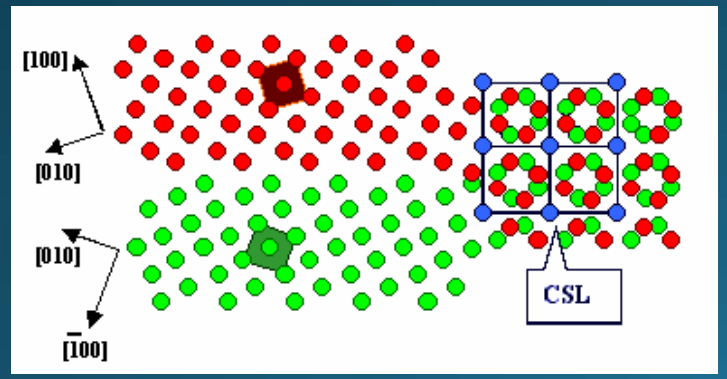

Dislocation

- Started by Read-Shockley model
- Frank-Bilby and Bollmann's O-lattice expand on Read-Shockley
- Distribution of dislocations facilitating small misorientations
- Simple linear GB energy model

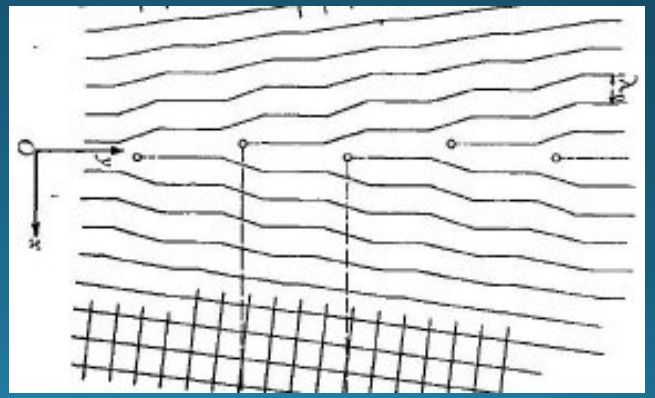

Current Approaches to Determine GB Energy and their Limitations

Molecular Dynamics (MD)

- Most accurate method to date for single boundaries
- Time consuming
- Not suitable for mesoscale analysis due to time constraints

Multi-Scale Models

- In development
- Large scale models using small scale physics
- Enable fast analysis of large data sets

Formal Definition of Excess Free Energy

For two clusters of atmos (b, w) interacting through interatomic energy,
Total free energy of general incoherent surface (Gibbs):

$$E_{tot} = \int_{\Omega b} E^b(x)dx + \int_{\Omega w} E^w(x)dx + \int_{\Omega b \cap \Omega w} \gamma(x)d\mathcal{H}^2$$

… rearranging, substituting, and taking the limit to get free excess energy:

$$\gamma = \lim_{L\to+\infty} \frac{1}{L^2} \left(\lim_{H\to\infty} \left(E_{tot}\left(x^b_{L,H}, x^w_{L,H}\right) - N^b_{L,H}E^b_{coh} - N^w_{L,H}E^w_{coh} \right) \right)$$

total energy at equilibrium — Number of atoms x cohesive energy per atom

Goal: define γ as a function of the interface geometry.

Lattice Matching Energy and Thermalization (Brandon Runnels et al)

What is the "cost" from white to perfect gray lattice?

- Define local energy density as (minimized) cost of transformation
- Integrate over Ω to get total Energy

$$e(\chi, z) = \inf\left\{ C(\chi, R\mathcal{L} + \tau, z):\ R \in SO(3),\ \tau \in \mathbb{R}^3 \right\}.$$

$$E(\chi, \Omega) = \int_\Omega e(\chi, z)\, dz.$$

- Thermalization process based on the principal of maximum entropy
- Energy and morphology of interfaces are temperature dependent
- Enables approximation of energy by L^2-bound.

Local energy density bound:

$$e(\chi, z) \leq \inf\left\{ c \int_{B_\lambda(z)} |\rho_\beta^\chi(x) - \rho_\beta^{R\mathcal{L}+\tau}(x)|^2 \theta(x - z)\, dx:\ R \in SO(3),\ \tau \in \mathbb{R}^3 \right\},$$

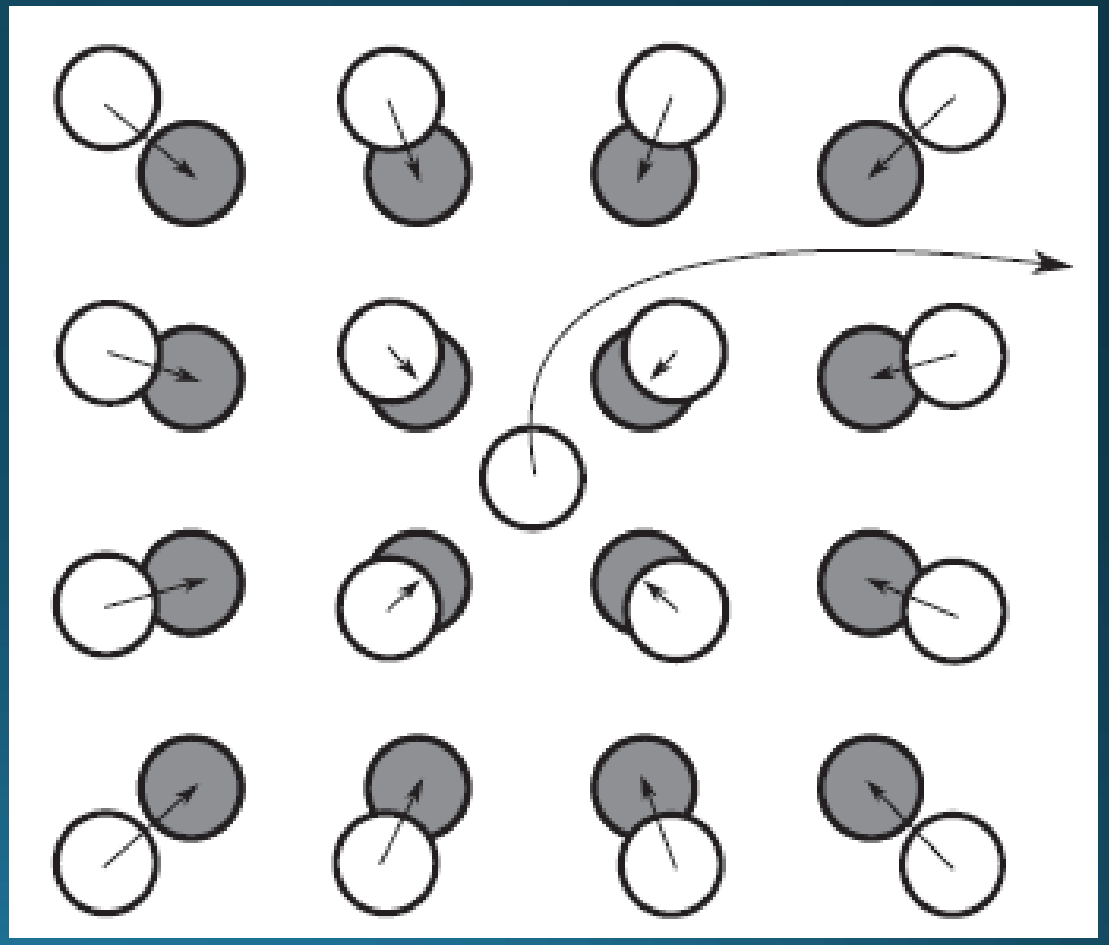

Interfacial Energy (Brandon Runnels et al)

Two lattices with different rotation and translation. Assumptions:

- Both rigid > cost of transformation will give upper bound for energy density.
- Local rotation and translation about z is of reference lattice
- L^2 bound from thermalization

Below an expression for upper bound of grain boundary energy. Does not account for relaxation mechanisms.

$$\gamma \approx \lim_{L\to\infty}\frac{1}{L^2}\left(\int_{\Omega_{L,\nu}\cap\mathbb{R}^3_b}\left(\int_{B_\lambda(z)} c\left|\sum_{x\in\mathcal{L}^w\cap\mathbb{R}^3_w}\psi_\beta(x-p)-\sum_{y\in\mathcal{L}^b\cap\mathbb{R}^3_w}\psi_\beta(y-p)\right|^2\theta(z-p)\,dp\right)dz\right.$$
$$\left.+\int_{\Omega_{L,\nu}\cap\mathbb{R}^3_w}\left(\int_{B_\lambda(z)} c\left|\sum_{x\in\mathcal{L}^b\cap\mathbb{R}^3_b}\psi_\beta(x-p)-\sum_{y\in\mathcal{L}^w\cap\mathbb{R}^3_b}\psi_\beta(y-p)\right|^2\theta(z-p)\,dp\right)dz\right).$$

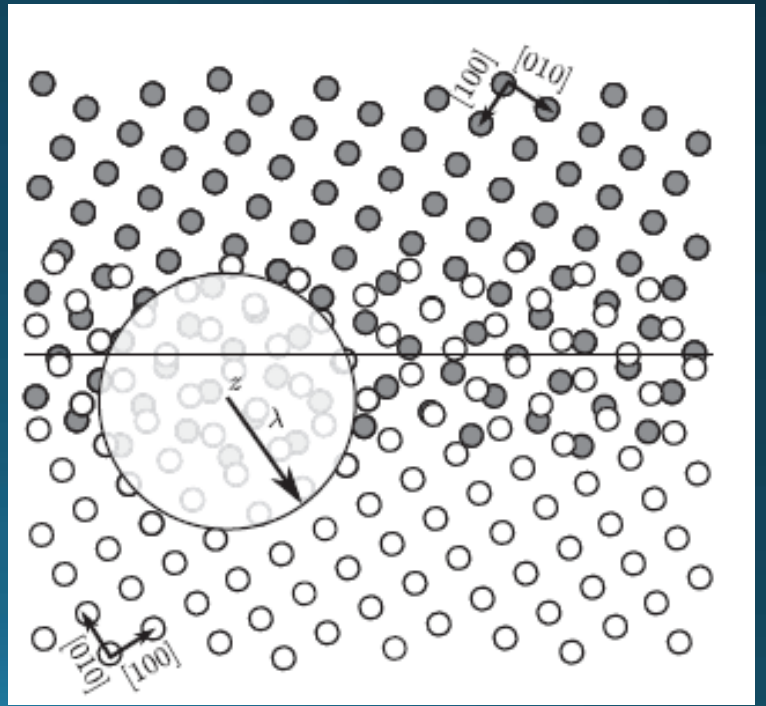

Summary (Brandon Runnels et al)

- Model achieves reasonable qualitative agreement to MD
- Location of all significant energy cusps recovered.
- General shape of the energy function recovered.
- Significant outliers: FCC (111)(111) and BCC(011)(011)
- Does not consider relaxation

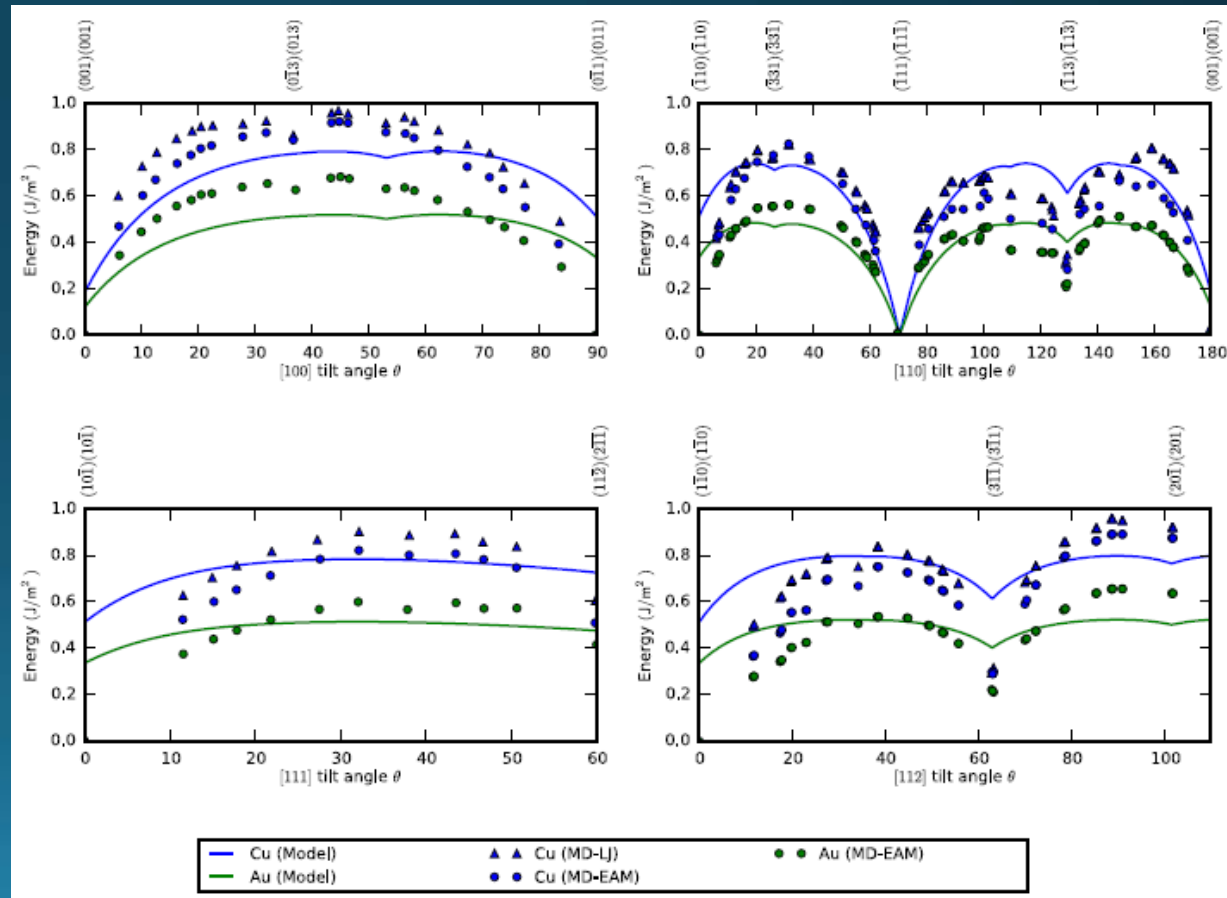

Experimental Observations in Copper (J. P. Escobedo et al)

- Effect of grain boundary structure on void nucleation

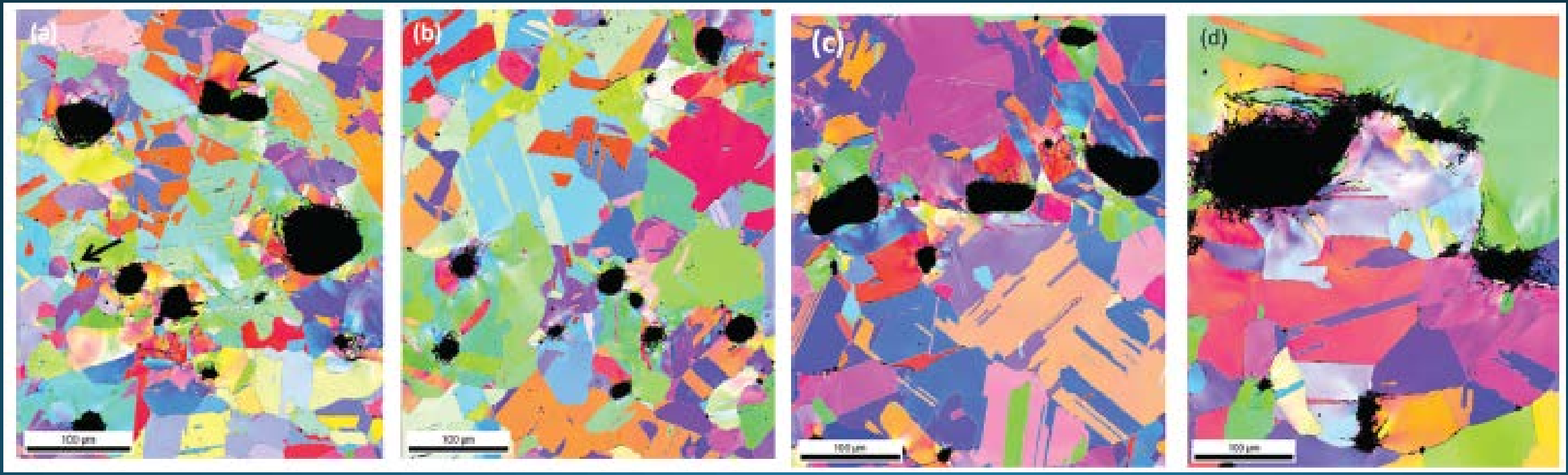

Void Nucleation at Grain Boundaries (J.P. Escobedo et al)

Boundaries excluding low angle and Σ3 parallel to shock

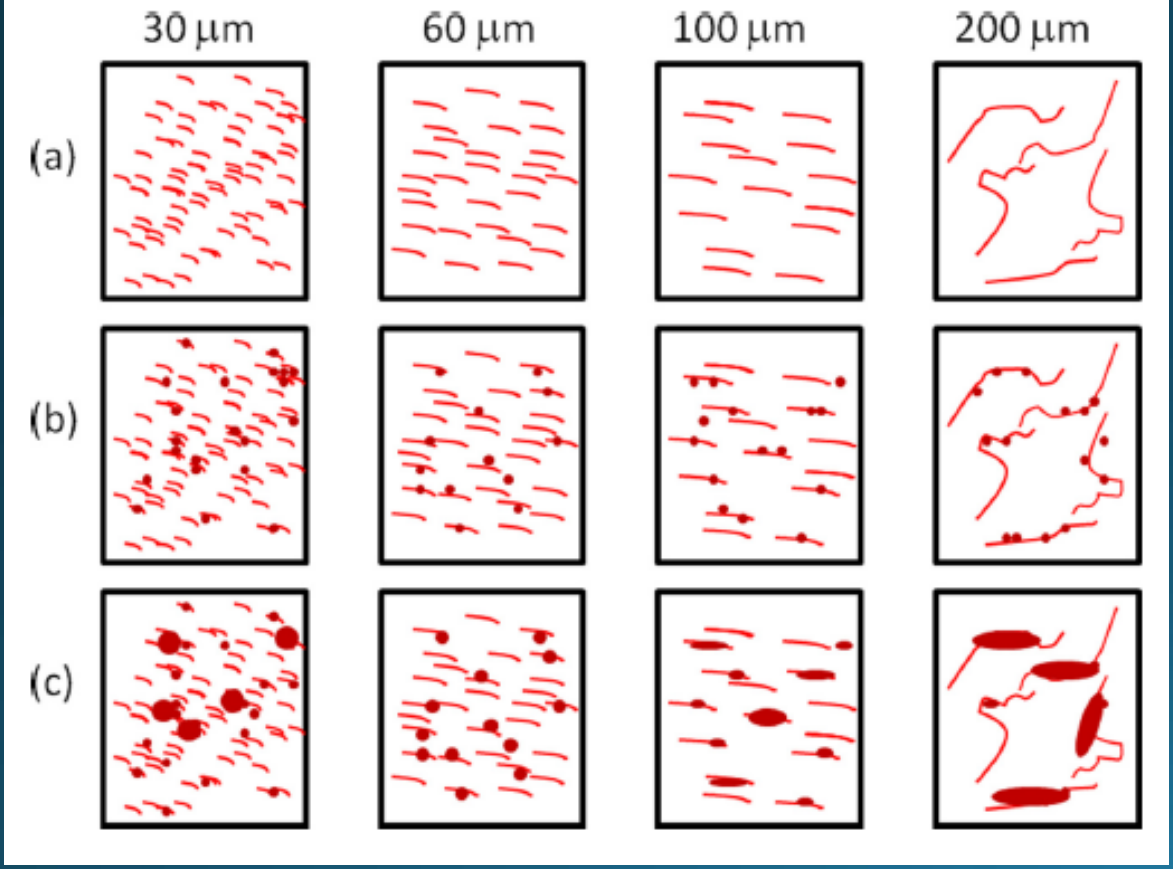

- Most voids at ~15°- 55° misorientation
- Low angle and Σ3 seem immune
- What is the reason voids preferentially nucleate at certain boundaries?
- Can we get more detailed information about the energy state of these particular boundaries?

Propensity for Void Nucleation (J.P. Escobedo et al)

- "Experimental evidence suggests that there is no demonstrable relationship between misorientation and probability for pore nucleation within the 10 to 58 degree range – equal probability within that misorientation range."

- "The probability of grain boundary pore nucleation is greater for boundaries that have normal vectors which form smaller angles with the principal direction of tensile loading."

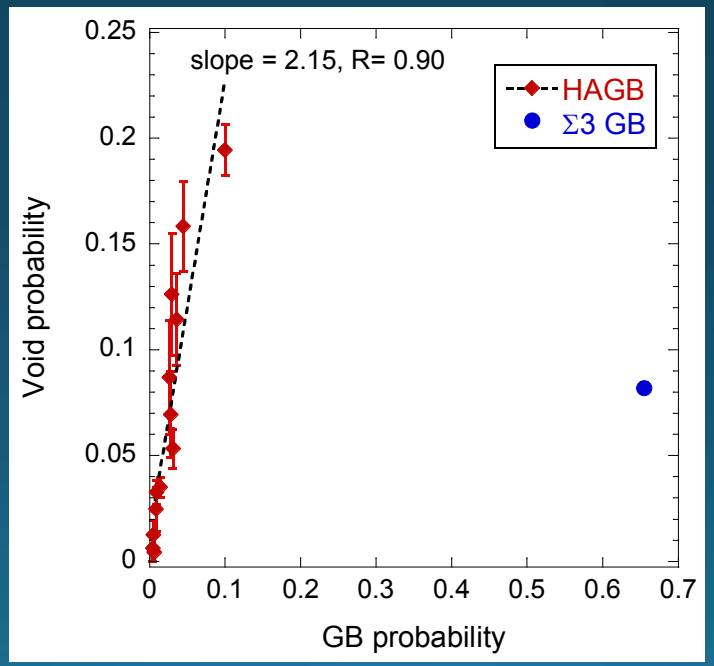

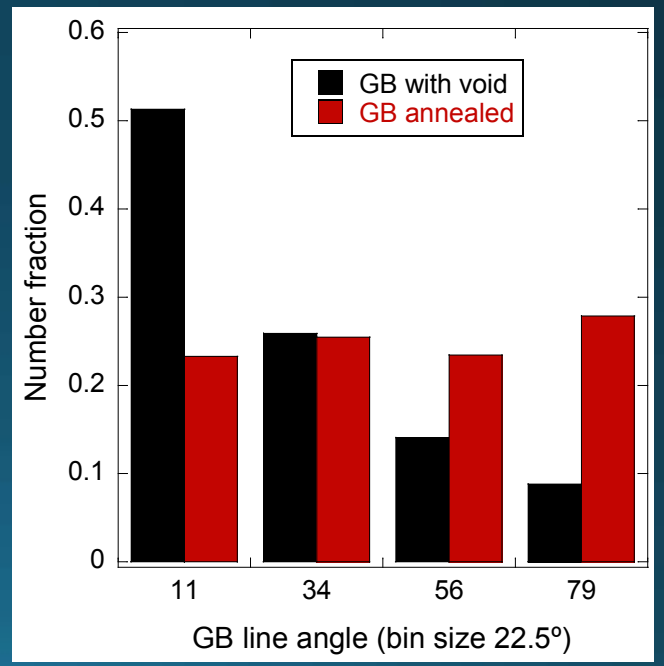

Summer 2016: Python Code

Uses OIM Analysis output files to

- Analyze simplified GB geometry
- Allow user to select boundaries of interest (around voids) for bulk operations
- Run different operations such as
  - Energy calculations using Brandon Runnels' model
  - Statistics about grain boundary distribution
  - Comparison of sample averages and selected GBs

GOAL: Create a powerful tool to examine large data sets quickly

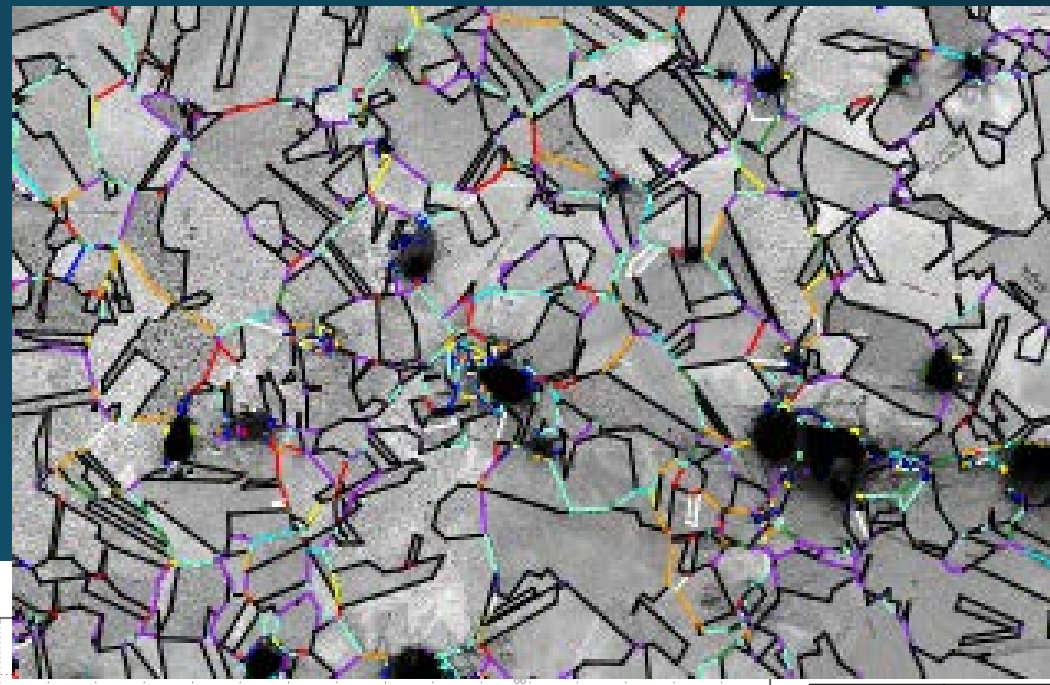

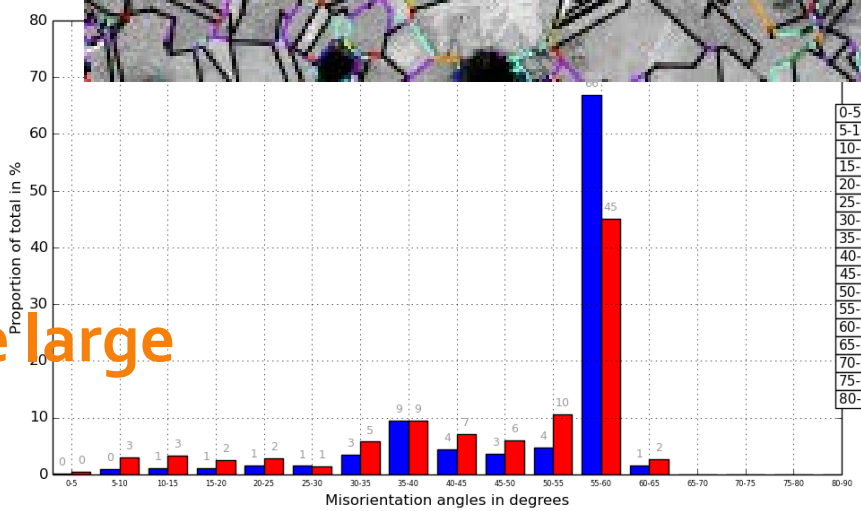

	Change in %	Increase Ener
0-5	0.26	5
5-10	2.08	0
10-15	2.28	10
15-20	1.44	25
20-25	1.31	24
25-30	-0.09	10
30-35	2.33	27
35-40	-0.0	30
40-45	2.67	30
45-50	2.44	25
50-55	5.84	42
55-60	-21.71	25
60-65	1.16	45
65-70	0.0	0
70-75	0.0	0
75-80	0.0	0
80-90	0.0	0

Summer 2016: Results and Observations

- More detailed analysis of misorientation angle distribution

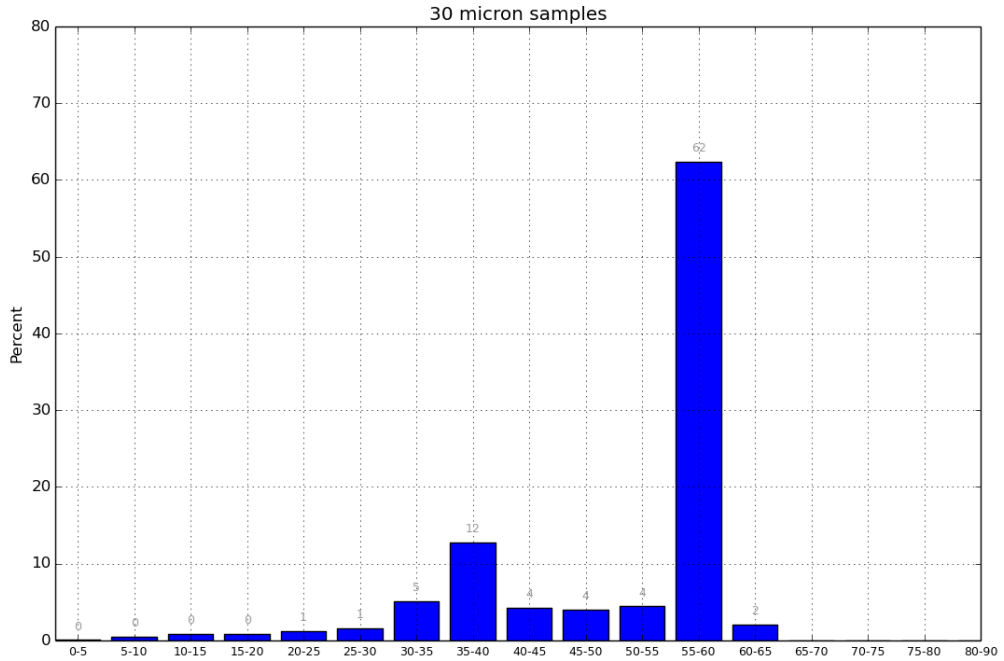

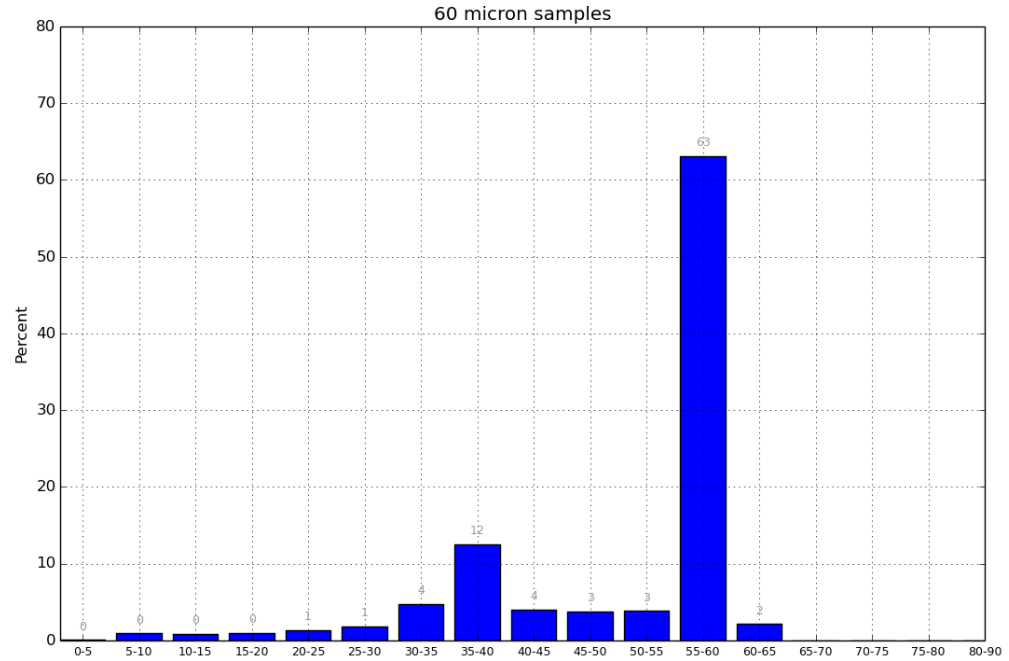

Summer 2016: Results and Observations

- Peak of 35-40° misorientation angles inversely proportional to grain size.

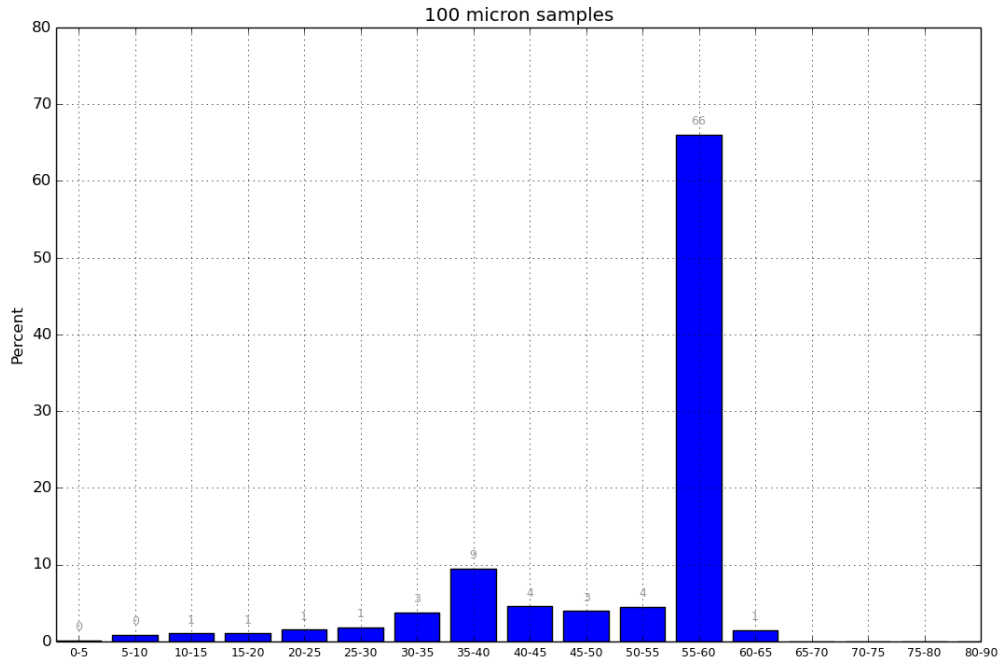

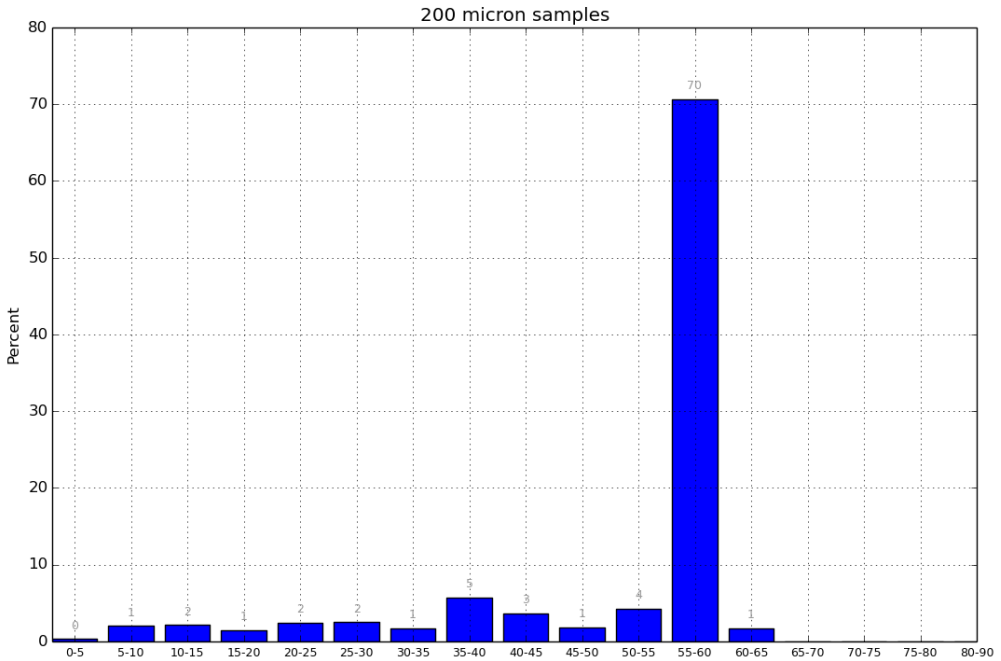

Summer 2016: Results and Observations 30 micron samples

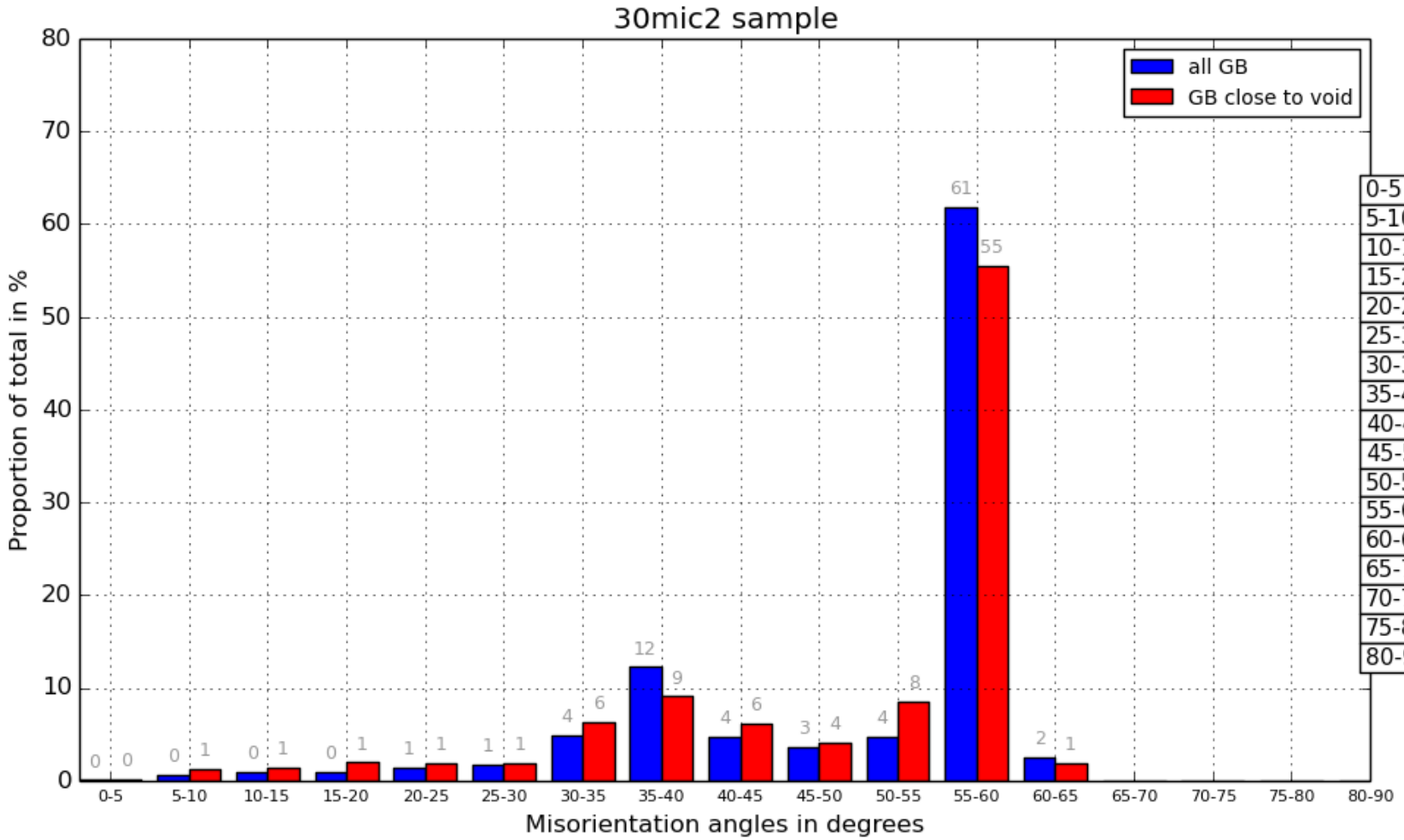

	GF Propensity	Energy min	Energy avg
0-5	3.0	311.271	382.761
5-10	2.0	373.952	418.867
10-15	1.4	394.34	425.86
15-20	2.0	369.08	416.79
20-25	1.4	384.763	429.73
25-30	1.1	402.027	433.509
30-35	1.3	387.093	426.509
35-40	0.7	398.429	433.949
40-45	1.3	384.651	426.917
45-50	1.1	394.331	427.941
50-55	1.8	403.239	434.28
55-60	0.9	387.415	426.659
60-65	0.8	356.026	407.353
65-70	nan	0.0	0.0
70-75	nan	0.0	0.0
75-80	nan	0.0	0.0
80-90	nan	0.0	0.0

Summer 2016: Results and Observations 60 micron samples

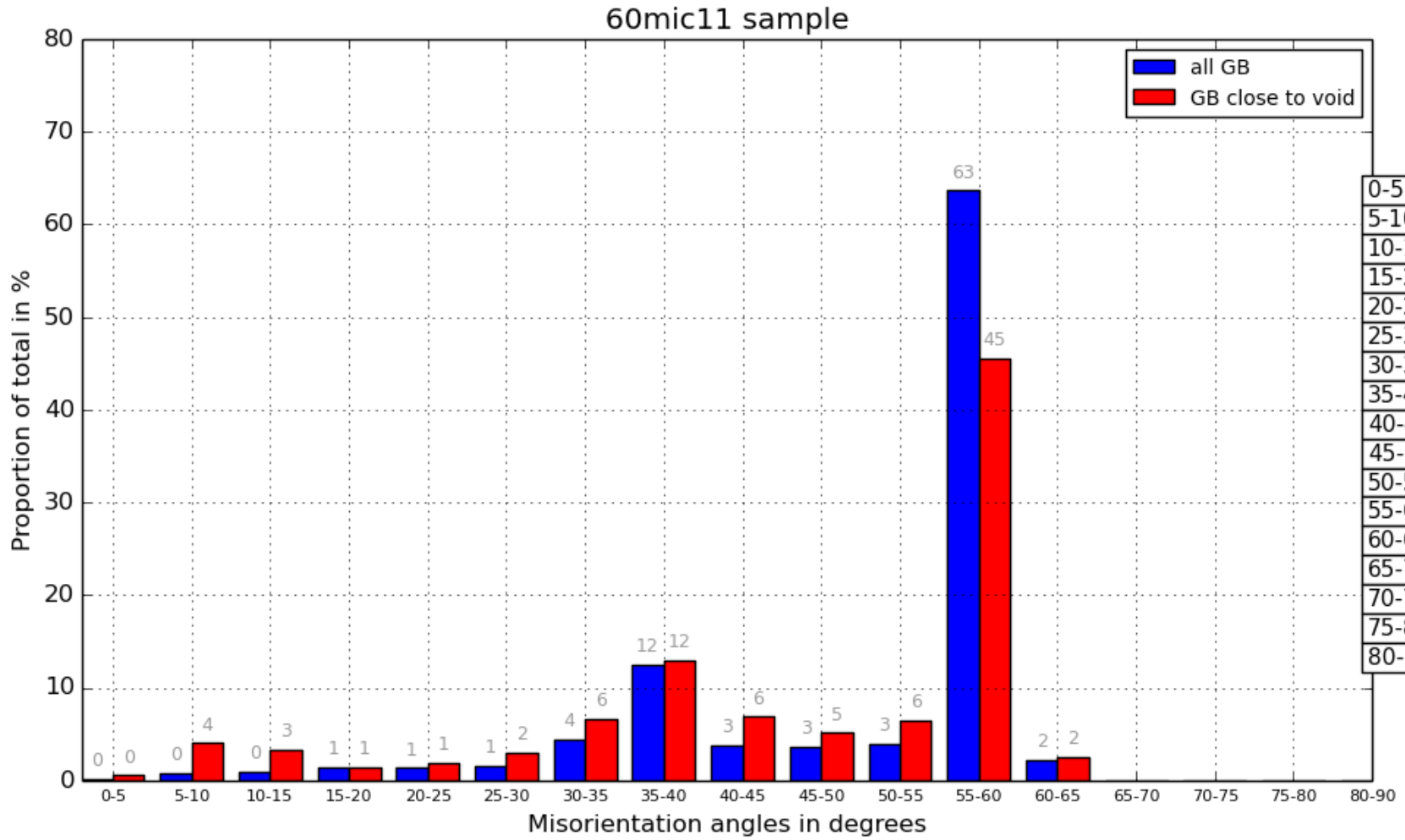

	GF Propensity	Energy min	Energy avg
0-5	6.5	361.148	420.514
5-10	5.7	368.049	418.505
10-15	3.4	379.512	421.755
15-20	1.0	374.49	415.628
20-25	1.5	378.989	419.2
25-30	1.9	407.713	433.16
30-35	1.5	406.188	434.976
35-40	1.0	408.045	434.96
40-45	1.8	394.593	430.143
45-50	1.4	394.815	429.623
50-55	1.6	390.962	426.468
55-60	0.7	392.339	429.377
60-65	1.2	383.088	424.59
65-70	nan	0.0	0.0
70-75	nan	0.0	0.0
75-80	nan	0.0	0.0
80-90	nan	0.0	0.0

Summer 2016: Results and Observations 200 micron samples

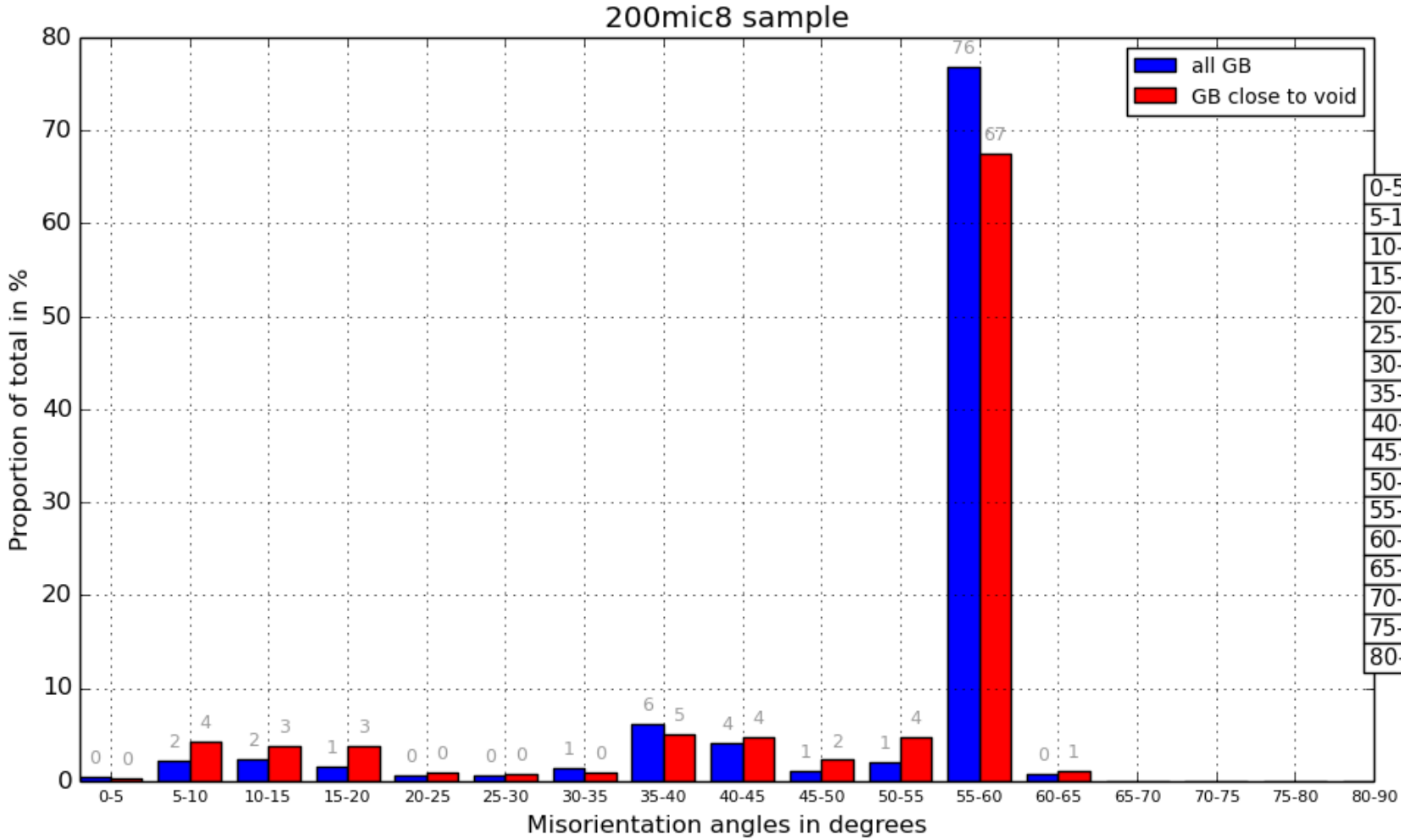

	GF Propensity	Energy min	Energy avg
0-5	0.7	363.75	419.778
5-10	2.0	370.865	419.964
10-15	1.6	386.577	423.625
15-20	2.3	395.943	425.315
20-25	1.7	394.722	430.605
25-30	1.3	406.821	439.476
30-35	0.7	358.635	416.054
35-40	0.8	373.117	424.467
40-45	1.1	389.855	429.718
45-50	2.1	377.54	428.878
50-55	2.4	393.993	431.809
55-60	0.9	389.698	426.157
60-65	1.4	399.769	434.721
65-70	nan	0.0	0.0
70-75	nan	0.0	0.0
75-80	nan	0.0	0.0
80-90	nan	0.0	0.0

Summer 2016: Results and Observations 100 micron samples

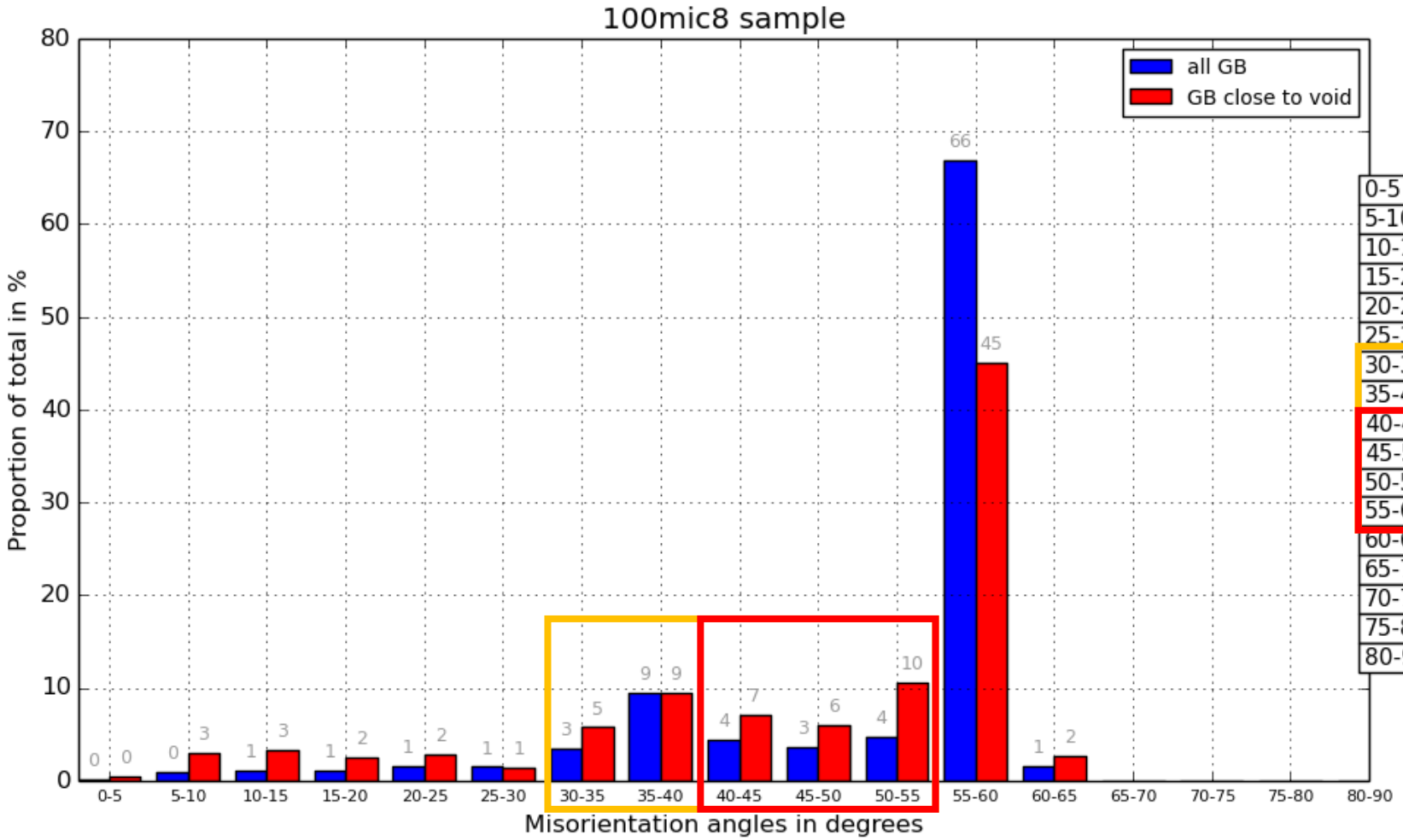

	GF Propensity	Energy min	Energy avg
0-5	2.8	371.283	428.752
5-10	3.2	365.937	414.663
10-15	3.1	376.12	417.051
15-20	2.4	391.507	427.054
20-25	1.9	390.126	426.716
25-30	0.9	376.014	423.728
30-35	1.7	392.976	428.325
35-40	1.0	396.61	430.25
40-45	1.6	396.444	428.346
45-50	1.7	391.581	426.922
50-55	2.2	408.002	436.024
55-60	0.7	391.588	428.467
60-65	1.8	411.121	432.202
65-70	nan	0.0	0.0
70-75	nan	0.0	0.0
75-80	nan	0.0	0.0
80-90	nan	0.0	0.0

Summer 2016: Results and Observations

Summary:

- 55 – 60° more resilient
- Peak of 35 – 40° boundaries, decreasing with grain size
- Close to voids, high concentration of 40 – 55° misorientation boundaries
  - 50-55° degrees highest concentration
- GB energy results so far inconclusive
  - Further improvements needed

Challenges

- Solving a 3D problem with 2D information
  - Missing boundary inclination
- No information on pre-shock geometry
  - Difficult to estimate where void initially nucleated
- Verification of results demanding
  - No MD values widely available for boundaries between Σ-values
- Analysis still cumbersome
- Missing enclosed grains
- Grain Boundary anisotropy is not the only factor in void nucleation

Future steps

- Improve data handling and expand functionality
- Incorporate
  - Trace angles with respect to shock loading direction
  - Analyze geometry of boundary in more detail
  - Triple points and their relation to voids (especially large grain samples)
  - Surroundings of boundaries (increased density of boundaries to average)
- Verify multi-scale model results with MD
  - Improve accuracy of the model
- More experiments targeted towards void nucleation
  - Appropriate grain size and low peak stresses to reveal and preserve initial nucleation site
  - Chose material with consistent known properties
  - Keep grain structure as “simple” as possible to reduce other factors for failure

Thank You!

- Curt Bronkhorst, T-3
- Irene Beyerlein, T-3
- Brandon Runnels, UCCS
- Eric Hahn, UC San Diego
- Pierre Schnarz, TU Clausthal